

THE SYNAPTIC AND ELECTROPHYSIOLOGICAL
PROPERTIES OF PRINCIPAL NEURONS IN THE
LATERAL SUPERIOR OLIVE OF TWO
MAMMALIAN SPECIES

Thesis submitted at UCL

by

Jason Mikiel-Hunter

for the degree of

Doctor of Philosophy, PhD

Declaration

I, Jason Mikiel-Hunter confirm that the work presented in this thesis results from the combined efforts of Dr Roberta Donato and myself. Dr Donato provided the electrophysiological recordings from the MSO and was fundamental in introducing the ZAP protocol and the concept of resonance to this study. Where other ideas, data or information has been derived from sources external to the McAlpine group, I confirm that it has been indicated in the thesis.

Abstract

The lateral and medial superior olives (LSO and MSO respectively) receive inputs from the two ears and represent the first station in the binaural localization pathway. The need for two discrete nuclei to locate sound sources on the horizontal axis was long assumed to reflect the binaural acoustic cue that each nucleus' principal neurons employed when processing sounds in a restricted frequency range. This arrangement proves to be overly simplistic however: even though the MSO is restricted to processing temporal information within low-frequency sounds, LSO principal neurons are sensitive to interaural discrepancies in both the intensity and arrival time of high-frequency auditory stimuli. The ability of these neurons to extract temporal information from the envelope of amplitude-modulated carrier stimuli raises the possibility that responses to binaural stimuli may be continuous across the two nuclei. The purpose of this thesis was to determine whether synaptic and biophysical properties are specialised in guinea pig LSO principal cells for temporal and intensity difference processing. Whole cell patch clamp recordings demonstrated that LSO principal neurons responded to superthreshold current injection with a continuous range of phasic and tonic firing patterns whilst maintaining low input resistances and fast membrane time constants across the neuronal population. The importance of these fast passive properties was made clear when it was revealed that LSO principal neurons rely more on their passive properties to integrate excitatory synaptic potentials than do MSO principal neurons. Furthermore the passive properties of principal neurons appeared fastest in the low-frequency, lateral limb of the LSO where contralateral excitation and band-pass filtering were also present. These findings suggest that many lateral guinea pig principal neurons may actually retain the biophysical and synaptic machinery to process pure tone and envelope temporal processing whilst still being sensitive to rapidly changing intensity differences.

Acknowledgements

I must first offer my joint thanks to both my principal and “direct” supervisors, David McAlpine and Roberta Donato respectively.

David’s mercurial ability to convey his enthusiasm for binaural hearing has proven highly infectious, only being surpassed by his unerring confidence and patience. Conversations with David have always been highly stimulating, opening several doors of inquiry, often at the same time, and I only wish some of those conversations would have proven longer.

Only Roberta knows how much I owe her over the course of this PhD. Her support and patience have been invaluable; her willingness to impart her scientific knowledge, electrophysiological experience and rigour, beyond compare. I thank her from the bottom of my heart for all she has provided.

As my second supervisor, I thank Jonathan Ashmore for his constant source of wisdom, assistance and patience. As the person who first brought the cochlea to my attention as an undergraduate, I am eternally indebted to him for introducing me to the world of hearing.

I give my thanks to all those past and present in the McAlpine and Ashmore groups (Ben Robinson; Torsten Marquadt, Isabel Dean, Ade Deane-Pratt, John Agapiou, Nicol Harper; Juan de D. Navarro Lopez and Pavel Mistrik) and at the same time extend my gratitude to colleagues of the Ear Institute who have often felt like members of one big group. In particular I would like to thank Jonathan Gale, Andy Forge, Ruth Taylor, Dan Jagger, Torsten Marquardt, Graham Nevill and Joerg Albert for their academic support. I would also like to thank AC Tan, Kate Faxen and Neil Roberts for their help as well as the “back room” for its changing faces but indomitable spirit and companionship over the years. I give special thank to members of the Pedarzani/Stocker lab for being a lab from lab. For helping with the modelling, I also thank Michiel Remme and John Rinzel in New York.

My warmest thanks to my dear friends, Marisol and Stephen (and family). At the bottom of a list which these acknowledgements cannot do justice, I thank them for introducing me to Goodenough College which was my home for so much of the PhD. I would like to especially thank Michael, Daffne, Geoffrey, Krithika, Shakti and Mary for being pillars during my thesis and being wonderful friends to boot.

My most tender affections and thanks go to Joseph, Andrea and Chiara, who have brought me so much joy throughout the PhD, reminding me what is truly important.

Words cannot express how much I thank my mother for her unstemmable love and support. I thank her for always making the grass seem greener at home wherever I was and however I felt. Thank you.

Finally thanks to Deafness Research UK and sponsors for funding my PhD and giving me this unparalleled opportunity to explore auditory sciences at UCL.

Table of Contents

Title	1
Declaration	2
Abstract	3
Acknowledgements	4
Table of Contents	6
List of Figures	12
Chapter One Introduction	16
1.1 Binaural hearing and its importance	16
1.1.1 Horizontal vs Vertical	16
1.2 Duplex theory	17
1.2.1 The Superior Olivary complex and the Duplex theory	19
1.2.2 Exceptions to the Duplex theory	19
1.3 The binaural pathway	21
1.3.1 A map of frequencies originals in the cochlea	23
1.3.2 Temporal coding in the periphery and the auditory nerve ...	25
1.3.3 Intensity coding in the periphery and the auditory nerve	26
1.3.4 Coding for temporal envelope of sounds in the auditory periphery and the auditory nerve	28
1.3.5 Anterior ventral cochlear nucleus can improve stimulus-locked neural discharge	28
1.3.6 MNTB relay information to the MSO and LSO	29
1.4 Anatomy of MSO principal neurons	30
1.4.1 The sublocalization of postsynaptic glycine receptors.....	30
1.4.2 Physiology of MSO principal neurons	31
1.4.3 Coding for ITDs in MSO principal neurons	33
1.4.4 Role of inhibition in ITD coding	36
1.5 Anatomy of LSO principal neurons	38

1.5.1	Physiology of LSO principal neurons	39
1.5.2	Binaural sensitivity of LSO principal neurons	41
1.6	Strategy for ITD coding across the SOC	44
1.6.1	Strategy for envelope ITD coding	45
1.7	Naturalistic sounds and the auditory system	46
1.7.1	Optimal coding of naturalistic sounds may affect binaural localization	47
1.8	The hearing ranges of guinea pig and rat	48
1.9	Aims of the project	49

Chapter Two **Material and Methods**

2.1	Electrophysiology	52
2.1.1	Animals	52
2.1.2	Slice preparation	52
2.1.3	Whole cell patch clamp	56
2.1.4	Electrophysiology protocols	57
2.1.5	ZAP protocol	58
2.1.6	Electrical stimulation of trapezoid body fibres	59
2.1.7	Analysis of passive and active property data	61
2.1.8	Analysis of synaptic data	65
2.2	Immunohistochemistry	66
2.2.1	Protocol	66
2.2.2	Preparation	66
2.2.3	Sectioning	67
2.2.4	Fixation	67
2.2.5	Immunohistochemical labelling	68
2.2.6	Confocal microscopy	69
2.2.7	Analysis	69

Chapter Three **Results**

3.1	Electrophysiology	71
3.1.1	Classification of guinea pig pLSO neurons	71
	A range of firing patterns are observed in guinea pig pLSO neurons.....	74
	The input resistances of guinea pig pLSO neurons	

	does not support the existence of two subtypes.....	75
	Other passive properties of guinea pig pLSO neurons also negate the existence of two subtypes	76
3.1.2	The intrinsic and firing properties of guinea pig pLSO neurons do not appear to develop postnatally	80
3.1.3	The tonotopic arrangement of guinea pig pLSO neuronal properties	82
3.1.4	Resonance of guinea pig pLSO neurons.....	86
	Hyperpolarization affects resonance in pSOC neurons; duration of the stimulus does not.....	87
	Resonance along the tonotopic axis in guinea pig pLSO neurons	88
3.1.5	Comparison with rat pLSO neurons indicates species differences.....	89
3.2	Synaptic properties	94
3.2.1	Excitatory inputs	94
	Excitatory inputs and the LSO tonotopic axis	94
	The time course of depolarizing PSPs in the LSO ...	95
	Relationship between the time course and the peak amplitude of dPSPs	98
	Short term plasticity of dPSP amplitude	99
	Stimulus frequency and summation of dPSPs	101
	Synaptically evoked APs in pLSO neurons	104
3.2.2	Inhibitory inputs	107
	Inhibitory inputs and the tonotopic axis	108
	Time course of hyperpolarizing PSPs in the LSO and its relationship to their peak amplitudes.	107
	Short term plasticity in the amplitude of hPSPs.....	111
	Frequency dependence of STSD in hPSP amplitude	114
	Stimulation frequency and summation of hPSPs	117

3.3	Immunohistochemistry	120
3.3.1	Localizing principal cells in the SOC	120
3.3.2	Morphology of LSO cells in the guinea pig	121
3.3.3	MSO cells have larger cross-sectional somatic areas than LSO cells	128
3.3.4	Gephyrin staining in the SOC of guinea pigs	129
	Gephyrin Staining in the guinea pig MSO is mainly somatic	129
	LSO gephyrin staining does not differ significantly from the MSO staining	130
	Comparisons of dendritic gephyrin staining in guinea pig LSO show no significant regional differences	131
3.3.5	Separation of LSO cells based on their gephyrin staining reveals somatic differences between LSO regions	132
3.3.6	The somatic size of MSO cells is invariant	133
3.3.7	pLSO neurons in the guinea pig medial limb are not significantly smaller than MSO cells	133
 Chapter Four Discussion		135
4.1	Passive and Active properties	135
4.1.1	Overview of results	135
4.1.2	Differentiating between pLSO neurons and alternative neuronal types	137
4.1.3	The passive and active properties of pLSO neurons in the rat	137
4.1.4	The passive and active properties of pLSO neurons in the guinea pig	139
4.1.5	Tonotopic differences in the active and passive properties of guinea pig pLSO neurons	143
4.1.6	Subthreshold resonance in guinea pig pLSO and pMSO neurons	144
	The biophysics of resonance in guinea pig pSOC neuron	147

	Peak resonance frequency and the tonotopic axis of the LSO and MSO	149
4.2	Synaptic Electrophysiology	152
4.2.1	Contralateral synaptic inputs	152
4.2.2	Comparing temporal properties of PSPs in the guinea pig LSO with findings from previous studies	153
4.2.3	Temporal properties of dPSPs in guinea pig LSO and MSO The relationship between peak amplitude and time course of dPSPs	155 158
4.2.4	Temporal properties of hPSPs in guinea pig LSO and MSO	158
4.2.5	Comparing the temporal properties of hPSPs in the LSO of different species	160
4.2.6	Comparing the temporal properties of hPSPs and dPSPs In the guinear pig LSO	160
4.2.7	Short term depression of dPSP amplitude	161
	Summation of dPSPs	163
4.2.8	Short term depression of hPSP amplitude	164
	Frequency dependence of STSD in hPSP amplitude dPSPs undergo greater STSD than hPSPs in the guinea pig LSO	165 166
4.2.9	Superthreshold dPSPs and graded APs	166
	Threshold for generating APs	169
4.3	Immunohistochemistry	170
4.3.1	Quality of gephyrin Staining in the SOC of guinea pig	170
4.3.2	The sublocalization of gephyrin staining in the guinea pig LSO	172
4.3.3	Cell types encountered in the guinea pig LSO	174
4.3.4	Alternative cell types in the SOC of rats and guinea pigs	175
4.3.5	pLSO neurons in the guinea pig LSO	177
	General Conclusions	179
	Appendix: List of guinea pig pLSO neurons and their properties	184
	References	185
	List of abbreviations and standard units of measurements	204

List of Figures

Figure 1.	Schematic of ITD and ILD cues	18
Figure 2.	The binaural pathways of the auditory brainstem	22
Figure 3.	The tonotopy of the BM and structure of the organ of Corti	24
Figure 4.	Temporal coding in the auditory periphery and auditory nerve ...	26
Figure 5.	Intensity coding in the auditory periphery and auditory nerve	27
Figure 6.	Morphology and firing pattern of guinea pig pMSO neurons	33
Figure 7.	The Jeffress model of ITD coding	35
Figure 8.	Contralateral inhibition and the two-channel model for ITD-coding	37
Figure 9.	Morphology and firing pattern of rat pLSO neurons	40
Figure 10.	Potential basis for IPD sensitivity in the LSO	43
Figure 11.	A potential arrangement of synaptic inputs to achieve a continuum of responses in the SOC	45
Figure 12.	Statistics of naturalistic sounds causes adaptive changes in the filtering properties of auditory midbrain neurons	47
Figure 13.	Contralateral electrical stimulation of the LSO synaptic pathway	60
Figure 14.	Division of LSO nucleus into medial and lateral limbs to localize patched pLSO neurons.....	62
Figure 15.	Calculation of impedance profile using ZAP protocol	64
Figure 16.	Voltage responses of three individual guinea pig pLSO neurons to depolarizing and hyperpolarizing current steps.....	72
Figure 17.	The electrophysiological properties of the three pLSO neurons in Figure 16.....	73
Figure 18.	Histogram displaying the number of action potentials potentially evoked across the guinea pig pLSO neuronal population.	74
Figure 19.	Histogram displaying the range of input resistances across the guinea pig pLSO neuronal population.	75
Figure 20.	Number of action potentials evoked plotted against the input resistance of guinea pig pLSO neurons	76
Figure 21.	Histogram displaying the range of membrane time constants across the guinea pig pLSO neuronal population	77
Figure 22.	The input resistance of guinea pig pLSO neurons plotted against their membrane time constants	78

Figure 23.	Histogram displaying values of capacitance across the guinea pig pLSO neuronal population.	78
Figure 24.	Histogram displaying the range of resting membrane potentials across the guinea pig pLSO neuronal population.	79
Figure 25.	The input resistances of guinea pig LSO neurons arranged by the post-natal day of recording.	80
Figure 26.	The resting membrane potentials of guinea pig LSO neurons arranged by the post-natal day of recording	81
Figure 27.	The values of capacitance of guinea pig LSO neurons arranged by the post-natal day of recording.	81
Figure 28.	The number of action potentials evoked in a guinea pig LSO neuron arranged by the post-natal day of recording	81
Figure 29.	The number of action potentials evoked in guinea pig pLSO neurons from different LSO limbs.	82
Figure 30.	The input resistances of guinea pig pLSO neurons compared in different LSO limbs	83
Figure 31.	The membrane time constants of guinea pig pLSO neurons compared in different LSO limbs.	84
Figure 32.	The impedance profile of two pLSO neurons demonstrates the existence of resonance.	85
Figure 33.	A tonotopic gradient in resonance was found in the SOC nuclei	86
Figure 34.	Hyperpolarization of a pLSO neurons led to the reduction of resonance.	88
Figure 35.	Voltage responses of rat type 1 and type 2 pLSO neurons to 80ms depolarizing current steps	90
Figure 36.	The electrophysiological properties of the two pLSO neurons in Figure 35.	91
Figure 37.	Histogram displaying the number of action potentials potentially evoked across the rat pLSO neuronal population.	92
Figure 38.	Input resistances of type 1 and type 2 rat pLSO neurons.	93
Figure 39.	Depolarizing post-synaptic potentials in the LSO and MSO.	97
Figure 40.	Half-widths were plotted as a function of peak amplitudes for the first five dPSPs evoked by a pulse train in a representative example pLSO neuron and pMSO neuron	99

Figure 41.	Depression of dPSP amplitude evoked by 50Hz electrical pulse trains in a single guinea pig pLSO neuron	101
Figure 42.	Voltage records of dPSPs elicited by 50Hz and 1kHz electrical pulse trains in the same guinea pig pLSO neuron from Figure 39	103
Figure 43	Voltage records of dPSPs elicited by 100Hz electrical pulse trains in a different guinea pig pLSO neuron	104
Figure 44.	Synaptically evoked APs are graded in the MSO and the LSO. APs were evoked by synaptic stimulation as well as somatic current injection in a pMSO and pLSO neuron	106
Figure 45.	PSPs mainly dominated by inhibition reversed at potentials close to the E_{Cl}	107
Figure 46	Hyperpolarizing post-synaptic potentials in a pLSO and pMSO neuron	110
Figure 47	The peak amplitudes of hPSPs were plotted against their half-widths for the guinea pig pLSO neuron shown in Figure 46	111
Figure 48.	Depression of dPSP amplitude evoked by 100Hz electrical pulse trains in the guinea pig pLSO neuronal population	113
Figure 49.	The frequency dependence of STSD in hPSP amplitude.	116
Figure 50.	Voltage records of hPSPs elicited by 100Hz and 250Hz electrical pulse trains in a guinea pig pLSO neuron	118
Figure 51.	Voltage records of hPSPs elicited by 1kHz electrical pulse trains in a guinea pig pLSO neuron	119
Figure 52	Schematic of LSO showing how the nucleus was separated into three parts.	121
Figure 53.	A 3-D reconstruction of a guinea pig mediolateral LSO cell is displayed from two different angles to demonstrate that the gephyrin puncta were located near the neuronal membrane	122
Figure 54.	Cells with single dendrites from the LSO medial region of guinea pig	123
Figure 55	Guinea pig mediolateral cells	124
Figure 56.	Banana-like cell from the mediolateral region of the guinea pig LSO	125
Figure 57.	Lateral banana-like cell with truncated dendrite	126
Figure 58	Gephyrin “rings” in the MSO and LSO cells.	127
Figure 59	Somatic areas of LSO cells	128

Figure 60	Length of gephyrin stained dendrites across different regions of guinea pig LSO and MSO	130
Figure 61	Somatic areas grouped into cells with and without dendritic staining for gephyrin	132
Figure 62	Resting membrane potential plotted against maximum number of action potentials evoked in guinea pig LSO neurons	142
Figure 63	Sub-threshold resonance in the guinea pig MSO	146
Figure 64	A tonotopic gradient in resonance was found in the guinea pig SOC nuclei	151
Figure 65	Gephyrin staining in the rat pLSO neurons	171
Figure 66	Medial region of rat LSO stained for GlyR alpha 1 subunit	173

Introduction

1.1 Binaural hearing and its importance

Where ears with tympana are concerned, two are more beneficial than one. Functional hearing organs have been found paired in all such animals apart from the praying mantis (*Parasphendale agrionina*) (Yager and Hoy, 1986), bestowing on their possessor the ability to compare sounds arriving at the two hearing organs in order to locate its source. It therefore makes hearing an incredibly potent sense in a vast number of ethological contexts: a predator's search for food, a prey's escape to safety or even the coupling of a mating pair. Such two-eared, or "binaural" hearing, allows not only for the localization of sound sources but also potentially the ability to hear out sounds from background noise. One such example is the human ability to detect, differentiate and recognize speech in ambient noise otherwise known as "the cocktail party effect" (Sayers and Cherry, 1957). Speech intelligibility has been shown to improve when subjects are tested binaurally as opposed to monaurally (Mackeith and Coles, 1971).

1.1.1 Horizontal vs Vertical

Although the impression of three-dimensional auditory space is seamlessly created to facilitate the tracking of targets in any direction, the ability to locate a sound with any precision involves identifying its position on different axes. Locating sources in the vertical axis does not require two ears, benefiting from spectral differences arising from the interaction of sounds with the outer ears (Blauert, 1997). Localization in the horizontal axis, on the other hand, is wholly dependent on the sensitivity to binaural cues. In fact as the binaural hearing apparatus is

typically separated by the full width of the head, the distance between the two ears and the shape of the head can be exploited as bases for the calculation of a sound's position on the horizontal axis.

1.2 Duplex Theory

Whilst the retina possesses an intrinsic map of space which extends as far as the visual cortex through retinotopic projections (Inouye, 1909; Holmes, 1918), the peripheral auditory system lacks any such map. It had long been assumed that the intensity or “level” difference (ILD) between the two ears created by the acoustic shadowing of the listener's head was an acoustic cue employed by humans to locate a sound source on the azimuthal axis (Figure 1 *b1* and *b2*). Therefore Lord Rayleigh developed the duplex theory in 1907 when he discovered that interaural discrepancies in the arrival time of a sound at either ear, or “interaural time differences” (ITDs), were utilized as a second binaural cue for sound localization (Figure 1 *a1* and *a2*) (Rayleigh, 1907).

Lord Rayleigh (1907) associated ITDs in particular with low-frequency sounds (<800Hz); later studies confirmed this and, in addition, proposed that ILDs were closely allied to high frequency sounds (>1500Hz) whilst the intervening frequency range (i.e. between 800Hz and 1500Hz) was serviced by both binaural cues (Stevens and Newman, 1936). This can be explained by the relative efficiency of each cue at conferring information about the location of stimuli in the low and high range of frequencies.

Low frequency sounds have long wavelengths ($L=V/F$ where V is the velocity of sound; F is sound frequency and L is wavelength); this allows them to diffract more easily around objects

and means that their ILD cues are much smaller than is true for high frequency sounds originating from the same location. However, thanks to their longer wavelengths, low-frequency sounds will always arrive at the two ears within the same cycle of their waveforms. Thus stimulus-locked neural responses will also be in temporal register and can be used to compare the arrival times of the auditory stimulus at either ear. Multiple cycles of high frequency sounds, on the other hand, can elapse between the two ears given their much shorter periods.

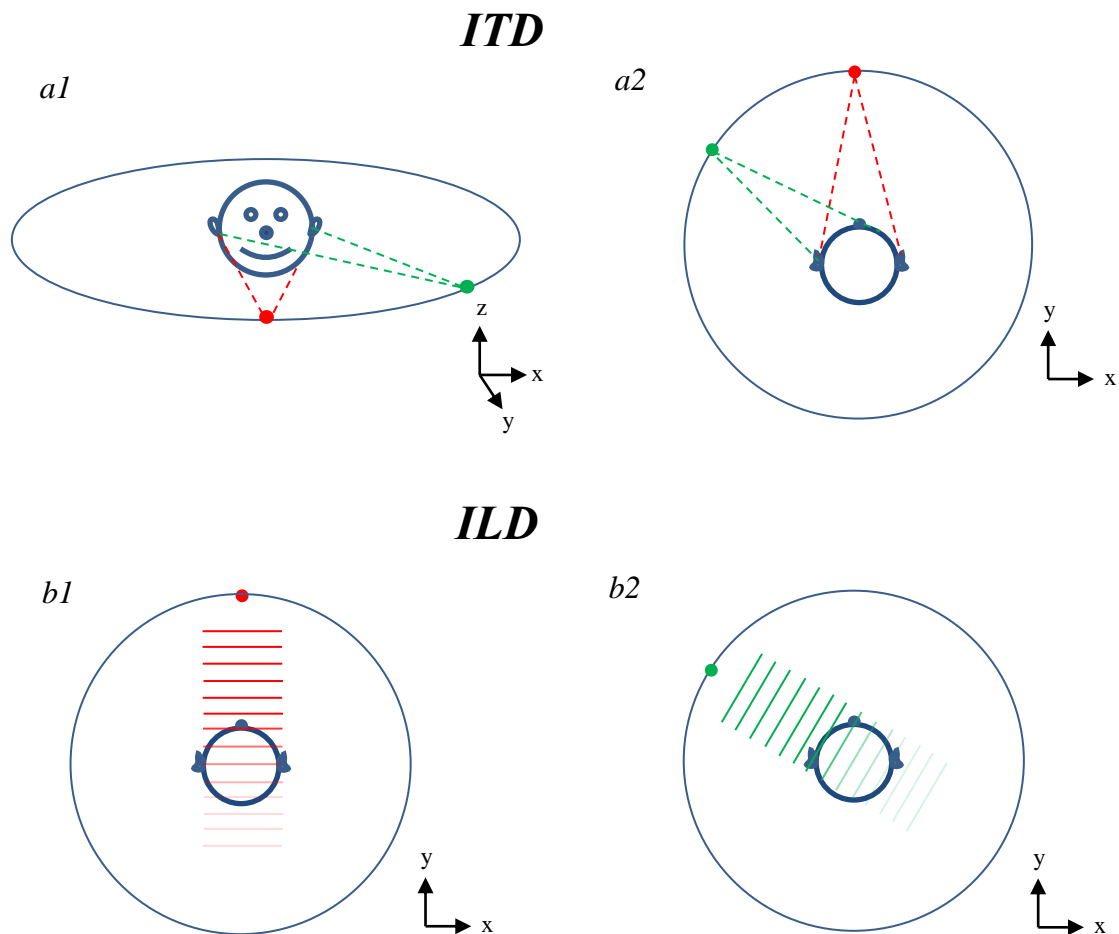


Figure 1. Schematic of ITD(*a1* and *a2*) and ILD (*b1* and *b2*) cues. A low-frequency (<800Hz) pure tone originating from directly in front of the subject on the horizontal axis (*red, a1* and *a2*) will arrive at both ears simultaneously (0 ITD). When the same stimulus comes from an angle close to 45° on the left (*green, b1* and *b2*), then it must travel around the subject's head to reach the ear on the right side. This leads to an interaural time delay in the arrival of the sound at the two ears (up to 660µs ITD). In contrast a high-frequency (>1500Hz) stimulus cannot diffract around the subject's head; therefore its intensity is reduced in the head's umbra (*b1* and *b2*). When a sound originates from in front of the subject (*red, b1*), the intensity remains the same at the two ears (0 ILD); in contrast, a sound will be louder in the left ear than the right ear when the stimulus comes from the left (up to 25dB), creating an interaural level difference (*green, b2*).

1.2.1 The Superior Olivary Complex and the Duplex theory

As receptors are not organized topographically in the auditory periphery, signals from either ear must be integrated to process ITDs and ILDs and therefore identify a sound's source. Whilst binaural interactions are observed in both the cochlea (via efferent connections (Lieberman, 1988) and the cochlear nucleus (both via efferent connections (Conlee and Kane, 1982; Brown et al, 1988; Weedman and Ryugo, 1996) and direct contact from the opposing cochlear nucleus (Mast, 1970; Adams and Warr, 1976)), the superior olivary complex (SOC) is considered to be the first location in the central nervous system (CNS) where binaural processing takes place for sound localization. Amongst the SOC nuclei in the auditory brainstem, the medial superior olive (MSO) and the lateral superior olive (LSO) are recognized as the primary binaural nuclei. Electrophysiological recordings from principal neurons in these nuclei indicate them to be predominantly sensitive to either ILDs (the LSO (Goldberg and Brown, 1969; Yin and Chan; 1990; Joris and Yin, 1995; Spitzer and Semple, 1995; Batra et al, 1997)) or ITDs (the MSO (Goldberg and Brown, 1969; Yin and Chan; 1990; Joris and Yin, 1995; Spitzer and Semple, 1995; Batra et al, 1997)). This apparent dichotomy has been regarded as potential biological correlates for the duplex theory (Joris et al, 1998; Tollin, 2003). The apparent over-representation of neurons with low-frequency characteristic frequencies, (CF - the frequency at which sound-evoked thresholds for generating action potentials are lowest) in the MSO and high frequency CFs in the LSO appears to support the claim that the two SOC nuclei exploit different binaural cues to help localize azimuthal sounds binaurally (Goldberg and Brown, 1969).

1.2.2 Exceptions to the Duplex theory

Although the duplex theory appears to hold for more complex sounds (Macpherson and Middlebrooks, 2002), psychoacoustical as well as electrophysiological studies have offered

findings which contradict the dichotomy suggested by the duplex theory. Studies in the 1950s showed that ITD sensitivity was possible for both high-frequency pure tones and sinusoidally amplitude-modulated (SAM) tones (Klump and Eady, 1956; Leakey et al, 1958). Several factors however distinguish this envelope ITD sensitivity in high frequency stimuli from ITD sensitivity in low frequency tones. Firstly envelope ITDs in SAM tones are perceived as originating from less lateral sources than ITDs in the fine frequency of similar amplitude (Blauert, 1982; Bernstein and Trahiotis, 1985). This would appear to be associated with a best frequency of amplitude modulation for envelope ITDs that is much lower than for low-frequency pure tone frequency that gives best ITD discrimination (McFadden and Pasanen, 1976; Nuetzel and Hafter, 1976; Bernstein and Trahiotis, 1994). Lastly envelope ITD sensitivity is more level dependent than ITD sensitivity (McFadden and Pasanen, 1976; Nuetzel and Hafter, 1976; Simon et al, 1994)

A more recent study by Bernstein and Trahiotis (2002) used transposed tones (a half-wave rectified low-frequency tone multiplied with a high-frequency carrier tone) to specifically provide high frequency channels with a phased-locked firing patterns similar to that in low frequency channels. This demonstrated that envelope ITD detection can in fact be as sensitive as it is for ITDs at low frequencies although the upper cut-off limit in modulation frequency still existed for this sensitivity (Bernstein and Trahiotis, 2004).

Two explanations exist for the biological origins of this decreased envelope ITD detection in SAM stimuli. The first proposes that this sensitivity to ITDs in high frequency sounds is in fact a by-product of high frequency LSO neurons being responsive to rapid ILD changes (Caird and Klinke, 1983; Joris and Yin, 1995; Tollin, 2003). The second suggests that the SAM stimulus simply does not offer an optimal input for phase-sensitive, high frequency SOC neurons to perform ITD processing (Colburn and Esquissaud, 1976). This second hypothesis is supported

by the transposed tone studies of Bernstein and Trahiotis (2002) as well as evidence that LSO neurons also display IPD sensitivity to pure tones (Tollin and Yin, 2005). This raises the question of how ITD sensitivity is organized within the SOC nuclei especially with regards to LSO neurons. Are LSO neurons sensitive to both ITD and ILD sensitivity, and do these cues interact? If LSO neurons display discrete ILD and ITD sensitivity, is envelope ITD sensitivity an acquired consequence of one or both neuronal subsets? This latter question is of especial importance as amplitude-modulated sounds are abundant in the natural world (Rosen, 1992); therefore understanding the biological limitations and capabilities of different species' envelope coding, including coding of envelope ITDs might potentially advance a more complete ethological perspective of binaural localization.

1.3 The binaural pathway

Before addressing the relative importance of LSO and MSO neurons to binaural localization, an overview of the binaural pathway including coding strategies for the acoustic properties of a stimulus are presented from the transduction of sound to the actual processing of ILDs and ITDs by neurons in the SOC nuclei (Figure 2).

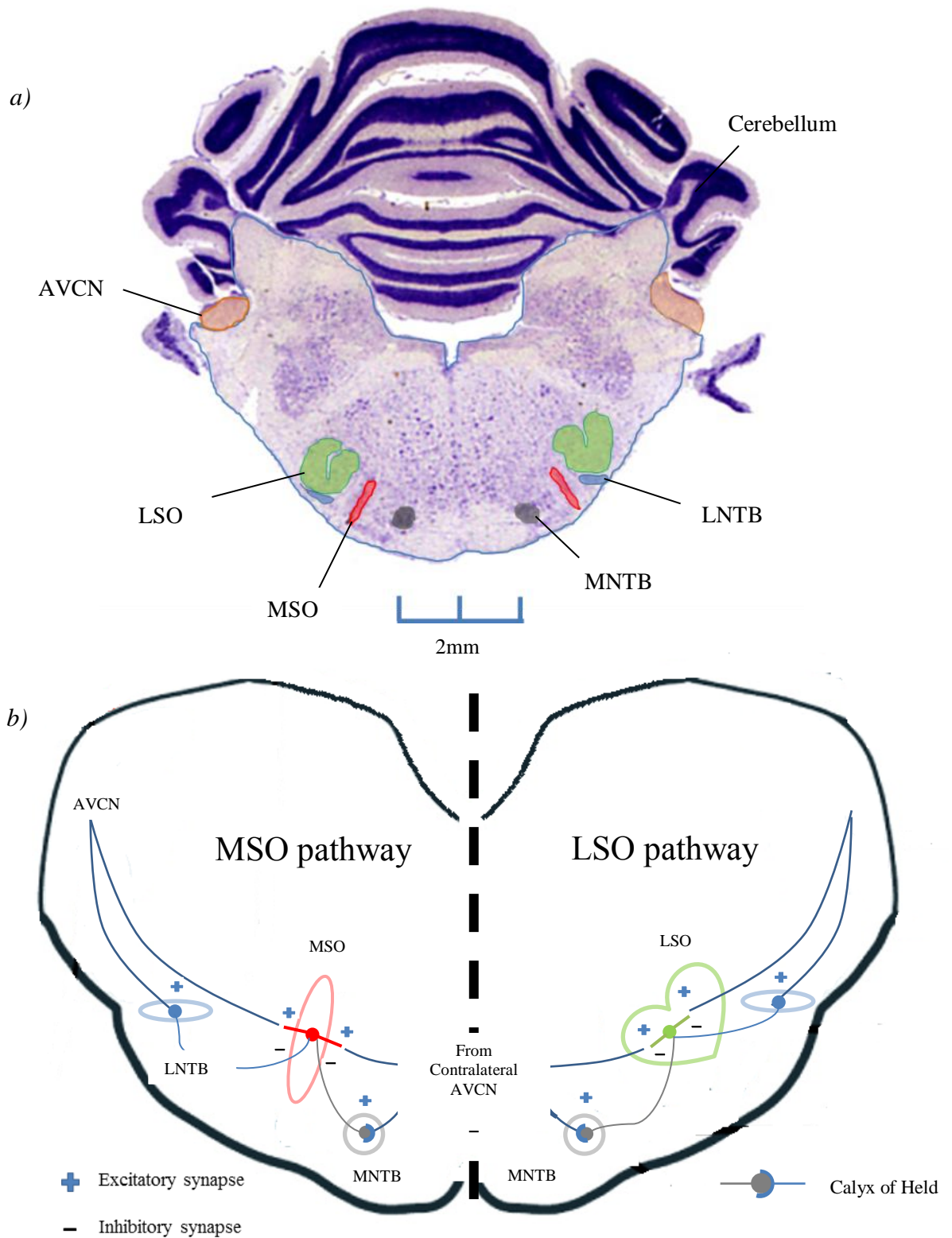


Figure 2. The binaural pathways in the auditory brainstem. A coronal slice of the auditory brainstem is shown in *a*); thionin-stained neurons in the auditory nuclei are highlighted and labeled (Madison brain collection). A schematic of the nuclei and their synaptic pathways are shown in *b*) Principal neurons of the MSO (*red neuron*) and the LSO (*green neuron*) and their respective binaural pathways are portrayed in different halves of the slice. Excitatory inputs arrive bilaterally from either AVCN whilst inhibitory inputs are conveyed by the MNTB and LNTB. Scale bar in *a*) = 2mm.

1.3.1 A map of frequencies originates in the cochlea

In the mammalian cochlea, inner hair cells (IHCs) convert sound-induced movements of the basilar membrane (BM) into electrical signals that are subsequently conveyed to the central nervous system by auditory nerve fibres (ANFs). The mechanical properties of the BM change from base to apex of the cochlea and confer it with the ability to separate frequencies spatially (Figure 3a). When a pure tone of moderate volume is presented as a stimulus, the BM vibrates with a sharp peak confined to location which is specific to that frequency. IHCs atop this BM region register the resulting movement of endolymphatic fluid with their specialized stereocilia and therefore respond preferentially to this stimulus frequency at low/middle intensities (Figure 3b). Extended across the whole cochlea, this arrangement creates a systematic map of pure-tone frequency which is maintained by the cochleotopic projections of the ANFs (Figure 3a). This map is vital in the most popular models of ITD and ILD processing as it allows frequency-match input to be compared in the SOC nuclei (Tollin, 2003).

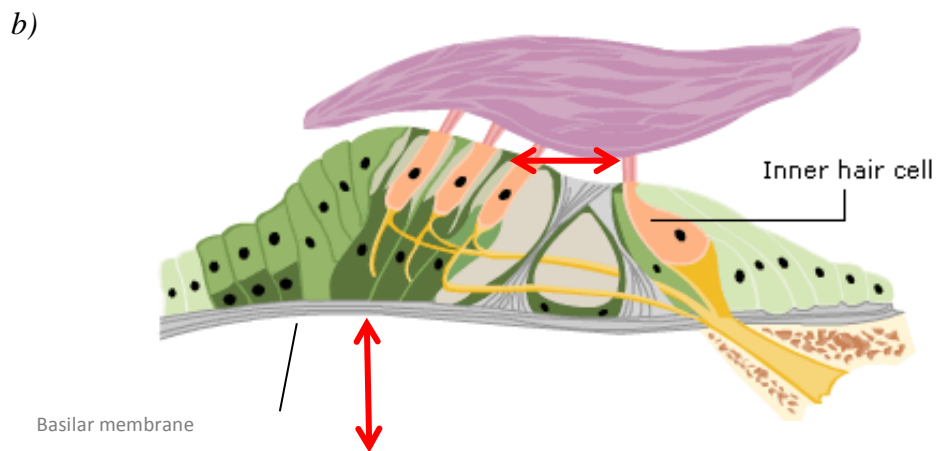
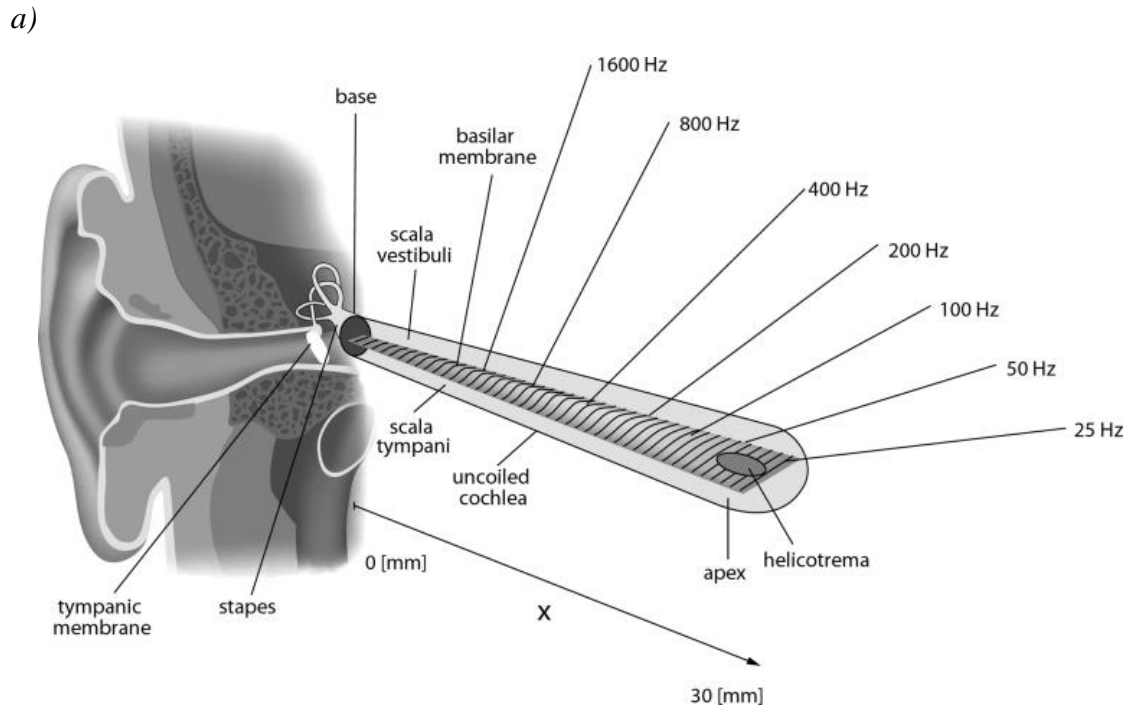


Figure 3. The tonotopy of the BM and structure of the organ of Corti. The BM is presented from base to apex in the uncoiled cochlea (a): the preferential response frequencies of the different regions decreases towards the apex (Kern et al, 2008). A cross-section of the organ of Corti in b) shows how IHCs sit upon the basilar membrane (adapted from Encyclopedia Britannica, 1997). The sound-evoked motion (*vertical red arrow* shows direction of BM movement) of the basilar membrane leads to the stereocilia of IHCs being displaced in an oscillatory manner (*horizontal red arrow* displays direction of stereocilia movement).

1.3.2 Temporal coding in the periphery and auditory nerve

The transduction of low frequency (<3.5kHz) sounds into electrical signals by IHCs intrinsically preserves the stimulus' temporal structure in the firing pattern of ANFs. From the sound-evoked vibration of the BM to the resultant oscillating current input that flows through mechanoreceptors in the stereocilia of the hair cells, responses remain phase-locked to the auditory stimulus up until very high frequencies. The transformation of this current input into a membrane potential however, is highly frequency dependent due to low pass filtering of the hair cell's membrane. Significantly this means that the membrane potential of a rat or guinea pig IHC stimulated by a pure tone of frequency <3.5Hz displays an AC component which reflects the BM's velocity (Figure 4a) (Palmer and Russell, 1986; Fettiplace and Fuchs, 1999; Paolini et al, 2001). As a result, the subsequent cycle-by-cycle release of excitatory neurotransmitter occurs within a well-defined window of the period of low-frequency sounds, triggering action potentials (APs) in ANFs that are phase-locked to the original waveform (Figure 4b). It is this firing pattern that conveys the stimulus' temporal fine structure to the rest of the auditory system. As stimulus frequency increases beyond 600Hz, the hair cell membrane increasingly filters the a.c. component of guinea pig IHC's membrane potential; this causes a linear decrease in phase-locked ANF firing (Palmer and Russell, 1986). Above 3-4 kHz, any oscillatory voltage responses disappears altogether in IHCs, leaving only a raised plateau potential which results in the cessation of phasic glutamate neurotransmitter release (Figure 4a) (Palmer and Russell, 1986).

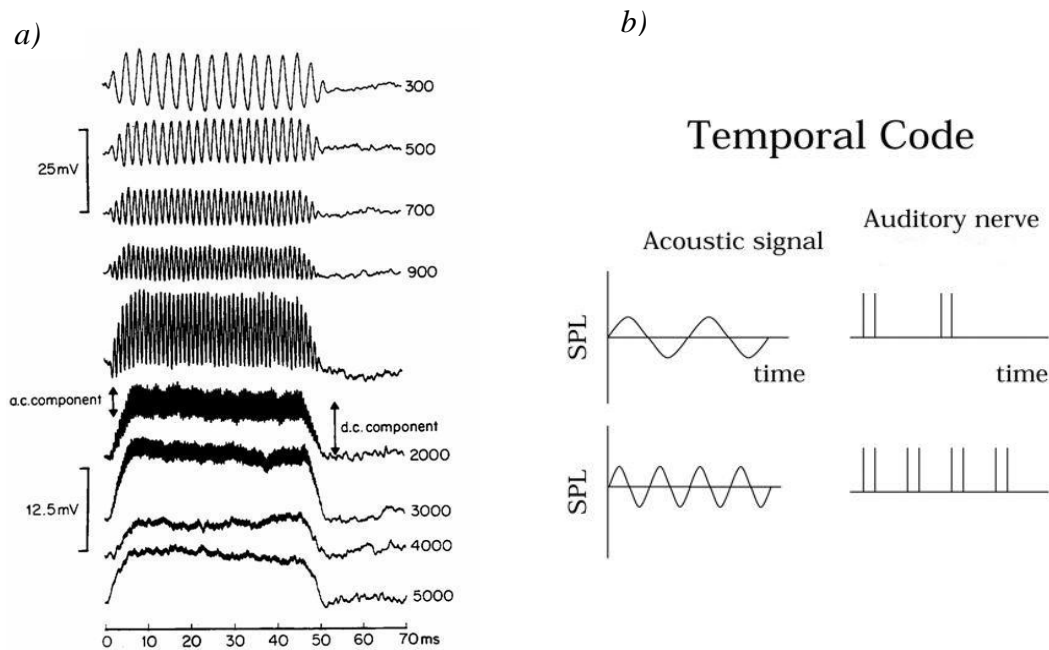


Figure 4. Temporal coding in the auditory periphery and auditory nerve. Voltage traces in *a)* are recorded from guinea pig inner hair cells which display a phase-locked AC component up until 3000Hz in response to 50ms pure tones (Palmer and Russell, 1986). This leads to the stimulus-locked release of neurotransmitter, triggering APs in ANFs which follow the waveform of the original low-frequency stimuli (*b)*).

1.3.3 Intensity coding in the auditory periphery and the ANF

The firing rates of ANFs are considered to be the primary means by which sound intensity is coded in the auditory system. This is because, regardless of the stimulus frequency, the magnitude of a hair cell's membrane potential is dependent on the displacement of the BM; louder generate larger BM vibrations, leading to greater probability of excitatory transmitter release at the IHC-ANF synapse and increased firing rates (Figure 5*a*) (Nomoto et al, 1964; Sachs and Abbas, 1974; Cody and Russell, 1987). A population of ANFs with the same CF but displaying a range of rate vs. sound intensity functions has been proposed to explain how individual fibres with a range of sensitivities typically between 35-40dB can produce an overall

dynamic range spanning more than 100dB (Figure 5c) (Winter and Palmer, 1991). Another factor which improves individual fibres' dynamic range is the frequency-dependent nonlinear compression of responsiveness in transduction (Ruggero et al, 1997; Martin and Hudspeth, 2001). Increasing the intensity of a sound from an initial value close to the threshold produces greater BM vibrations than stimuli that start from medium or high intensities, this non-linear compression therefore can prevent ANF responses from saturating in response to high intensity sounds. However sounds at the higher end of the intensity scale can exploit the increased spread of excitation along the BM they cause as ANFs with CF proximal to the actual stimulus frequency are recruited (Figure 5b).

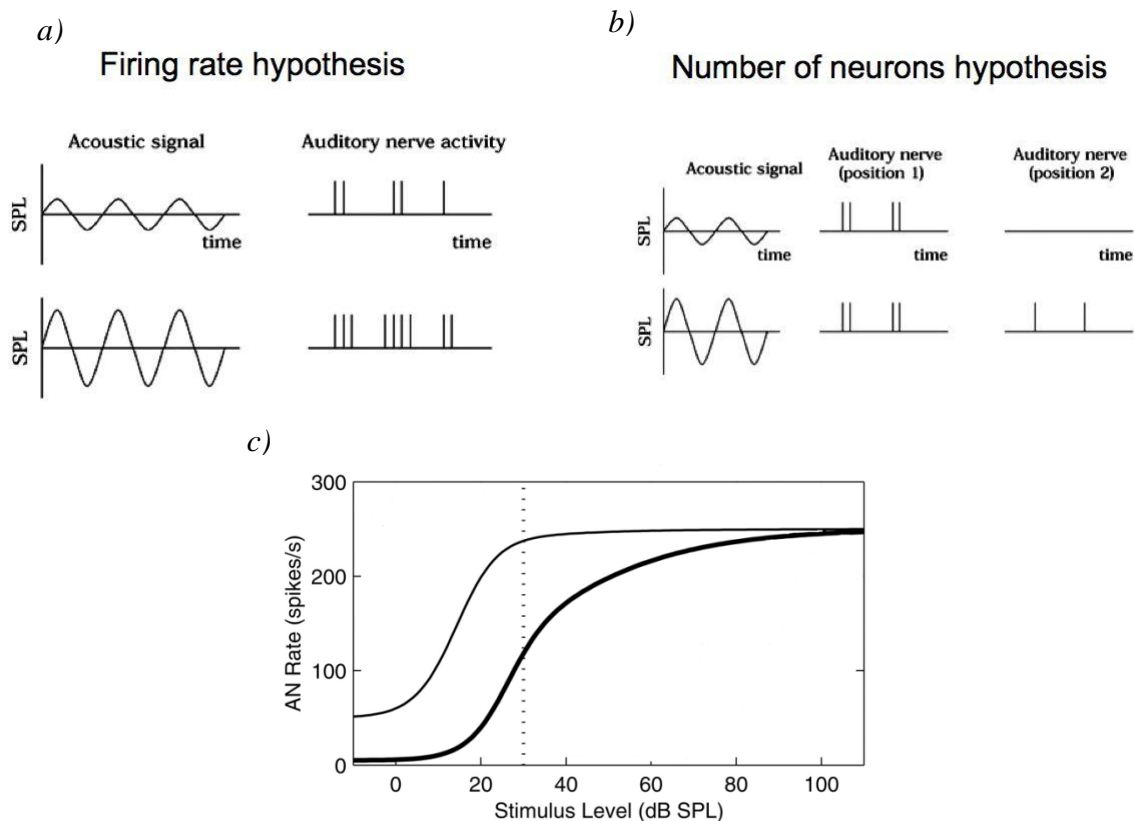


Figure 5. Intensity coding in the auditory periphery and auditory nerve. As the amplitude of an auditory stimulus' waveform increases, the concomitant increase in firing rate that follows in individual ANFs can form the basis of an intensity code (a). When spike rates are plotted against the stimulus level for two ANFs with different thresholds and spontaneous rates (c), the range of stimulus levels that are coded is found to increase (dotted line displays where response saturates in ANF with lower threshold). Another way to code intensity involves the spread of excitation across the BM with higher intensity signals; this leads to ANFs firing which are associated with IHCs stimulated at locations further along the BM (b).

1.3.4 Coding for temporal envelope of sounds in the auditory periphery and ANF

As mentioned above, low-frequency temporal information can be introduced to a region of the cochlea that predominantly transduces high frequency sounds by including them in the carrier stimulus as amplitude modulations. ANFs with high CFs follow changes in intensity generated by the stimulus envelope with phase-locked firing patterns. However since IHCs respond to a restricted range of stimulus frequencies- a function of their location along the BM, their associated ANFs display narrow bandwidths and present a bottleneck to the range of modulation frequencies that can be transmitted. Even as the bandwidth of IHCs increases towards the basal, high frequency region of the BM, the cut-off frequency for modulation tuning remains lower than is observed for ITD tuning of pure tones (Joris and Yin, 1992). Nevertheless envelope coding in ANFs does cover a sufficiently large range of modulation frequencies to explain psychoacoustic sensitivity (Joris et al, 2004; Dreyer and Delgutte, 2006).

1.3.5 Anterior Ventral Cochlear nucleus can improve stimulus-locked neural discharge

ANFs project from the cochlea via the 8th cranial nerve to innervate the first auditory centre in the CNS, the cochlear nucleus (CN). Upon reaching the CN, ANFs bifurcate to innervate the three CN subnuclei: the dorsal cochlear nucleus (DCN); posteroventral cochlear nucleus (PVCN) and the anteroventral cochlear nucleus (AVCN). Signals are transformed in these subnuclei for a variety purposes and upstream targets; however the temporal processing associated with binaural localization is predominantly associated with the spherical and globular bushy cells (SBCs and GBCs respectively) of the AVCN. Whilst SBCs provide excitatory inputs to the MSO and LSO, inhibition and is relayed to the SOC nuclei via principal neurons of the medial nucleus of the trapezoid body (pMNTB neurons) which are excited by GBCs (Figure 2) (Cant and Benson, 2003). However SBCs and GBCs do more than just relay an excitatory

signal from ANFs to auditory brainstem nuclei; their firing pattern in response to pure tones of frequency <1000Hz actually displays improved phase-locking over ANFs of similar CF (Joris et al, 1994). Although *in vivo* and *in vitro* studies appear to disagree on the exact biophysical mechanism for this transformation, it would appear that multiple inputs must converge onto bushy cells within a narrow time window (due to their short time constants) in order to generate a very precisely timed AP (Rothman et al, 1993). Aside from reducing temporal jitter, integrating information from across several isofrequency ANFs between 600Hz and 3500Hz produces a more complete representation of the stimulus' temporal waveform. This could be paramount for a range of pure tone frequencies at which phase-locked responses may still exist but neural discharges in individual ANFs cannot follow the stimulus on a cycle-by-cycle basis. When firing patterns in bushy cells are compared against those of ANFs for amplitude-modulated stimuli in the cat and the rat, enhanced phase-locking is also observed alongside higher cut-off frequencies for modulation tuning (Joris et al, 1998; Paolini et al, 2001; Frisina, 2001).

1.3.6 MNTB relays information to the MSO and LSO

Although the MNTB forms part of the SOC, it is not discussed here beyond its ability to relay a signal from GBCs to MSO and LSO neurons as an inhibitory input. The synapse between GBCs and principle neurons of the MNTB is referred to as the Calyx of Held (Held, 1893; Morest, 1968). It is the largest synapse in the adult mammalian auditory CNS, consisting of a cup-shaped, dendrite whose fenestrations encapsulate a neurons' large, spherical soma (Satzler and Sohl, 2002; von Gersdorff and Borst, 2002). In conjunction with large, glutamatergic synaptic currents, the extent of contact between pre- and post-synaptic terminals at the calyx of Held ensures that synaptic transmission is very secure and that firing patterns of GBCs are reproduced faithfully in MNTB principal neurons. Specialized K⁺ conductances help to reduce neuronal

membrane time constant and therefore allow the rapid integration of synaptic currents; these conductances can also help maintain firing rates over a large range of frequencies so that pMNTB neurons can follow their GBC inputs (Kaczmarek et al, 2005; Song et al, 2005; Hardman and Forsythe, 2009).

1.4 Anatomy of MSO principal neurons

Arranged in a “ladder-like” structure along the dorsal-ventral axis of the nucleus, MSO principal (pMSO) neurons are organized tonotopically in the MSO: neurons with their lowest CFs are found in the dorsal limb and those with the highest CFs in the ventral limb. Sharing a single morphology, all pMSO neurons are bipolar with dendrites emerging 180° to each other from large, fusiform somata (~20µm) (Figure 6a). Whilst the medial and lateral dendrites receive excitatory inputs (glutamatergic) from contralateral and ipsilateral SBCs respectively, inhibitory inputs (mainly glycinergic in adults) from the MNTB are largely restricted to the somata and proximal dendrites of adult gerbil pMSO neurons (Figure 2) (Grothe, 1994; Smith et al, 2000; Kapfer et al, 2002; Cant and Benson, 2003). Ipsilateral inhibition from the lateral nucleus of the trapezoid body (LNTB) has also been observed however its properties have been studied less extensively across species (Figure 2) (Cant and Hyson, 1992; Grothe and Sanes, 1993).

1.4.1 The sublocalization of postsynaptic glycine receptors.

In the gerbil MSO, postsynaptic glycine receptors (GlyRs) are redistributed over the course of development (Kapfer et al, 2002): a diffuse somato-dendritic arrangement of GlyRs in juveniles is replaced by one mainly restricted to the perisomatic region of adult pMSO neurons (i.e. the soma and the first 50µm of proximal dendrite). It appears that a species hearing range is

correlated to the sublocalization of GlyRs on particular compartments of pMSO neurons as a similar perisomatic configuration has been noted in the adult cat and chinchilla, both of whom are proficient at hearing low-frequencies whereas high-frequency hearing species such as the rat, opossum and bat retain a somato-dendritic pattern of GlyR distribution into maturity (Fay, 1998; Kapfer et al, 2002). It has been speculated that the lack of somatic compartmentalization in those species insensitive to frequencies of a several hundred Hertz may reflect their poor fine structure ITD processing abilities (Kapfer et al, 2002). The idea that GlyR sublocalization in the MSO is determined by the experience of fine structure ITD cues is supported by evidence from gerbils, reared in white noise and therefore an environment poor in correlated ITD cues (Kapfer et al, 2002); the developmental transition observed in control subjects is interrupted so that a somato-dendritic distribution of GlyR receptors on pMSO neurons is preserved in these noise-reared animals. Little is known however about how sublocalization of inhibitory synapses on principal neurons varies in either limb of the LSO and how this may be related to their ILD or ITD sensitivity.

1.4.2 Physiology of MSO principal neurons

The intrinsic properties of pMSO neurons appear to be homogenous in the Mongolian gerbil. They are characterized by their single-figure low input resistances (between 8.2 ± 0.6 and 12.3 ± 0.4 M Ω on average in the gerbil), sub-millisecond membrane time constants and highly phasic firing patterns (Smith et al, 1995; Svirskis et al, 2002; Scott et al, 2005 and 2007; Chirila et al, 2007; Mathews et al, 2010; Khurana et al, 2011). Most of these properties can be attributed to the array of voltage-gated membrane channels open at rest, chief amongst these being the low threshold voltage-gated K⁺ current, I_{KLT}.

Thanks to I_{KLT} 's low-voltage threshold of activation, depolarization from resting membrane potentials can induce large outward currents (Scott et al, 2005; Mathews et al, 2010). These decrease the overall excitability of pMSO neurons and mean that depolarizing inputs must have fast rise times for membrane voltages to bypass I_{KLT} activation and reach threshold for AP generation (Svirskis et al, 2004; Jercog et al, 2010; Mathews et al, 2010). In conjunction with a rapidly inactivating Na^+ conductance, I_{KLT} limits the number of APs generated in response to superthreshold current injections, producing a single onset AP that constitutes its highly phasic firing pattern (Figure 6b) (Svirskis et al, 2004; Scott et al, 2005 and 2007).

I_{KLT} 's rapid kinetics mean that brief stimuli such as excitatory postsynaptic potentials (EPSPs) can activate the conductance (Rothman et al, 2003; Mathews et al, 2010); the transient decrease that follows in a pMSO neuron's membrane time constant (beyond already low resting values) accelerates the EPSP's time course, causing the time window for summation of excitatory inputs from either ear to narrow (Mathews et al, 2010). By carefully controlling the relative proportion of the conductance in different compartments of the pMSO neurons, I_{KLT} even appears to play a role in ensuring that EPSPs of different amplitude have a similar time course thus preventing any accompanying ILD cues from biasing ITD processing (Mathews et al, 2010).

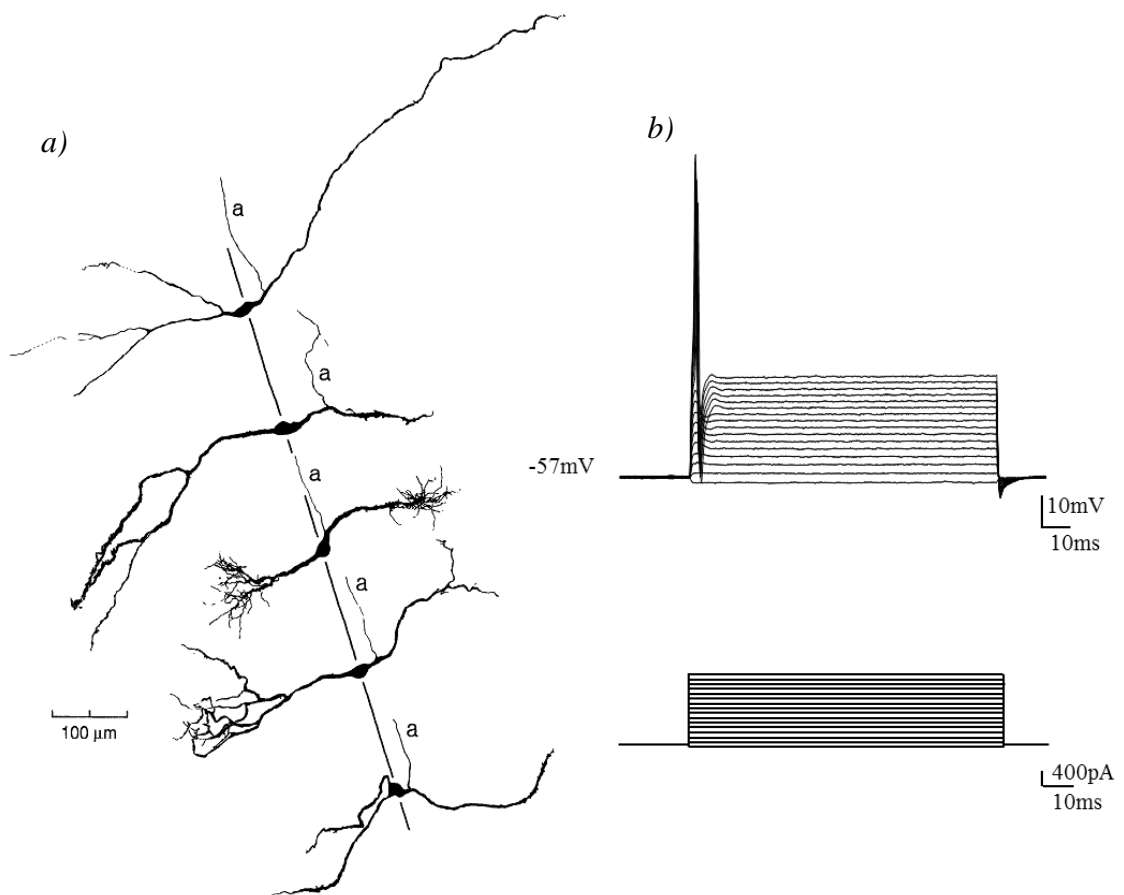


Figure 6. Morphology and firing pattern of guinea pig pMSO neurons . Neurobiotin-filled pMSO neurons display their bipolar morphology with axons (marked by letter a) that generally emanate from the cell somata (a) (Smith, 1995). Their parallel arrangement of pMSO neurons along the rostralcaudal axis is similar to the orientation of the cartoon neuron in Figure 2b. Voltage traces (b, above) in response to depolarizing current steps (b, below) are displayed for a guinea pig pMSO neuron in b). Due to the low input resistance (<10MΩ), larger current steps are necessary for suprathreshold responses. Only a single onset AP with short latency can be evoked by a current step regardless of its amplitude.

1.4.3 Coding for ITDs in MSO principal neurons

Although extracellular recordings are difficult from single pMSO neurons *in vivo* due to their small amplitude of their APs and large neurophonic potentials, a number of studies have demonstrated in the MSO of several species that firing rates are indeed modulated by ITDs and

the envelope ITDs of SAM tones (cat: Yin and Chan, 1990; Joris, 1996, rabbit: Batra et al, 1997 and bat: Grothe and Park, 1998). This supports the idea that pMSO neurons perform coincidence detection of phase-locked excitatory inputs from each ear. A maximal response is not typically obtained however when a stimulus reaches the two ears simultaneously i.e. 0ms ITD but instead when the signal from the contralateral ear leads (see Figure 8 *b*). This was assumed for a long period to be evidence for a particular representation of ITDs that was proposed by Jeffress in 1948. He suggested that, at each frequency channel, an array of coincidence detectors exists in which each neuron represents a particular ITD within the physiological range (Figure 7 *a*) (i.e. range of ITDs that can be created by head) by its maximum firing rate (see Figure 7). Since coincidence of phase-matched inputs from either ear would be required for maximum firing, a range of ITDs could be simply represented by different axonal path lengths bilaterally (Figure 7*b*). This would create internal delays that compensate for the differences in a sound's arrival times at either ear.

Although the separation of ipsilateral and contralateral inputs on bipolar dendrite as well as the “ladder-like” arrangement of pMSO neurons suggests that they are specialised to perform coincidence detection (Agmon-Snir et al, 1998; Beckius et al, 1999; Zhou et al, 2005), no strong anatomical evidence for delay lines has yet been found in mammals (Smith et al, 1993; Beckius et al, 2000). Furthermore when the maximum firing rates of guinea pig IC neurons (which receive their input from pMSO neurons) with different CFs is grouped, it is found that their values are distributed around 45° IPD (Yin and Kuwada, 1983; Spitzer and Semple, 1998; McAlpine et al, 2001; Shackleton et al 2003; Hancock and Delgutte, 2004; Joris and Yin, 2007). Since peak IPD is correlated to corresponding peak ITD by frequency, guinea pig IC neurons of low CF show peak firing rates for ITDs beyond the physiological range of ITDs for a species of such small head size (Palmer et al, 1990). This finding has also been replicated in other species including the gerbil MSO (Brand et al, 2002; Seidl and Grothe, 2005; Pecka et al, 2008) and cat

IC (Hancock and Delgutte, 2004), suggesting that the peak firing rates of these neurons might convey little information about the ITD of a stimulus in these species. McAlpine et al (2001) has proposed that the slope of the ITD-tuning function (whose maximum lies close to $0\mu\text{s}$) instead forms the basis of ITD coding in the mammalian brainstem (Figure 8c) (Shackleton et al, 2003). Rather than an array of coincidence detectors conferring ITD information, two broadly tuned channels (one for each hemisphere of space) now provide the most efficient ITD-coding strategy (McAlpine et al, 2001; Harper and McAlpine, 2004).

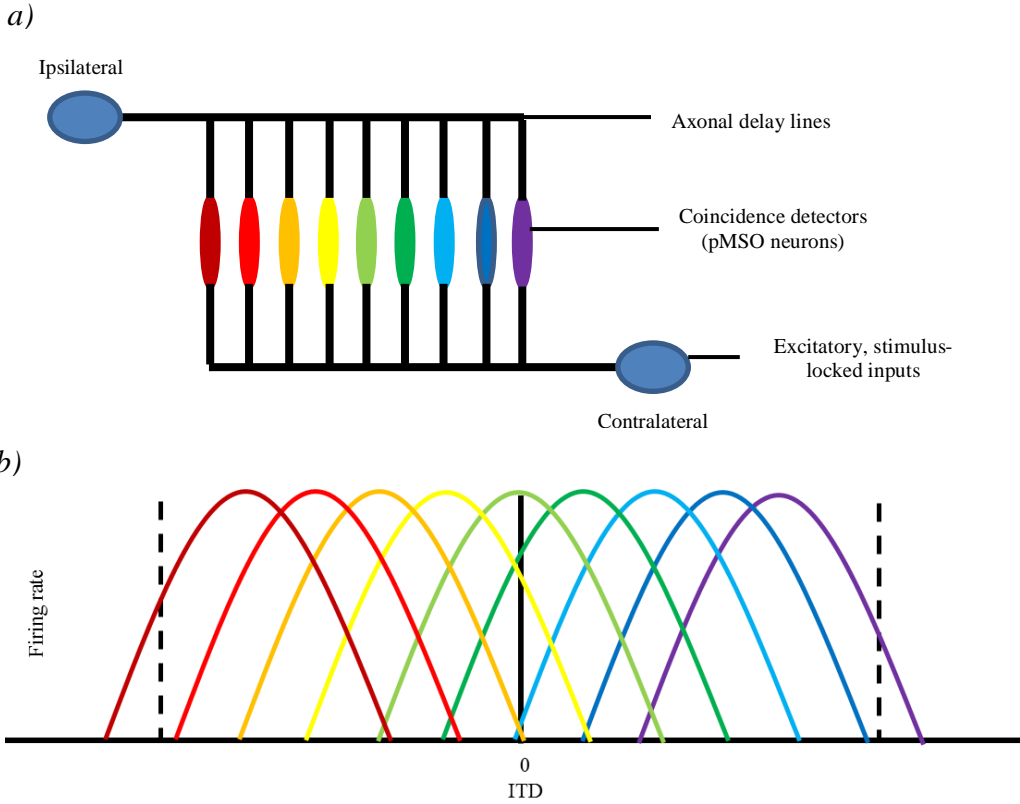


Figure 7. The Jeffress model of ITD coding. As described in the Jeffress (1948) model, ITD coding can be performed by an array of isofrequency neurons which receive stimulus-locked, excitatory inputs from either ear (a). Axonal path lengths vary across the array and therefore compensate for the full physiological range of ITDs (a). The firing rates of the coincidence-detecting neurons are subsequently tuned to different ITDs (b). Dotted lines represent the physiological range of ITDs.

1.4.4 Role of inhibition in ITD coding

Batra et al (1997) suggested that a well-timed inhibitory input from the MNTB could potentially shift the ITD-tuning function of rabbit pSOC neurons so that its peak laid at intermediate IPDs (Figure 8a). Brand et al (2002) blocked glycinergic transmission using iontophoresis of strychnine onto the gerbil MSO and found that the peak firing rate of principal neurons moved towards a distribution around zero ITD/IPD (Figure 8b), suggesting that MSO neurons are pure coincidence detectors whose ITD-tuning function is indeed modulated by timed inhibition.

Several models for this mechanism have been proposed. Brand et al (2002) used a fast inhibition which preceded excitatory input from the same side to produce a contralaterally-leading peak in the ITD-tuning function. However the time constant of inhibition used in this model has proven unrealistically fast when tested *in vitro* (Batra et al (2002) model = 0.1ms; Magnusson et al (2004) electrophysiological study = ~1ms). Zhou et al (2005) suggested a separate model which did not require inhibition to have temporal precision or fast kinetics; it attributed the shift in the peak of the ITD-tuning function to the sublocalization of the axon's initiation site on one of the two dendrites. Although this is compatible with the observed inhibition, the asymmetric morphology has not proved consistent across gerbil pMSO neurons (Scott et al, 2005). A more recent model by Jercog et al (2010) has postulated that the shift in ITD-tuning function is actually associated with the asymmetrical rise slopes of EPSPs arriving from each ear. The temporal ordering of bilateral inputs is vital as summation of EPSPs is nonlinear due to the activation of I_{KLT} by slower rising voltage deflections. The role of inhibition in this model is to determine the relative difference in EPSP rise slope bilaterally (Jercog et al, 2010). A more direct interaction between inhibitory inputs and I_{KLT} has also been advocated in a separate model. Svirskis et al (2004) found that depolarizing inputs were more likely to elicit an AP if they were preceded by a period of hyperpolarization. This was explained by the need to

deactivate I_{KLT} , open at rest, before slower depolarizing inputs could reach threshold for AP generation (Svirskis et al, 2004). If contralateral inhibition can produce a sufficient reduction in membrane potential and if it precedes a delayed contralateral excitation then this could help to bias all coincidence detection towards contralateral leading stimuli.

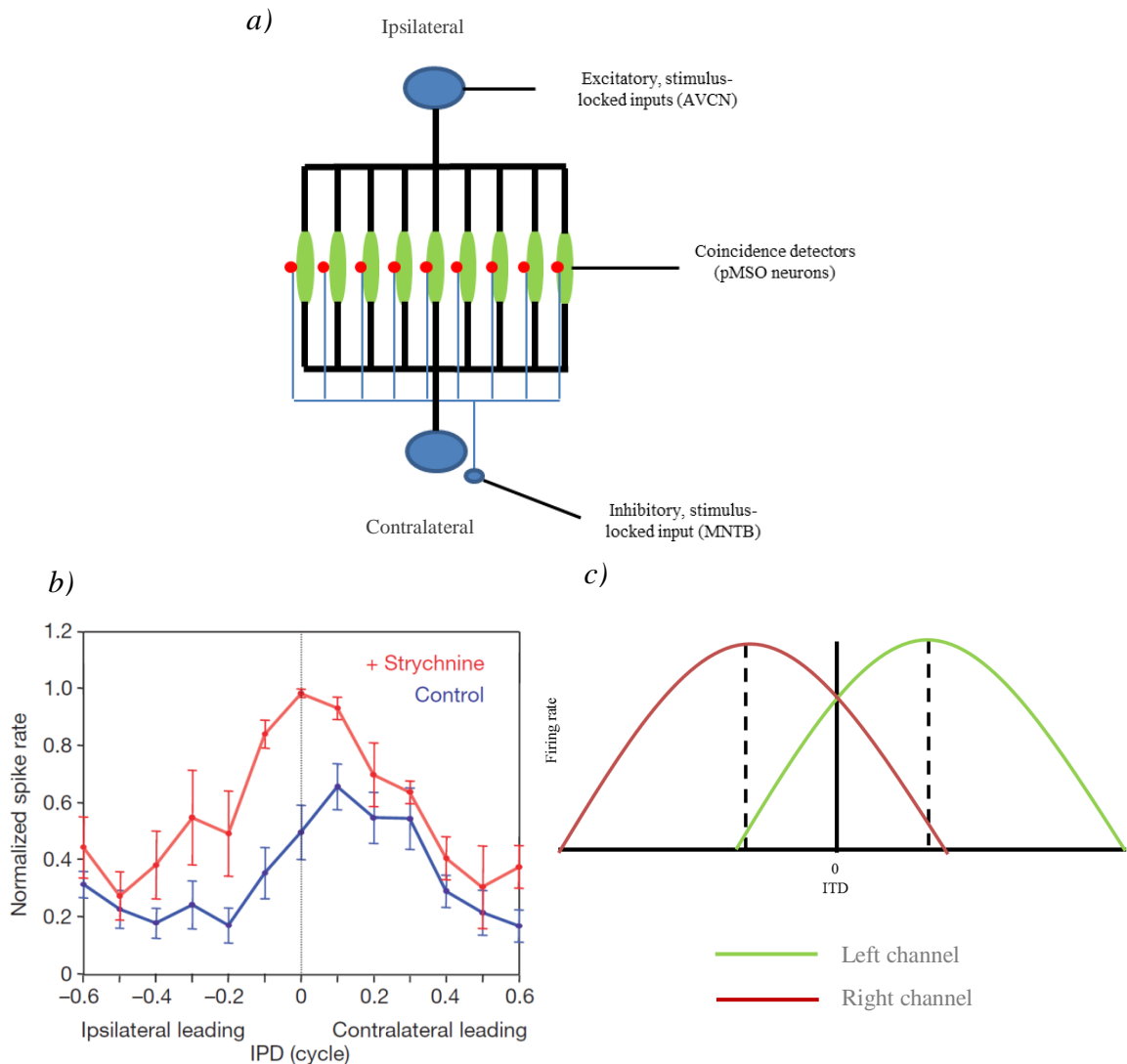


Figure 8. Contralateral inhibition and two-channel model for ITD-coding. In *a*), coincidence-detecting neurons of different CFs receive inhibition as well as excitation from the contralateral. Iontophoresis of strychnine, the GlyR blocker, has demonstrated that such well-timed inhibition can modulate the ITD tuning functions of gerbil pMSO neurons, shifting the peak firing rate towards more positive IPDs (*b*) (Brand et al, 2002). Thus, instead of an array of coincidence detectors representing the full azimuthal space (as proposed by the Jeffress (1948) model (Fig. 7*b*)), the slope of individual neurons' ITD-tuning functions can convey information about the complete physiological range of ITDs (*c*). This also entails a different ITD encoding strategy from the Jeffress model as the relative activation of two broadly-tuned binaural channels (i.e. from either MSO) replaces “a map of ITD-tuned neurons” as a means to localize sounds on the azimuthal plane (*c*).

1.5 Anatomy of LSO principal neurons

Like their counterparts in the MSO, principal neurons of the LSO (pLSO neurons) are tonotopically organized, with low CF neurons found in the lateral region of the nucleus and high CF pLSO neurons located more medially (Boudreau and Tschutani, 1968; Guinan et al, 1972; Adam et al, 1999). Unlike pMSO neurons however, pLSO neurons appear to span more than one morphological class in the rat, guinea pig, cat and gerbil (Barnes-Davies et al, 2004; Helfert and Schwartz, 1986; 1987; Schofield and Cant, 1991). Of the seven morphological subtypes previously observed in rat LSO (Rietzel and Friauf, 1998), principal neurons have been identified as belonging to the unipolar and bipolar classes (Figure 9a and c) (Barnes-Davies et al, 2004). Bipolar cells possess large fusiform somata (15-33 μ m in diameter) from which between two and six dendrites project (Figure 9a) (Rietzel and Friauf, 1998). In contrast, unipolar neurons have “drop-shaped” somata (16-20 μ m in diameter) with between one and two thick dendrites emerging from the tapered end (Figure 9b). In the guinea pig LSO, two potential candidates for principal neurons have been identified (Schofield and Cant, 1991): the first has a fusiform somata (20-25 μ m in diameter) and is a disk-shaped, multipolar cell with which appears bipolar when viewed coronally and the second is also multipolar and of a similar size but appears more rounded in coronal slices due to its orientation (Schofield and Cant, 1991).

As the most prominent cell type in their respective LSOs, both the bipolar fusiform neurons in the rat (Figure 9b) and fusiform neurons in the guinea pig appear to be the main principal neuronal types. They are arranged similarly in the LSO with the longest axes of their somata perpendicular to the main axis of the nucleus (see Figure 6). The classical arrangement of synaptic inputs to the LSO has been considered a contralateral inhibitory input from the

ipsilateral MNTB and an excitatory input from the ipsilateral AVCN (Yin, 2001). However many studies have noted the potential existence of a contralateral excitation to pLSO neurons (Figure 2) (Finlayson and Caspary, 1991; Sanes and Siverls, 1991; Wu and Kelly, 1991 and 1992; Tollin and Yin, 2005). There has even been speculation that an ipsilateral inhibitory input from the LNTB also contacts pLSO neurons (Figure 2) (Wu and Kelly, 1994). Whilst excitation is presumed to be impinging upon the dendrites, it has been claimed that inhibitory synapses are located close to the soma (Figure 2) (Cant, 1984; Helfert et al, 1992; Smith et al, 1998).

1.5.1 Physiology of LSO principal neurons

Analysis of whole cell recordings in the gerbil indicates that the average input resistance and membrane time constant of pLSO neurons are larger/slower than in gerbil pMSO neurons (average input resistance = $109 \pm 64.4 \text{ M}\Omega$; average membrane time constant = $8.5 \pm 4.5 \text{ ms}$ (Adam et al, 2001)). The large variance in input resistance across the population of gerbil pLSO neurons appears may be explained by the existence of two subtypes of principal neurons as has been demonstrated in the rat LSO (Barnes-Davies et al, 2004). Depending on how many APs are generated during suprathreshold current steps, rat pLSO neurons can be separated into single-firing neurons that respond with a single onset AP (Figure 9c) (average input resistance = $70.0 \pm 6.7 \text{ M}\Omega$) and multi-firing neurons that respond with a train of APs (Figure 9d) (average input resistance = $174.2 \pm 29.1 \text{ M}\Omega$) (Barnes-Davies et al, 2004). With little difference in membrane capacitance between the two subtypes (single-firing = $23.1 \pm 1.8 \text{ pF}$ vs. multi-firing = $21.7 \pm 1.8 \text{ pF}$), the larger average input resistance in multi-firing neurons has been attributed to a decreased I_{KLT} expression in this pLSO neuronal subtype (Barnes-Davies et al, 2004). Indeed application of Dendrotoxin-I to block selectively Kv1.1 channels associated with I_{KLT} causes single-firing neurons not only to fire like multi-firing pLSO neurons but also to have similarly high input resistances (Barnes-Davies et al, 2004). It has also been proposed in the same study

that single-firing pLSO neurons were more prominent in the lateral region of adult rat LSO (Barnes-Davies et al, 2004). This tonotopic organization of single- and multi-firing pLSO neurons also appears to be correlated with the total expression of I_{KLT} in each sub-region of the nucleus (medial < central < lateral) (Barnes-Davies et al, 2004). Although the role of I_{KLT} has been emphasized, in particular its influence over the excitability of pLSO neurons, a host of other voltage-gates conductances has been observed including the hyperpolarization-activated mixed cationic conductance, I_h (Leao et al, 2006; Barnes-Davies et al, 2004; Adam et al, 2001). Its strong dendritic expression may prevent temporal summation of EPSPs originating from the ipsilateral ear and can therefore help to detect synchronous excitatory input (Leao et al, 2011).

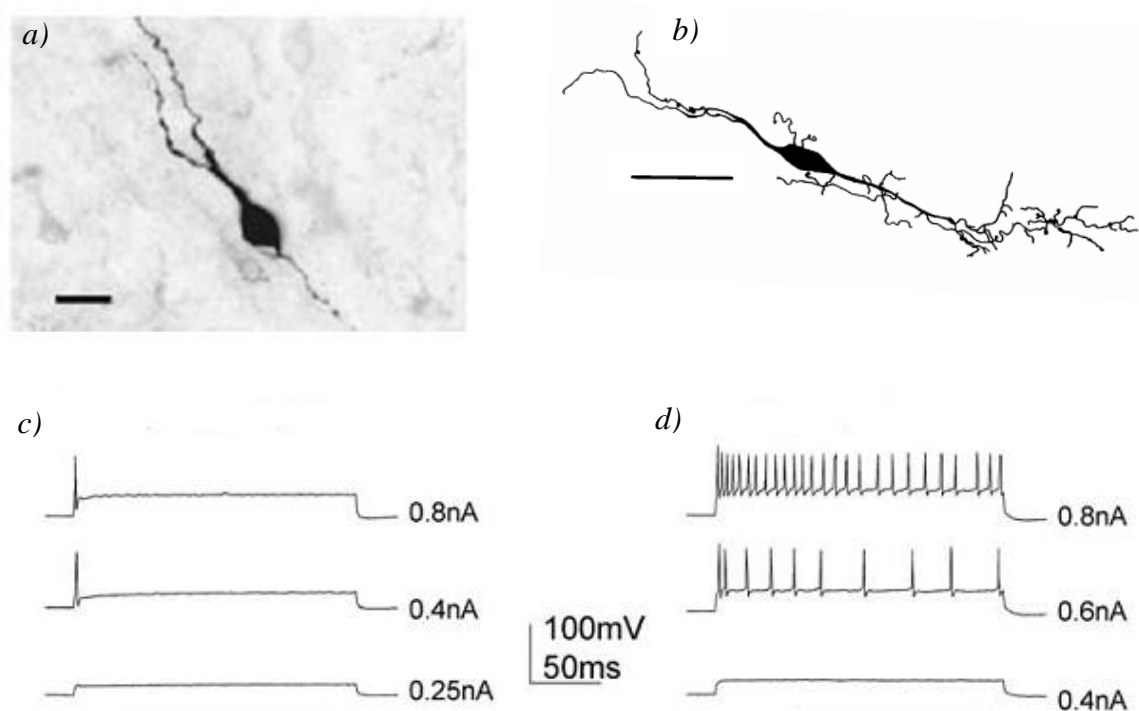


Figure 9. Morphology and firing pattern of rat pLSO neurons. Lucifer yellow-filled rat pLSO neurons display two distinct morphologies (Barnes-Davies et al, 2004): a unipolar neuronal type (*a*, taken from Barnes-Davies et al, 2004) and bipolar neuronal type (*b*, taken from Rietzel and Friauf, 1998). They can also be divided on the basis of their firing patterns when injected with superthreshold current steps (*c* and *d*) (Barnes-Davies et al, 2004). Those pLSO neurons which fired a single, onset AP are classified as single firing (*c*) whereas those that responded with a train of APs are called multi-firing (*d*) neurons. No correlation was found between electrophysiological properties and morphological subtype of pLSO neurons in the rat (Barnes-Davies et al, 2004). Scale bars in *a*) and *b*) were 20 μ m and 50 μ m respectively.

1.5.2 Binaural sensitivity of LSO principal neurons

By raising contralateral sound levels whilst keeping the ipsilateral stimulus constant, it has been demonstrated that the firing rate of pLSO neurons is modulated as a function of ILD (Galambos et al, 1959; Boudreau and Tsuchitani, 1969; Caird and Klinke, 1983; Sanes and Rubel, 1988; Joris and Yin, 1995; Park et al, 1997). It is believed that these responses are predominantly a result of EI (Excitation from ipsilateral ear; Inhibition from the contralateral ear) pLSO neurons. Thus, the integration of synaptic inputs at most pLSO neurons represents the subtraction of stimulus level at the contralateral ear from the stimulus level at the ipsilateral ear. The characteristic chopping pattern of pLSO neurons has been associated with active properties of pLSO neurons associated with their tonic firing properties (Zacksenhouse et al, 1995; Adam et al, 1999; Adam et al, 2001). This begets a scalar code where firing rates are dependent on the magnitude of the ILD (Tollin and Yin, 2002a; Tollin and Yin 2002b)

Low CF pLSO neurons have also been shown to be ITD sensitive (Caird and Klinke, 1983; Finlayson and Caspary, 1991; Batra et al, 1997; Tollin and Yin, 2007); apparently via a process similar to coincidence detection in pMSO neurons. In contrast with ITD discrimination in the MSO, peaks in pLSO neurons' neural discharge are generally observed where synaptic input from either ear arrives at somata out of phase and contralateral inhibition does not negate the ipsilateral excitation. However this is not true for all pLSO neurons as peak firing rates often occur at IPDs less than 90° IPD; it has been proposed that the ITD-tuning functions of these pLSO neurons is shaped by well-timed contralateral excitation (Tollin and Yin, 2005).

The sensitivity of pLSO neurons to ITDs in the envelope of high frequency tones has also been demonstrated and arises from the rapid comparison of changing sound levels at either ear (Joris

and Yin, 1998; Tollin, 2003). The subtractive process associated with ILD computations has therefore been implicated in envelope ITD calculations as well (Figure 10) (Joris and Yin, 1998). It has been noted however that the upper frequency limit for modulation tuning is reduced in the LSO ($\leq 800\text{Hz}$): the upper limit in pLSO neurons being an octave lower than is observed in their monaural inputs (Joris and Yin, 1998). This reduction in upper frequency of modulation tuning may help minimize errors in binaural processing (Joris et al, 2004)

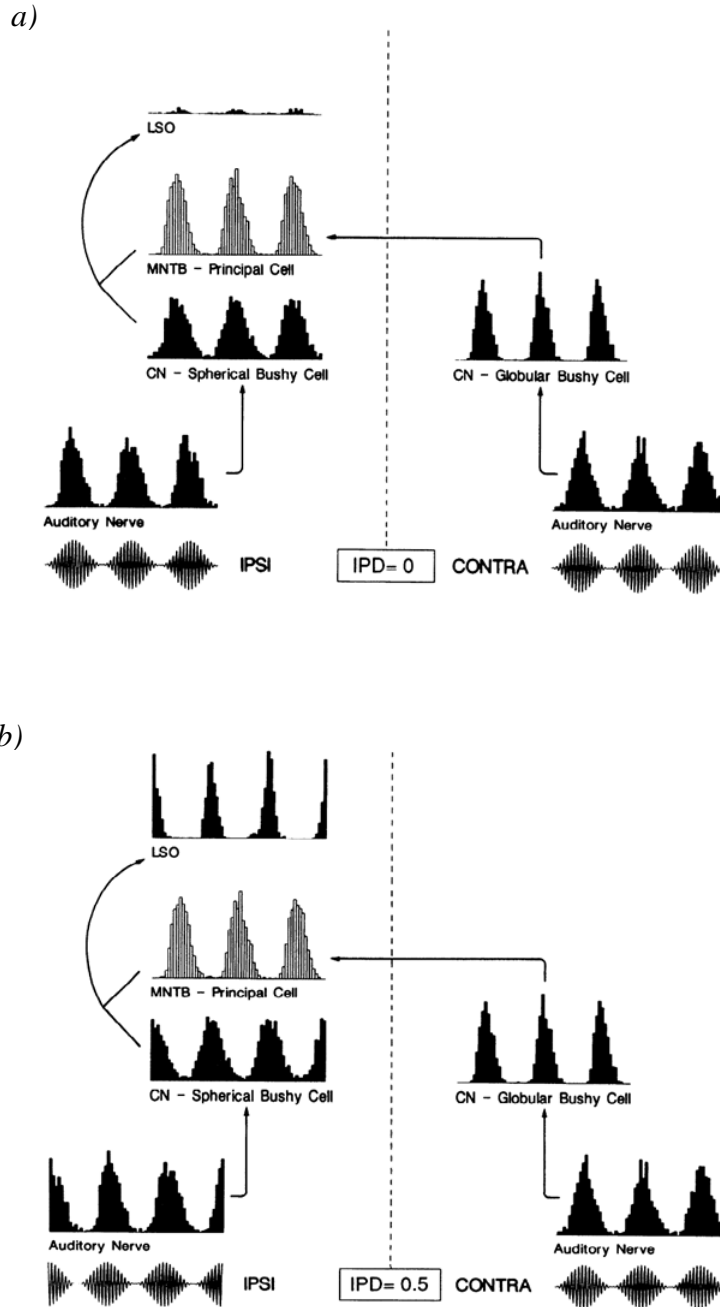


Figure 10. Potential basis for IPD sensitivity in the LSO. Poststimulus histograms of model LSO neurons in response to in-phase (*a*, IPD = 0) and out-of-phase (*b*, IPD = 0.5) AM stimuli suggest that the subtractive mechanism underlying ILD sensitivity can also produce envelope ITD/IPD sensitivity (Joris and Yin, 1995). Phase-locking of ANF firing to the low-frequency envelope of the AM stimuli propagates to CN and MNTB neurons through fast and secure synapses. If the afferent pathways to LSO neurons introduce balanced delays bilaterally, then in-phase stimuli will cause excitatory and inhibitory inputs from either to coincide at LSO neurons and negate each other so that the neurons fire minimally (*a*). In contrast, when the stimuli are out-of-phase, excitatory and inhibitory inputs overlap very little in their time of arrival, producing maximal firing in LSO neurons (*b*).

1.6 Strategy for ITD coding across the SOC

The responses of IC neurons to fine structure and envelope ITD appear to suggest that, in spite of subtle transformations, their binaural sensitivity is directly inherited from pSOC neurons (Fitzpatrick et al, 2002). It has been suggested that the different types of ITD-sensitivity found in pSOC neurons i.e. peak-type, trough-type and intermediate responses may be maintained as far as the auditory cortex to produce a single perceptual continuum of ITD sensitivity (Fitzpatrick et al, 2002). One explanation for the continuum originating in the MSO and LSO is that different response types may reflect the pSOC neurons' synaptic arrangements (Figure 11) (Fitzpatrick et al, 2002). This model predicts that peak-type principal neurons in the ventral, high CF region of the MSO perform pure coincidence detection and thus receive purely excitatory inputs from either ear. The increasing influence of inhibition on ITD-tuning functions towards the dorsal region of the MSO leads to the generation a range of intermediate-type responses in low-CF and middle-CF pMSO neurons. Extending this trend into the LSO, intermediate-type pLSO neurons in the low CF, lateral limb are replaced by trough-type pLSO neurons as contralateral inhibition and ipsilateral excitation prevail in the high CF, medial limb (see Figure 11). Together with findings suggesting that lateral pLSO neurons receive contralateral excitation (Finlayson and Caspary, 1991; Sanes, 1991; Wu and Kelly, 1991 and 1992; Kil et al, 1995) and that inhibition modifies peak firing rates of pMSO neurons (Brand et al, 2002; Pecka et al, 2008), evidence also exists for a systematic organization of inhibition and excitation in different frequency regions of the LSO (Glendenning et al, 1985).

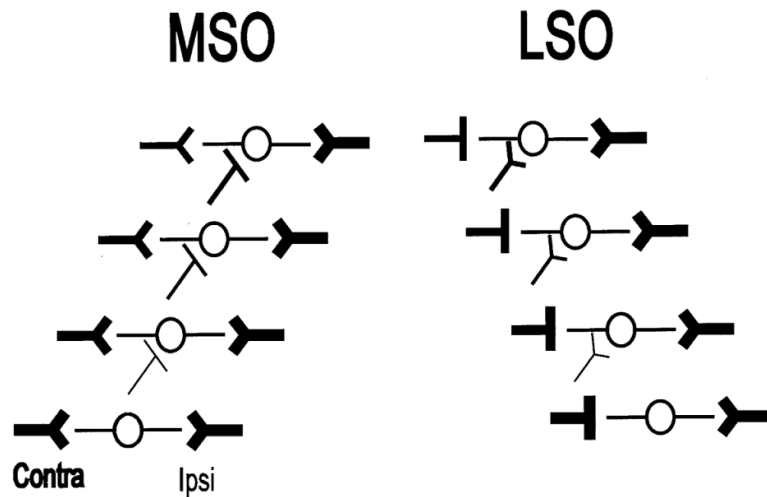


Figure 11. A potential arrangement of synaptic inputs to achieve a continuum of responses in the SOC. Although the generic arrangement of EE neurons in the MSO and EI neurons in the LSO would only allow for a dichotomy between peak- and trough- type ITD sensitivity, by varying the strength of contralateral excitation and inhibition across the MSO and LSO, it is possible to create a continuum of ITD functions including intermediate responses (Fitzpatrick et al, 2002). Given the relative importance of ITD cues to localizing pure tones of low frequencies, it is likely that low CF pLSO neurons displaying IPD sensitivity will possess stronger contralateral excitation but weaker contralateral inhibition than high CF pLSO neurons. This would entail that pLSO neurons in the low-frequency, lateral limb of the nucleus would resemble low CF pMSO neurons more in their ability to detect coincidence between stimulus-locked inputs from the two ears.

1.6.1 Strategy for envelope ITD coding

Amplitude modulations are particularly prominent in natural sounds such as vocalizations (Nelken et al, 1999) and the ITDs associated with the envelopes of these stimuli are potentially extremely important for binaural localization. Although responses in gerbil and rabbit IC neurons are mainly peak-type or trough-type, studies have observed intermediate responses (Fitzpatrick et al, 2002; Griffin et al, 2005), suggesting that the coding strategy for envelope ITDs may mirror that for fine-structure ITDs. However these studies have also demonstrated that the range of AM frequencies at which IC neurons are most sensitive to envelope ITDs is between 60 and 310Hz (Fitzpatrick et al, 2002; Griffin et al, 2005). For animals with small

heads such as the rabbit and the gerbil, this means that peak ITD of any intermediate neurons sits so far outside the physiological range that the slope of individual IC neuron's envelope ITD tuning functions are too shallow to actually provide information about azimuthal position (McAlpine et al, 2001; Sterbing et al, 2003). It has been suggested that regions of the IPD tuning curves may actually display greater accuracy for ITD discrimination however it is also likely that by integrating responses across a pool of envelope ITD sensitive neurons, the necessary temporal resolution observed in psychoacoustic studies may be achieved (Shackleton et al, 2003; Griffin et al, 2005).

1.7 Naturalistic sounds and the auditory system

When natural sounds are examined in narrow frequency bands, the power of the enclosed amplitude modulations (AMs) decreases proportionally with increasing AM frequency, leading to a "1/f power law" (Figure 12a) (Voss and Clarke, 1975; Attias and Schreiner, 1997; Singh and Theunissen, 2003; Lesica and Grothe, 2008; Rodriguez et al, 2010). Neural responses in the auditory system appear optimised to preferentially process these natural sounds over auditory stimuli with artificial statistics (Rieke et al, 1995; Nelkin et al, 1999; Escabi et al, 2003; Garcia-Lazaro et al, 2006). This finding supports the proposal that sensory systems have evolved to encode natural stimuli as efficiently as possible (Attneave, 1954; Barlow, 1961): maximal neural responses are restricted to a range of input frequencies so that neurons act a band-pass filter and encode a signal efficiently by removing redundancy in neural representation (Figure 12b) (Van Hateren, 1992; Lesica and Grothe, 2008).

One problem associated with this strategy however is that neural responses are more susceptible to the effects of noise (Kretzmer, 1954). As ambient noise displays a flat power spectrum irrespective of carrier frequency, neurons that extend their receptive fields to lower input

frequencies and therefore act as a low-pass filters, can convey more information about a signal in noisy environments (Figure 12a) (Voss and Clarke, 1975; Van Hateren, 1992; Attias and Schreiner, 1997; Singh and Theunissen, 2003; Lesica and Grothe, 2008; Rodriguez et al, 2010). Such an adaptive mechanism has indeed been observed in the AM frequency tuning when natural sounds have been presented with reduced signal-to-noise ratio to neurons in the gerbil IC and songbird forebrain (Figure 12b) (Nagel and Doupe, 2006; Lesica and Grothe, 2008).

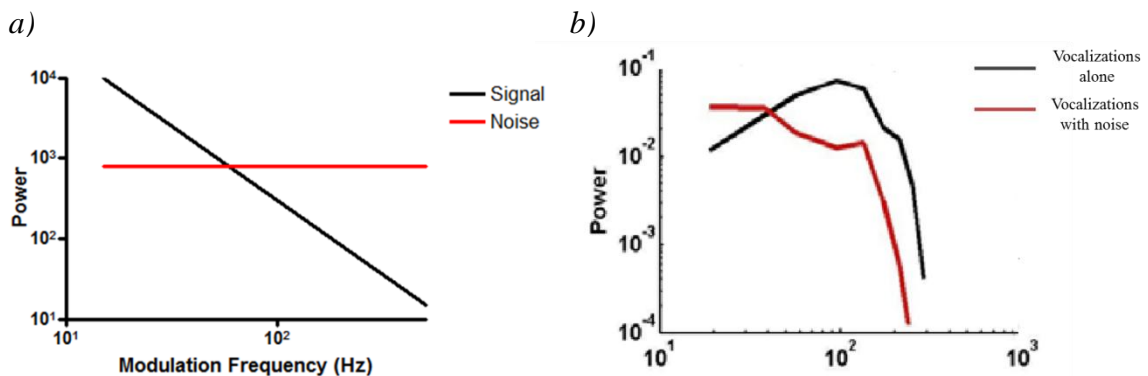


Figure 12. Statistics of naturalistic sounds causes adaptive changes in the filtering properties of auditory midbrain neurons. A schematic representation shows how the power associated with AM components in a narrow frequency band of a naturalistic stimulus is inversely proportional to the modulation frequency (a). This contrasts with ambient noise that displays a flat power spectrum across all modulation frequencies. As a consequence, the signal-to-noise ratio of naturalistic sounds decreases with increasing modulation frequency. Neurons in the gerbil IC respond to vocalizations as band-pass filter (b, black line) (Lesica et al, 2008) however, when ambient noise is added, their temporal receptive field becomes more low-pass (b, red line). It has been proposed that this is evidence for adaptive efficient coding of naturalistic sounds.

1.7.1 Optimal coding of naturalistic sounds may affect binaural localization

Given that binaural cues are restricted to particular frequency ranges, the signal to noise ratios associated with these cues may also vary in natural conditions. This may implicate different filtering strategies in MSO and LSO neurons in order to optimize binaural localization. Since ITD cues are restricted to carrier frequencies <1500Hz, relatively high signal to noise ratios are expected; thus MSO neurons may possess band-pass filtering properties that allow them to extract temporal information more efficiently from low frequency AM stimuli. Envelope ITDs and ILDs, on the other hand, are the only binaural cues available at carrier frequencies >1500Hz

and therefore are subject to reduced signal to noise ratios. Thus LSO neurons, sensitive to level differences in the fine frequency and envelope, are more likely to act as low-pass filters, extracting energy from across input frequencies with improved efficacy. Given that neurons in both nuclei are arranged along tonotopic axes, with some LSO neurons even possessing low CFs and displaying ITD sensitivity (Tollin and Yin, 2005), it is equally possible that a continuum of filtering properties exists across the SOC neurons, forming the basis for efficient coding of azimuthal sounds with complex, naturalistic statistics.

1.8 The hearing ranges of guinea pig and rat

Although the hearing ranges of guinea pigs (54-50,000Hz) and rats (200-76,000Hz) overlap considerably (Warfield, 1978; Fay, 1988), their upper and lower limits are dissimilar. These differences reflect the disparate frequency channels the two species use to communicate in the wild. Both species are capable of producing audible as well as ultrasonic sounds (Nygby et al, 1978; Sanders et al, 2001): however the fundamental frequencies of audible calls in the rat (2-4kHz, [Nitschke, 1982]) are higher on average than those in the guinea pig (“purr” can be as low as hundreds of Hertz, [Wallace et al, 2002]) whilst ultrasonic calls (i.e. >20,000Hz) are more common in the rat than the guinea pig across a range of ethological situations, both aversive and appetitive (Nitschke, 1982; Brudzynski, 2006; Litvin et al, 2007). Thus rats tend to vocalize at higher frequencies than guinea pigs and their hearing range is adapted to improve conspecific communication.

This could have potential implications for binaural processing: with rats relying more heavily on envelope ITDs and ILDs and guinea pigs being also able to benefit from ITDs in the fine frequency waveform to lateralize a call more accurately. Anatomical and electrophysiological evidence supports such a relationship as the rat MSO nucleus appears to be small in volume and

its neurons display some level difference sensitivity (Grothe, 2000; Paxinos, 2004). Given that rat ANs can achieve phase-locked responses to 3000Hz stimuli as well as ANs in the guinea pig (Palmer and Russell, 1986; Paolini et al, 2001), it is unlikely that poorer ITD sensitivity in the rat arises from failure to encode temporal information in the auditory periphery and instead may be a feature created *de novo* in the rat SOC.

1.9 Aims of the project

Although it has been well documented that both pMSO and pLSO neurons can display fine structure ITD sensitivity (Goldberg and Brown, 1969; Tollin and Yin, 2005), few studies have explored whether this arises from the two pSOC classes sharing synaptic or intrinsic neuronal properties. One of the project's main objectives was to answer this question and, in so doing, determine whether a continuum of neuronal properties and responses may exist across the MSO and LSO. The potential existence of a continuum in the SOC would offer greater insight into how individual principal neurons contribute to the overall representation of a stimulus's location on the azimuth.

Without *in vivo* intracellular recordings to definitively associate a principal neuron's ITD sensitivity with its electrophysiological profile, several channels of inquiry were employed to determine how similar pLSO neurons were to their MSO counterparts. Under the working hypothesis that low CF pLSO neurons, sensitive to fine structure ITDs, do indeed possess properties matching those observed in pMSO neurons, intracellular recordings were performed *in vitro* to first compare the passive and active properties of principal neurons from different regions of the LSO and MSO. Previous efforts to find a continuum have been limited by the lack of heterogeneity encountered in the electrophysiological properties of pMSO neurons along

the tonotopic axis: a fact likely attributable to the restricted nature of DC step/ramp protocols used by such studies. This project introduces a sinusoidal current injection protocol of linearly increasing frequencies that may help to tease apart the relative expression of different voltage-gated conductances in the pSOC neuronal population.

A study of synaptic profiles was also performed to determine whether similarities existed between the pMSO and low CF pLSO neurons that process fine structure ITDs. Electrical stimulation was used to target the contralateral pathways to the MSO and LSO in the *in vitro* preparation. It was hypothesized that principal neurons process fine structure ITDs in the LSO's low frequency, lateral limb would not retain a synaptic arrangement postulated by the duplex theory (i.e. inhibition alone) but instead resemble more pMSO neurons, receiving contralateral excitation as well as inhibition (Tollin and Yin, 2005). Analysis of synaptic properties was also used to determine how pLSO neurons, located at different positions along the tonotopic axis, might filter synaptic inputs of different polarity and therefore integrate information from the contralateral ear.

In parallel with the electrophysiological study, immunohistochemical techniques were employed to visualize the sublocalization of inhibitory synapses on pLSO neurons. This presented an opportunity to explore where inhibitory inputs impinged on the neuronal morphology of pLSO neurons along the tonotopic axis; comparisons could then be made with the somatic inhibition shown to exist in gerbil pMSO neurons (Kapfer et al, 2002). Although no specific hypothesis was formulated, differences in inhibition's sublocalization between the medial and lateral limb of the LSO were sought as part of a possible, continuous transition in the arrangement of pSOC neurons' synaptic inputs. A basic morphological characterization was also performed to help identify principal neurons and to give an initial indication of morphologically divergent subpopulations which may hold distinct functional roles in binaural processing.

The aforementioned hypotheses are applicable when considering species with low frequency hearing ranges like the guinea pig. Such species are particularly reliant on fine structure ITDs to localize auditory stimuli binaurally and hence retain a well-developed MSO and low-frequency, lateral limb of the LSO. Nevertheless many of the experiments above were also performed using the rat, a high frequency hearing species. If there exists a strong ethological pressure for these species to rely on envelope ITD rather fine structure ITD processing, then is likely that any continuum of properties in the SOC nuclei would be altered, making it easier to localize amplitude-modulated naturalistic stimuli within ambient noise.

Material and Methods

2.1 Electrophysiology

2.1.1 Animals

Two species with different frequency hearing ranges were used in this study. Tri-coloured guinea pigs (*cavia porcellus*) (of ages P1 to P19) were taken as a species specialising in low frequencies and Sprague-Dawley rats (*rattus norvegicus*) (P19 to P21) represented high-frequency hearing animals. 137 guinea pigs and 46 rats were sacrificed in order to attain the recordings in this thesis. Both strains are not known to suffer from any hearing problems within the ages specified and their peripheral hearing has matured sufficiently to exclude developmental factors as a possible explanation for any finding (Borg, 1982; Simpson et al, 1985; Ingham et al, 1998; Rietzel and Friauf, 1998; Nabekura et al, 2004; Barnes-Davies et al, 2004). The broader range of guinea pig ages reflects the dearth of available animals; this paucity arises from both the species prolonged gestation period (3 months) as well as the ‘time-locked pregnancies within a small breeding colony. Animal handling, care and all other procedures were in accordance with the Animal Welfare Act 1988 and had been approved by the UCL Biological Services.

2.1.2 Slice preparation

Animals were decapitated and brains were harvested in a low sodium, high sucrose dissection solution (pH 7.4 after bubbling with carbogen and preheated to 30C⁰ in a water bath) (Table 1).

The superior olivary nuclei are located in the region of the brainstem ventral to the cerebellum in both species; thus this region was isolated from cranial nerves and adjacent brain regions before the meninges were carefully removed. The brain tissue was then attached rostral face-down to a 2cm x 2cm x 1cm block of agar using cyanoacrylate glue (Vetbond, 3M US). The brainstem is notoriously sensitive to anoxia so the block of agar was quickly transferred to a custom-made chamber where it was glued down to a metal platform (Superglue, Superglue Corporation) and immersed once more in dissection solution. Once the chamber was been installed in the vibratome (Integraslice 7550 PSDS, Camden instruments), coronal slices 300-325 μ m thick in the guinea pig, and 305 μ m in the rat, were cut using a sharp ceramic blade (7550-1-C blades, Camden Instruments). These thicknesses were chosen as they best balanced efforts to preserve the auditory brainstem circuitry whilst permitting adequate perfusion with carboxygenated external solution during recordings. The tissue block was orientated in such a manner that it was sectioned in a rostral to dorsal direction. To this end, in order to determine whether the level of the SOC nuclei had been reached, a dissection microscope on the vibratome was used to identify the facial nerve (which acted as a visual landmark). The nerve appeared highly conspicuous as a white line transecting the tissue laterally to the LSO, which itself was recognized as an S-shaped white region when sectioned at the appropriate depth. Typically 2-3 slices containing the lateral superior olive were obtained from each animal.

Once cut, brain slices were carefully transferred to a 100ml beaker containing carboxygenated Krebbs (Table 1) heated to 37°C in a water bath (Universal water bath SUB14, Grant). To enable access of the bathing solution to all surfaces, slices were suspended on freshly-cut medical gauze (Medical gauze, Boots) stretched across a plastic frame (35mm culture dishes, BD Falcon). After 30-45 minutes, the temperature was lowered and held at room temperature (about 21C°). Slices remained at this temperature until they were moved individually to the recording chamber. Given the prolonged time spent in these conditions, care was taken that the

volume of solution (and thereby osmolarity (tested using a Camlab Osmometer)) remained constant by placing a temporary cover over the beaker.

		Internal solution	External Solutions	
		Low Chloride	Low Sodium, High Sucrose	Normal Krebs
KCl		5mM	2.5mM	2.4mM
KGlu		130mM		
CaCl ₂			0.5mM	2mM
MgCl ₂			4mM	1mM
NaCl			87mM	125mM
NaH ₂ PO ₄			1.25mM	1.1mM
NaHCO ₃			25mM	26mM
MgATP		2mM		
Na ₂ ATP		2mM		
Na ₃ GTP		0.3mM		
Na ₂ PCr		10mM		
EGTA		1mM		
HEPES		10mM		
Glucose			25mM	25mM
Sucrose			75mM	
ASC			0.5mM	

Table 1. The ionic composition of internal and external solutions used for slice preparation and electrophysiological recordings. A pH of 7.4 ± 0.1 was considered acceptable for both internal and external solutions. Adjustments to pH were made using KOH and NaOH for the internal and external solutions respectively (pH 210 pH meter, Hanna Instruments) An osmolarity of 305 ± 5 mOsm was used for the internal solution whilst a suitable external solution had a value of 320 ± 10 mOsm (CamLab Osmometer).

2.1.3 Whole cell patch clamp

Slices were secured in the circular recording chamber by means of a custom-made platinum harp. An external Krebs solution (Table 1) was carboxygenated and perfused in the chamber at a constant rate of 3ml/min with the point of entry and exit placed diametrically apart to improve flow over slices (Miniplus-3 perfusion pump, Gilson Inc). An in-line heater (SH27B inline heater, Warner Instruments Corporation) connected to a proprietary temperature controller maintained slices close to physiological temperature throughout recordings (30-34 C⁰). Slices were viewed with an Olympus upright microscope (BX51WI Microscope, Olympus): the LSO or MSO being located with the 10× objective lens before individual principal neurons were identified by switching to the combination of a 60× objective lens and a CCD camera (w82C CCIR, Watec Cameras) connected to a monitor (M/0922 monitor, Mitsubishi Electric). pSOC neurons were identified on the basis of their large fusiform somata. Where they lay superficially in the slice, their viability was assessed based on the opacity and luminosity of their somatic membrane, viewed on the monitor. Viable neurons appeared more opaque and retained their lucre, whilst neurons close to death possessed translucent somata that were often spherical and showed signs of blebbing.

Before each recording, borosilicate capillaries (GC120TF pipette glass, Harvard Apparatus) were cut to 7.5cm with a diamond knife and “fire polished” before they were pulled using a vertical puller (PP-83 pipette puller, Narashige Group). Pipettes were then back-filled with a pre-filtered (0.22 µm syringe filter units, Millex-Millipore) potassium gluconate-based internal solution (Table 1) that, over the course of recordings, was kept on ice. The filled pipette was then inserted into the pipette holder on the head stage (CV 203BU headstage, Axon Instruments), making sure that the Ag/AgCl wire electrode (AG10W silver wire, Harvard Apparatus) was at least partially immersed in the internal solution. Wandering baseline

potentials were avoided during recordings by re-chloriding electrodes regularly (sanding down and placing it in 15% Sodium Hypochlorite solution for 15-30 minutes or until it turned matt-brown in appearance). Reference electrodes (E205 Ag/AgCl pellet and wire electrode, Harvard Apparatus) were replaced when their AgCl pellets attached to a silver wire had been exhausted.

The pipette was lowered into the bath using a Luigs-Neumann Micro25 manipulator (controlled by a Luigs and Neumann SM5 unit), whilst positive pressure was applied by mouth through a 1ml syringe to prevent blockage of the aperture by material on the meniscus. If the pipette's resistance fell within the range of 4-6.5 M Ω and its aperture appeared as a regular rounded shape, the pipette was deemed suitable for patching. At this stage, the offset was adjusted on the Axopatch 200B patch-clamp amplifier (Axon Instruments) so that the baseline potential was returned to zero.

Positive pressure was held throughout the approach to the cell and could be kept steady for prolonged periods by closing a three-way valve attached to the 1ml syringe. When the pipette was close enough to engage the cell, as indicated by a jump of a few M Ω in the pipette's resistance, positive pressure was replaced by a gentle negative pressure in order to form a stable seal. Both the fast and slow capacitances were compensated in cell-attached mode after a gigaseal was achieved. Extra suction was then administered to break into whole cell configuration. At this point, the resting membrane potential was noted i.e. when zero current was injected

2.1.4 Electrophysiology protocols

All recordings were made using the Axopatch 200B amplifier in current-clamp mode at a sampling rate of 50kHz; a 5kHz Bessel filter was used to filter out high-frequency electrical

noise. A Digidata 1320A (Axon Instruments) was used to digitize the acquired data. Although a bridge balance was not used as it produce unstable recordings, any neuron that displayed rapidly rising offsets in response to current injection was rejected if the series resistance could not be reduced by improving access to the cell through increased suction.

Neurons were selected on the basis of the stability of their membrane potential (<-40mV) and the capacity to evoke APs upon current injection. In order to compare firing patterns from different cells, a small DC current ($\leq \pm 100\text{pA}$) was employed where necessary to hold a cell at a potential of $-55\text{mV} (\pm 5\text{mV})$ throughout recordings. For the purposes of characterizing the passive and active properties of principal neurons, 100ms current steps, ranging from 10 to 1750pA, were used to depolarize cells whilst 400ms long hyperpolarizing current steps between -5pA and -1500pA were employed. Current pulse generation in conjunction with data acquisition was performed using a PC (Dell) running pClamp 9 software (Axon Instruments).

2.1.5 ZAP protocol

In order to determine how pSOC neurons responded to inputs that varied in the frequency domain, a DC current was first used to hold a neuron at a desired membrane potential before a ZAP function was injected somatically (Puil, 1986). The ZAP function is a sinusoidal current waveform whose frequency increases linearly: it can be described by the equation:

$$I(t) = a \sin \left[2\pi \left(f_0 + \frac{k}{2} t \right) t \right], 0 \leq t \leq T$$

where $I(t)$ is the instantaneous current value at time point t (total duration is represented by T); a and k determine the waveform's amplitude and rate of frequency increase respectively and f_0 equals the initial sinusoidal frequency.

In this study, f_0 was held constant at 1Hz and the sinusoidal frequency increased until it reached a fixed maximum of 1000Hz at time T . ZAP waveforms were comprised of 50,000 time points and the total duration, T , was set at either 1 or 5 seconds. The peak-to-peak amplitude of the current was set between 50 and 75pA to ensure that only subthreshold responses were produced. The waveform was generated using a custom-written program in Matlab v7.0 (MathWorks) before the stimulus waveform was imported into pClamp 9 via Excel 07 (Microsoft Corporation).

2.1.6 Electrical stimulation of trapezoid body fibres

To target contralateral inputs, a bipolar electrode (WDF), attached to a separate Luigs-Neumann Micro 25 manipulator, was positioned across the trapezoid body fibres at the midline of each brain slice (Figure 13). By delivering focal stimulation here, it was possible not only to recruit excitatory fibres directly contacting the pSOC neurons but also to stimulate the inhibitory pathways that, relayed via neurons of the MNTB, innervate the LSO and MSO.

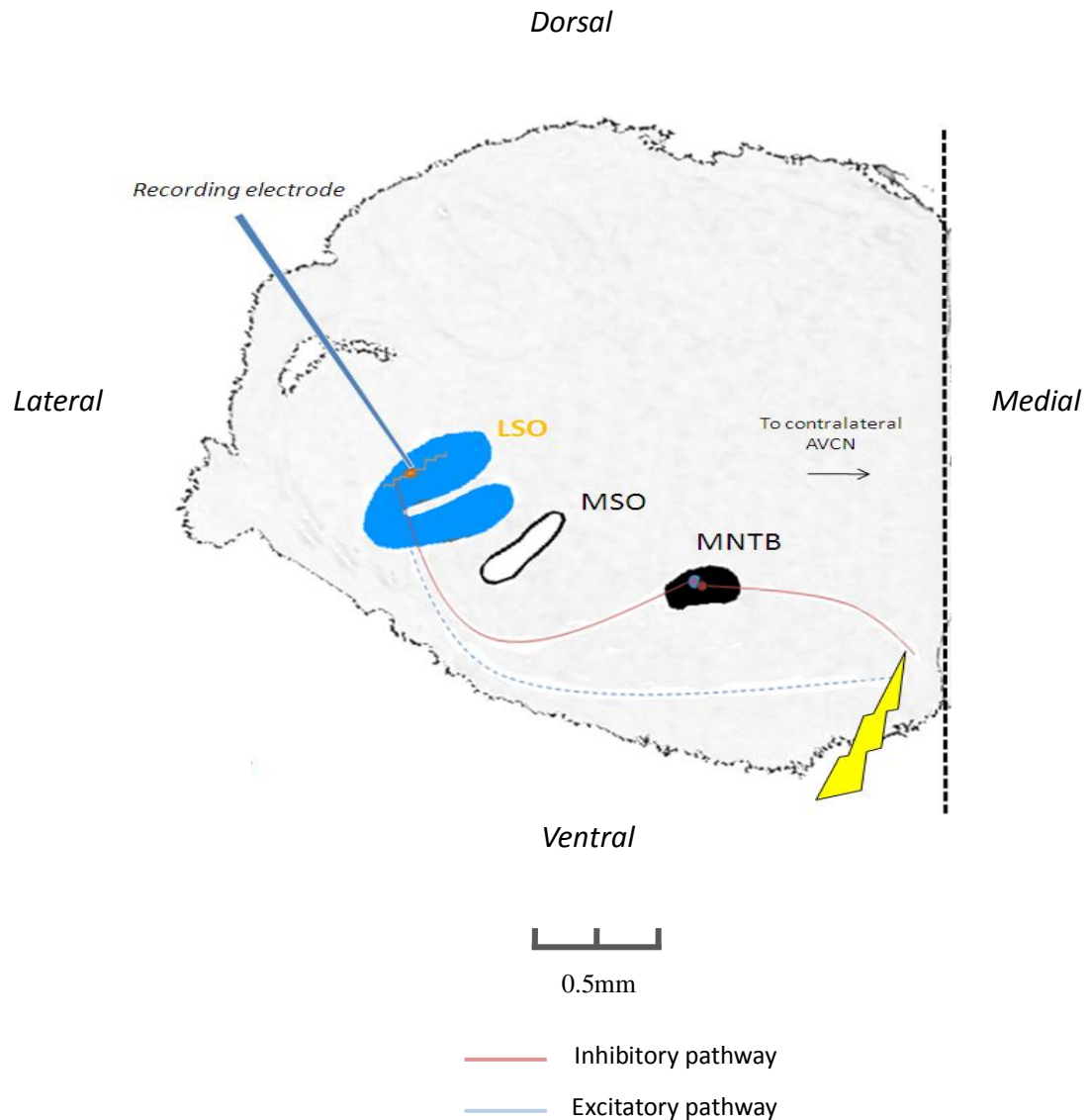


Figure 13. Contralateral electrical stimulation of the LSO synaptic pathway. Half a coronal auditory brainstem slice, (*dotted line* indicates midline), is represented to demonstrate how extracellular stimulation of pLSO neurons' contralateral excitatory and inhibitory pathways was achieved. A bipolar electrode was placed medial to the MNTB at a location where trapezoid body fibres originating from the contralateral ear were most tightly bundled together. Only once a stable recording had been attained from a pLSO neuron were pulse trains of different amplitude (7-70mV) employed to determine whether contralateral synaptic connections were present. A similar protocol was performed to evoke synaptic potentials when recording from pMSO neurons.

To stimulate the fibres, pulses were generated in pClamp 9 and delivered via the Axopatch 200B amplifier to a stimulator (S9 stimulator, Grass Technologies), triggering 200 μ s long square pulses. Stimulus intensity was adjusted (range 7 - 70mV) until a consistent synaptic response, reproducible across repeated stimuli, was recorded. If no synaptic stimulation was observed then either the polarity of the pulse was switched, or the electrode was physically moved. Pulse trains contained either 15 or 30 pulses presented at a rate in the range 50Hz to 1kHz. A minimum of three repeats was required for analysis to be performed. The interval between consecutive sweeps was fixed at 10s for all stimulus protocols, as experience suggested this to be the minimum interval to provide for full recovery of any short term synaptic plasticity. A negative or positive DC current was injected to change the baseline potential where necessary. Data acquisition was performed using pClamp 9 on a PC.

2.1.7 Analysis of passive and active property data

On account of the variety of forms the LSO took across coronal slices obtained from a single brain, the nucleus was partitioned broadly into medial and lateral limbs in order to pinpoint the location of a pLSO neuron on the tonotopic axis (Figure 14). Analysis was mainly performed using the Clampfit 9 program although linear regression and tests of significance were performed using Graphpad Prism 4 (Graphpad Software). Where averaged data are shown, standard errors are employed, unless indicated otherwise. All values presented in this thesis were calculated without subtraction of the liquid junction potential which was calculated as 17.3 mV (liquid junction calculator in pClamp 9).

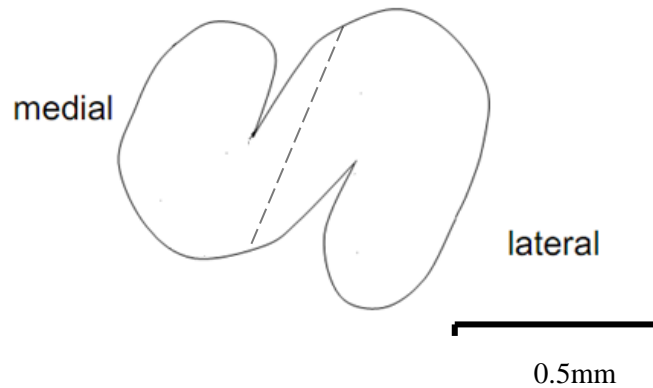


Figure 14. Division of LSO nucleus into medial and lateral limbs to localize patched pLSO neurons. Given that the LSO nucleus manifested a different shape depending on the height and angle of the slice in the auditory brainstem, it was divided into medial and lateral limbs so that patched pLSO neurons could be assigned a position along the LSO's axis.

Input resistances of cells were calculated from the voltage traces evoked in response to the smallest hyperpolarizing steps presented (in the range 5-50pA). The voltage difference produced by such current steps was calculated by subtracting the average voltage response over a 10ms period at the very end of the 400ms stimulus from the average value observed for a 10ms region before stimulus onset. The membrane time constant was calculated using the rising portion of the response in the smallest hyperpolarizing voltage traces, to fit an exponential curve (assessed using pClamp 9 software). A cell's capacitance was thereby calculated by multiplying the membrane time constant of this fit by the cell's input resistance. Current-vs.-voltage (IV) curves were plotted using two sets of voltage values: peak and sustained. The peak response was considered to be the largest sub-threshold voltage measured across the whole stimulus,

whilst the sustained response was an average subthreshold voltage calculated over the final 10ms of the depolarizing or hyperpolarizing current steps.

To study cell firing patterns, action potentials were identified and the interspike intervals were calculated between the 1st and 2nd APs (the 1st ISI) using a semi-automatic threshold detection program (pClamp 9). An absolute threshold was set manually at 0mV for classifying voltage deflections as APs; although events with half-widths larger than 3ms were also rejected as failed APs or oscillations following APs.

The frequency-dependent impedance ($Z_{(f)}$) was calculated by taking the square root of the ratio between the Fast Fourier Transforms (FFTs) of voltage and current traces ($Z_{(f)} = \sqrt{\frac{FFT[V_{ZAP}(t)]}{FFT[I_{ZAP}(t)]}}$; Puil et al, 1986, 1988; Schreiber et al, 2004). The impedance amplitude profile of a neuron was produced by plotting impedance values (y-axis: linear scale) against the sinusoidal frequencies at which they were measured (x-axis: log scale). The average FFTs of at least 5 current and voltage traces were used to create impedance amplitude profiles.

If a neuron displayed band-pass properties i.e. peak impedance value was at a non-zero frequency, then it was considered to possess resonant properties and further analysis was performed. The peak resonant frequency (F_c) was taken as the frequency at which the peak impedance was observed and indicated what the preferred input frequency of a resonant neuron was. The Q value, on the other hand, was calculated as the ratio between the impedance at F_c and the impedance at a frequency of 0Hz (equivalent to the input resistance (R_{in}) (Q value = Z_{F_c}/R_{in}) (Figure 15). It shed light on how narrow the range of input frequencies was which caused this resonance.

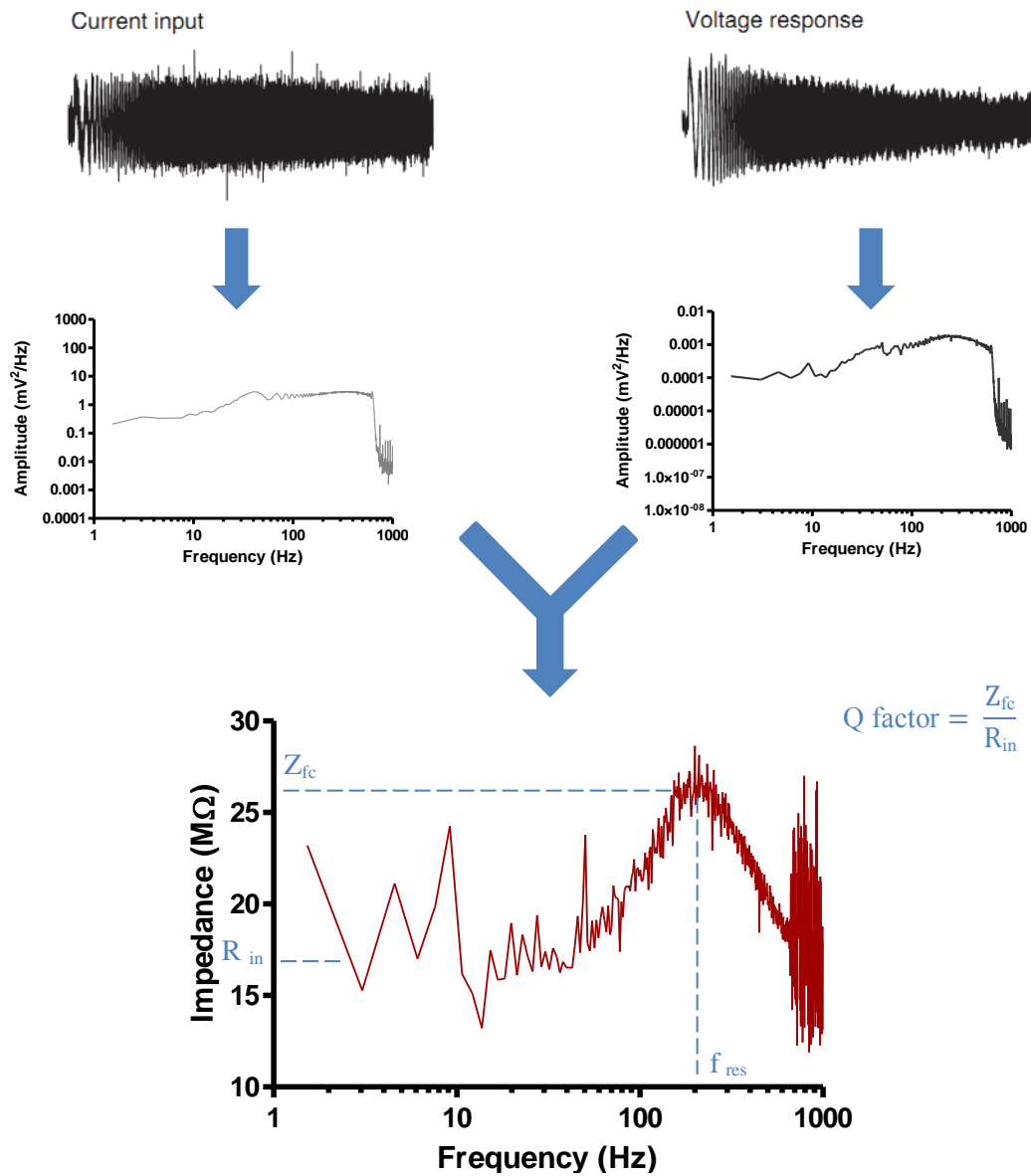


Figure 15. Calculation of impedance profile using ZAP protocol. A sinusoidal current input whose frequency increased linearly from 1-1000Hz (top left) was injected into a pLSO neuron producing a corresponding voltage response (top right). The impedance at each frequency was calculated by first dividing the average power spectrum for a minimum of 5 current traces (middle left panel) by the average power spectrum for a similar number of voltage traces (middle right panel) before taking the square root of the answer. These impedances were then plotted against the input frequency (on a log scale) to produce the impedance profile (bottom panel). Where a peak impedance was observed at a resonant frequency (f_{res}), the Q factor was calculated by dividing the impedance at this peak by the impedance for a 0Hz stimulus i.e. the input resistance.

2.1.8 Analysis of synaptic data

When the potential of a pLSO or pMSO neuron was held at -55mV, inhibitory and excitatory synaptic potentials showed opposite polarities, making it possible to determine whether one or the other dominated synaptic transmission. This arose because the relative reversal potentials of inhibition and excitation lay either side of a neuron's resting potential. Whilst EPSPs reverse close to 0mV due to the mixed cationic permeability of glutamatergic AMPA receptors, inhibition was largely dependent on the reversal potential of the chloride ion as it was the monovalent ion most permeable through GABA and glycine receptors in the internal and external solutions (Fatima-Shad and Barry, 1993). The reversal potential for chloride was calculated as -85mV using the Nernst equation (or -68 mV with liquid junction potential included).

An event-detection program (part of the pClamp 9 software), was used to identify individual dPSPs and hPSPs in traces. The parameters assigned as criteria for detection were the amplitude and duration of the PSP. The threshold amplitude was set at ± 2 mV depending on the polarity of the PSP, whilst the minimum required duration was 1ms in the LSO and 0.5ms in the MSO. No filtering was performed on traces unless otherwise indicated in text.

The peak amplitude, rise slope (slope over 10% to 90% of the peak amplitude), half width (width of PSP at half peak amplitude) and inter-event intervals of subthreshold PSPs were all measured automatically in pClamp 9 after PSPs had been detected. In order to calculate the 10% to 90% rise slope of suprathreshold dPSPs, it was assumed that the voltage threshold of synaptically evoked APs was the same as the "peak amplitude" of underlying dPSPs. To this end, the second derivative of the voltage traces was calculated and the second peak taken as

marking AP initiation: once the “peak amplitude” of the dPSP was found, the 10% to 90% rise slope was then calculated manually. Short-term plasticity in PSP amplitude was measured by normalizing the peak amplitudes of PSPs in each pulse train to the largest peak amplitude. Values at each pulse were then averaged across sweeps to produce the temporal profile of changes in PSP amplitude for each cell within each pulse train for each frequency tested. This profile was finally fitted with a one phase exponential decay in Graphpad Prism 4 and the plateau value taken as the normalized steady state value whilst the decay time constant was calculated as the inverse of the time constant of the fit.

2.2 Immunohistochemistry

2.2.1 Protocol

The protocol for tissue preparation (Schneider Gasser et al, 2006) was followed to better preserve morphology and antigenicity especially where puncta were involved. No alteration in the protocol was made based on which species was being processed.

2.2.2 Preparation

Unlike perfusion fixation which fixes tissue immediately post-mortem, this protocol required freezing of harvested brain in liquid nitrogen and its subsequent slicing before fixation took place. The extraction of brain tissue from a decapitated animal was performed as previously described in the electrophysiological study. The region containing the auditory brainstem was placed in a petri dish, partially filled with ice-cold PBS, and dissected to make it more compact

and stable on the cryostat chuck. An interface between chuck face and brain tissue was reinforced with either a drop of PBS or a more substantial volume of O.C.T (Tissue-Tek). Once the orientation had been optimized to produce transverse slices, the brain tissue and chuck were plunged into liquid nitrogen (BOC UK) for 2-3 minutes making sure that no part was exposed to air. The frozen tissue was then either transferred directly to the cryostat or was kept in a -80 freezer wrapped air-tight in aluminium foil.

2.2.3 Sectioning

The brain tissue was kept in the freezer for a maximum of 2-3 days before it was mounted in a cryostat chamber (CM1850, Leica) cooled to -20 to -25 C° and allowed to equilibrate for 30 minutes. Sections 20-25µm thick were made with the cutting knife which was held at the same temperature as the chamber before the slices were then collected with cooled gelatin-coated slides (VWR International). At first sections were checked under a light microscope to judge the depth in the brain tissue from which they had been taken. When slices from the MSO and LSO were being cut, subsequent sections were allowed to air dry for 30 seconds before being returned to the chamber on the slides. 20-25µm slices had the advantage of allowing better primary antibody penetration but this unfortunately also meant that many dendritic processes were severed at this stage if they did not lie in the plane of the slice.

2.2.4 Fixation

As it was paramount that the slides should not dry out, slides were placed on plastic straws raised above Whatman filter paper (Grade 1 filter paper, Whatman) that had been soaked in PBS. The straws were secured to the plastic container by sellotape and a lid covered the slides to

prevent moisture loss. Fixation took place using 2% PFA (Sigma-Aldrich); the fixative was carefully pipetted on to slides for ten minutes at 4C ° before a PBS wash was performed for 15 minutes. In rat the fixation was also attempted for 30 minutes at 4C ° in attempt to improve levels of background fluorescence.

2.2.5 Immunohistochemical labeling

Permeabilization was performed in PBS (Sigma-Aldrich) with 10% Goat serum (Sigma-Aldrich) and 0.5% TRITON-X 100 (Sigma-Aldrich) at room temperature for an hour. The slides were next washed six times with PBS for 10 minutes each. Primary antibodies against Gephyrin were then applied at concentrations of 1:100; 1:250; 1:500 or 1:1000 (1:500 was most common concentration) from an original concentration of 1mg/ml (Mouse Anti-Gephyrin Monoclonal, Oyster®550 conjugated, Synaptic Systems GmbH). Antibodies against MAP2 (Microtubule associated protein 2, a neuronal specific marker of microtubules in somata and dendrites (Drewes et al, 1998)) were also used at 1:500 from an original 1mg/ml to help visualize neurons (Rabbit Anti-MAP2 polyclonal, Synaptic Systems GmbH). Incubation occurred overnight at 4C°. Three, 5 minute washes followed with PBS before the secondary antibodies were applied. Since the anti-Gephyrin primary antibody had a fluorophore pre-attached, there was no need to include a secondary antibody for this target. Thus only 1% Horse serum (Sigma Aldrich); 0.01% TRITON-X100; FITC, goat anti-rabbit secondary antibody for the MAP2 (Sigma Aldrich) at 1:500 (1mg/ml) and PBS were used to make a total volume of 5mL per slide. Three PBS washes of five minutes were finally performed. Touching a tissue to the slide's edge, capillary action carefully removed all the PBS solution so that 2 drops of the mounting medium (VECTASHIELD, VECTOR Labs) could be added. Vectorshield also included the nuclear marker, DAPI, included at a concentration of 1.5µg/ml (VECTASHIELD HardSet Mounting

Medium with DAPI, VECTOR Labs). Coverslips of dimensions, 60mm x 25mm (VWR International), were placed on top of the slides, making sure that no air bubbles were trapped beneath.

2.2.6 Confocal microscopy

Regions in the LSO and MSO were first singled out using the brightfield settings on the microscope (AxioPlan 2 LSM 510 META Confocal Microscope, Carl Zeiss Microimaging GmbH) and epifluorescence was employed to locate individual cells stained for gephyrin. Single images or image stacks were then made using the confocal technique. In the latter case, the depth of each image ranged from 0.75 μm to 1 μm . Acquisition protocols, controlling the dichromatic mirrors and filters, were taken from previous users given their suitability to the fluorophores involved in this study. Data was collected using the Zeiss proprietary software supplied for the PC (Fujitsu) accompanying the microscope.

2.2.7 Analysis

LSO and MSO neurons were identified by their fusiform somata which lay within their respective nuclei and were highly stained for MAP2. Dendrites were considered as first protruding from somata where their diameter was smaller than 4 μm in the LSO and 6 μm in the MSO. The cross-sectional somatic area was used as it was considered more robust to slight artefactual changes in the cell morphology caused by the preparation protocol. Cross-sectional somatic area was measured at the level of the confocal image stack where its value was judged to be largest: this was usually the image in which the nucleus (or the space where the nucleus would have been also appeared largest). Due to the punctate nature of gephyrin staining, it was

possible to assign a definite dendritic location where puncta were 75% less concentrated than on the soma: the dendritic length was measured from this point to the soma.

Image re-adjustments and measurements of cell somatic area were performed using the using Zeiss LSM Image Browser software (Carl Zeiss MicroImagine GmbH). To make 3-D reconstructions from image stacks, Volocity v.7 (Perkin-Elmer) was used. Brightness, Contrast and Density of the voxels were the only parameters changed for the purposes of the reconstructions.

3.1 Electrophysiology

Whole cell recordings were attained from 20 LSO neurons (all were recorded by Jason Mikiel-Hunter) and these are reported here. The total population of cells was 186 and results from the whole population will be described as required. In all neurons recorded, the resting membrane potential was below -40mV and voltage traces displayed no obvious “current bridge” in response to stepped injections of current.

3.1.1 Classification of guinea pig pLSO neurons

19/20 neurons were classified as guinea pig pLSO neurons based on their voltage responses to constant, current steps of varying amplitude (Figure 16). Suprathreshold depolarizing current steps evoked action potentials of reduced latency (<3ms at current steps greater than 1nA in amplitude, Figure 17 *a, b* and *c*) and short first inter-spike intervals (between 3 and 6ms for current steps greater than 1nA amplitude, Figure 17 *a, b* and *c*) in the pLSO neurons. In addition, repolarizing sags during maintained steps associated with the activation of the cation selective conductance, I_H , were observed when hyperpolarizing currents were used to probe the pLSO neurons (Figure 16 *d* and 17 *d, e* and *f*). The input resistance, membrane time constant and capacitance of these 19 guinea pig pLSO neurons were $52.9 \pm 3.8 \text{ M}\Omega$, $1.5 \pm 0.2 \text{ ms}$ and $28.9 \pm 2.1 \text{ pF}$ respectively. The single neuron to be excluded on the basis of its voltage responses had a resistance of $175 \text{ M}\Omega$ and membrane time constant of 11ms. In conjunction with its calculated capacitance of 15.9 pF, these properties suggest that the neuron was likely to have been a smaller “intrinsic” lateral olivocochlear neuron. Further analysis was not applied to this neuron.

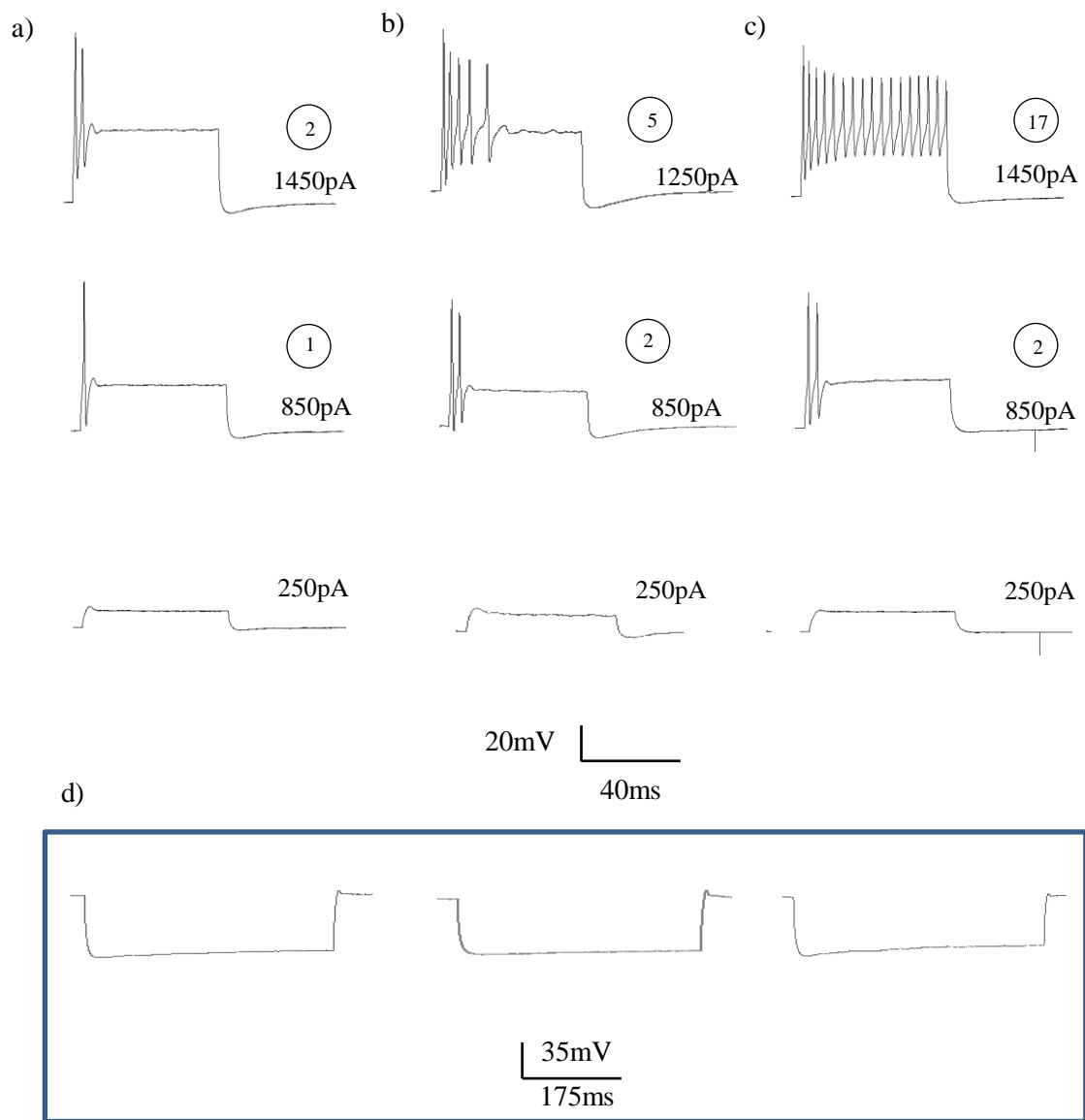


Figure 16. Voltage responses of three individual guinea pig pLSO neurons to depolarizing and hyperpolarizing current steps. The three neurons (*a*, *b* and *c*) displayed different maximum number of action potentials (*top panels*) in response to 80ms depolarizing current steps (step amplitude shown on right of traces). The encircled figure represents the number of APs evoked at that current injection. Action potentials were identified as voltage deflections that surpassed a 0mV threshold. In response to a 400ms hyperpolarizing current step of -500pA, all three guinea pig pLSO neurons displayed a repolarizing sag (*d*). Note the subthreshold oscillations that followed APs in middle neuron (*top panel, b*)

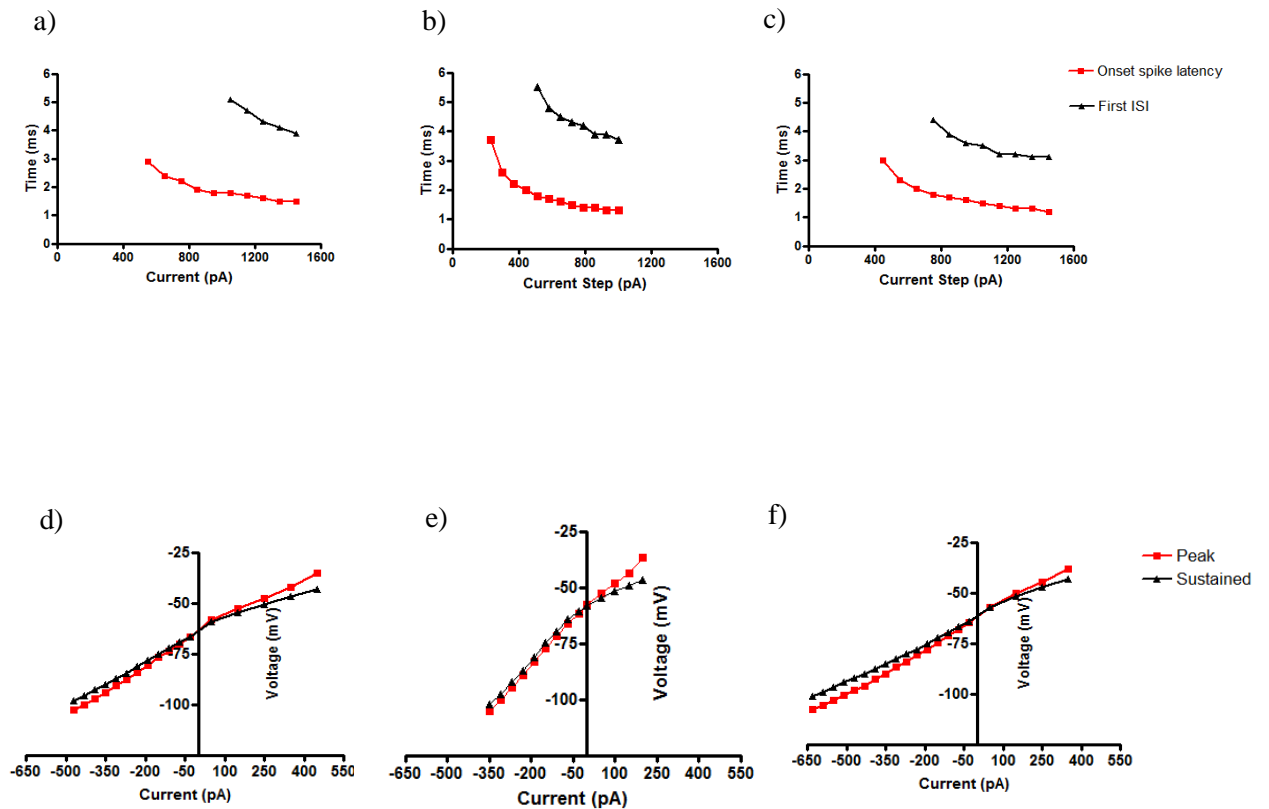


Figure 17. The electrophysiological properties of the three pLSO neurons in Figure 16. The latency of the onset AP (*red trace*) and the interval between the 1st and 2nd AP (*black trace*) were plotted for the three neurons (*a*, *b* and *c*) in figure 16 (ISI was calculated for the cell in *a* as it responded with a second AP above 850pA). Both parameters decayed with increasing current step size, eventually reaching a stable minimal value at the highest current steps. Subthreshold IV profiles of the three neurons (*d*, *e* and *f*) cells displayed non-linearities especially in the hyperpolarizing direction.

A range of firing patterns are observed in guinea pig pLSO neurons

A study of pLSO neurons in the rat has previously proposed that two subpopulations exist with distinct firing patterns (Barnes-Davies et al, 2004). ‘Single-firing’ cells are those which responded to depolarizing current steps with a single onset action potential, whilst ‘multiple-firing’ cells are those which respond to action potentials following an initial spike. An initial observation that all guinea pig pLSO neurons responded to large depolarizing current steps (>850pA) with multiple action potentials suggested that a different arrangement may be true for guinea pig pLSO neurons. Therefore to determine whether pLSO neurons could be separated into two distinct groups based on their firing patterns, the number of action potentials evoked as a result of a large amplitude current step (fixed to a range of 1.25nA to 1.45nA) was measured for each guinea pig pLSO neuron and displayed in a histogram (Figure 18). Although the histogram presented a distribution which is skewed towards neurons which only fire twice maximally (10/19 or 53% of the cells), a continuum of neuronal firing patterns was evident across the pLSO population recorded here. Example traces of guinea pig pLSO neurons which fired two, five or seventeen times in response to current steps of either 1.25nA or 1.45nA amplitude are displayed in Figure 16.

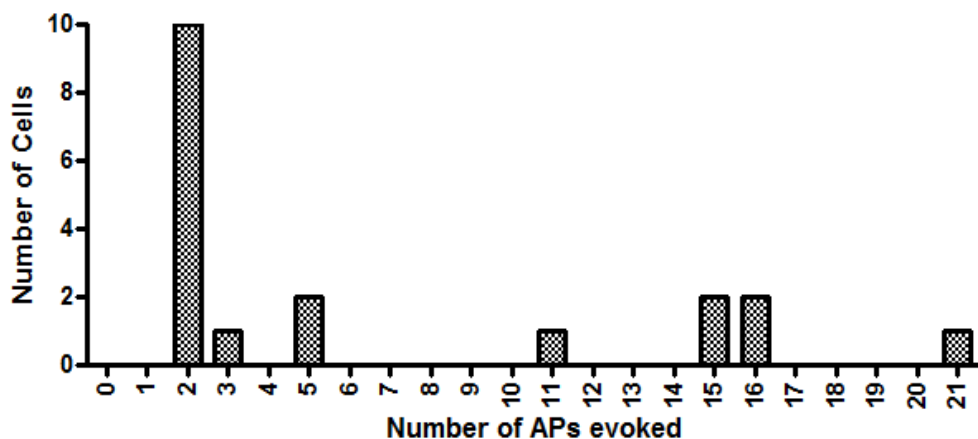


Figure 18. Histogram displaying the number of action potentials potentially evoked across the guinea pig pLSO neuronal population. The number of action potentials was counted in response to a depolarizing step between 1.25 and 1.45nA. At least two APs were observed per cell with a variable number evident in half the population of cells.

The input resistances of guinea pig pLSO neurons does not support the existence of two subtypes

It has also been demonstrated in the rat LSO that the two pLSO subtypes display differing intrinsic properties (Barnes-Davies et al, 2004): “single-firing” neurons possessing lower input resistances than “multi-firing” principal neurons. In contrast when the input resistances of all guinea pig pLSO neurons were plotted in a histogram, a continuous set of values was observed with no evidence of discrete modes. A Gaussian distribution could be fitted to the data (best-fit mean = $48.2 \pm 2.6 \text{ M}\Omega$, $R^2 = 0.60$, Figure 19). Furthermore when the number of action potentials evoked in each guinea pig pLSO neuron was plotted against its input resistance (Figure 20), no clustering or correlation was found (Pearson product-moment correlation, $r = 0.104$). Both findings substantiate the conclusion that only a single subtype of principal neuron exists in the guinea pig LSO.

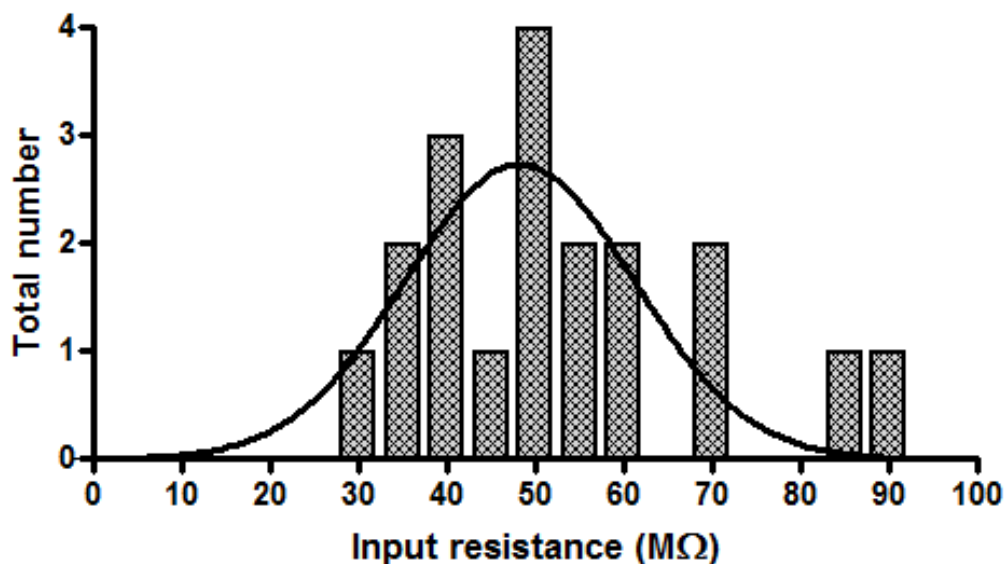


Figure 19. Histogram displaying the range of input resistances across the guinea pig pLSO neuronal population. A standard Gaussian distribution gave a good fit of the data ($R^2 = 0.58$), suggesting that pLSO neurons had been sampled from a continuous population.

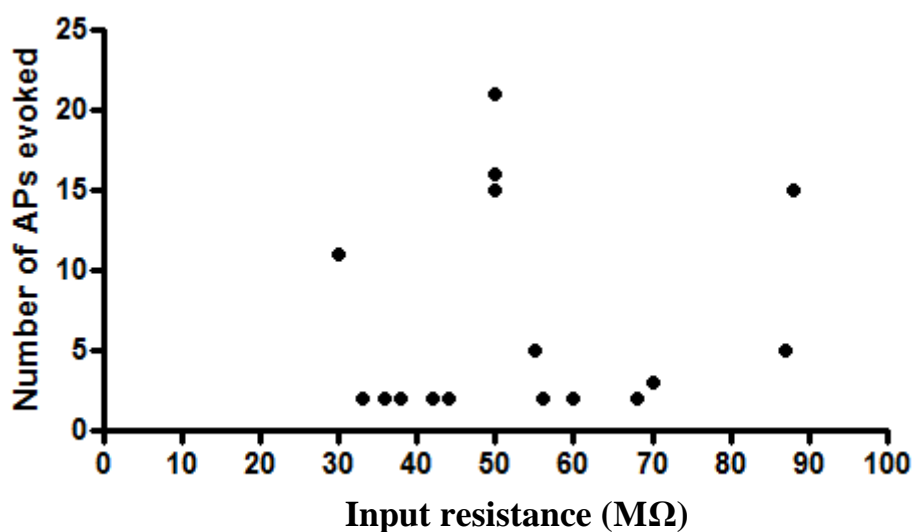


Figure 20. Number of action potentials evoked plotted against the input resistance of guinea pig pLSO neurons (*same as those in figure 18*). No correlation could be derived between the two parameters.

Other passive properties of guinea pig pLSO neurons also negate the existence of two subtypes

The membrane time constant ($\tau = \text{input resistance} \times \text{capacitance}$) provides a very basic assessment of how rapidly a neuron can integrate synaptic inputs at its soma passively, as well as offering an insight into a neuron's size. To determine whether different subtypes of guinea pig pLSO neurons could be distinguished based on their membrane time constants; a histogram plotting all values was produced in Figure 21. Although the distribution of pLSO neurons appeared continuous (see above), suggesting that no pLSO subpopulations do exist in the guinea pig LSO; it is interesting to note that almost half of the populations (8/19) possessed membrane time constants of either a millisecond or less. These values are therefore comparable to those calculated for principal neurons in the gerbil and guinea pig MSO (0.3ms (gerbil, Scott et al, 2005) and $0.50 \pm 0.07\text{ms}$ (n =10, guinea pig, Donato, personal communication)).

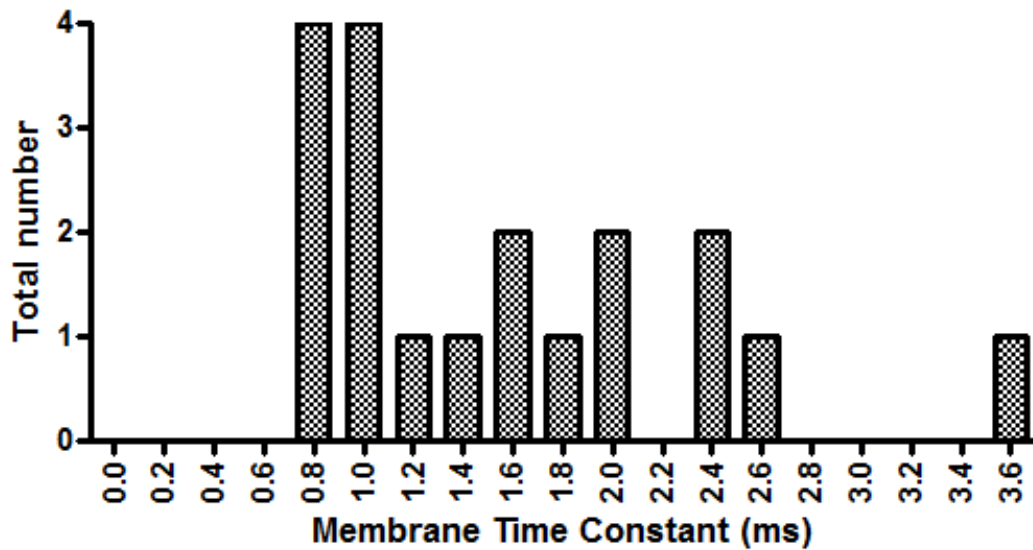


Figure 21. Histogram displaying the range of membrane time constants across the guinea pig pLSO neuronal population. Although skewed towards lower membrane time constants, the dataset appeared continuous.

Since the membrane time constant of a neuron is the product of its input resistance and capacitance, guinea pig pLSO neurons' membrane time constants were plotted against their input resistances in Figure 22. A positive correlation was evident with no visible clustering (slope of linear fit = 0.04 ± 0.007 mV/ms ($R^2 = 0.58$)), suggesting that the population of pLSO neurons displayed a continuous range of capacitances. A histogram of all capacitance values in the guinea pig pLSO population indeed demonstrated the existence of such a continuum (Figure 23): 15/19 (80.0 %) of the principal neurons possessing capacitances between 16pF and 34 pF. As the capacitance of a neuron is correlated with the amount of membrane it possesses, this result points to a continuous range of sizes for guinea pig pLSO neurons

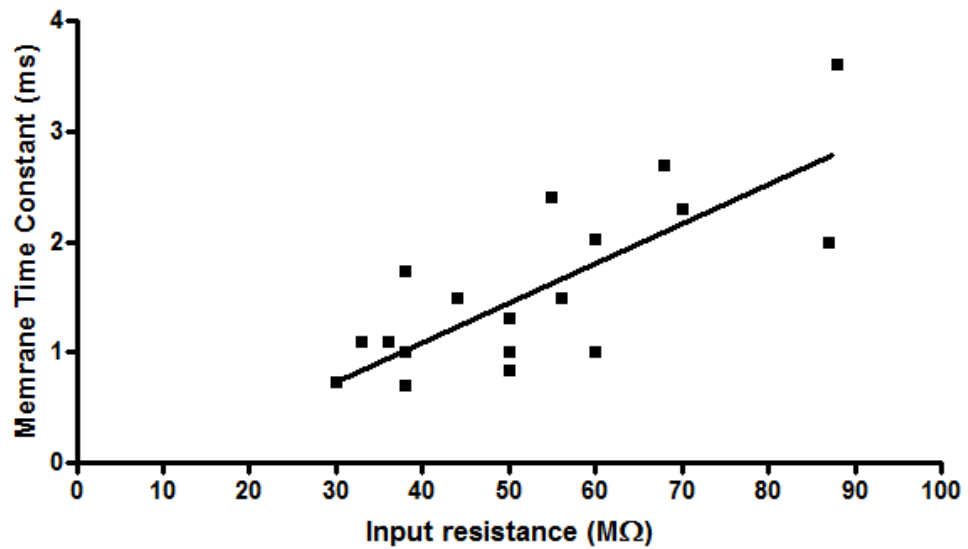


Figure 22. The input resistance of guinea pig pLSO neurons plotted against their membrane time constants. A positive correlation was found between the two parameters [slope of linear fit = 0.04 ± 0.007 mV/ms ($R^2 = 0.58$)].

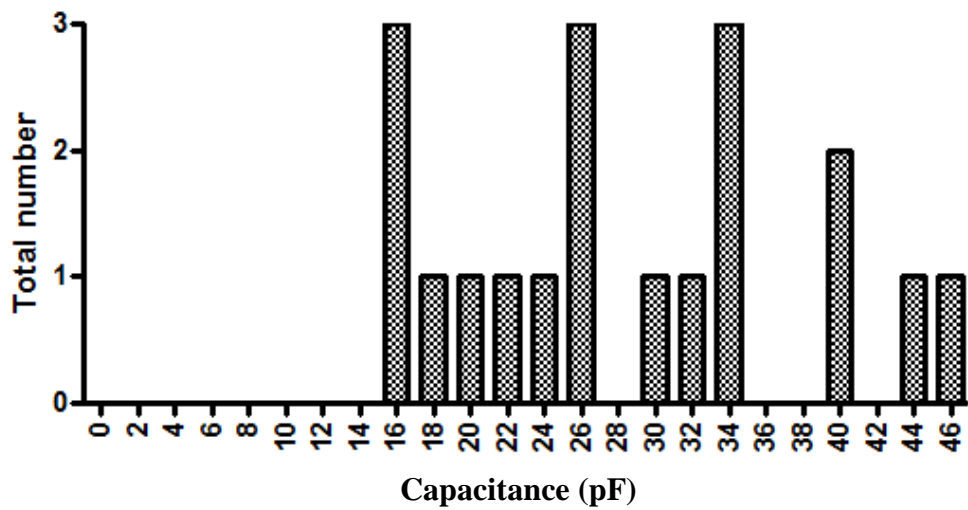


Figure 23. Histogram displaying values of capacitance across the guinea pig pLSO neuronal population.

A continuous dataset of potentials ranging from -40 to -65mV was also observed when the resting membrane potentials of guinea pig pLSO neurons were plotted as a histogram (Figure 24). Taking into account the results described above for guinea pig pLSO neurons' passive properties, it therefore will be assumed in the remainder of the analysis that the recordings in this study were sampled from a single population of guinea pig pLSO neurons whose intrinsic properties form a continuum.

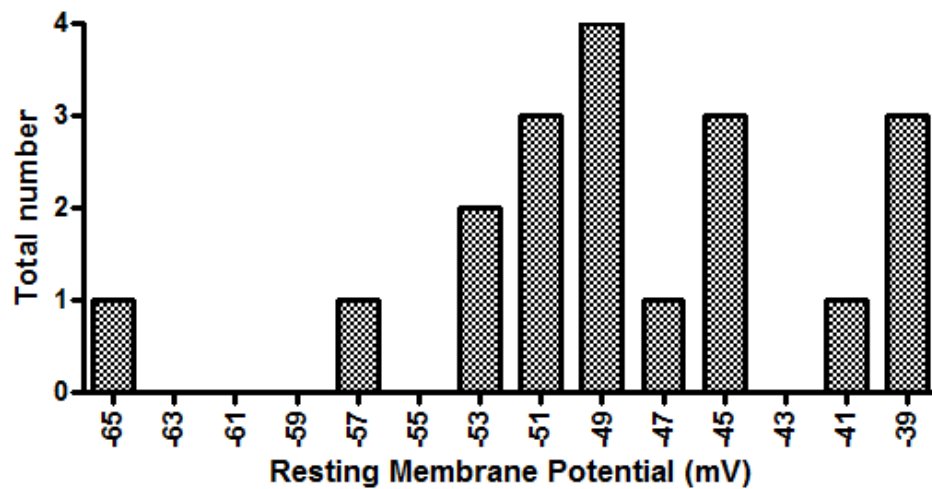


Figure 24. Histogram displaying the range of resting membrane potentials across the guinea pig pLSO neuronal population.

3.1.2 The intrinsic and firing properties of guinea pig pLSO neurons do not appear to develop postnatally.

Developmental changes in the passive properties of pLSO neurons have been observed in the gerbil and rat (Barnes-Davies et al, 2004; Magnusson et al, 2005); in both species hearing onset occurs postnatally (P12 in both species). Guinea pigs, on the other hand, have a precocious ability to hear *in utero*. It is therefore reasonable to expect that the dramatic postnatal changes observed in the passive properties of immature animals would not occur in a more developmentally (at birth) mature species. To satisfy the demand for guinea pigs to harvest brain tissue, animals of varying ages (P1-P19) were sacrificed in this study. As a result, trends in the development of guinea pig pLSO neurons' intrinsic and active properties could be monitored across a wide age range. Passive properties such as input resistance (Figure 25), resting membrane potential (Figure 26) and capacitance (Figure 27) remained constant across the first postnatal weeks whilst it was evident that the number of action potentials evoked by a large current step (between 1.25nA and 1.45nA) was not correlated with the age of the guinea pig (Figure 28). This suggests that guinea pig neurons possess mature passive properties from birth and the continuum of intrinsic/firing properties observed in the guinea pig LSO cannot be attributed to different developmental stages.

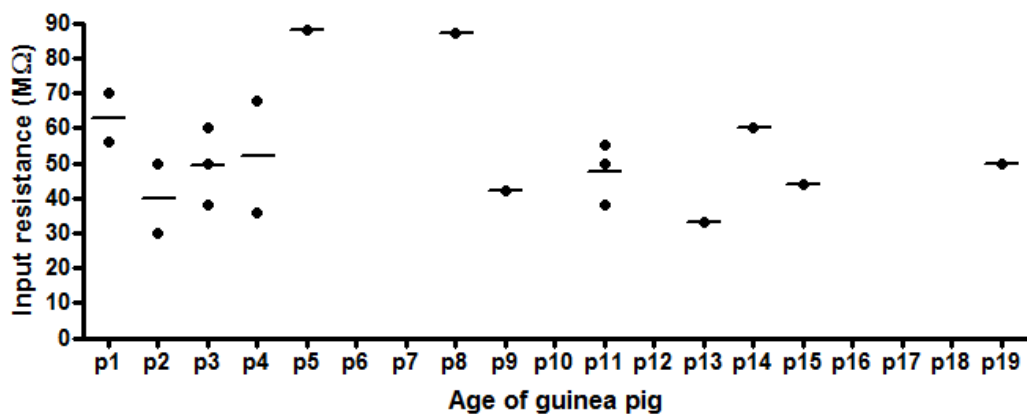


Figure 25. The input resistances of guinea pig LSO neurons arranged by the post-natal day of recording. No age-dependent trend was observed in this parameter.

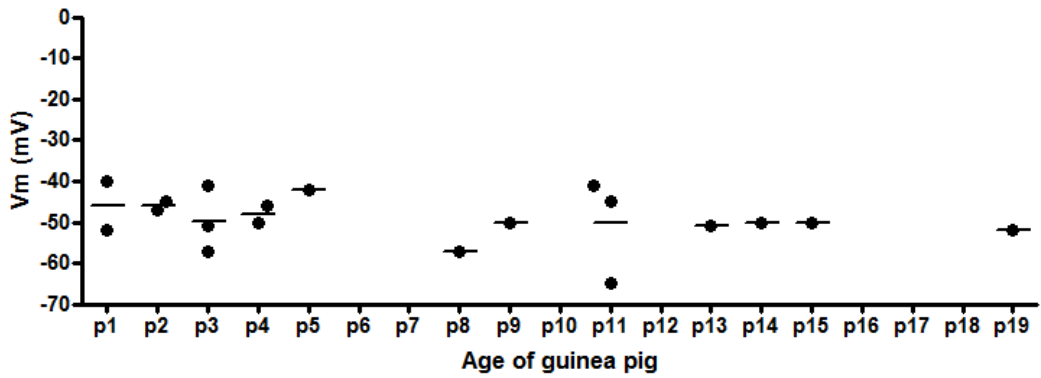


Figure 26. The resting membrane potentials of guinea pig LSO neurons arranged by the post-natal day of recording. No age-dependent trend was observed in this parameter.

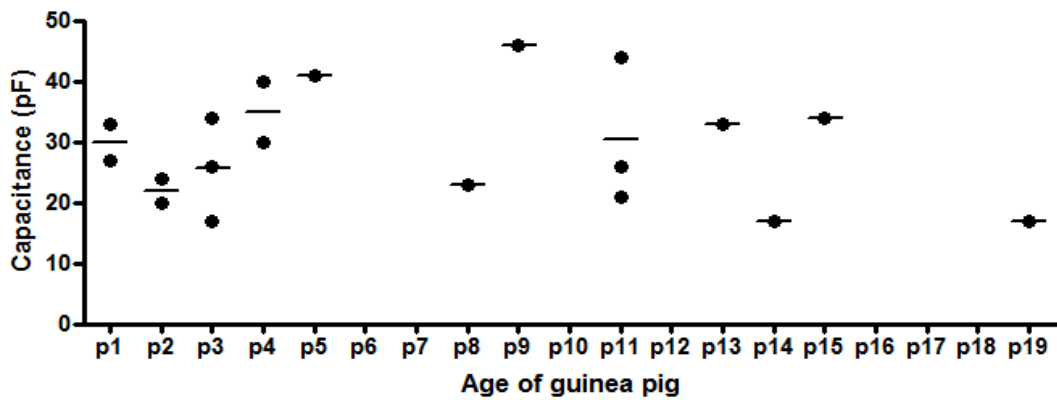


Figure 27. The values of capacitance of guinea pig LSO neurons arranged by the post-natal day of recording. No age-dependent trend was observed in this parameter.

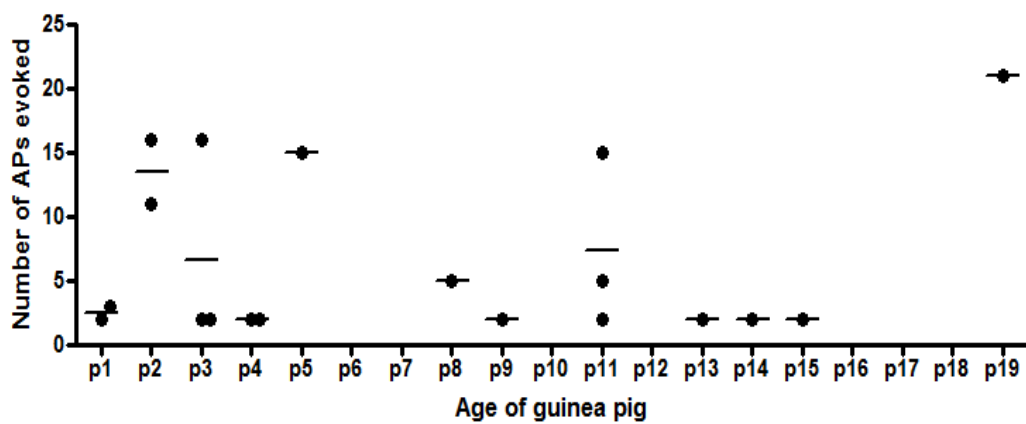


Figure 28. The number of action potentials evoked (in response to a depolarizing step between 1.25nA and 1.45nA in amplitude) in a guinea pig LSO neuron arranged by the post-natal day of recording. No age-dependent trend was observed in this parameter.

3.1.3 The tonotopic arrangement of guinea pig pLSO neuronal properties

Spatial segregation of single and multi-firing principal neurons has been observed in the LSO of post-weaned rats (Barnes-Davis et al, 2004); thus in order to establish whether their firing properties also correlated to their position in the LSO (and hence the tonotopic axis), guinea pig principal neurons were considered as belonging to either the medial or lateral limb (Figure 29). 7/19 (37%) pLSO neurons were from the medial limb whilst 12/19 (62%) pLSO neurons were patched in the lateral limb.

No significant difference was found between the average number of action potentials observed in a pLSO neuron from the medial (4.9 ± 1.8 action potentials, $n = 7$) and lateral limb (7.8 ± 2.1 action potentials, $n = 12$) ($p=0.37$, Independent two-tailed t-test).

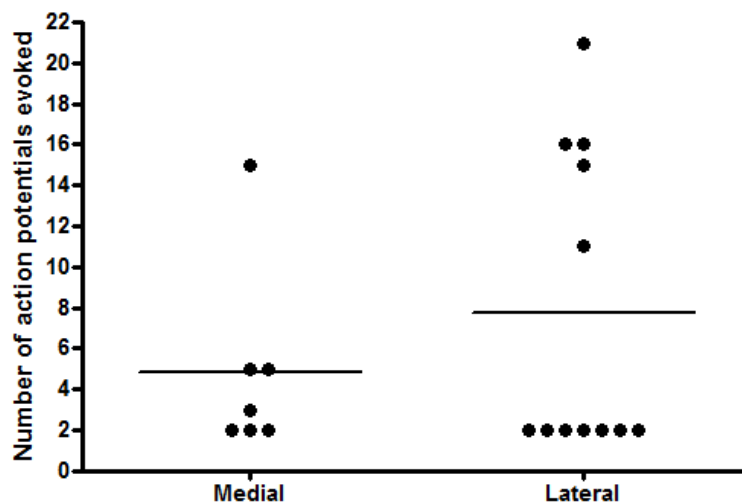


Figure 29. The number of action potentials evoked in guinea pig pLSO neurons from different LSO limbs. No significant difference was observed between the average number of action potentials evoked in a cell from either limb (Independent two-tailed t-test)

The input resistances of the guinea pig principal neurons in different regions of the LSO were also compared in Figure 30. The seven pLSO neurons in the medial limb possessed significantly larger input resistances (65.9 ± 7.2 M Ω) than the twelve pLSO neurons in the lateral limb (45.0 ± 2.6 M Ω) ($p < 0.01$, Independent two-tailed t-test). This result suggests that

input resistance of principal neurons might not vary according to different phenotypes (as in rats) but according to their location along the tonotopic axis in the guinea pig LSO.

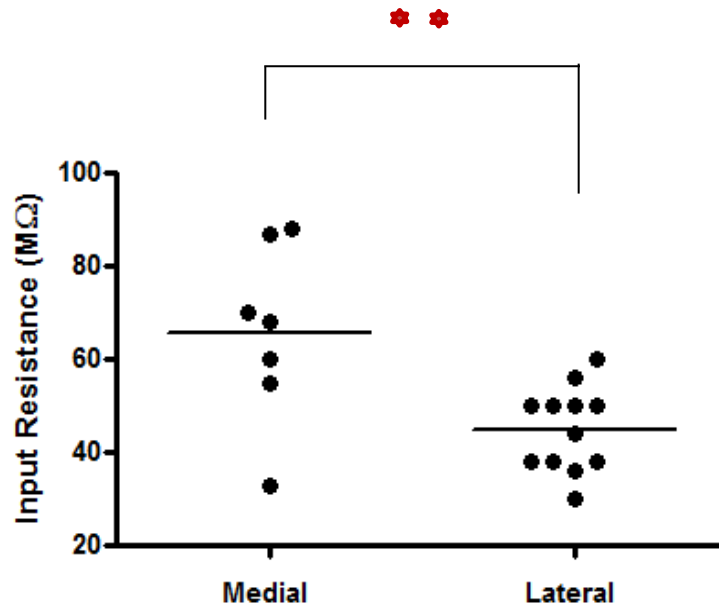


Figure 30. The input resistances of guinea pig pLSO neurons compared in different LSO limbs. The pLSO neurons in the lateral limb were significantly smaller than their medial counterparts ($p < 0.01$; Independent two-tailed t-test).

Given the functional implications of increased input resistances on a medial guinea pig pLSO neuron's ability to integrate rapidly changing level differences in envelope ITD cues, the membrane time constants of guinea pig pLSO neurons in either limb were next compared (Figure 31). Values of membrane time constants proved to be significantly larger in the medial (2.3 ± 0.3 ms) than in the lateral limb (1.1 ± 0.1 ms) ($p < 0.001$, Independent two-tailed t-test). If their passive properties are only considered, the present results would suggest that medial guinea pig principal neurons integrate synaptic inputs more slowly than their neighbouring neurons in the lateral limb and therefore may display different envelope ITDs processing.

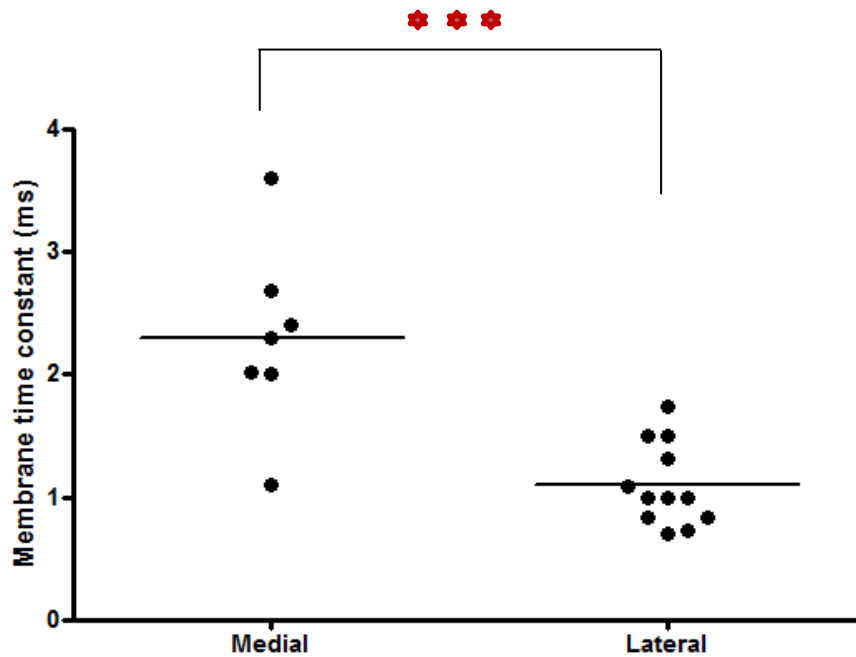


Figure 31. The membrane time constants of guinea pig pLSO neurons compared in different LSO limbs. The pLSO neurons in the medial limb possessed significantly longer membrane time constants than their medial counterparts ($p < 0.001$; Independent two-tailed t-test).

It was next determined whether pLSO neuronal capacitances varied in the two limbs and so contributed additively to the larger membrane time constants found medially (Figure 32). The average capacitance of a medial pLSO neuron (35.3 ± 2.6 pF) indeed proved to be larger than the average value calculated for a lateral pLSO neuron (25.2 ± 2.5 pF) ($p < 0.5$, Independent two-tailed t-test). As the capacitance is correlated with the size of a neuron (if the neuron is strictly spherical the C_m varies as the square of the cell diameter), it is therefore predicted that principal neurons from the medial limb of the guinea pig LSO are larger on average than those from the lateral limb. Combined with the larger input resistances in the medial limb, this difference in size could explain why longer membrane time constants were observed medially.

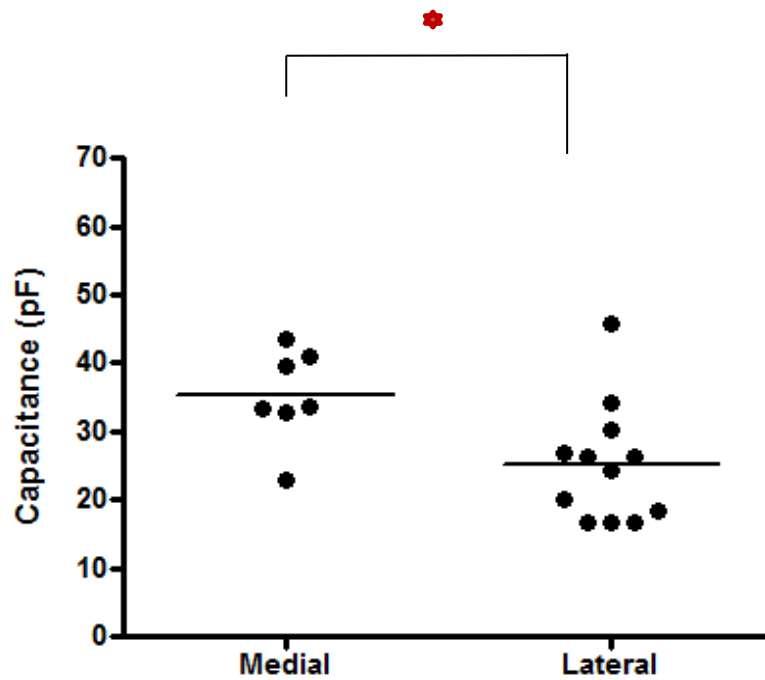


Figure 32. The capacitances of guinea pig pLSO neurons compared in different LSO limbs. The pLSO neurons in the medial limb possessed significantly larger capacitances than their lateral counterparts ($p < 0.05$; Independent two-tailed t-test).

In summary, a continuous population of principal neurons was found to exist within both limbs of the guinea pig LSO. Variations in of pLSO neurons' intrinsic properties were observed between the medial and lateral limbs however suggesting that these neurons may be segregated along the tonotopic axis with smaller, faster-integrating cells appearing in the lateral, low-frequency region of the nucleus. The implications of these differing intrinsic properties on fine structure and envelope ITD processing are discussed further in the general conclusions.

3.1.4 Resonance of guinea pig pLSO neurons.

Electrical resonance has been noted in a number of non-mammalian auditory systems (avians, reptiles and amphibians). In all cases, it has been speculated that resonance helps the sensory hair cells to filter inputs with improved frequency selectivity and therefore respond preferentially to specific acoustic stimuli (Art et al, 1986; Strohmann et al, 1994). To investigate whether similar ideas could be applied to the LSO, sub-threshold resonance was therefore probed in the guinea pig LSO using sinusoidal currents of linearly increasing frequency (a 'ZAP') to stimulate principal neurons (Figure 15). Subsequent voltage responses were analysed to create impedance profiles and resonance was identified in neurons with non-monotonic profiles (Figure 33). Of the eight pLSO neurons assessed, only two displayed resonant properties and hence were considered band-pass (filter) neurons (as opposed to neurons that display no such resonance and hence act as low-pass filters).

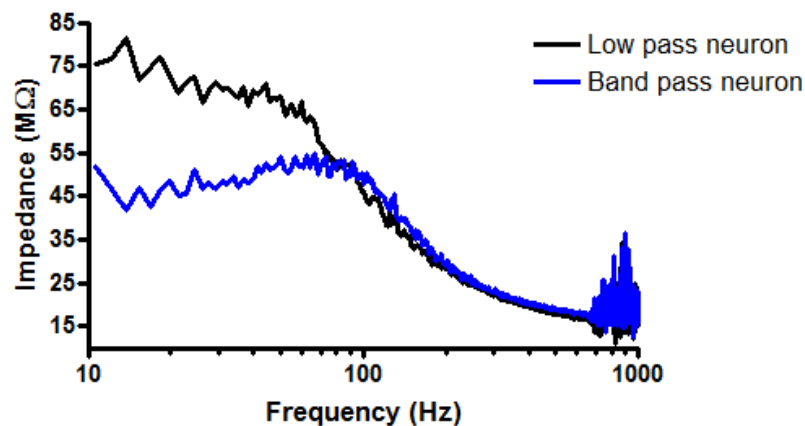


Figure 33 The impedance profile of two pLSO neurons demonstrates the existence of resonance. Impedance profiles were calculated using voltage responses to sinusoidal current injections called a ZAP. Resonance was observed as a peak in the profile around a specific frequency (*blue trace*), as opposed to an impedance profile where only the impedance was high at low frequencies and decreased monotonically with increasing frequency (*black trace*).

In order to characterize the resonant properties and determine how selective pLSO neurons might be to particular rates of synaptic input *in vivo*, measurements of peak resonant frequency and Q factor were made for both resonant pLSO neurons (Puil et al, 1986).

Although they can be considered as dampened resonators in comparison to non-mammalian hair cells (Average Q factor of pLSO neurons = 1.2 ± 0.02 , n=2) (Crawford and Fettiplace, 1980; Art et al, 1986), the average peak resonant frequency of the two pLSO neurons was 86 ± 15 Hz. This is between two and three orders of magnitude higher than has been previously reported for neurons in the mammalian central nervous system (Gutfreund et al, 1995; Hutcheon et al, 1996). Since low frequency resonances have also been proposed to underpin specific physiological roles in the olfactory bulb and the hippocampus (Skaggs et al,1996; Margrie and Schaeffer, 2003), the high peak resonant frequencies, observed here in the pLSO neurons, may signify their improved ability to integrate relatively fast input rates.

Hyperpolarization affects resonance in pSOC neurons; duration of the stimulus does not.

The observed resonances arise from the interplay of a neuron's active and passive electrical properties. In the simplest biophysical model of resonance, just two components are necessary to account for resonant behaviour: 1) a membrane that acts as a low pass filter and 2) a voltage-gated conductance whose activation lags the membrane time constant and therefore acts as a high pass filter (Hutcheon and Yarom, 2000). The fast kinetics and constitutive activation at a holding potential of -55mV make I_{KLT} a prime candidate for the voltage-gated conductance underlying high frequency resonance in pSOC neurons. Since I_{KLT} can be inactivated at hyperpolarized potentials, injecting a negative, hyperpolarizing DC current step during the ZAP protocol should reduce or abolish sub-threshold resonance in pSOC neurons.

To determine whether hyperpolarization led to a reduction in resonance, one of the resonant pLSO neurons was hyperpolarized by 5mV during stimulation with the ZAP protocol (Figure 34). The peak resonant frequency shifted from 71Hz under control conditions to 60Hz in the hyperpolarized state whilst the Q factor value also decreased from 1.18 to 1.05.

This would support the notion that the low-threshold K^+ conductance is the main contributing conductance to the resonance in these neurons.

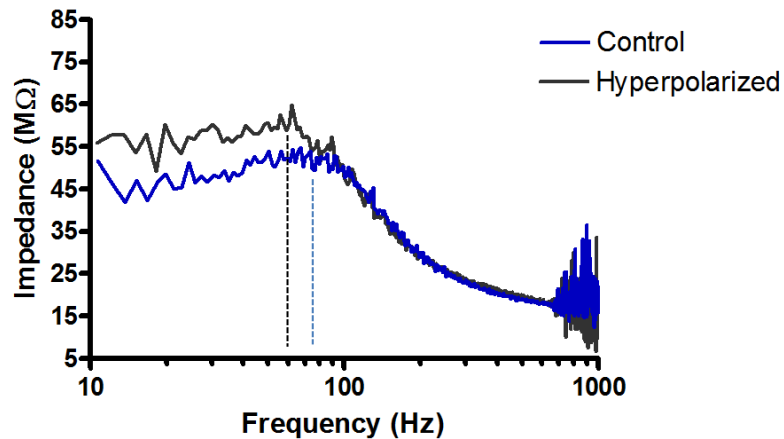


Figure 34. Hyperpolarization of a pLSO neurons led to the reduction of resonance. A pLSO neuron was hyperpolarized by 5mV before being assessed for resonance again. The resonance peak frequency decreased from 71Hz in the control (*blue trace*) to 60Hz in the hyperpolarized condition (*black trace*). The Q value also decreased from 1.18 to 1.05 when the neurons were hyperpolarized.

Resonance along the tonotopic axis in guinea pig pLSO neurons.

If resonance is a phenomenon specifically associated with ITD coding, its existence might be expected in regions of the SOC nuclei known to process ITDs such as the lateral limb of the LSO (Tollin and Yin, 2005). In order to test this hypothesis, the resonant properties of the eight pLOC neurons were correlated with their positions along the tonotopic axis of the LSO by superimposing their location onto the schematic of an LSO nucleus. Three of the eight principal neurons were found in the lateral, low-frequency limb including both resonant neurons; the five remaining pLSO neurons were located in the high-frequency medial limb and displayed low-pass properties.

This suggests that pLSO neurons may be arranged so that neurons possessing resonance are found in the low-frequency limbs of the LSO. The function of such a sub-threshold resonance in pSOC neurons is discussed in the general conclusions.

3.1.5 Comparison with rat pLSO neurons indicates species differences.

It has been proposed that technical differences between studies could underlie the variations in pLSO neuronal firing patterns observed across species (Walcher et al, 2011). To determine whether this could explain the present findings from the guinea pig LSO, a small number of recordings was also made in the rat LSO, allowing the rudimentary comparison of their firing properties with those of rat pLSO neurons described in previous studies (Adam et al, 2001; Barnes-Davies et al, 2004).

Using the same criteria applied to identify rat pLSO neurons in previous studies [presence of I_H conductance as well as short latency action potentials and first inter-spike intervals (Adam et al, 2001; Barnes-Davies et al, 2004)], 6 of the 9 neurons patched were considered to be principal neurons (Figure 35). The average values of input resistance, membrane time constant and capacitance of these 6 rat pLSO neurons were $80 \pm 20 \text{ M}\Omega$, $2.3 \pm 0.7 \text{ ms}$ and $30.04 \pm 5.9 \text{ pF}$ respectively. The three remaining rat neurons, excluded on the basis of their voltage responses, displayed average input resistance and membrane time constant of $303 \pm 173 \text{ (SD) M}\Omega$ and $11 \pm 5.8 \text{ (SD) ms}$ respectively and thus were likely rat LOC neurons given their similarity to values previously reported in rat LOC neurons [$445 \pm 191 \text{ (SD) M}\Omega$ and $18 \pm 11.7 \text{ (SD) ms}$; Fujino et al, 1997]. The firing properties of these three rat LOC neurons were not studied further.

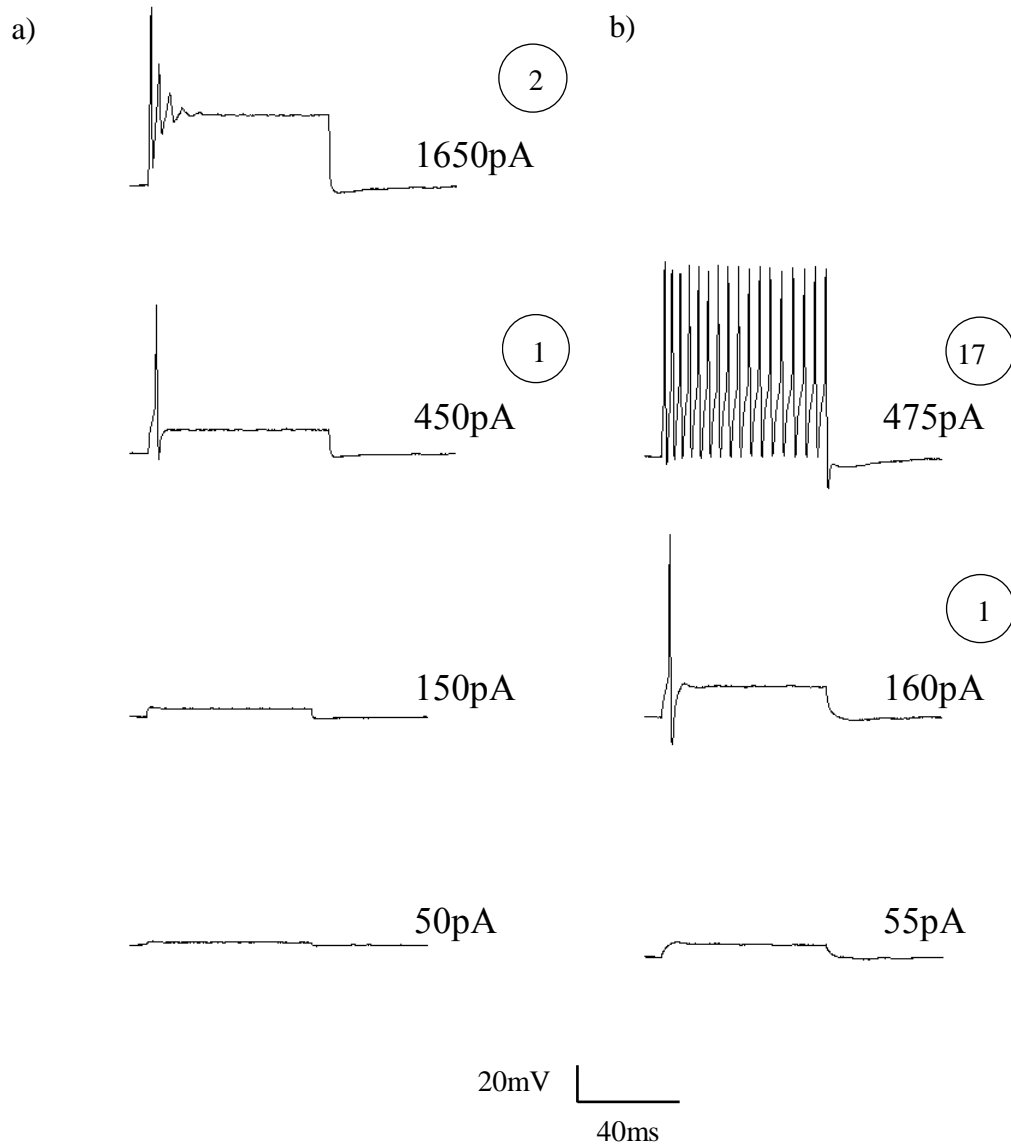


Figure 35. Voltage responses of rat type 1 (a) and type 2 (b) pLSO neurons to 80ms depolarizing current steps (step amplitude shown on right of traces). The input resistance of the encircled figure represents the number of APs evoked at that current injection. The type 1 neuron typically responded with a single onset AP (a, second panel from top) however at current steps of 850pA and above, two APs were elicited. The type 2 pLSO neuron already responded maximally at 475pA. (b, top)

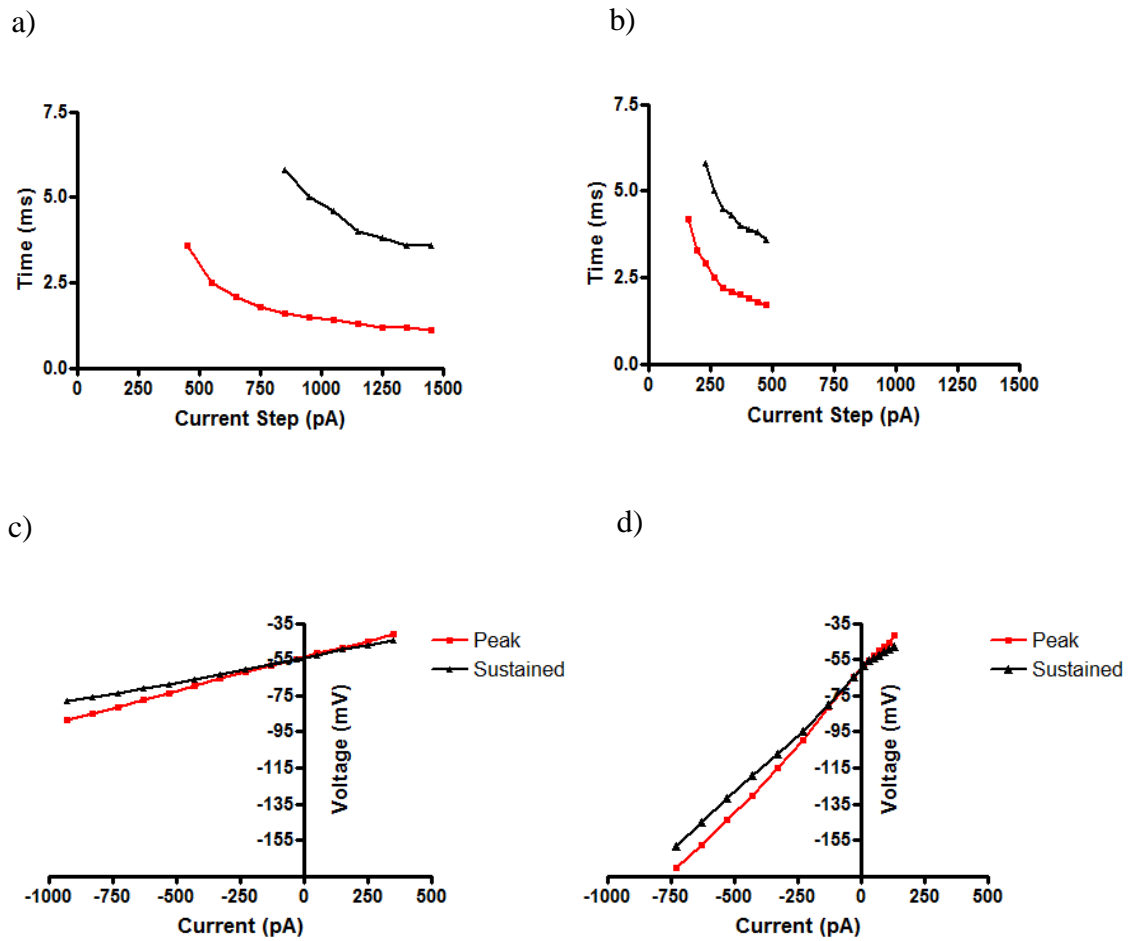


Figure 36. The electrophysiological properties of the two pLSO neurons in Figure 35. The latency of the onset AP (*red trace*) and the interval between the 1st and 2nd AP (*black trace*) were plotted for the type 1 (*a*) and type 2 (*b*) in figure 35 (ISI was calculated for the type 1 cell as it responded with a second AP above 850pA). Both parameters decayed with increasing current step size, eventually reaching a stable minimal value at the highest current steps. Subthreshold IV profiles of the type 1 (*c*) and type 2 (*d*) cells displayed non-linearities especially in the hyperpolarizing direction.

A histogram displaying the number action potentials evoked by a large depolarizing current step (between 0.6 and 1 nA) in the six rat pLSO neurons demonstrated that this case does show a divide between neurons that fired only twice (3/6 or 50%) and those that fired ten or more action potentials (3/6 or 50%) (Figure 37). This result is similar to the “single-firing” and “multi-firing” neurons described by Barnes-Davies and colleagues (2004). It should be noted however that the “single-firing” cells described in the previous study appeared to fire more than one action potential at current steps greater than 850pA. For this reason “single-firing” and “multi-firing” neurons are called “type 1” and “type 2” neurons respectively when referring to rat pLSO neurons patched in this study..

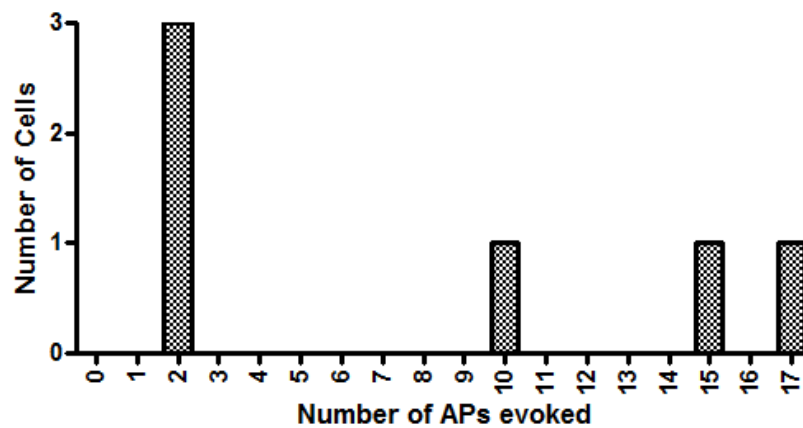


Figure 37. Histogram displaying the number of action potentials potentially evoked across the rat pLSO neuronal population. The number of action potentials was counted in response to a depolarizing step between 0.6 and 1nA. A discontinuity between neurons that fired only two action potentials in response to such a large depolarizing step and those that fired ten or more existed.

In the study by Barnes-Davies and colleagues (2004), the two classes of rat pLSO neuron were also distinguished by their differing input resistances: “multi-firing” pLSO neurons possessing significantly higher input resistances than their “single-firing” counterparts. In line with this finding, the individual input resistances of the three rat type 2 pLSO neuron (average input resistance = $120 \pm 20 \text{ M}\Omega$) proved to be larger than those of the three type 1 rat pLSO neurons (average input resistance = $39 \pm 8.2 \text{ M}\Omega$) (Figure 38).

The present study therefore supports the finding that rat pLSO neurons can be separated into discreet groups based on their firing patterns and passive properties. In contrast to the observations made in the guinea pig LSO, the present results suggests that there may indeed be a biological origin for the reported difference in properties of principal neurons between the two species.

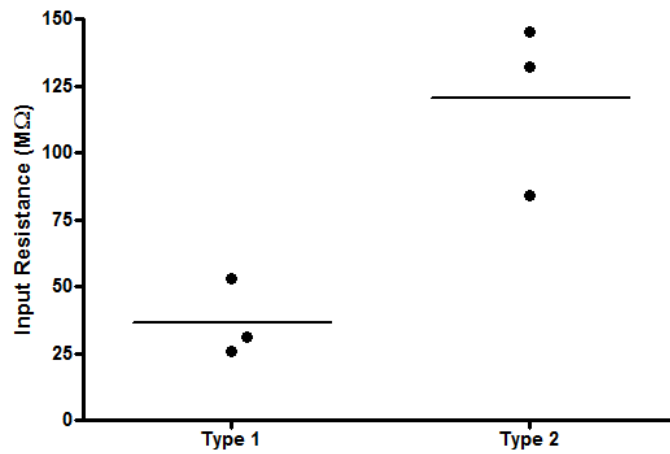


Figure 38. Input resistances of type 1 and type 2 rat pLSO neurons. Although statistical tests were not performed due to the dataset size, values for all type 2 neurons were larger than those observed in type 1 neurons. The average input resistances of type 1 and type 2 neurons are demarcated by horizontal lines (Type 1 = $39 \pm 8.2 \text{ M}\Omega$, n= 3 Vs Type 2 = $120 \pm 20 \text{ M}\Omega$, n= 3)

3.2 Synaptic properties

Electrical stimulation of the contralateral trapezoid body fibres was performed in all 20 guinea pig pLSO neurons however only 12/20 (60%) of these neurons displayed synaptically evoked, post-synaptic potentials (PSPs). The motive for this analysis was to understand how the active and passive properties of pLSO neurons might determine the shape of PSPs at their somatic integration sites. Possible ramifications of differing response properties were then considered with binaural processing in mind.

Although excitatory or inhibitory PSPs were not isolated pharmacologically in this study, the experimental conditions designated Cl⁻ or cation-mediated PSPs with opposite polarities. In these recordings, stimulation almost always resulted in a monophasic potential exhibiting either net membrane depolarization or hyperpolarization overall. Hence, in this section, I refer to the former as dPSPs (depolarizing PSPs) and the latter as hPSPs (hyperpolarizing PSPs).

3.2.1 Excitatory Inputs

Excitatory inputs and the LSO tonotopic axis

dPSPs were observed in 6/12 (50%) pLSO neurons, suggesting that excitatory inputs arising from the contralateral AVCN are common in guinea pig LSO. Extracellular recordings made in the lateral limbs of several species' LSOs have emphasized the predominance of contralateral excitation in low-frequency pLSO neurons (Batra et al, 1997; Tollin and Yin, 2005). In the guinea pig, half (3/6) of the contralaterally excited pLSO neurons were found

in the lateral limb of the LSO. Analysis of medial cells is not shown here due to the small sizes of the depolarization evoked ($<2\text{mV}$) and the irregular occurrence of dPSPs in regular trains.

Time course of depolarizing PSPs in the LSO

The sub-millisecond temporal sensitivity of pMSO neurons in response to acoustic stimulation in vivo requires the existence of short-lasting dPSPs (Chirila et al, 2007; Jercog et al, 2010); pLSO neurons, on the other hand integrate input more slowly, typically responding to depolarizing current steps with several action potentials. It might therefore be expected that they would process synaptic inputs more slowly. Indeed the time course of the average dPSP in an example pLSO neurons proved to be twice as long as the time course of the average dPSP in an example pMSO neuron patched by Roberta Donato (8.3ms Vs. 4.2ms, Figure 39b).

In order to calculate the average half-width of dPSPs recorded across the 3 pLSO neurons, analysis was restricted to a range of dPSP amplitudes (between 3 and 6mV) as a neuron's membrane potential can alter its membrane time constant. Since the average amplitude of the first dPSPs in the three guinea pig pLSO neurons was $10.8 \pm 1.0 \text{ mV}$, it was necessary to select dPSPs evoked within the first 5 current pulses to make the calculation possible. The average half-width of the dPSPs in guinea pig pLSO neurons was $2.71 \pm 0.2\text{ms}$.

The relatively short-duration dPSPs in the MSO can be attributed to their rapid rise times and decays (Figure 39b). Both the rising and falling phases of dPSPs are influenced heavily by the action of the low-threshold K^+ conductance, I_{KLT} (Mathews et al, 2010), which not only contributes to the input resistance and membrane time constant at rest, but also determines the decay phase, underlying the after-hyperpolarization that is typically observed following a dPSP (Magnusson et al, 2005; Scott et al, 2005; Mathews et al, 2010). In the

guinea pig pLSO neurons, the average rise time of dPSPs in the three pLSO neurons was 1.22 ± 0.15 ms whilst the average decay time was calculated as 3.08 ± 0.61 ms. In addition to the slow decay, no after-hyperpolarization was ever observed following amplitude-matched dPSPs in the LSO (Figures 39 *a* and *b*).

This slow average rise and decay in pLSO neurons likely results from longer membrane time constants as well as fewer active membrane conductances determining dPSP temporal profiles. The absence of after-hyperpolarization in the LSO especially suggests a lack of an active K^+ conductance during the decay phase; thus it would appear that I_{KLT} may not be as abundant in pLSO neurons as has been previously demonstrated in pMSO neurons (Mathews et al, 2010).

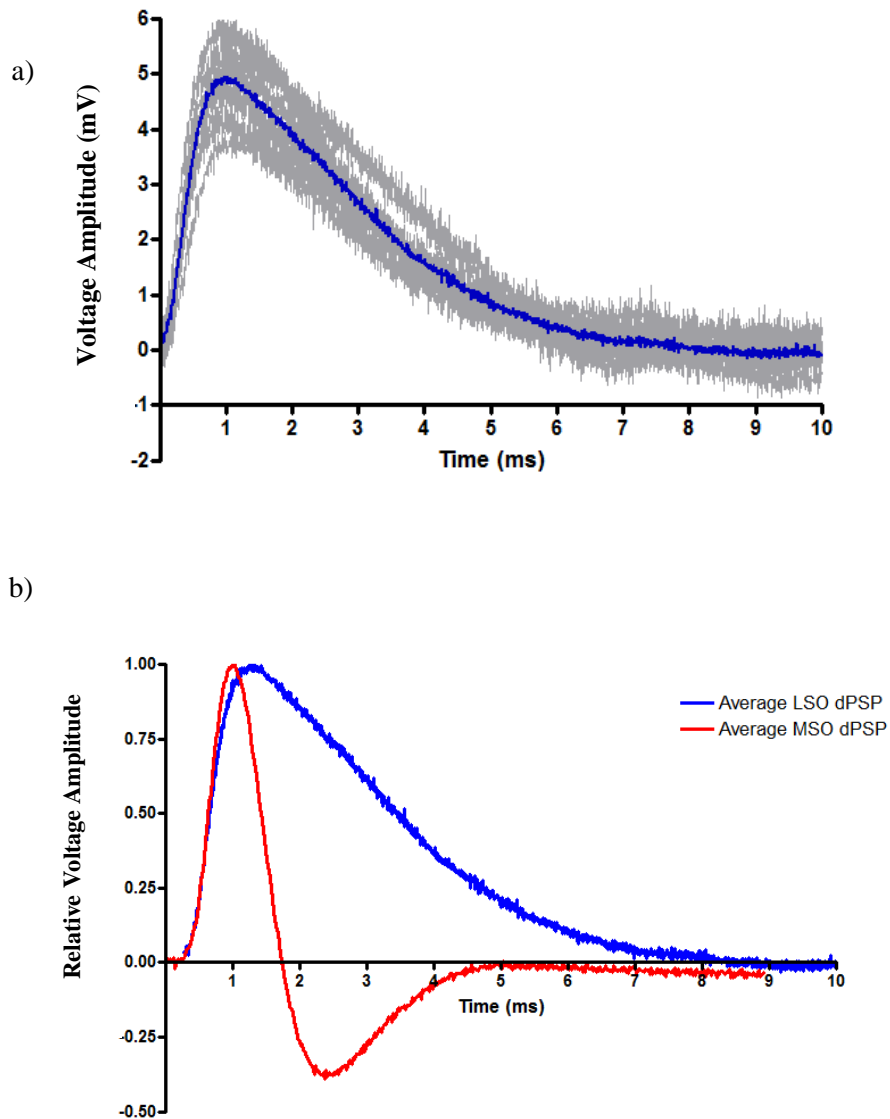


Figure 39. Depolarizing post-synaptic potentials in the LSO and MSO (latter patched by Roberta Donato). Voltage traces (*grey lines*) depict aggregated dPSPs evoked in a single guinea pig pLSO neuron (*a*). The average of these traces is shown in *blue* (the peak amplitude of the average dPSP in the pLSO neuron was 5.0mV). dPSPs were amplitude-matched in order to compare times courses with a pMSO neuron (between 3 and 6mV). The duration of the pLSO neuron's average dPSP was much longer than encountered in a guinea pig pMSO neuron (*red trace*) (*b*): both traces were normalised to peak amplitude. The average rise time of first dPSPs in the example pLSO neuron was significantly longer ($0.67 \pm 0.03\text{ms}$) than in the pMSO neuron ($0.5 \pm 0.01 \text{ms}$) ($p < 0.05$, Independent two-tailed t-test). A hyperpolarization commonly followed the dPSP in the pMSO neuron (Input resistance = $15\text{M}\Omega$). Values of input resistance and membrane tau in the pLSO neurons were $30\text{M}\Omega$ and 0.7ms ; whilst in the pMSO neuron, they were $10\text{M}\Omega$ and 0.2ms .

Relationship between the time course and the peak amplitude of dPSPs

In the gerbil MSO, it has been demonstrated that dendritic I_{KLT} ensures that the half-width of a simulated dPSP (i.e. one in which current is injected dendritically and responses recorded somatically) decreases with increasing peak amplitude of the PSP (Mathews et al, 2010). This may improve coincidence detection by sharpening the integration window for even the largest PSP amplitudes (Mathews et al, 2010). Similarly, data from the guinea pig MSO has also shown that dPSP half-widths are independent of the voltage of their peak amplitude when stimulated electrically (Mikiel-Hunter et al, ARO 2010).

Given that spherical bushy cells of the AVCN provide the excitatory drive to pMSO and pLSO neurons and have been shown to fire at up to a few hundred Hertz *in vivo* (Rhode and Smith, 1986; Winter and Palmer, 1990; Smith, 1993; Kunzel et al, 2011); pLSO neurons are likely to integrate convergent excitatory inputs at high rates over prolonged durations. As models of ILD encoding propose that synaptic responses in pLSO neurons are proportional to the intensity of the stimulus at that ear (Tollin, 2003), it might be expected that a single dPSP, arising from a higher intensity acoustic stimulus, would induce a greater depolarization and in so doing potentially promote the summation of multiple dPSPs. A means of achieving this would be for half-widths of dPSPs to increase with peak amplitude as stimuli get louder.

To study how the peak amplitude affected the kinetics of differently-sized dPSPs in the LSO, half-widths were plotted as a function of peak amplitude for the first five (amplitude-unmatched) dPSPs of each stimulus train in the example pLSO neuron from Figure 39. The slope of the linear fit was 0.20 ± 0.008 ms/mV which was significantly different than the slope of the linear fit calculated for the example pMSO neuron in Figure 40 (0.002 ± 0.007 ms/mV; Donato, personal communication) [$p < 0.005$, comparison of linear regression lines (Zar, 1984)]. Across the 3 lateral guinea pig pLSO neurons, a significant positive correlation was also observed between the two parameters (neuron 1, 2 and 3 = $p < 0.0001$,

0.0001, 0.0001 and $r = 0.79, 0.62$ and 0.55 ; Pearson product product-moment correlation) and the average slope of the fit by linear regression was $0.14 \pm 0.03 \text{ms/mV}$. This indicates that, in contrast to what has been observed for gerbil and guinea pig pMSO neurons, the half-widths of dPSPs in pLSO neurons increased with their amplitude. This supports the idea that principal neurons in the LSO extract intensity information from contralateral excitation by integrating synaptic input.

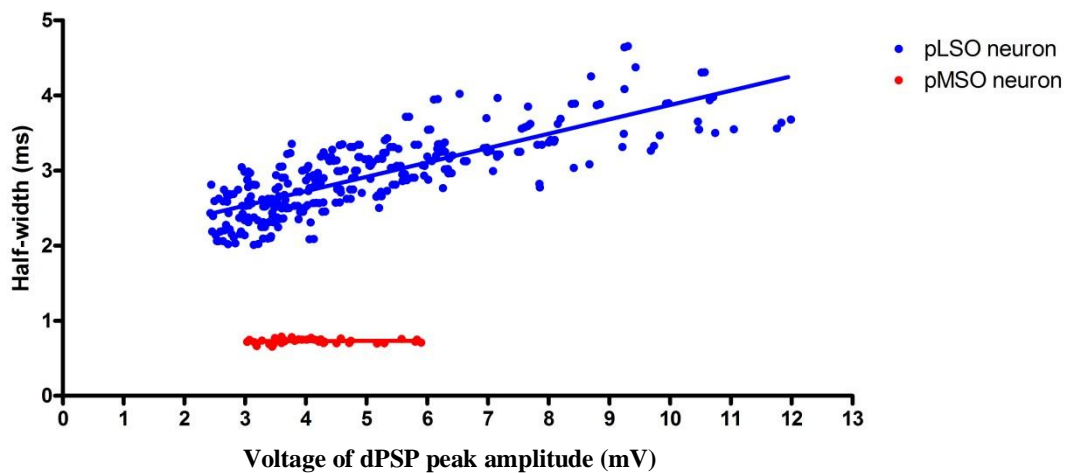


Figure 40. Half-widths were plotted as a function of peak amplitudes for the first five dPSPs evoked by a pulse train in a representative example pLSO neuron (*blue*) and pMSO neuron (*red*) (same neurons as in Figure 38 *b*). dPSPs were not amplitude-matched in this graph. The slope of the fit for the pLSO and pMSO distribution were significantly different [$p < 0.005$, comparison of linear regression lines (Zar, 1984)].

Short term plasticity of dPSP amplitude

Studies in the avian *nucleus angularis* have shown that neurons processing intensity information possess excitatory inputs with varying degrees of short term synaptic facilitation (STSF) and depression (STSD) (Macleod et al, 2007). It has been proposed that those neurons combining facilitation with depression compensate for neurons with pure depression by helping to convey intensity information concerning ongoing stimuli. Since on-going component of signals contain level and temporal information necessary for envelope ITD

processing, encoding them is vital to principal neurons in the high frequency, medial limb of the LSO. It therefore might be expected that the population of pLSO neurons would reflect this heterogeneity with some neurons purely depressing and others displaying either some facilitation or just steady amplitude across pulse trains. Although measurements were performed here in current clamp, the effects of short term synaptic plasticity should be mirrored in the dPSP amplitude at non-summing frequencies of response.

In order to determine whether STSD or STSF affected contralaterally-derived dPSP amplitudes in the guinea pig LSO, the average amplitudes of dPSPs were normalised to the peak value and presented in the order they were evoked by the stimulus train (Figure 41). Three of the contralaterally-excited pLSO neurons in the guinea pig, stimulated with 50Hz synaptic inputs, displayed depression from similar initial peak amplitudes (10.8 ± 1.0 mV); the average normalized steady state amplitude was 0.35 ± 0.02 and the average τ was 57ms. This suggests that dPSPs in the LSO do indeed experience STSD. When a small negative current was injected to change the baseline potential from -55mV to -40mV during the pulse train, there was no difference in the degree of STSD (steady state amplitude was 0.34 in both conditions), suggesting that synaptic mechanisms underlying STSD are unaffected by postsynaptic membrane potential and are therefore likely presynaptic.

The frequency dependence of STSD was not tested comprehensively due to the limited number of the frequencies tested in each cell; however, the 1kHz train in Figure 41 *b1* suggested that some STSF could exist as dPSPs following the first response were of a similar size or larger. It is unlikely that this shares a similar biophysical explanation with the STSF observed at low frequencies in the *nucleus angularis* (Macleod et al, 2007). Indeed it is more likely to be an epiphenomenon of any presynaptic mechanism that secured synaptic transmission at this high frequency.

In summary, these findings suggest that STSD was prevalent at synaptic input rates of 50Hz and at 100Hz (Figure 42). Since the average spike frequency rate was ~63Hz for a 1kHz

stimulus, the apparent facilitation is unexpected given the STSD at 50 and 100Hz. Alongside the preservation of temporal information observed at 1kHz in Figure 42 *b1*, this “normalization” of dPSP amplitude could potentially be important to the processing of envelope ITDs.

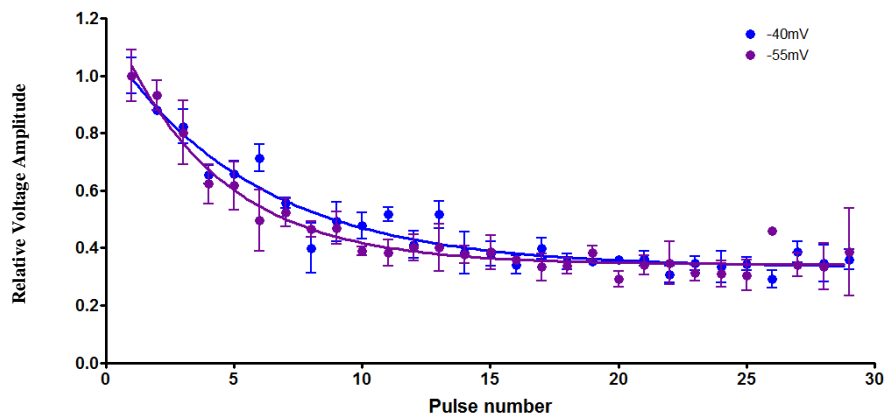


Figure 41. Depression of dPSP amplitude evoked by 50Hz electrical pulse trains in a single guinea pig pLSO neuron (*purple data*) (Same as in Figure 39 and 40). dPSPs were normalised to the amplitude of the first response. The strength of STSD, evoked at 50Hz was not dependent on the postsynaptic baseline potential (*blue data*) (F-test). Steady state amplitude was 0.34 in both conditions.

Stimulus frequency and summation of dPSPs

Recordings made from the LSO of mice, employing sharp glass-pipette recording electrodes, have shown that pLSO neurons can respond with an AP to each current pulse somatically injected in a train at frequencies up to 143Hz (Wu and Kelly, 1993). Some temporal summation was observed at frequencies above 333Hz, with the incrementally increasing voltage response eventually reaching threshold for AP generation. It has been shown that membrane conductances such as the hyperpolarized-activated mixed cationic conductance, I_H , help reduce temporal summation of dPSPs in mouse pLSO neurons at an input frequency of 50Hz (Leao et al, 2011). Located dendritically, I_H reduces the input resistance and

membrane time constant of this compartment, preventing asynchronous dPSPs from summing and helping pLSO neurons to phase-lock to the amplitude envelope of high frequency sounds (Leao et al, 2011). To determine the ability of the lateral guinea pig pLSO neurons to follow different frequencies inputs without summation, trains of dPSPs evoked by electrical stimuli of 3 different frequencies (50Hz, 100Hz and 1kHz) were analysed as were the inter-event interval between successive dPSP responses (Figures 42 and 43).

Individual depolarizing responses were observed after every stimulation artefact at 50Hz (Figure 42 *a1*) and at 100Hz (Figure 43 *a*). Considering that the durations of single dPSPs were between 6 and 10ms long, it is evident that no temporal summation will occur at frequencies lower than 100Hz. Therefore it would appear that the inability of pLSO neuron's postsynaptic membrane to integrate dPSPs more rapidly is probably implicated in setting the upper frequency limit for temporal summation at lower frequencies.

Although a 1kHz stimulus train was much higher than this frequency limit, it was surprising to find that no indication of any temporal summation (Figure 42 *b1*). The absence of summation in pLSO neurons at 1kHz likely occurs because trains of current pulses fail to translate into a high rate of synaptic responses: an issue that is likely underplayed by a presynaptic mechanism. It should be noted however that this high failure rate did not lead to random generation of dPSPs as temporal information was still preserved by dPSPs precisely timed across trials at 1kHz (Figure 42 *b2*).

In summary, these findings suggest that non-summing responses can be evoked after every pulse in train of up to 111-166Hz in the guinea pig. Since this is much lower than the 250Hz limit that has been observed in recordings from pMSO neurons patched in the same species, it would appear that pLSO neurons operate more slowly in the temporal domain

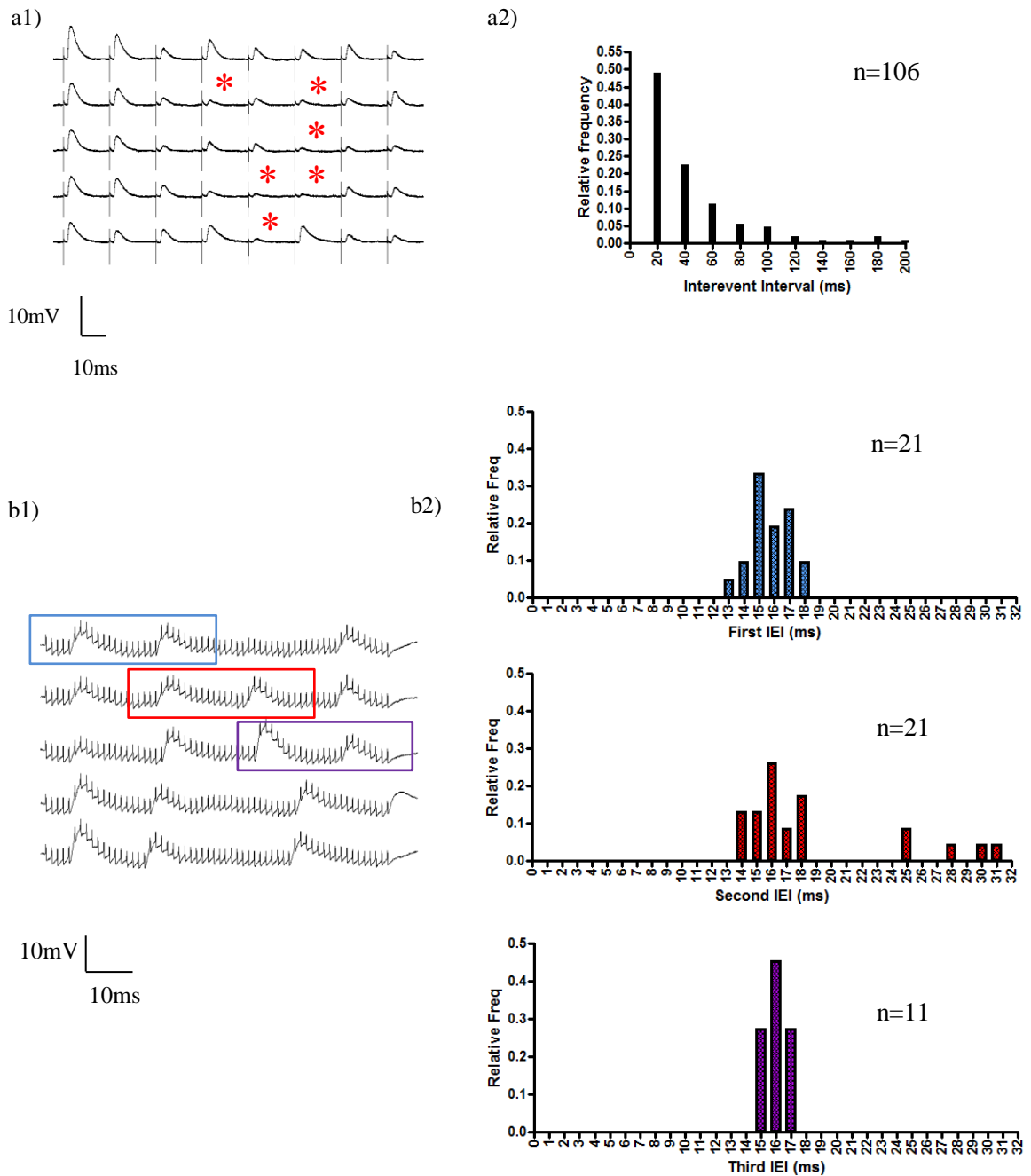


Figure 42. Voltage records of dPSPs elicited by 50Hz (*a1*) and 1kHz (*b1*; filtered at 3kHz) electrical pulse trains in the same guinea pig pLSO neuron from Figure 39 (stimulus artefacts preceded (*a1*) or were superimposed (*b1*) on synaptic responses; red asterisks represent failed events). Histograms of the inter-event intervals in *a1* indicate that synaptic responses could follow the 50Hz stimulation well (*a2*; bin width = 20ms, n value represents totals number of inter-events intervals analysed). The histograms in *b2* (bin width = 1ms) display the range of intervals between pairs of synaptic events (Inter-event intervals or IEI). The three histograms represent the different classifications of inter-event interval according to the order they occurred within a trace (Example classifications are shown in *b1*; blue box = 1st IEI, red box = 2nd IEI and purple box = 3rd IEI). Although the second pair occasionally displayed prolonged intervals (*middle panel, b2* and *traces 1, 4 and 5 in b1*); the majority of inter-event intervals were clustered around 16ms, advocating the temporal precision of the responses (*b2*). Note that no temporal summation was evident yet amplitudes of individual dPSPs evoked at 1kHz were similar to the amplitudes of the individual dPSPs evoked at 50Hz in the same neuron.

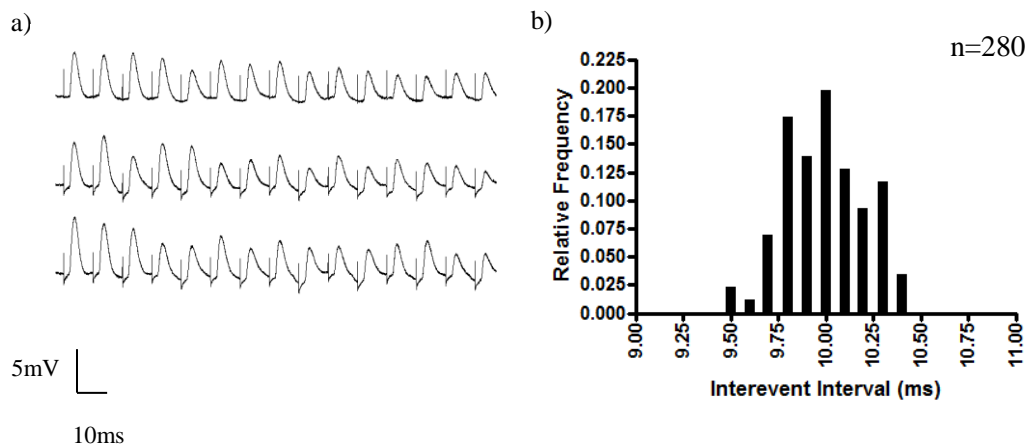


Figure 43. Voltage records of dPSPs elicited by 100Hz electrical pulse trains in a different guinea pig pLSO neuron (a). Though some jitter existed around the median inter-event interval of 10ms, the histogram shows that synaptic responses followed the 100Hz stimulus (b; bin width = 0.1ms, n value represents total number of inter-event intervals analysed).

Synaptically evoked APs in pLSO neurons

In the mammalian MSO and the avian *nucleus laminaris* (NL) (both implicated as the primary site of ITD processing) amplitudes of synaptically-evoked APs are not only smaller than those of APs evoked by somatic injections of current but are also graded, depending on the rising slope of the underlying EPSP (Kuba et al, 2006; Scott et al, 2007). This phenomenon appears to facilitate ITD detection at high frequencies and has been attributed to the location of the AP initiation site (Kuba et al, 2006).

In the guinea pig, synaptically-evoked APs were also graded in pMSO neurons (Roberta Donato, personal communication): the peak voltage never surpassing 0mV (unlike APs evoked by somatic injections of current whose peak voltage were consistently greater than 0mV) (Figures 44 a and c). In 2/3 guinea pig pLSO neurons which displayed contralaterally-evoked dPSPs, the peak voltage of APs elicited at the beginning of stimulus trains were smaller than 0mV (Figures 44 b and c). These findings suggest that synaptically-evoked APs are also initiated at a site distal to the somata of guinea pig pLSO neurons. As

they then propagate towards the somatic site of integration, their amplitude is reduced by electrotonic filtering of the interstitial axonal region.

When the peak voltages of underlying dPSPs were plotted as a function of AP peak amplitude, differences were noted between guinea pig pLSO and pMSO (Figure 44 *c*). First, the threshold rise slope (i.e. the lowest rising slope required to evoke an AP) was 6mV/ms lower in the pLSO neuron; secondly the range of graded AP amplitudes was smaller in the pLSO neuron (range in pLSO neuron: 38-46mV; range in the pMSO neuron: 34-54mV) in spite of a larger array of underlying rising slopes PSP rise slopes (range in pLSO neuron: 16-29mV/ms; range in the pMSO neuron: 22-28mV/ms). Indeed Figure 44 *c* suggests that the rise slope of the dPSP in the pLSO neuron may not have been as effective at triggering an AP as in the pMSO neuron. Since it would appear that the rise slope of subthreshold dPSPs is directly proportional to their peak voltage for pLSO neurons (Figure 44 *c*), it is possible that the absolute amplitude of a dPSP, rather than its rising slope, acts as the threshold for generation of APs in pLSO neurons.

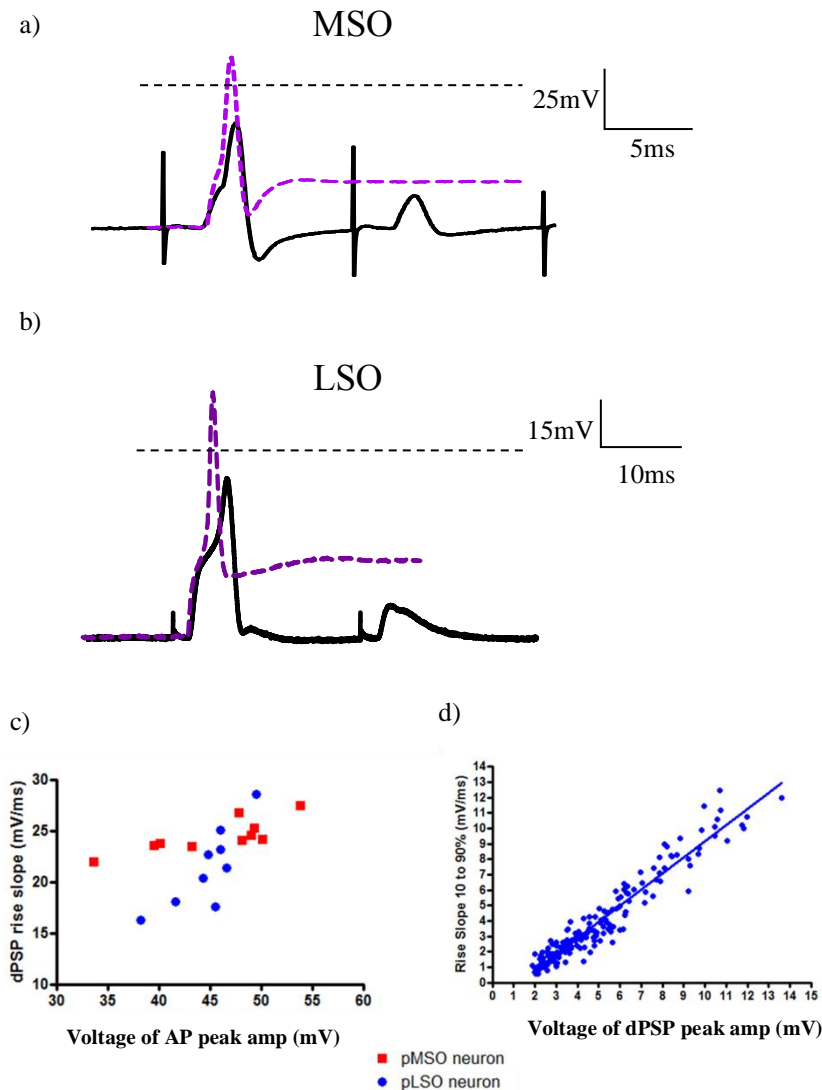


Figure 44. Synaptically evoked APs are graded in the MSO and the LSO. APs were evoked by synaptic stimulation (black traces) as well as somatic current injection (purple traces) in a pMSO (a) and pLSO (b) neuron (MSO neuron patched by Roberta Donato). Synaptically evoked APs never exceeded 0mV (dotted lines) and were consistently of smaller amplitude than somatically evoked APs (Both neurons were held at -55mV during synaptic or electrical stimulation). Following the graded APs in both a and b, sub-threshold dPSPs were observed in response to a subsequent stimulus. The smaller peak amplitude of sub-threshold dPSPs made it easy to distinguish between them and super-threshold responses. A range of synaptically evoked AP peak amplitudes was found in both the pMSO (blue) and pLSO (red) neurons (c). The relationship between voltage of the AP amplitude and the rise slope of its underlying dPSP differed between the two neuronal classes. The rise slopes of sub-threshold dPSPs in the pLSO neuron were directly proportional to the voltage of peak amplitude (d) (slope of linear fit regression fit = $1.04 \pm 0.02 \text{ ms}^{-1}$)

3.2.2 Inhibitory Inputs

Hyperpolarising PSPs (hPSPs) were observed in 7/12 (58%) of guinea pig pLSO neurons. Of the 7 guinea pig pLSO neurons in which hPSPs were observed, one neuron displayed synaptic events dominated by excitation and thus was not included for the purposes of analysis here. The dominant presence of inhibitory PSPs could be demonstrated by hyperpolarizing a pLSO neuron such that the amplitude of an hPSP decreased to 0mV at around -65mV (the reversal potential for chloride ions in our experimental conditions) before the sign reversed and it became excitatory at -80mV. (Figure 45).

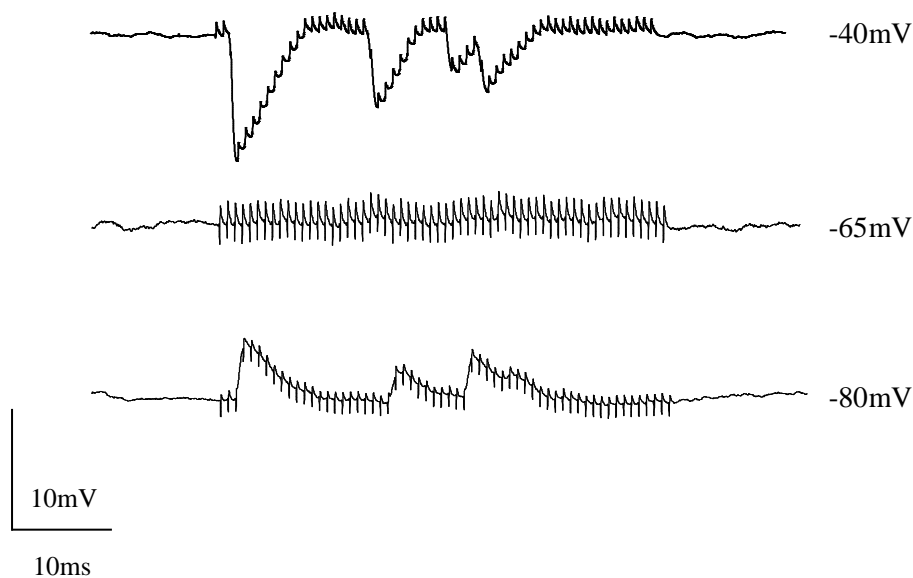


Figure 45. PSPs mainly dominated by inhibition reversed at potentials close to the E_{Cl} . A 1kHz stimulus (filtered at 3kHz to reduce size of superimposed artefacts) showed hyperpolarizing responses in a guinea pig pLSO neuron. Current injections of different amplitude and sign were used to hold the cell at varying potentials. At -40mV (top trace), responses were temporally consistent and did not summate to produce a prolonged envelope. At -60mV(middle trace), no responses were observed, a phenomenon attributed to the reversal potential of the chloride ion, which had been artificially set close to this value. At -80mV(bottom trace), the responses were again visible with a similar temporal pattern but were now depolarizing.

Inhibitory inputs and the tonotopic axis.

Of the pLSO neurons that showed evidence of contralateral inhibition, 5/6 (83%) were found in the lateral limb of the guinea pig LSO. Although inhibition was not observed in all pLSO neurons recorded, this cannot be attributed to its absence from the same neurons *in vivo*, as the preservation of all synaptic connections in a slice cannot be guaranteed. Indeed the finding that contralateral inhibitory input to pLSO neurons was the norm in the lateral limb demonstrates that they are predominantly binaural and not monaural as was suggested by some classical *in vivo* studies (Boudreau and Tsuchitani, 1968; Guinan et al, 1972).

Time course of hyperpolarizing PSPs in the LSO and its relationship to their peak amplitudes.

Models of pMSO neurons have postulated that only a fast inhibition can shift its ITD function's peak towards 0 ITD (Brand et al, 2002; Leibold, 2010). An electrophysiological study in the gerbil MSO has indicated that mature hPSPs have an average half-width of 3.1 ± 1.2 ms and an average rise time of 1.0 ± 0.6 ms (mean \pm SD, Magnusson et al, 2005). Sharp electrode recordings, made *in vitro*, have indicated that evoked IPSPs have absolute durations between 3.2ms and 8.1ms long in the gerbil LSO (Sanes, 1990); however envelope ITD functions suggest that inhibition can suppress ipsilaterally evoked discharges in the LSO for only about 1-2ms and therefore can produce temporally well-defined troughs in otherwise persistent high-firing rates (Joris and Yin, 1998; Irvine et al, 2001; Tollin and Yin, 2005). This indicates that the duration of inhibitory potentials may be of equal importance to the processing of envelope ITDs in pLSO neurons (Tollin, 2003).

In order to calculate hPSP time courses in the guinea pig LSO (Figure 46c), analysis was restricted to synaptic potentials satisfying two criteria: firstly, they were selected from the first five potentials observed in a train and secondly they were larger than -2mV but smaller

than -4.5mV (Figure 46a). The former criterion limited the effects of synaptic plasticity on analysis whilst the amplitude-matching of hPSPs negated possible membrane potential effects on the results. The time course of an average hPSP in an example pLSO neuron was measured at 7.5ms which was longer than the 4.5ms duration of the average hPSP observed in the example pMSO patched by Roberta Donato (Figure 46c). The average half-width and rise time of the hPSPs calculated for the 6 guinea pig pLSO neurons was 3.6 ± 1.15 ms (n=6) and 1.30 ± 0.10 ms (n=6) respectively.

A further observation made about the profile of hPSPs in the LSO was that a rebound after-depolarization was observed after hPSPs in guinea pig pLSO neurons (Figure 46c). This after-depolarization is likely associated with a membrane conductance that is activated or inactivated by hyperpolarization as its amplitude was correlated with the size of the preceding hPSP (Figure 46b). Much as is the case for after-hyperpolarizations following dPSPs in the MSO, the after-depolarization likely reflects the action of an conductance to curtail decay times and therefore reduce hPSPs' durations as a whole. This after-depolarization was not observed in the two principal neurons recorded in the guinea pig MSO.

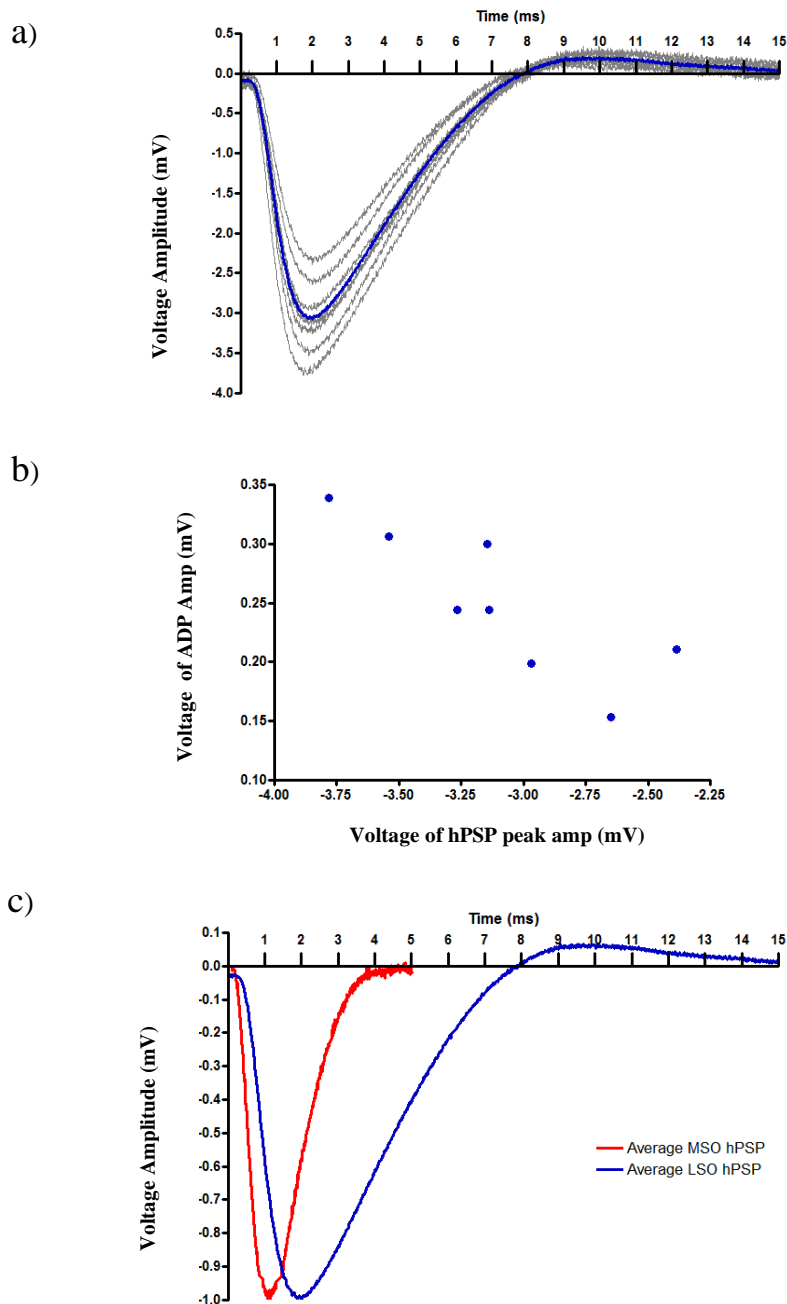


Figure 46. Hyperpolarizing post-synaptic potentials in a pLSO and pMSO neuron (latter patched by Roberta Donato). Voltage traces (grey lines) depict aggregated hPSPs evoked by the first pulse of a train in a single guinea pig type 1 pLSO neuron (Input resistance = 31 M Ω) (a): the average of these traces is shown in blue (the peak amplitude of the average hPSP in the pLSO neuron was -3.1mV). Note that an after depolarization was observed after hPSPs in the LSO which proved to be correlated with the size of the hPSP peak amplitude ($p < 0.01$, Pearson product-moment correlation). In c, the duration of the pLSO neuron's average hPSP (blue) was longer than that the average hPSP of a guinea pig pMSO neuron (red) both traces were normalised to peak amplitude. The peak amplitude of the average hPSP in the pMSO neurons was -2.8mV and its input resistance was 13M Ω . Afterdepolarizations were not noted in hPSPs recorded in the MSO.

As would be expected if hyperpolarization did not activate or inactivate membrane conductances in guinea pig pLSO neurons, a significant positive correlation ($p < 0.0001$ for all cells, Pearson product-moment correlation) was observed when the half widths of hPSPs were plotted as a function of peak amplitude (for the first five hPSPs in repeated 100Hz trains) (Figure 47). The average Pearson R value was 0.78 ± 0.04 ($n=6$) in the guinea pig whilst the linear fits had an average gradient of $-0.27 \pm 0.33\text{ms/mV}$ ($n=6$). No amplitude matching was utilised to plot this data.

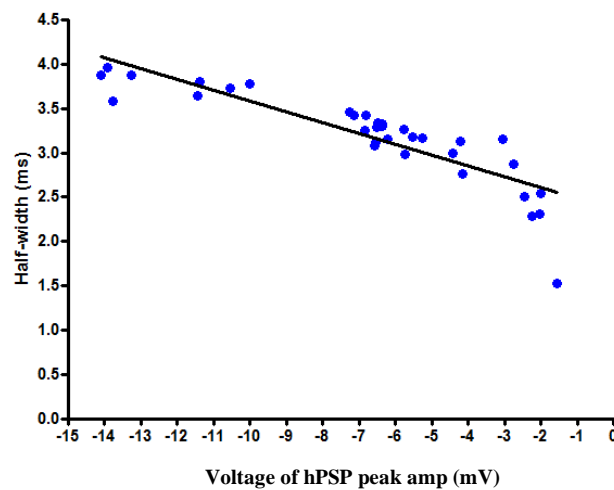


Figure 47. The peak amplitudes of hPSPs (analysing only the first five synaptic potentials in a train. No amplitude matching was used) were plotted against their half-widths for the guinea pig pLSO neuron shown in Figure 46. The gradient of linear fit was -0.12 ± 0.01 ms/mV and was significantly different from zero ($p < 0.0001$, F-test)

Short term plasticity in the amplitude of hPSPs

STSD of IPSCs has been observed at the MNTB-MSO synapse (Couchman et al, 2010). Although its function has not been studied extensively in the MSO, a decrease in the amplitude of inhibition might help match the synaptic depression evoked by excitation across the course of a stimulus and therefore balance the weight of excitatory and inhibitory synapses onto individual pMSO neurons. A similar role would arguably be more important

in a neuron coding ILDs; it was therefore hypothesized in light of the results attained for depolarizing potentials that the amplitude of hPSPs would depress over the course of a train of pulses.

In order to determine whether short-term plasticity of hPSP amplitudes also exists in pLSO neurons, average hPSP amplitudes were analysed across the course of repeated stimulus trains of 100Hz. Short-term depression in the amplitude of hPSPs was observed in all pLSO neurons with the first hPSP in a train always the largest (Figures 48 *a*). The average normalized steady state value was 0.47 ± 0.06 (n=6) and the average τ was 33 ± 5.5 ms (n=6).

Since normalized steady state amplitudes were measured relative to the initial hPSP in a train and these ranged from 4.5mV to -11mV, it was important to see whether a relationship between the actual amplitude and the amount of STSD existed. To that end, the actual values of the average steady state hPSP amplitude were plotted as a function of the first hPSP amplitude for the guinea pig pLSO neurons (Figure 48*b*). Linear regression gave a fit with a positive slope of 0.19 ± 0.06 which proved to be significantly different from zero ($p < 0.05$, F-test). As values of fitted slopes were considerably less than 1, it appears that STSD's strength increased with the amplitude of the initial hPSP. The reduction in the τ of decay with increasing first hPSP amplitude (Figures 48*c*) also supports the biological legitimacy of this finding and perhaps even points to the pre-/post-synaptic mechanism underlying STSD in hPSPs as discussed in Chapters 4.2.7 and 4.2.8.

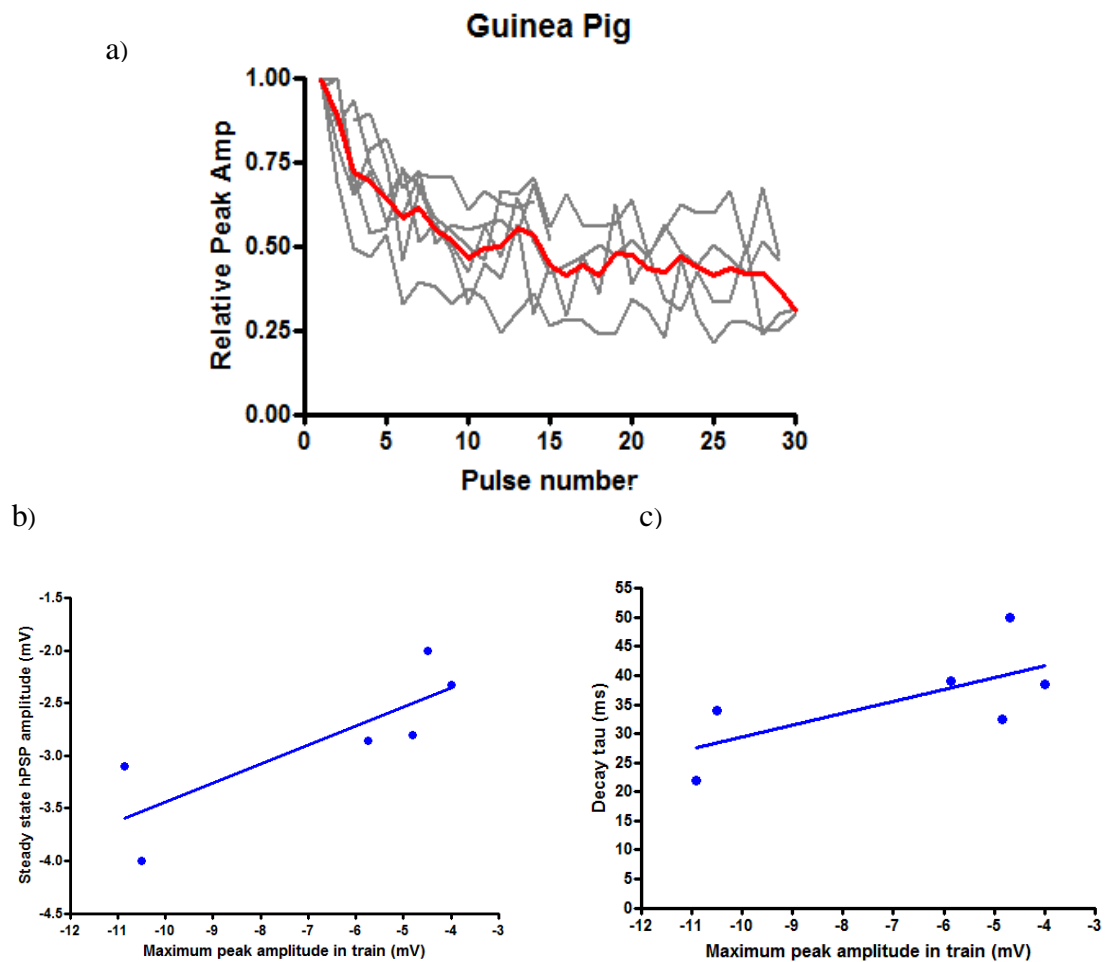


Figure 48. Depression of dPSP amplitude evoked by 100Hz electrical pulse trains in the guinea pig pLSO neuronal population. The profile of depression was averaged across repeated trains of electrical inputs for individual guinea pig pLSO neurons (*grey lines*) and displayed alongside the average profile for all cells (*red line*). The actual steady state amplitude was plotted as a function of the maximum peak amplitude of each guinea pig cell (*b*). This was also performed for the τ of STSD decay and the maximum peak amplitude (*c*). In both *b* and *c*, parameters were linearly proportional.

Frequency dependence of STSD in hPSP amplitude.

At the MNTB-MSO synapse, inhibition has been demonstrated to undergo frequency-dependent synaptic depression: both the steady state amplitude of IPSPs and the τ of the decay in STSD decreased as the stimulus frequency increased (Couchman et al, 2010). The frequency dependence of STSD has not been studied extensively at the mature MNTB-LSO synapse although there are suggestions that it too experiences STSD. To this end, it is likely that excitation and inhibition possess very similar short-term synaptic plasticity at different stimulation frequencies, as has been demonstrated in the gerbil MSO (Couchman et al, 2010). Evidence of an underlying STSF was observed in the first few dPSPs evoked by a 50Hz train in a guinea pig pLSO neuron (*middle trace*, Figure 42 *a*), drawing potential similarities with the STSF found in *nucleus angularis* (Macleod et al, 2007). As at the MNTB-MSO synapse, some neurons in this avian nucleus only display synaptic depression at all stimulation frequencies; however they are outnumbered by neurons that also incorporate STSF. The influence of this STSF is greatest at low frequencies of stimulation but declines with increasing stimulation rate, leaving pure STSD at the highest frequencies (Macleod et al, 2007). It was therefore hypothesized that, although some pLSO neurons in the guinea pig might possess inhibition that only undergoes STSD at all frequencies of stimulation, many principal neurons would incorporate a mixture of STSF and STSD whose ratio would change with the rate of stimulation.

To determine whether the STSD of inhibition observed at 100Hz was masking a smaller STSF, a selection of stimulation frequencies from 10Hz, 50Hz, 100Hz, 250Hz and 1kHz was employed in 5/6 (83%) guinea pig pLSO neurons (although not all were used in the same cell): normalized steady state hPSP amplitude and τ s of decay were the parameters used for comparison. No changes in maximum hPSP amplitude were encountered across different stimulus frequencies in each neuron.

STSD was observed at every stimulus frequency employed in each neuron although its properties did change with stimulus frequency. Increasing the stimulus frequency from 50Hz to 100Hz in three guinea pig pLSO neurons had two possible consequences. The normalized steady state amplitude decreased by 19% in 1 neuron (Figure 49 *a*); however in the other 2 neurons, STSD changed very little (-1% in 1 neurons and +2.3% in the other; Figure 49 *b*). Evidence still existed for STSD's frequency-dependence in the latter two neurons however as the average decay time constant decreased in all 3 neurons (by $37 \pm 1.5\%$). This suggests that the magnitude of STSD plateaued at 50Hz in 2 of the guinea pig pLSO neurons and would likely not change at higher stimulus frequencies. In the third guinea pig neuron, increasing the stimulus frequency from 50Hz to 100Hz caused an increase in STSD and it is possible that it would have continued to do so at higher stimulus frequencies.

This variation in STSD frequency dependence across the pLSO population is highlighted by two other neurons: one which was stimulated at either 10Hz or 100Hz (Figure 49 *c*) and another that was stimulated at 100Hz or 250Hz (Figure 49 *d*). In the former case, STSD appeared to have reached its limit by 10Hz, as the normalised steady state amplitude increased from 0.24 at 10Hz to 0.25 at 100Hz (an increase of 4%). The decay time constant of STSD decreased from 93ms to 34ms as the stimulus frequency increased. In the latter neuron, increasing the rate of electrical stimulation from 100Hz to 250Hz led to a reduction in both the normalized steady state amplitude (from 0.47 to 0.22 (-53%)) and in the decay time constant (from 42ms to 9ms). This suggests that for input rates below 250Hz, STSD had not reached a maximum in this neuron. Although hyperpolarizing responses were not measured at stimulations of 1kHz, STSD was always observed for this frequency of stimulation (Figure 45).

In summary, STSD in hPSP amplitude was frequency dependent in most pLSO neurons in both the rat and the guinea pig. There was no indication, however, that the amplitude of hPSPs was subject to STSF at any stimulation frequency. The range observed in the profiles

of frequency dependence appears to arise from the parameters of synaptic depression and not due to a secondary form of short term synaptic plasticity, as is the case in *nucleus angularis* (NA) in birds (Macleod et al, 2007).

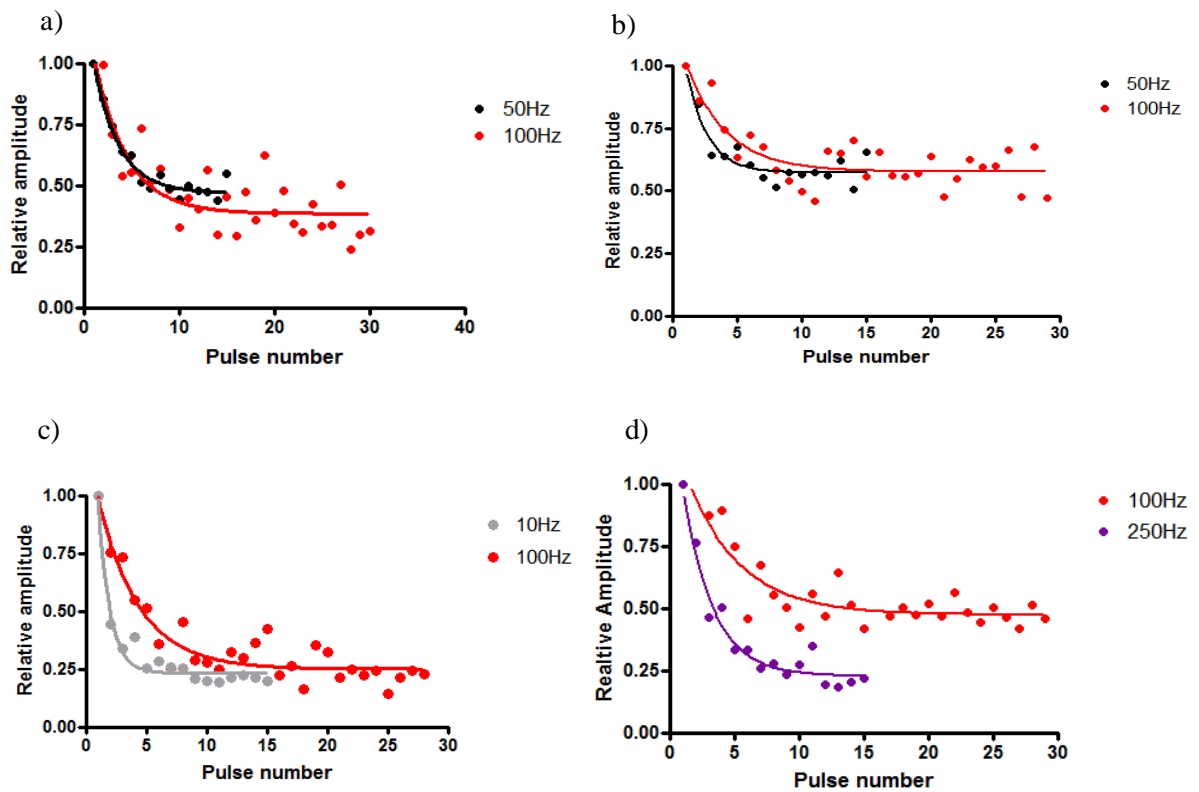


Figure 49 The frequency dependence of STSD in hPSP amplitude. Different frequency electrical pulse trains were used to assess STSD in separate guinea pig pLSO neurons (a,b,c and d). In a and b, 50Hz (black traces) and 100Hz (red traces) stimuli were used. STSD increased with stimulus frequency in a however had reached a maximum strength at 50Hz already in b. In c, 10Hz and 100Hz were employed whilst in d, 100Hz (red trace) and 250Hz (purple trace). The steady state amplitude did not change from 10Hz (grey trace) to 100Hz (red trace) in c, suggesting that STSD had already plateaued. This was not the case when a different pLSO neuron was probed first with 100Hz (red trace) and then 250Hz (purple trace) stimuli (d), as the STSD increased considerably

Stimulation frequency and summation of hPSPs

In the MSO, where collateral pMNTB fibres contact principal neurons, IPSPs have been observed following electrical stimulation of up to 160Hz, without summation (Smith et al, 1998; Chirila et al, 2007). The slower membrane time constant of pLSO neurons was expected to limit more severely the maximum non-summating frequency at which responses could follow each cycle of stimulation in this study.

5/6 of the guinea pig pLSO neurons were able to follow a 100Hz stimulus with individual responses after each pulse that did not summate (Figure 50 *a1*). Instances of summation at 100Hz were observed in those neurons that also displayed the longest half-widths. At 250Hz all pLSO neurons displayed some summation within the first 10 pulses, however individual hPSP responses were still visible atop the summated envelope (Figure 50 *b1*). Surprisingly very little summation was observed at 1kHz stimuli however; this was especially true of the first hyperpolarizing potentials in a train which were of typical amplitude and half-width and were succeeded by a longer interval before subsequent responses (Figure 45).

As previously suggested for dPSPs, it appears that two biophysical mechanisms may determine whether a stimulation frequency resulted in summation of hPSPs. At lower stimulus frequencies, there appears to be a postsynaptic limit on summation which is associated with a pLSO neurons' ability to integrate individual synaptic responses. The 8-10ms maximum duration of an onset hPSP in the guinea pig LSO indicates that 125Hz should be the highest stimulus frequency at which any pLSO neuron would be able to display non-summating hPSPs after each current pulse. At the higher frequency of 1kHz stimulation, summation was mostly absent (Figure 51 *a*). In conjunction with the precisely timed occurrence of the hPSPs (Figure 51 *b*), this absence of summation at 1kHz is likely associated with limitations on how fast presynaptic fibres can follow high rates of stimulation.

In summary, the data suggest that guinea pig pLSO neurons are able to follow input rates of at least 100Hz. It is unlikely, however, that they could respond with non-summating hPSPs at 160Hz, given the recorded duration of hPSPs. At higher frequencies, the inputs still produce a sharp and phasic inhibition, evident even at 1kHz. This is potentially of great importance to envelope ITD processing.

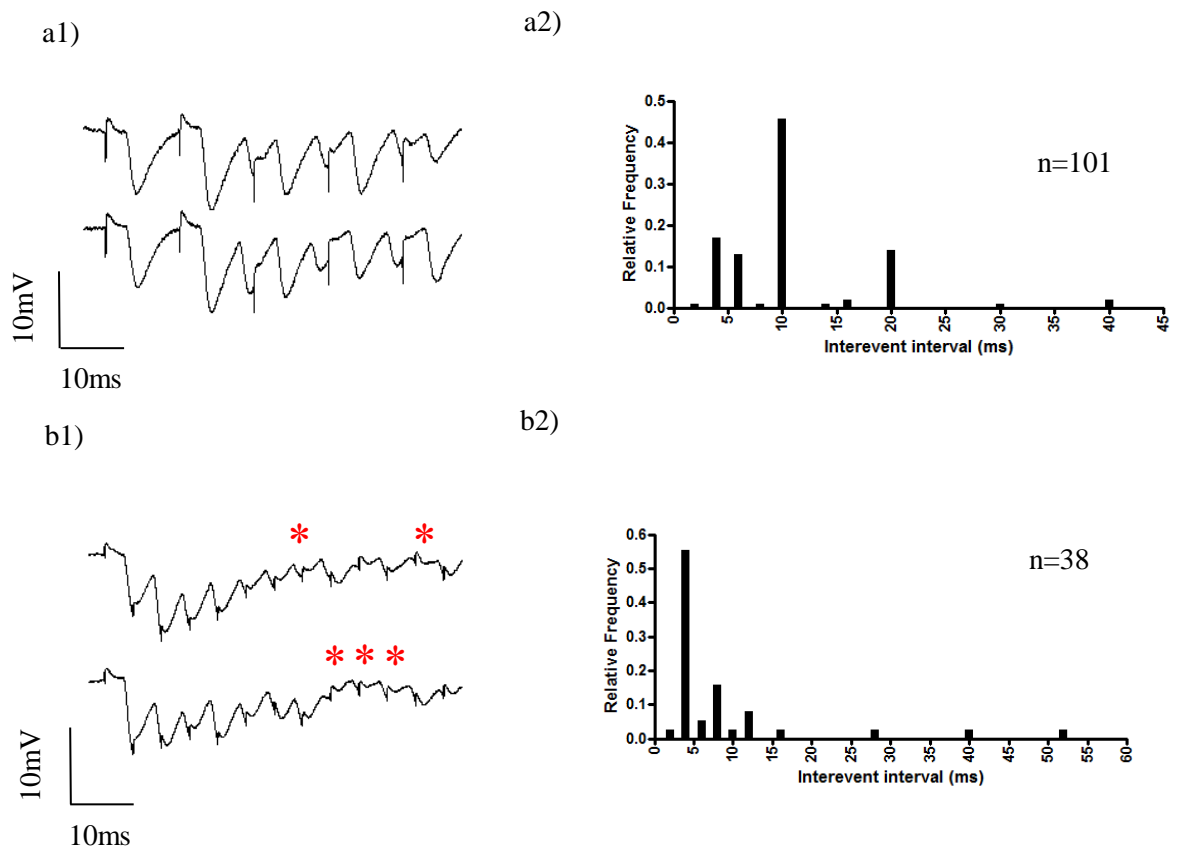


Figure 50. Voltage records of hPSPs elicited by 100Hz (*a1*) and 250Hz (*b1*); filtered at 3kHz) electrical pulse trains in a guinea pig pLSO neuron (stimulus artefacts preceded the responses in *A1* and were superimposed in *B1*). Traces and histograms of the inter-event intervals (*a1* and *a2*) indicate that synaptic responses could follow without summation at 100Hz however there appeared a proportion of stimulus cycles that caused the neuron to respond with two hPSP for every stimulus pulse At 250Hz (*B1* and *B2*), a temporary summation was evident at the beginning of traces but individual responses were still visible atop the envelope every 4ms (*a2*; bin width = 2ms and *b2*; bin width = 2ms). The red asterisks represent failed events

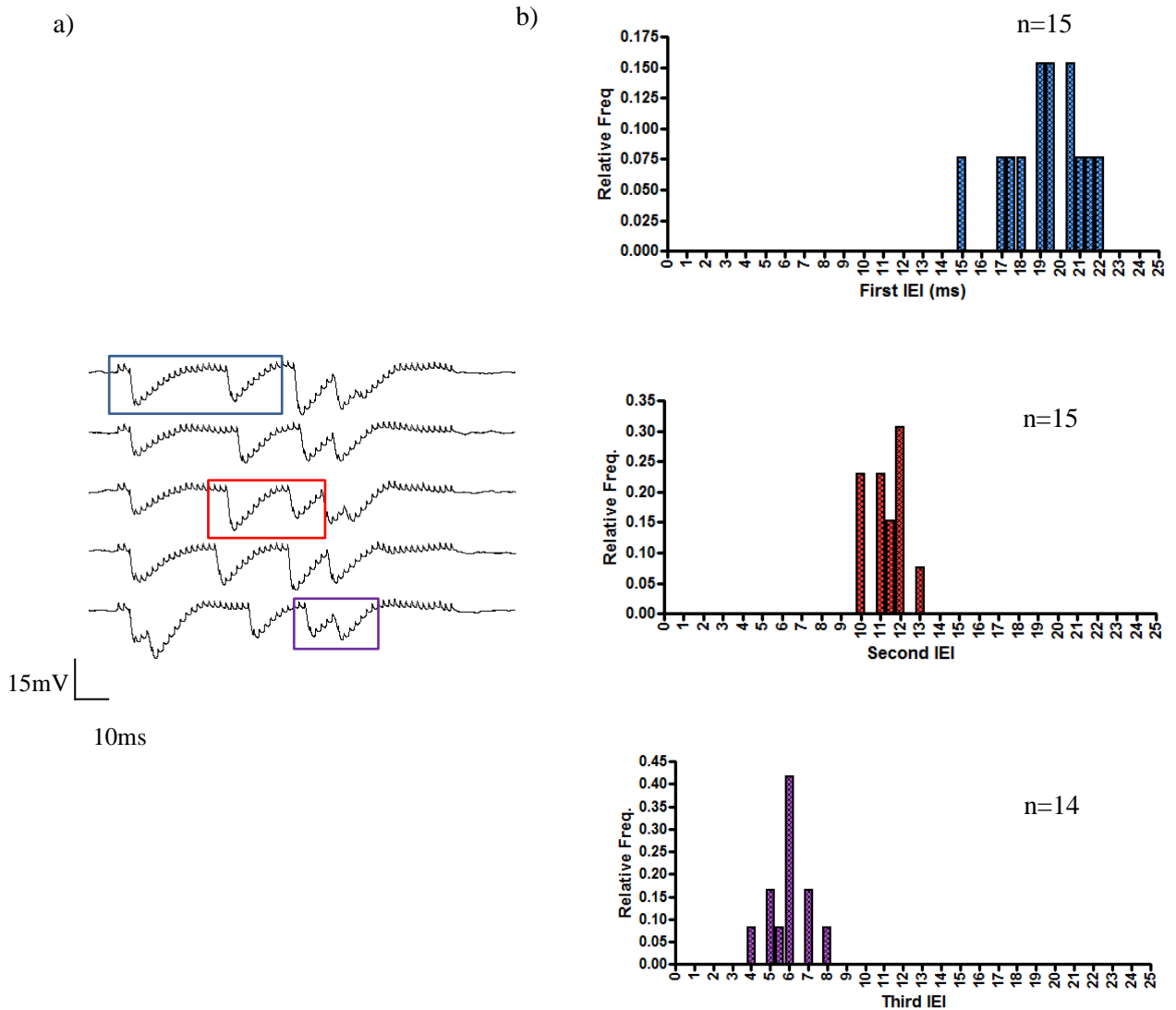


Figure 51. Voltage records of hPSPs elicited by 1kHz (*a*; filtered at 3kHz) electrical pulse trains in a guinea pig pLSO neuron (stimulus artefacts can be seen superimposed on responses in *a*). Traces in *a* displayed few instance of summation. The histograms in *b* (bin width = 0.5ms) display the range of intervals between synaptic events. The three histograms represent the different classifications of inter-event interval according to the order they occurred with a trace (Example classifications are shown in *a*; bluebox= 1st IEI, red box= 2nd IEI and purple box= 3rd IEI). Whilst the initial IEIs displayed dome variation between traces, they were clustered around 19-20ms, subsequent IEIs were shorter and displayed even greater temporal precision.

3.3 Immunohistochemistry

3.3.1 Localizing principal cells in the SOC.

Using light microscopy, the LSO was identified in both species as a darker region medial to the facial nerve; its form was typically S-shaped though this depended on the level in the brainstem at which the slice had been made.

In order to identify neurons in the SOC, MAP2 staining was used to detect their somata and dendritic processes (Figures 53*c* and 55*b*) whilst their nuclei were visualised by DAPI staining. The gephyrin channel was next overlaid (Figures 53*b* and 55*c*) before qualitative descriptions and dendritic measurements were made from the final image.

Neurons in the guinea pig LSO were separated into three categories based on their location in the S-shaped nucleus: medial, mediolateral and lateral (Figure 52). No dendritic processes were seen to leave the nucleus and all cell bodies lay within the LSO.

Guinea pig pMSO neurons were identified by the “ladder-like”-arrangement of bipolar cells slightly rostromedial to the LSO (Smith, 1995).

3.3.2 Morphology of LSO cells in the guinea pig

No previous study has described the morphology of LSO cells in the guinea pig and whilst numerous truncated appendages and weak MAP2 staining prevented a detailed reconstruction of cells, it did allow their identification as well as measurement of cross-sectional somatic areas.

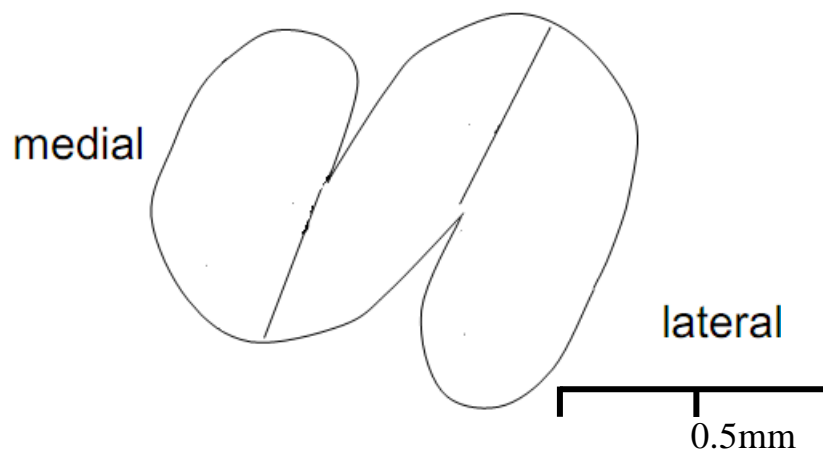


Figure 52: Schematic of LSO showing how the nucleus was separated into three parts. Although not shown in this diagram, the facial nerve lays laterally to the LSO and, in conjunction with the LSO nucleus itself, was used as a landmark to identify the appropriate level of the brainstem. The scale bar represents 0.5mm.

Of the neurons identified in the LSO and MSO nuclei as being MAP2 positive, none displayed more than two dendritic processes positive for the marker. Bidendritic cells were observed across the whole guinea pig LSO but, as a percentage of all cells visualised, they became increasingly prevalent towards the lateral limb. Amongst their number, cells with two dendrites arranged orthogonally (i.e. oriented at 90° to each other) were found in all regions of the guinea pig LSO (Figures 55d, 56a, 57a). These cells were reminiscent of the “banana-like” cells observed in the lateral limb of the rat (Rietzel and Friauf, 1998).

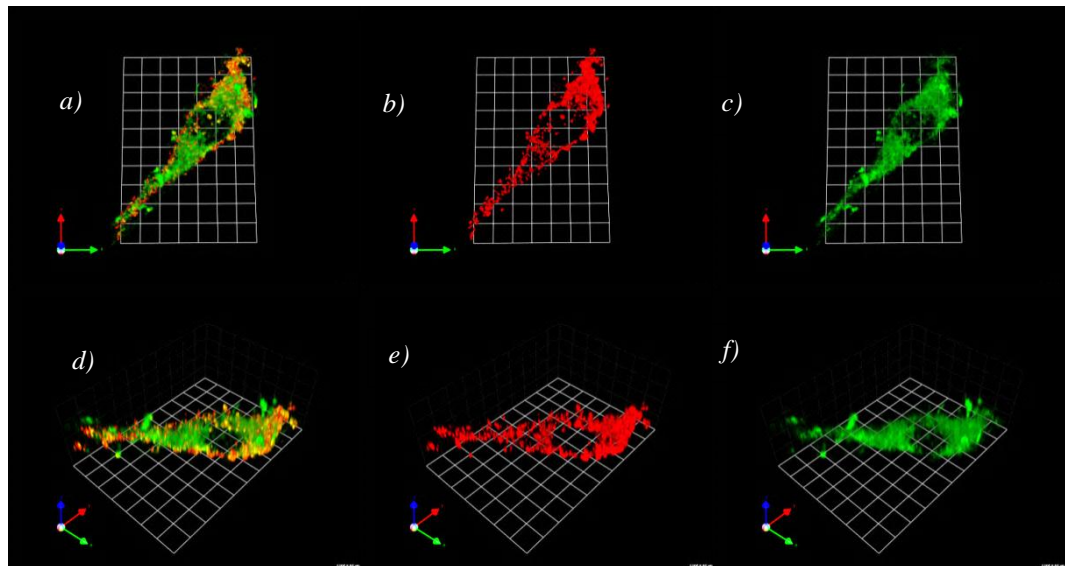


Figure 53. A 3-D reconstruction of a guinea pig mediolateral LSO cell is displayed from two different angles (a,b,c and d,e,f) to demonstrate that the gephyrin puncta were located near the neuronal membrane. The full reconstructed image is shown in a and d with gephyrin stained in red and MAP2 in green (colocalization is yellow). The gephyrin and MAP2 channels are next split in b/e and c/f respectively. Figure 53 f also shows that certain MAP2 staining visible is not associated with the cell. The axes accompany each image (x= green, y= red and z= blue) whilst the grid behind provides the scale (each square box = $4.6\mu\text{m} \times 4.6\mu\text{m}$)

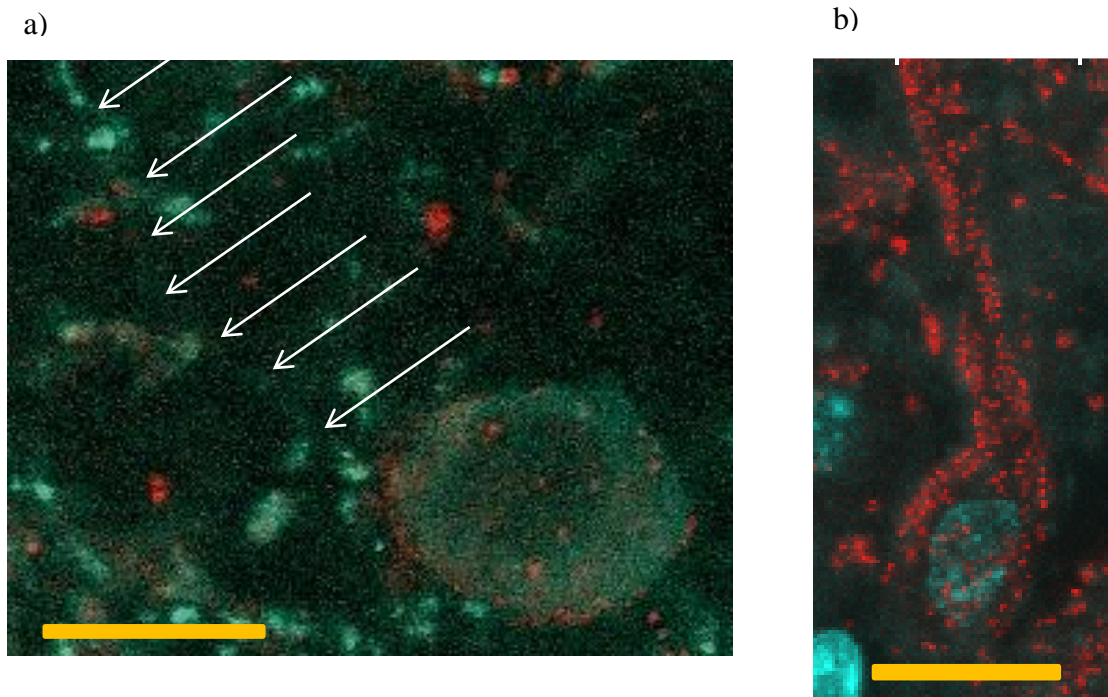


Figure 54. Cells with single dendrites from the LSO medial region of guinea pig. The cell in a) displayed gephyrin puncta somatically but not dendritically (gephyrin=red and MAP2 = green). The arrows display the path of a potential dendrite. Prominent gephyrin staining was observed along the dendrite and soma of the cell in b) (nucleus in blue). The scale bar for a) and b) was 15 μ m.

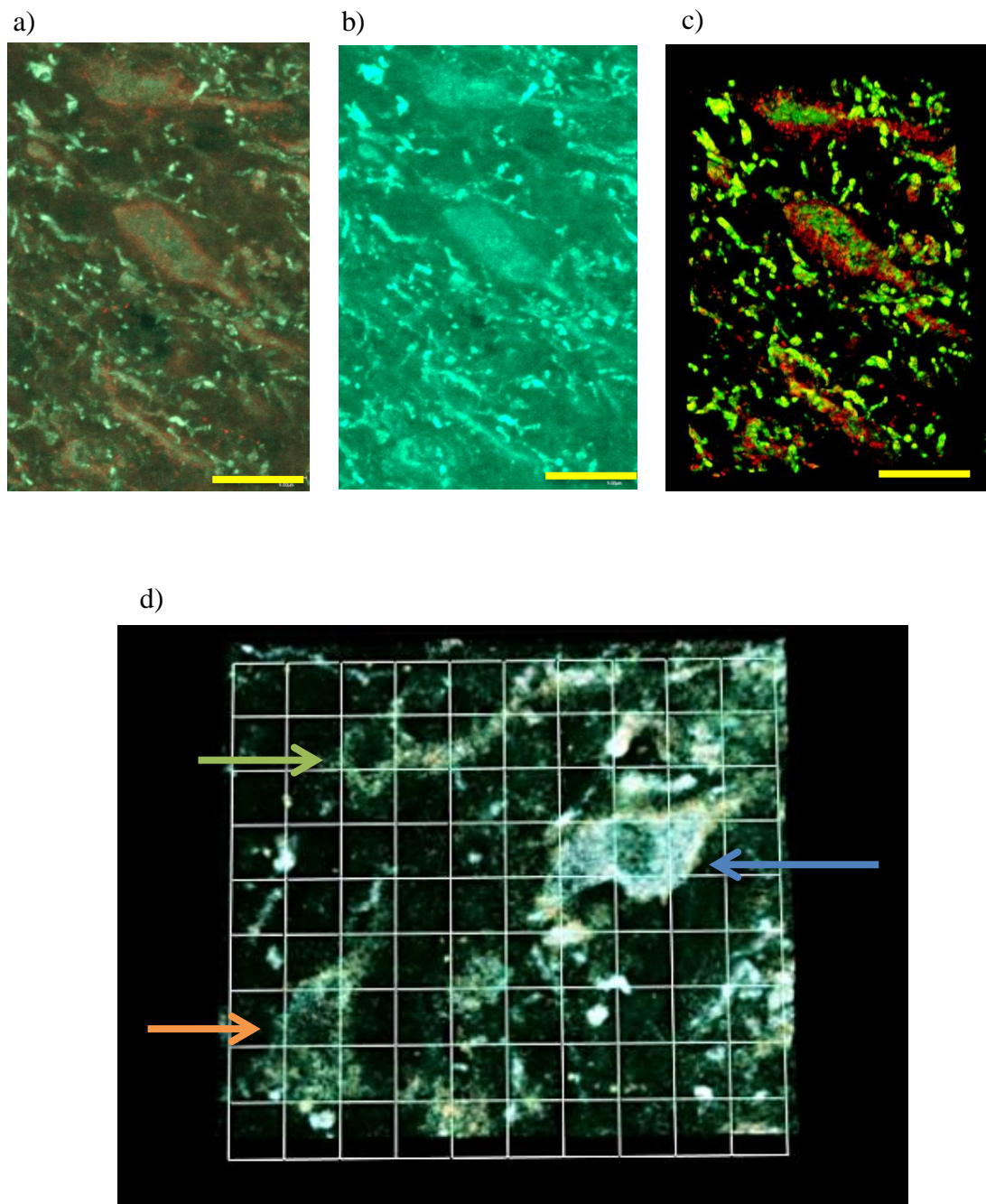


Figure 55. Guinea pig mediolateral cells. Images in a), b) and c) show large cells in the mediolateral region orientated parallel to each other (gephyrin=red and MAP2 = green). a) and b) are 2-D projections across the stack whilst c) is a 3-D reconstruction. a) and c) show both gephyrin and MAP2 channels whilst b) only includes the MAP2 channel proving that cells can be identified by their MAP2 staining alone. The image in d) shows an amplified MAP2 channel to show two banana-like cells marked with green and orange arrows. A bipolar cell, indicated by the blue arrow, is shown for comparison. The scale bar for a), b) and c) was 20 μ m. The Scale grid in d) is 8.5 μ m x 8.5 μ m.

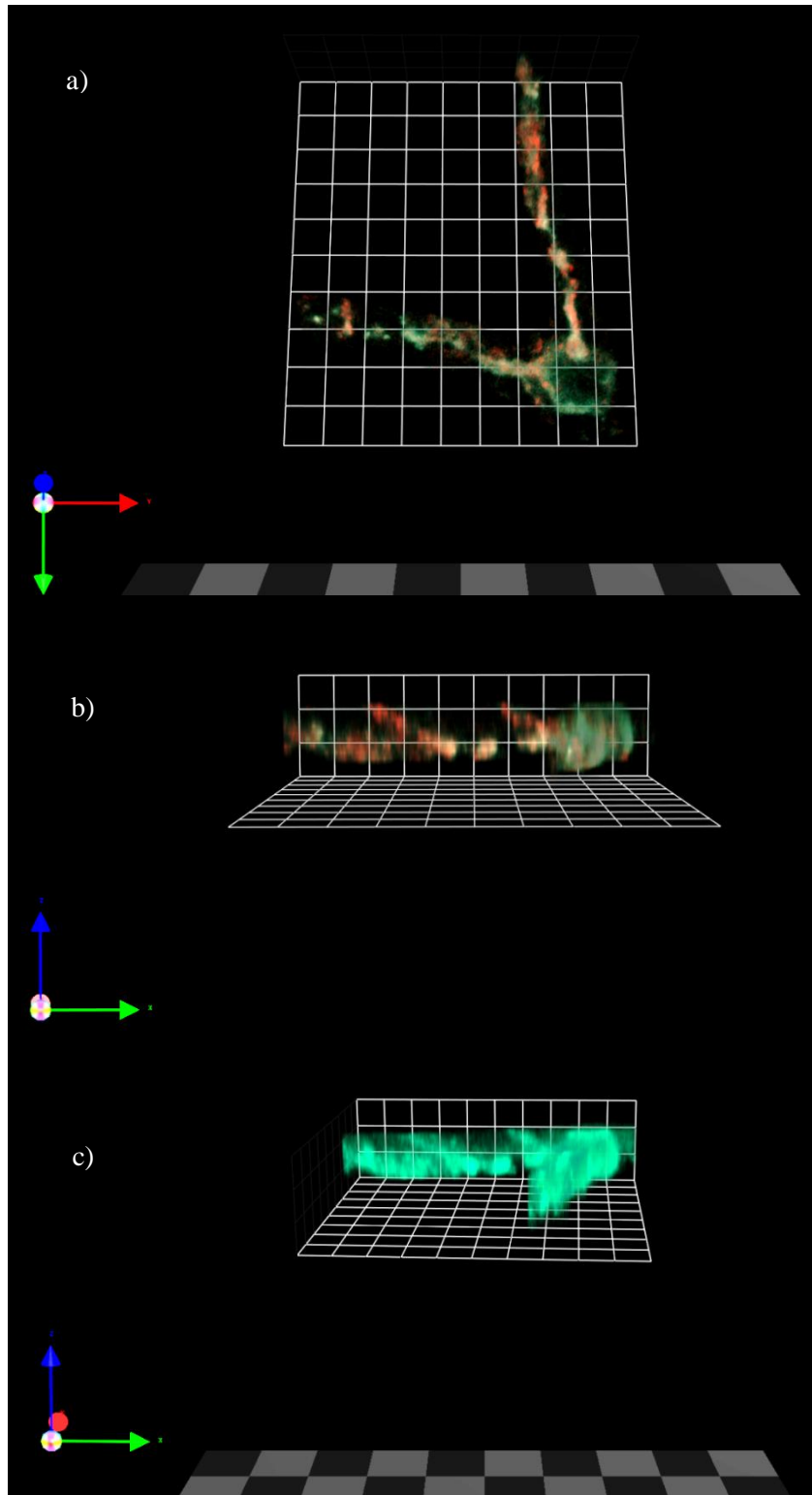


Figure 56. Banana-like cell from the mediolateral region of the guinea pig LSO (gephyrin= red and MAP2= green). Dendritic gephyrin staining in this cell was stronger than the staining observed in the somatic compartment. c) demonstrates that it was possible to resolve processes which branched off the primary dendrite. b) also showed gephyrin staining on this process The scale grid was $5.9\mu\text{m} \times 5.9\mu\text{m}$.

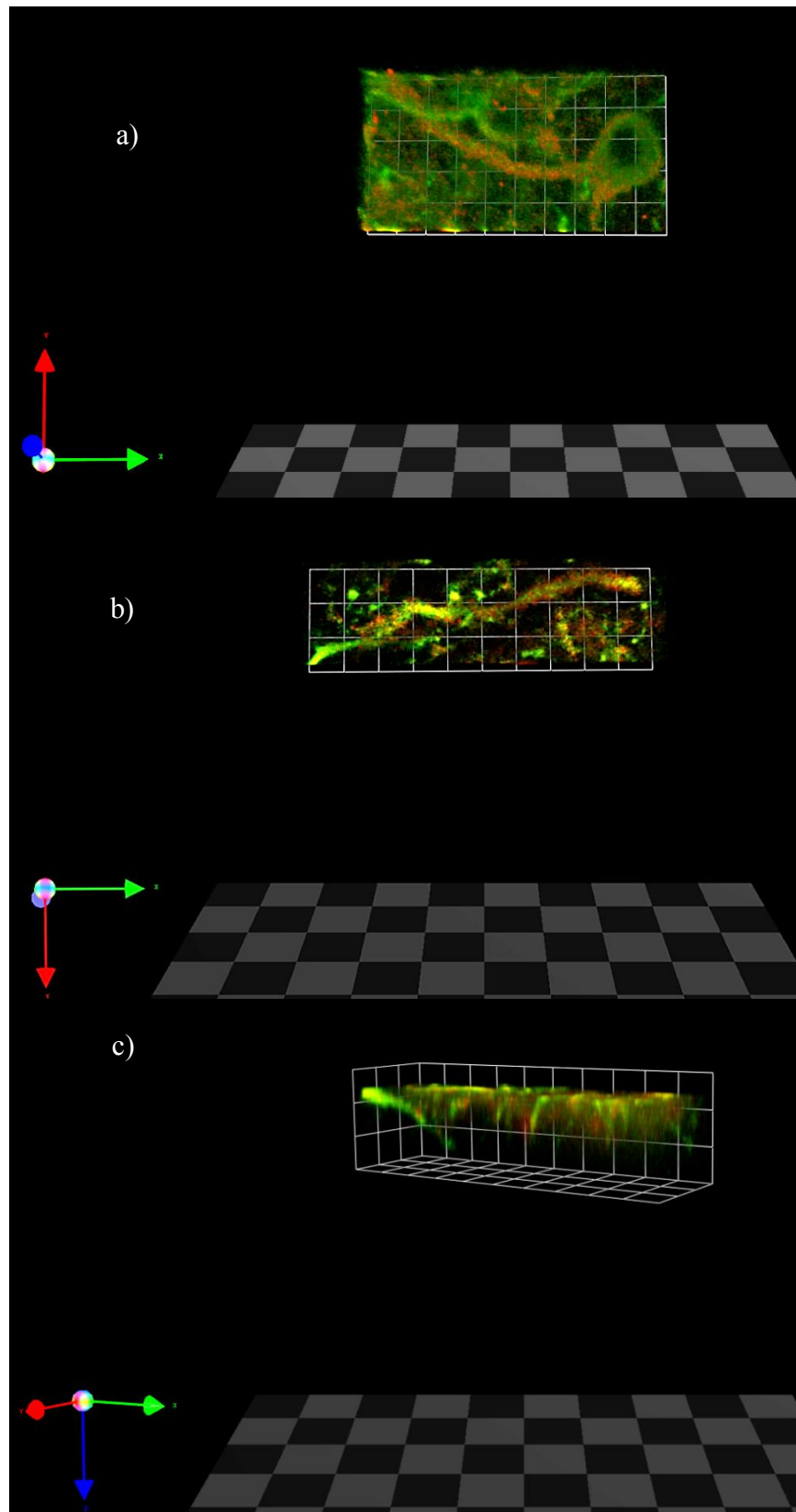
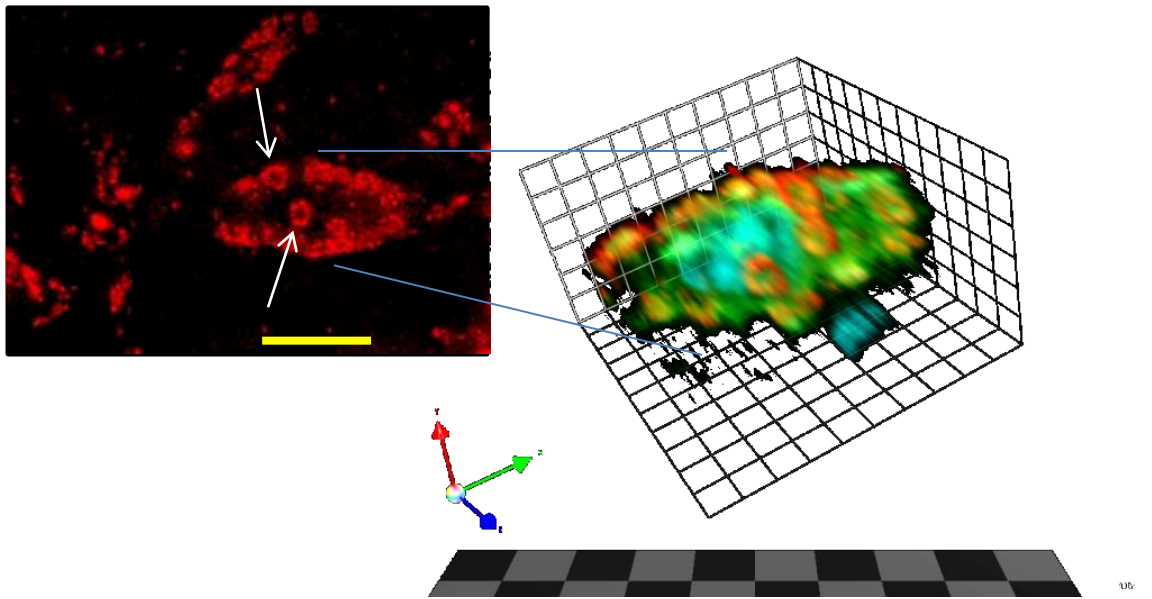


Figure 57. Lateral banana-like cell with truncated dendrite in a) (gephyrin= red and MAP2= green). b) and c) uses the same colour scheme but different orientations to show a severed dendrite stained for gephyrin along its 82μm length. c) shows that another process (on the left of image) gives the impression of a single continuous dendrite in b). Scale grid is 7 μm x 7μm for all three images.

a)



b)

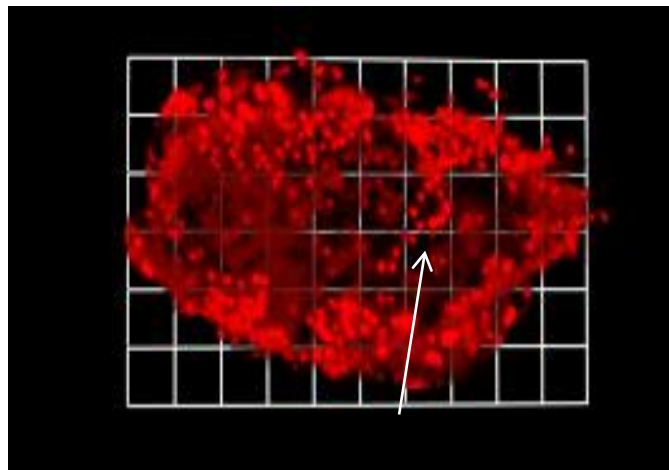


Figure 58. Gephyrin “rings” in the MSO and LSO cells. The fusiform soma of a MSO cell, (a), had high levels of somatic staining for gephyrin (red). This staining presented itself as several independent “rings” of gephyrin on a single soma, (a, white arrows and inset) (MAP2 (green) and DAPI (blue) channels are also displayed in inset). Although it was seen in LSO cells, (b, white arrow), the “rings” were limited in number and not as well defined. The scale bar in a) was 15 μ m; scale grids were 3.2 μ m x 3.2 μ m for a) inset and 4.2 μ m x 4.2 μ m for b).

3.3.3 MSO cells have larger cross-sectional somatic areas than LSO cells

In many species, the LSO nucleus has been shown to contain a heterogeneous population of cells which is believed to contain both pLSO and LOC neurons as well as alternative neuronal types as yet uncharacterized electrophysiologically (Helfert and Schwartz 1987; Henkel and Brunso-Brechtold, 1991; Rietzel and Friauf, 1998). Measurements of cross sectional somatic area potentially offer a preliminary indication of this heterogeneity. When the cross-sectional somatic areas from the medial ($197 \pm 16\mu\text{m}^2$); mediolateral ($192 \pm 21\mu\text{m}^2$) and lateral ($181 \pm 11\mu\text{m}^2$) regions of the guinea pig LSO were compared however, no significant difference was observed (Figure 59). Conversely, cells from each LSO region did prove to be significantly smaller than neurons in the MSO ($p < 0.001$, One-way ANOVA with Bonferonni post-correction test). It was also true that cells aggregated from all LSO regions (average = $191 \pm 9.5\mu\text{m}^2$) were significantly smaller than MSO cells (average = $296 \pm 13\mu\text{m}^2$) ($p < 0.0001$, Independent two-tailed t test).

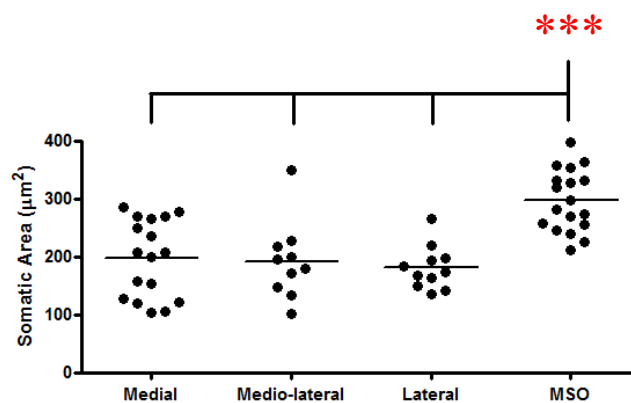


Figure 59: Somatic areas of LSO cells: across different regions of guinea pig LSO and guinea pig MSO cells. Horizontal lines represent the means of each dataset.

3.3.4 Gephyrin staining in the guinea pig SOC

All identified cells within the MSO and LSO had some degree of gephyrin staining, whether purely somatic or both somatic and dendritic. This staining generally appeared as well defined *puncta* surrounding the peri-membrane space (Figures 53*b*, 54*b*, 56*c* and 58*b*).

A maximum of two dendrites was stained on any cell and occasionally it was possible to observe the ramifications leading from proximal dendrites, noting gephyrin staining on these branches too (Figures 56*b* and 57*c*).

Gephyrin Staining in the guinea pig MSO is mainly somatic

Gephyrin staining in the guinea pig MSO was analysed to determine whether it was largely confined to the cell soma as is suggested to be the case for species of similar frequency hearing ranges (Kapfer et al, 2002). Consistent with this perspective, punctate staining was restricted to the somatic compartment, only marginally extending to the proximal dendrites. In fact, of 18 cells identified, 14 (77.7%) showed gephyrin staining extending on average just $24 \pm 2.0 \mu\text{m}$ from the soma although dendritic staining was evident bilaterally in all cases. This suggests that gephyrin staining is also largely somatic in nature in the juvenile guinea pig MSO and a mature postsynaptic configuration of inhibitory receptors may already exist at this early stage in the guinea pig

Interestingly, gephyrin puncta formed structures that appeared as “rings” (Figure 58*a inset*). These were mostly found on the soma although were also be observed in the proximal dendrites. The “rings” ranged from under $1\mu\text{m}$ to as large as $3\mu\text{m}$ in diameter.

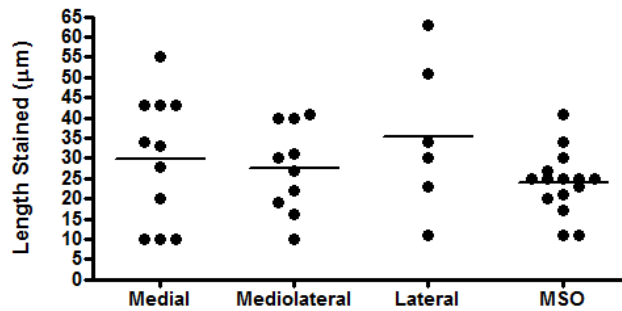


Figure 60. Length of gephyrin stained dendrites across different regions of guinea pig LSO and MSO. Horizontal lines represent the means of each dataset

LSO gephyrin staining does not differ significantly from the MSO staining

Since it has been shown that the somatic (or perisomatic i.e. defined in this study as including the cell body and the proximal dendrites up to a distance of 50µm) localization of glycinergic receptor is peculiar to MSO neurons, neurons that encode ITDs in the fine structure of low frequency sounds, we wanted to study whether LSO neurons, that are typically associated with ILD processing, possess gephyrin staining which extends further along the dendrites. The punctate gephyrin staining in the LSO was also observed to be mostly perisomatic although 2 out of 38 LSO cells were evident whose proximal dendrites were stained beyond the 50µm boundary. When all LSO cells were grouped (irrespective of sub-localization), the mean length of dendritic gephyrin-staining was $30.2 \pm 2.8 \mu\text{m}$ which did not prove to be significantly different from the length observed in the MSO ($p=0.13$, Independent two-tailed t test). This suggests that gephyrin staining is also mostly somatic in the guinea pig LSO. It is likely that measurements of dendritic length of gephyrin staining underestimate the true values as MAP2 staining of dendrites in the LSO never projected beyond the corresponding gephyrin staining, suggesting that almost all dendrites had been severed at their extreme. Somatically-stained cells were also affected by this with only one guinea pig LSO cell displaying a non-gephyrin stained dendrite projecting from its soma (Figure 54a). This issue is discussed in chapter 4.3.1.

Comparisons of dendritic gephyrin staining in guinea pig LSO show no significant regional differences.

To explore the possibility that a changing sensitivity to binaural cue along the LSO's tonotopic axis (Tollin and Yin, 2005) may be associated with variations in how far gephyrin staining stretches dendritically, comparisons were made between the guinea pig LSO regions.

The medial region displayed staining on average $29.9 \pm 4.7 \mu\text{m}$ from the soma (9 of the 17 cells visualised: 3 of which were bipolar); the dendrites in the mediolateral limb were stained on average $27.6 \pm 3.4 \mu\text{m}$ from the soma (7 of the 10 cells visualised: 4 of which were bipolar); whilst the most distal gephyrin staining was observed in the lateral region at $35.3 \pm 7.7 \mu\text{m}$ (8 of the 11 cells visualised: 5 of which had two dendrites). The mean values for the LSO regions did not show any significant difference between regions (One-way ANOVA with Bonferonni post-correction test) (Figure 60 a).

These data therefore do not support the existence of any gradient in the dendritic length of gephyrin staining across the guinea pig SOC.

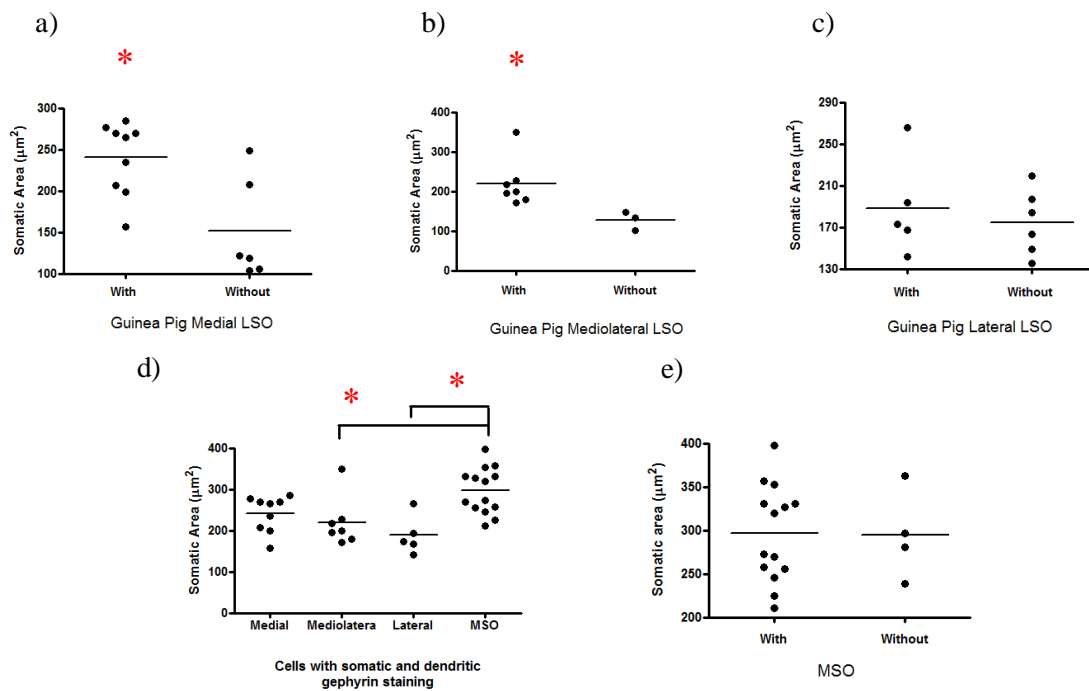


Figure 61. Somatic areas grouped into cells with and without dendritic staining for gephyrin. a), b) and c) display the somatic areas of neurons with and without somatodendritic gephyrin staining in different regions of the guinea pig LSO. e) displays the same but for the guinea pig MSO. In d), somatodendritically gephyrin stained cells from different guinea pig LSO regions and guinea pig MSO are compared. Horizontal lines represent the means of each dataset.

3.3.5 Separation of LSO cells based on their gephyrin staining reveals somatic differences between LSO regions

To determine whether any relationship between a cell's size and the sublocalization of its gephyrin staining existed, cells were separated into those with purely somatic gephyrin and those with staining that continued across both somatic and dendritic compartments. When the two classes were compared in the medial limb, it was found that cells with both dendritic and somatic gephyrin staining (average = $240 \pm 15 \mu\text{m}^2$) were significantly larger than those with purely somatic staining (average = $151 \pm 25 \mu\text{m}^2$) ($p < 0.05$, Independent two-tailed t test) (Figure 61 a). This was true when the two classes were compared in the mediolateral limb (average = $220 \pm 23 \mu\text{m}^2$ vs average = $127 \pm 14 \mu\text{m}^2$) ($p < 0.05$, Independent two-tailed t test)

(Figure 61 *b*). In the lateral limb however, no significant difference was found (somato-dendritic average = $188 \pm 21 \mu\text{m}^2$ vs purely somatic average = $175 \pm 13 \mu\text{m}^2$ respectively) (Independent two-tailed t test) (Figure 61 *c*).

In several species Lateral olivocochlear (LOC) neurons are demonstrably smaller than pLSO neurons (Sanchez-Gonzalez et al, 2003; Adam et al, 1999 Aschoff and Ostwald, 1988), so they are likely candidates for the population of cells with purely somatic gephyrin staining. The larger cells with dendritic and somatic gephyrin staining would therefore appear to be pLSO neurons. Since these cells are the focus of the current investigation, they are assessed exclusively in the remainder of this chapter.

3.3.6 The somatic size of MSO cells is invariant.

Unlike the LSO, the MSO proved to comprise a single homogenous population of cells when classified on the sublocalization of their gephyrin staining: average cross-sectional somatic areas were almost exactly the same for cells with dendritic and somatic staining (average = $297 \pm 15 \mu\text{m}^2$) and those with purely somatic (average = $295 \pm 28 \mu\text{m}^2$) (Figure 61 *e*).

3.3.7 pLSO neurons in the guinea pig medial limb are not significantly smaller than MSO cells

To determine whether regional differences exist in the somatic properties of guinea pig pLSO neurons (i.e. those LSO cells with somato-dendritic gephyrin), staining were next compared across the nucleus. Though the average somatic size does decrease from the medial to the lateral limb of the LSO, these differences were not significant (One Way ANOVA with Bonferonni post correction) (Figure 61 *d*).

pLSO cells from different regions were then compared to MSO cells with somato-dendritic gephyrin staining to determine whether a significantly larger somatic size still persisted in MSO after distinction between pLSO and LOC neurons (Figure 61 *d*). Whilst pLSO neurons from the mediolateral and lateral limbs continued to obey the relationship between cell size and location ($p < 0.05$ and $p < 0.01$ respectively, Independent two-tailed t-test), cells from the medial limbs were not significantly smaller than MSO cells. The simplest hypothesis, given the absolute values of the average cross-sectional somatic areas, is that the somatic size of pLSO cells increases towards the medial limb of the guinea pig.

Discussion

In this thesis, experiments were performed in the guinea pig LSO to study the intrinsic and synaptic properties of their principal neurons. Such biophysical specializations are fundamental in determining how well pLSO neurons can extract acoustic cues from binaural stimuli. To shed light here on guinea pig pLSO neurons' predisposition to process ILDs and envelope ITDs, the biophysical differences and similarities between guinea pig pLSO neurons and principal neurons from the rat LSO and guinea pig MSO are compared. The ensuing functional implications for high- and low-frequency hearing species are addressed in the general conclusions, highlighting potential strategies that might be employed across SOC nuclei.

4.1 Passive and Active properties

4.1.1 Overview of results

Whereas evidence from the rat, an altricial species, has indicated that the passive electrophysiological properties of their pLSO neurons continue to develop beyond the onset of hearing at P12 (Kandler and Friauf, 1995); this study showed that, in line with the guinea pig's precocious ability to hear, its pLSO neurons were mature at birth.

A continuous range of firing patterns was observed in the guinea pig LSO, pointing towards a single, broadly homogeneous population of principal neurons. This was corroborated by analysis of the pLSO neurons' passive properties including input resistance, membrane time constant and capacitance. These findings contrast with the data collected from the rat LSO both here and in previous studies which propose that two neuronal classes can be

distinguished in the rat LSO by their passive and active properties (Barnes-Davies et al, 2004). Since the absence of a heterogeneous population in the guinea pig pLSO population could not be attributed to artifactual concerns and therefore likely had a biological provenance, it may reflect a functional schism in the strategies employed by the two species to process ILDs and envelope ITDs in their LSOs.

Differences were observed in the passive properties of guinea pig principal neurons along the tonotopic axis of the LSO. Lateral pLSO neurons, which receive afferents from fibres representing low-frequency auditory stimuli *in vivo*, possessed the lowest input resistances as well as the fastest membrane time courses. Since low CF pLSO neurons in the lateral limb are particularly sensitive to interaural phase differences (Tollin and Yin, 2003), principal neurons, able to integrate synaptic information rapidly in this region, could play a specialized role in fine structure and envelope ITD processing.

The observation of resonance in guinea pig pLSO neurons was made for the first time, using a ZAP protocol to assess sub-threshold voltage responses. The peak resonant frequency in pLSO neurons was considerably higher than values previously observed in other CNS neurons suggesting that such resonant properties may be unique to the auditory pathway. The discovery that resonant pLSO neurons recorded were mainly localized in the low-frequency lateral limb of the LSO may be associated with a varying expression or different array of membrane conductances that has not been described before. Functionally, this may mean that resonance in pLSO neurons filter synaptic inputs in such a manner that improves their envelope ITD sensitivity and facilitates the localization of a sound in a noisy environment.

4.1.2 Differentiating between pLSO neurons and alternative neuronal types.

Before analysis of pLSO neurons could be performed, recordings from other neuronal types had to be identified in the collective group of recordings made in the SOC. “Intrinsic” LOC neurons, which provide efferent drive to the outer hair cells in the cochlea, are the main alternative neuronal type to be localized within the LSO of rats and guinea pig (Adam et al, 1999; Fujino et al, 1997; Barnes-Davies et al, 2004). In spite of the fact that electrophysiological characterizations have only been performed in the rat, it was still possible to use the same general criteria to identify LOC neurons in the guinea pig. For every LOC neuron patched in the two species, recordings were made from 7.3 pLSO neurons: this ratio appears to advocate the success of visually selecting potential principal neurons by microscope and CCD camera prior to patching.

Values obtained for the input resistance (303 ± 173 (SD) $M\Omega$) and membrane time constant (11 ± 5.8 (SD)) of rat LOC neurons in this study were smaller than previously found in the same species [445 ± 191 (SD) $M\Omega$ and 18 ± 11.7 (SD) ms] (Fujino et al, 1997): this is likely a result of the higher temperature implemented during recordings here (Fujino et al study was performed at room temperature). By increasing the bath temperature, membrane conductances would have increased as the underlying channels spent more time in the open state and pass a current. The LOC neurons would therefore be leakier and both input resistances and membrane time constants would be reduced.

4.1.3 The passive and active properties of pLSO neurons in the rat.

To understand how a continuous range of firing patterns is achieved across a population of guinea pig pLSO neurons possessing homogeneous passive properties, it is useful to first broach the relationship between firing patterns and passive properties in rat pLSO neurons.

In contrast to the guinea pig LSO, a schism in the firing patterns of pLSO neurons was observed in the rat when responses to somatic current injection were studied (Figure 36). type 1 pLSO neurons mainly displayed a single onset AP in response to superthreshold depolarizing current steps; when the stimulus exceeded 850pA, however, many type 1 neurons did respond with a second AP (Figure 35 *a*). Type 2 pLSO neurons, on the other hand, demonstrated a train of APs following the onset AP at current steps smaller than 850pA (Figure 35 *b*). Despite type 1 and type 2 pLSO neurons closely resembling classifications of single- and multi-firing neurons used by Barnes-Davies and colleagues in the rat LSO (2004), the emergence of a second AP in most type 1 neurons meant that it was difficult to appropriate these names here.

It has been proposed that the relative expression of I_{KLT} in rat pLSO neurons determines whether neurons are single- or multi-firing in the Barnes-Davies et al study (2004); it is therefore likely that I_{KLT} was involved in determining how many APs were generated in rat pLSO neurons after the onset AP. The increased expression of I_{KLT} in type 1 pLSO neurons does not appear, however, to be sufficient to prevent a second AP and therefore make pLSO neurons strongly phasic as has been suggested of single-firing pLSO neurons in the Barnes-Davies et al study (2004). In gerbil pMSO neurons, which only respond with an onset AP even in the presence of dendrotoxin, a K_{LT} blocker, it is the rapid inactivation of voltage-gated Na channels at surprisingly hyperpolarized potentials ($V_{1/2} = -77mV$) that causes the complete cessation of firing after an initial AP (Svirskis et al, 2004; Scott et al, 2005; Scott et al, 2010). It would therefore appear that whilst a Na^+ conductance with these properties is necessary to institute strong phasic behaviour in pMSO neuron, it is absent in both type 1 and type 2 pLSO neurons (or at least it exists with a more depolarized $V_{1/2}$ inactivation). This is conducive to both classes of pLSO neuron having more tonic firing properties than their pMSO counterparts.

Aside from the issue of how many APs were evoked by current steps in rat type1/single-firing pLSO neurons in the rat, the average input resistances of rat type 1 and 2 neurons also

differed from the values measured for single- and multi-firing pLSO neurons in the study of Barnes-Davies et al (Type 1 Vs. Single-firing neurons = $37 \pm 8 \text{M}\Omega$ Vs $70 \pm 7 \text{M}\Omega$ and Type 2 Vs. Multi-firing neurons = $121 \pm 18 \text{M}\Omega$ Vs. $174 \pm 29 \text{M}\Omega$). However, as was the case for the LOC neurons, these discrepancies in passive properties can be traced back to diverging recording conditions since Barnes-Davies et al (2004) was conducted at the lower temperature of 24C° . This conclusion is supported by the calculation of the average rat pLSO capacitance using the membrane time constant and input resistance ($\tau = \text{input resistance} * \text{capacitance}$). The average value for all rat pLSO neurons ($30 \pm 5.9 \text{pF}$) was similar to the values calculated for single- ($23.1 \pm 1.8 \text{pF}$) and multi-firing ($21.7 \pm 1.8 \text{pF}$) neurons in the previous study. Since the capacitance is proportional to neuronal size, which is not temperature dependent, it can be assumed with confidence that neurons patched in both studies arose from the same general population of neurons. Indeed even the distribution of rat type 1 and type 2 pLSO neurons along the tonotopic axis of the LSO followed the scheme observed in Barnes-Davies et al (2004) for single- and multi-firing neurons.

4.1.4 The passive and active properties of pLSO neurons in the guinea pig.

If I_{KLT} is also considered a suitable candidate to depress excitability in guinea pig pLSO neurons and thus regulate the maximum number of APs possibly elicited by a current step, then varying the expression of its underlying channel, Kv1.1, across the neuronal population could explain how a continuous range of firing patterns is implemented. Although Barnes-Davies and colleagues showed that I_{KLT} 's current density did vary along the tonotopic axis in "single-firing" rat pLSO neurons, it was apparently not enough to affect neurons firing patterns (Barnes-Davies et al, 2004). Indeed immunohistochemical assays by the same group pointed to an all-or-nothing Kv1.1 expression profile being responsible for the differing excitability amongst rat pLSO neurons. Thus any variations in I_{KLT} amplitude

would likely have to be extensive to permit such a full range of firing patterns across guinea pig pLSO neurons.

Were this the case and the continuous firing range in the guinea pig LSO was dependent solely on the varying amplitude of I_{KLT} , then a continuous range of input resistances values would be expected as a consequence. Such an observation was indeed made in the guinea pig LSO (Figure 19) however input resistances spanned a smaller range (30-90M Ω) than previously observed in the rat LSO (30-150M Ω in Figure 38 and 55-230M Ω in Barnes-Davies et al, 2004), suggesting a more homogeneous set of passive properties in the guinea pig LSO. This raises the question as to what diverse set of conductances could underlie different firing patterns in the guinea pig LSO, while still providing a very similar input resistance.

This is a particularly important question for those pLSO neurons which fired most frequently and yet still possessed low input resistances. In such cases where I_{KLT} was definitely absent, an additional conductance had to be constitutively open in order for the input resistance to be set so low without limiting the number of APs. The most likely candidates are the hyperpolarizing-activated mixed cationic conductance, I_h , and the inward rectifier, I_{KIR} . Both have been noted as particularly prominent in other species' pLSO neurons and can act to decrease the input resistance in this voltage range (Adam et al, 2001; Leao et al, 2006; Szalisznyó, 2006). Were I_h more prominent in the aforementioned group of guinea pig pLSO neurons its effects would be most conspicuous in the hyperpolarizing section of IV curves. Figures 17 *d*, *e* and *f* demonstrate that the IV profiles of three guinea pig pLSO neurons were comparable with no obvious increase in steady state rectification with maximum number of APs possibly evoked. This observation does not however preclude the presence of a larger I_h conductance in guinea pig pLSO neurons which fired more frequently. One explanation is that a large I_{KIR} conductance (inward rectifying potassium conductance) could have opened in the hyperpolarizing direction and masked the I_h conductance by "clamping" the pLSO neuron to the E_K reversal potential (Adam et al,

2001). A second explanation proposes that I_h could possess differing voltage-gated profiles across the guinea pig pLSO population. Different HCN channel isoforms are known to produce I_h currents with faster kinetics and more positive $V_{1/2}$ activations in the auditory brainstem and midbrain (Bal and Oertel, 2000; Leao et al, 2006; Koch and Grothe, 2003; Barnes-Davies et al, 2004). Although immunohistochemical studies suggest that it is unlikely that different HCN isoforms would be found within the guinea pig pLSO neuronal population (Leao et al, 2006), it is possible that differing modulation of a shared isoform could lead to diverging voltage-gating properties for I_h in the guinea pig LSO (Adams et al, 2001). If I_h had a more negative $V_{1/2}$ activation in those guinea pig pLSO neurons which fired more frequently, hyperpolarizing current steps would activate less additional conductance above constitutive levels in these neurons when compared to their pLSO counterparts which only fired twice maximally. As a consequence, the voltage sag observed in the hyperpolarizing direction could appear constant across the guinea pig pLSO neuronal population.

If the second scenario were true and I_h proved to be more active at rest in guinea pig pLSO neurons firing twice maximally, then their resting membrane potentials should appear more depolarized than those of pLSO neurons which responded with more than two APs. Figure 62 shows that there was no correlation existed between the resting membrane potential and the number of action potentials that could be evoked maximally in the guinea pig LSO. Thus it is likely that changes in I_{KIR} amplitude do accompany those in I_h , helping to clamp the resting membrane potential closer to the K^+ equilibrium in guinea pig pLSO neurons (Szalisnyó, 2006).

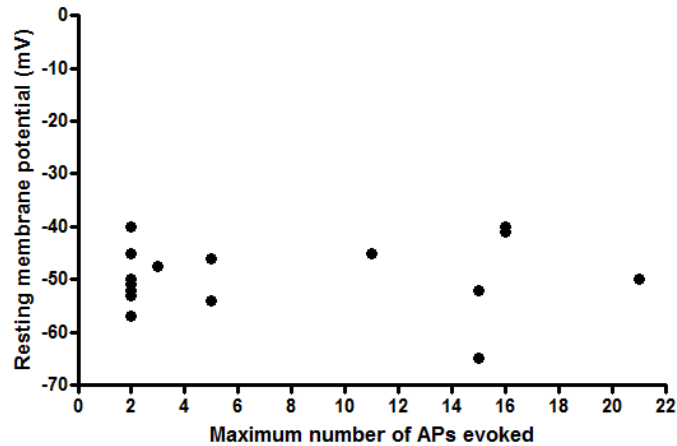


Figure 62. Resting membrane potential plotted against maximum number of action potentials evoked in guinea pig LSO neurons. No correlation was observed between the two parameters

Given that the maximum number of APs evoked by a current step is independent of a guinea pig pLSO neuron's input resistance (Figure 20), conductances that actively control spike frequency adaptation will be highly important in determining how frequently a neuron fires during a 100ms current step. It would be wrong to imagine that I_{KLT} is the only conductance able to directly regulate the number of APs evoked. Similar to I_{KLT} , the A-type transient potassium conductance has been found in rat pLSO neurons and can also curtail firing; indeed blocking it 50 μ M 4-AP leads to a sustained firing pattern devoid of spike frequency adaptation (Adams et al, 2001). In contrast to the effects of I_{KLT} and I_A , it is possible that a regenerative conductance such as a sub-threshold sodium conductance could actually promote excitability in guinea pig pLSO neurons whilst actually lowering the input resistance by being open at rest (Adams et al, 2001). In summary, pharmacological intervention will be necessary to better understand how this myriad of conductances might potentially interact, producing these firing patterns in the guinea pig LSO.

It is not only the active properties that can have functional implications for envelope ITD processing. Although the membrane time constants of the guinea pig pLSO neurons never approached the low values quoted for gerbil pMSO neurons in the literature (<0.4ms, Scott et al, 2005; Khurana et al, 2011), 8/20 (40%) of them were sub-millisecond indicating that

these neurons should be able to integrate synaptic inputs sufficiently fast to process the with rapidly changing levels differences associated with envelope ITDs.

4.1.5 Tonotopic differences in the active and passive properties of guinea pig pLSO neurons

The prevalence of “single-firing” principal neurons in the lateral limb and “multi-firing” principal neurons in the medial limb of the rat LSO has been previously observed by Barnes-Davies and colleagues (2004). This arrangement potentially has great functional significance as the associated variations in the passive properties may facilitate the processing of divergent binaural cues along the tonotopic axis.

Of the twelve principal neurons patched in the guinea pig LSO’s lateral limb, five (42%) responded maximally to depolarizing current steps with more than 10 APs (Figure 29). As a result, the proportion of pLSO neurons only firing twice maximally was not significantly larger in the lateral limb ($\chi^2=0.083$, Yates-corrected Chi-squared test), suggesting that firing patterns may also remain continuous within each limb of the guinea pig LSO. This observation did not however suggest the absence of tonotopic variations in the principal neurons’ passive properties: values of all three passive properties analysed (input resistance, capacitance and membrane time constant) being significantly smaller in the lateral limb of the guinea pig LSO (Figures 30, 31 and 32).

Although the variations in input resistance along the LSO’s tonotopic axis do not offer further clues as to the identities of any underlying conductances, they do suggest that these conductances display a tonotopic gradient of expression. Given the apparent similarity in the firing patterns between the two limbs, it is likely that the conductance in question is not fundamental to determining the number of APs evoked in response to a current step.

If it is assumed that the space clamp of a recording was not affected greatly by the tonotopic variations in input resistance, then the analysis of capacitance points to larger neurons in the medial limb of the guinea pig LSO. Anatomical studies in the rat and gerbil have suggested that dendritic arborizations are actually similar if not more extensive in the lateral limbs of their LSOs due to restricted dendritic pruning in this region during development (Sanes and Song, 1992; Rietzel and Friauf, 1998). If this were also true for the guinea pig, the somatic size of medial pLSO neurons would consequently have to be larger than is the case for neurons from the lateral limb to produce the result in Figure 32.

Potentially the most important result from a functional perspective is the faster membrane time constant of pLSO neurons from the lateral limb of the guinea pig LSO. Faster integration of synaptic inputs would allow guinea pig pLSO neurons in the lateral limb to process envelope ITDs with better resolution.

In regards to the membrane time constant, it would appear that the rat and guinea pig LSO are arranged in a similar manner, indicating a potential functional overlap (Barnes-Davies et al, 2004). The question still remains however why so many principal neurons in the guinea pig LSO with such a high firing rate (when stimulated by current steps) are found in the lateral limb. This and the functional implications of the tonotopic variations are discussed further in the general conclusions.

4.1.6 Subthreshold resonances in guinea pig pLSO and pMSO neurons

Resonance is a phenomenon that arises from the interplay between a neuron's passive and active properties and allows neurons to respond preferentially to particular input frequencies. Although spontaneous oscillations have been previously noted in rat type 2 pLSO neurons (Adams et al, 2001), they are only observed following APs in rat (Adams et al, 2001) and guinea pig pLSO neurons (Figure 16 *b*, top panel). Neuronal models have suggested that

such spontaneous oscillations are not associated with subthreshold resonances but are instead an epiphenomenon of the conductances that allow tonic firing patterns in type 2 pLSO neurons (Izhikevich, 1999; Szalisznyó, 2006). When tested with the ZAP stimulus to probe subthreshold resonance directly, 2 out of 8 guinea-pig pLSO neurons were indeed resonant, making this the first study to describe subthreshold resonance properties in the guinea pig LSO.

This finding complements the work performed by Roberta Donato in the guinea pig MSO which showed that band-pass filtering was common amongst principal neurons. All ten pMSO neurons possessed resonant properties: their impedance profiles offered similar Q values to the two pLSO neurons recorded in this study (average Q factor in guinea pig MSO = 1.3 ± 0.03 , n=10) but with peak resonances that reached much higher frequencies than in the pLSO neurons (average peak resonant frequency in guinea pig MSO = 188 ± 30 Hz; range = 73-380Hz, n=10) (Figure 63).

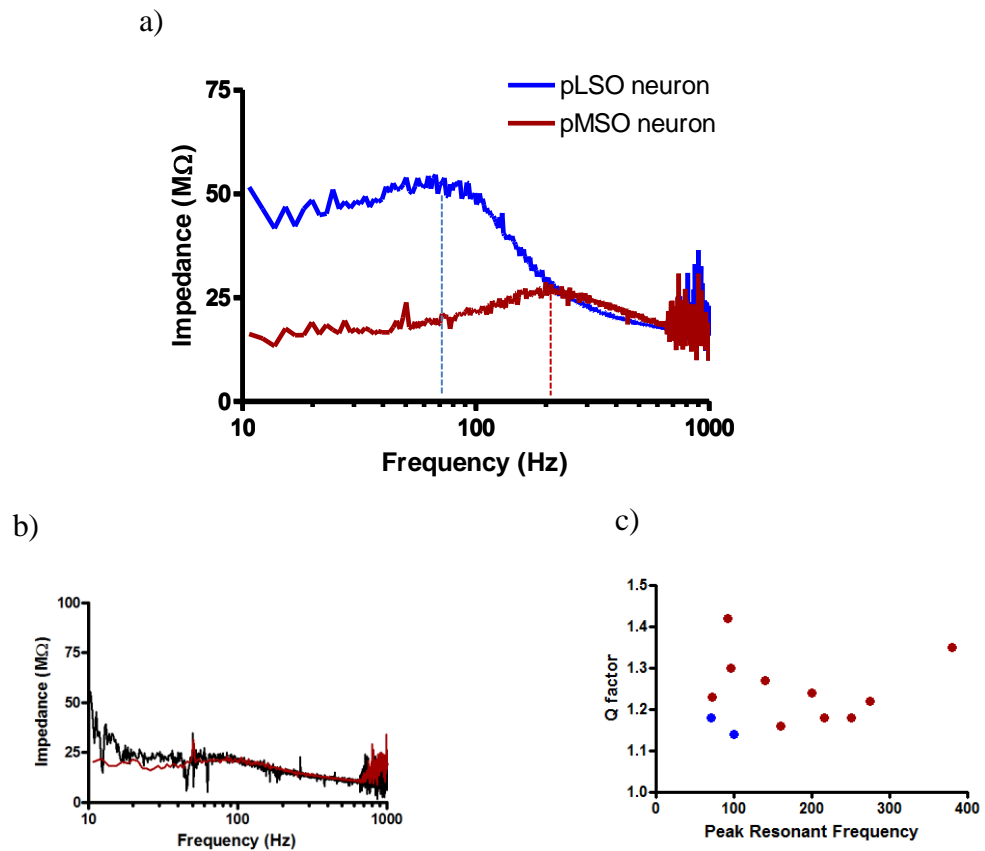


Figure 63. Sub-threshold resonance in the guinea pig MSO. The impedance profiles of example pMSO (*blue trace*) and pLSO neurons (*red trace*) are shown in *a*. Peak resonant resonance frequencies are represented by vertical dashed lines. Hyperpolarization of a pMSO neurons by 10mV led to the elimination of resonance in *b*. When Q factor was plotted as a function of peak resonant frequency for all resonant pSOC neurons, there was no correlation between the values

When comparing impedance profiles in the guinea pig SOC to those acquired in other regions of the central and peripheral nervous system, it is evident that subthreshold resonances in the pSOC have particular properties. The average Q factor values in both the LSO and MSO are very comparable to those observed in non-auditory neurons in the rat hippocampus (Hu et al, 2007; Bohlen et al, 2011), indicating that pSOC neurons are not in fact any more frequency selective than other resonant neurons in the central nervous system. In contrast, the range of peak resonant frequencies in the MSO (73-380Hz) and LSO (71-100Hz) are two or more orders of magnitude higher than has been previously noted in other

mammalian neurons (Leung and Yu, 1998). This means that peak resonant frequencies of guinea pig pSOC neurons actually match values observed in the turtle hair cell population (10-300Hz) (Art et al, 1986). Resonance in the turtle's auditory periphery however displays exquisite frequency selectivity (thanks to high Q factor values) allowing the hair cells to replace basilar membrane properties as a means of establishing a tonotopic map in lower vertebrates. Given the unique nature of the pSOC neuron's subthreshold resonance, it is highly unlikely that its function overlaps with other resonances in the central or peripheral nervous system. Their high peak-resonant frequency ranges do suggest, however, that the band-pass filters in the guinea pig SOC particularly suited to fast temporal processing, possibly even able to modulate input on a cycle-by-cycle basis at many frequencies.

The biophysics of resonance in guinea pig pSOC neurons

In light of the criteria proposed by Hutcheon and Yarom (2000) for resonance, I_{KLT} is a suitable candidate conductance to underlay resonant properties at peak frequencies in both guinea pig pLSO and pMSO neurons. Open at rest thanks to its low voltage activation, I_{KLT} reduces a neuron's input resistance and therefore raises the corner frequency of the low-pass filter created by a neuron's passive properties. As an outward rectifying potassium conductance whose reversal potential lies near the base of its activation curve (Barnes-Davies et al, 2004; Scott et al, 2005), I_{KLT} also opposes changes in the membrane voltage and can therefore act as an inductor. Thanks to its fast activation kinetics (1.1ms in the gerbil MSO (Mathews et al, 2010), I_{KLT} can "track and oppose" the low frequency stimuli, attenuating the corresponding voltage response and creating a high-pass filter with a high corner frequency (Hutcheon and Yarom, 2000; Day et al, 2008; Mathews et al, 2010 Remme et al, 2011). Together, these low- and high-pass filters' elevated corner frequencies are conducive to high peak resonant frequencies in pSOC neurons.

Evidence for I_{KLT} 's involvement in the resonance of pSOC neurons was also observed in this study. I_{KLT} is a conductance common to both gerbil MSO and rat single-firing (type 1) pLSO neurons (Svirakis et al, 2002; Barnes-Davies et al, 2004; Scott et al, 2005) and, given data from AP firing patterns accrued in this study, it is likely to be the predominant conductance in many of the guinea pig pSOC neurons. Therefore, the fact that resonance was only observed in pSOC neurons which responded maximally to current injection with either one (pMSO) or two (pLSO) APs could be due to prevalence of I_{KLT} in these neuronal types. Furthermore, injecting a DC hyperpolarizing current to reduce the baseline of the voltage response during a ZAP protocol reduced or eliminated resonance in the one pMSO and one pLSO neuron tested (Fig. 34 and 63). This can be explained by I_{KLT} 's lying close to the base of the activation curve at resting membrane potential in both neuronal types [as it does in pMSO neurons (Mathews et al, 2010)]. Therefore, when pSOC neurons are hyperpolarized, I_{KLT} is inactivated and cannot be recruited as effectively by the small subthreshold voltage responses to ZAP protocols: causing the reduced or eliminated resonance in turn.

The proposition that high peak resonant frequencies can be attributed to the predominance of I_{KLT} is supported by a model of subthreshold resonance in the guinea pig pSOC neurons performed as part of a laboratory collaboration with the Rinzel group in NYU (Remme et al, 2011). Using a linear membrane model, we fitted resonant impedance profiles from both pMSO and pLSO neurons extremely well and found that the activation time constant for I_{KLT} required a range from 1 to 4ms depending on the peak resonant frequency. This value for the activation time constant agrees well with those observed for I_{KLT} in pMSO and VCN neurons *in vitro* (Rothman and Manis, 2003; Mathews et al, 2010).

I_{KLT} is likely the main conductance involved in producing resonance. However, this does not exclude the involvement of other conductances. The relationship between the peak resonant frequency and the Q factor did not display any correlation and this potentially means that another conductance may be involved in amplifying the resonance (Hutcheon and Yarom,

2000). The aforementioned model suggests that a regenerative conductance with an activation constant of 0.5ms would have to exist for resonance with a peak below 100Hz in pMSO and pLSO neurons. One possible candidate that has been previously mentioned in regards to pLSO neurons' excitability is the sub-threshold Na^+ conductance. Its existence in gerbil pLSO neurons has been demonstrated and, interestingly, it appears to be open at rest since TTX induces hyperpolarization of the membrane potential. It therefore could be involved in a sub-threshold resonance (Adam et al, 2001).

In summary, resonance with a high peak resonant frequency exists in guinea pig pMSO and pLSO neurons thanks to the combination of a large neuronal size, a low input resistance and specialized voltage-gated conductances. The candidate voltage-gated conductance which most likely underpins this resonance is I_{KLT} whose expression in pMSO and a subset of pLSO neurons matches the pattern of resonant neurons in the guinea pig. Another conductance also appears to be involved where low frequency resonance is concerned, potentially the subthreshold Na^+ current previously observed in rat pLSO neurons.

Peak resonance frequency and the tonotopic axis of the LSO and MSO

The exclusive presence of resonant pLSO neurons in the lateral limb of the guinea pig LSO has both biophysical and functional implications. Whilst a restorative conductance like I_{KLT} may account for the restricted firing pattern in these resonant principal neurons, it appears that it must be allied with a regenerative conductance, such as I_{Na} , for resonance to be observed in the LSO. The existence of a single medial pLSO neuron displaying more phasic firing pattern but no resonant properties could therefore result from the amplitude of I_{Na} varying across the tonotopic axis of the guinea pig LSO. Were diverging patterns of I_{KLT} expression then additionally able to account for the continuous firing patterns across the guinea pig LSO (and also ensure low pass-filtering in those principal neurons firing more tonically), then only the homogeneous passive properties across the pLSO population would

remain unexplained. Although this is only speculation without experiments involving detailed pharmacological intervention, it does highlight the possibility that pLSO neurons with similar firing patterns might actually possess different active properties along the tonotopic axis of the LSO. This would further add weight to the idea that resonance is functionally important to ITD and envelope ITD processing in the low-frequency region of the guinea pig LSO

Whilst there was no possible discontinuity in resonant properties along the tonotopic axis of the guinea pig MSO, a tonotopic gradient of peak resonant frequencies was found when a composite MSO nucleus was reconstructed using the neurons' positions as localized by Roberta Donato (Figure 64). This would appear to not only indicate that pMSO possess heterogeneous biophysical properties but also that they are organized along the tonotopic axis. In light of the central role attributed to I_{KLT} in implementing resonance, the biophysical explanation for different peak resonant frequencies likely involves the conductance's properties diverging across the tonotopic axis. When the resonant properties in each pMSO neuron from Figure 64 were fitted using the linear membrane model developed by Remme (2011), it was predicted that the activation time constant and magnitude of I_{KLT} were particularly important parameters. Whilst the activation time constant decreased from 4 to 1ms towards the low frequency limb of the MSO where the peak resonant frequencies of principal neurons were highest, the conductance's amplitude increased (Remme et al, 2011).

To summarize, variations in I_{KLT} and I_{Na} expression as well as its kinetic properties may well underlie the range of resonant properties in pSOC neurons observed along the tonotopic axis. The positive correlation between a pSOC neuron's resonance and its ability to integrate synaptic inputs rapidly means resonance may be especially important to processing temporal cues.

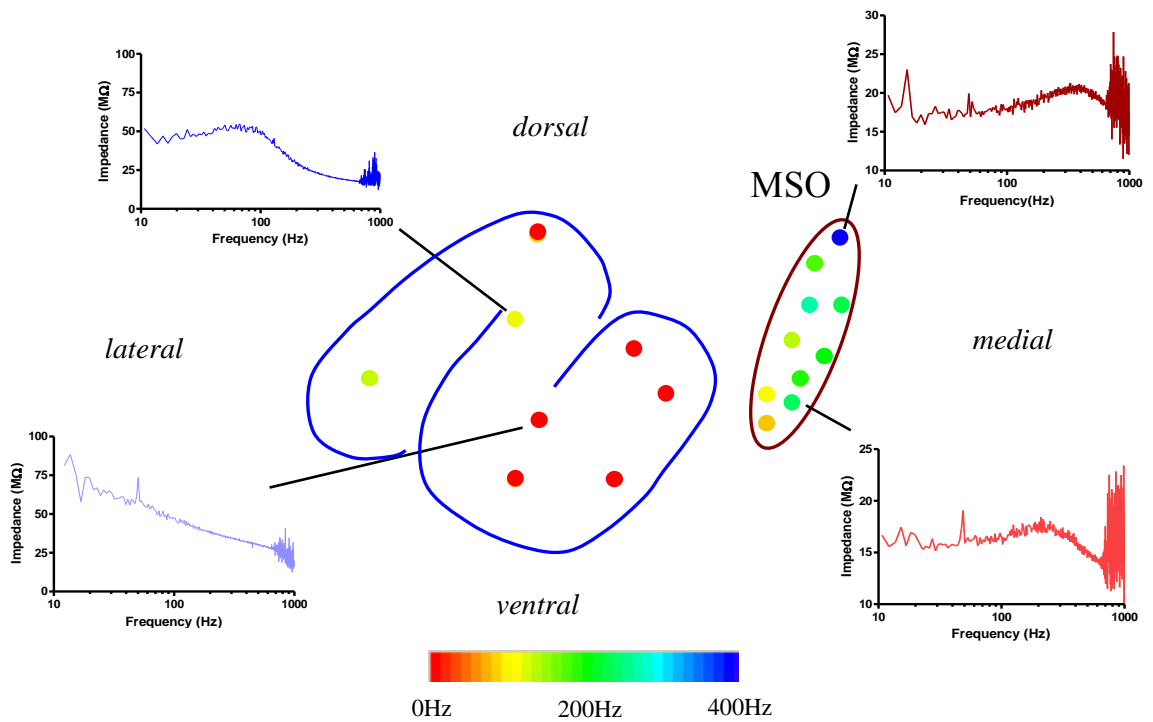


Figure 64. A tonotopic gradient in resonance was found in the guinea pig SOC nuclei. Each symbol represents a single pSOC neuron; its colour represents the peak resonant frequency observed in that neurons. In the LSO, resonant neurons were only encountered in the lateral limb. In the MSO, all principal neurons displayed resonance and were organized such that the highest peak resonant frequencies were found in the low-frequency dorsal region whilst the lowest values were found at the high-frequency, ventral region.

4.2 Synaptic Electrophysiology

4.2.1 Contralateral synaptic inputs in the guinea pig LSO

Results from this study confirm that synaptic inputs of contralateral origins do impinge upon principal neurons in the low-frequency, lateral limb of the guinea pig LSO (12/21 neurons). Prior to studying synaptic inputs in the guinea pig LSO, a pilot study using the same *in vitro* brainstem preparation was performed in the rat LSO by myself. PSPs were observed in 5/11 (55%) of rat pLSO neurons (n=11 rat pLSO neurons). These numbers likely underestimate how many pLSO neurons actually received contralateral inputs *in vivo* as slicing performed at a slightly oblique angle could have easily damaged fibre tracts.

Since it is unlikely that either the excitatory or inhibitory pathway would have preferentially remained intact after slicing, given the proximity of the two pathways in the brainstem, another explanation for why so few pLSO neurons displayed mixed excitatory and inhibitory input must be assumed to exist. If the impact of electrode placement on the selective recruitment of trapezoid body fibres at the midline is also excluded on the basis of the pathways' proximity, it leaves the conclusion that these results actually reflect the true contralateral arrangement of synaptic inputs to pLSO neurons. The potential existence of guinea pig and rat pLSO neurons that only received excitation as a contralateral input would be supported by evidence from low frequency neurons in the rabbit LSO which displayed a peak activity close to coincidence and thus were considered bilaterally excitable (Batra et al, 1997).

The proportion of pLSO neurons contacted by contralateral excitation in the rat (2/5 or 40% of cells) and guinea pig (50%) appeared to be higher than the percentage observed in the mouse (30%) (Wu and Kelly, 1991; Wu and Kelly, 1992). It is difficult to state whether this difference is significant or merely associated to the smaller sample size in this study. It is

however very unlikely that dPSPs in fact arose from ipsilateral fibres stimulated by current spread, as electrical stimulation was performed here at the midline [unlike in some previous studies (Sanes, 1990)].

In 83% of guinea pig, and 100% of rat, neurons receiving this contralateral excitation possessed phasic firing patterns (i.e. only responded with two APs maximally to current injection), suggesting that this subgroup of pLSO neurons was targeted preferentially by fibres arriving directly from the AVCN. This appeared to be irrespective of a neuron's location along the tonotopic axis, however, as half of all guinea pig pLSO neurons receiving contralateral excitation were located in the medial limb, contralateral excitation does not appear to be restricted to one or the other limb of the guinea pig LSO. As discussed in method, the division of the LSO nucleus into medial and lateral limbs is not especially precise, however it compensates for the difficulty in accruing data across slices from different individual animals. It is therefore difficult to state how far contralateral excitation actually extended into the high frequency, medial limb. The functional relevance of bilaterally excitable pLSO neurons are discussed in the general conclusions.

4.2.2 Comparing temporal properties of PSPs in the guinea pig LSO with findings from previous studies.

Two previous studies have used sharp electrode recordings at near physiological temperatures to measure PSPs in the rat (Kandler and Friauf, 1995) and gerbil (Sanes, 1990) LSOs. This form of intracellular recording entails penetrating the somata of pLSO neurons with a high resistance pipette which can underestimate the input resistance by introducing a significant leakage resistance across the membrane of a recorded cell (Staley et al, 1992; Li et al, 2004). It is therefore expected that the time course of PSPs will be artificially accelerated by this technique as the membrane time constant is greatly reduced.

Whilst hPSPs and dPSPs in the guinea pig pLSO neurons were twice as slow as PSPs of equivalent polarity in gerbil pLSO neurons (Sanes, 1990), the average hPSP half-width in guinea pig pLSO neurons (3.6 ± 1.15 ms, n= 6) proved to be shorter than has been previously observed in P13 rats (10.2 ± 7.6 ms, n = 3) (Kandler and Friauf, 1995). Although both findings could result from species difference, it is impossible to ignore the technical differences between this patch clamp study and the sharp electrode studies performed in the gerbil and rat LSOs. The hPSPs in the gerbil study likely appeared much faster than they are in reality, due to the use of sharp electrode recordings by Sanes at 31C° (1990). Such a technical concern cannot however explain why guinea pig hPSPs were of longer duration than rat hPSPs in the Kandler and Friauf study (1995). Indeed my own data from a previous pilot study probing synaptic inputs in the rat LSO indicated that the average half-width of hPSPs in the rat LSO was (3.5 ± 0.3 ms, n=3 rat pLSO neurons). This value is almost identical to the average half-width measured in the guinea pig LSO thus it would appear that the results from the Kandler and Friauf study (1995) are not related to species differences. One major factor that may have particularly influenced the hPSP time courses in the Kandler and Friauf study (1995) was the age at which brain tissue was harvested from the rat. Evidence from the gerbil, an altricial species like the rat, shows that pMSO neuron's passive properties only reach a mature, low input resistance after P17 (Magnusson et al, 2005). It is therefore likely that P13 rat pLSO neurons in the Kandler and Friauf (1995) study did not possess fully mature passive properties and would have undergone further development before reaching P19-21 when their lower input resistances would be conducive to faster hPSP time courses as was observed in this study.

In spite of the technical issues surrounding the different intracellular techniques, similarities and dissimilarities observed between guinea pig LSO PSPs and gerbil LSO PSPs (Sanes, 1990) are worth noting for their potential biological basis. The two most obvious similarities were that dPSPs displayed no after-hyperpolarization in the LSO and that the half-width of both dPSPs and hPSPs in the LSO increased with peak amplitude. One major dis-similarity

was that dPSPs were significantly shorter than hPSPs in the gerbil LSO study (Sanes, 1990) whereas this study suggests that PSPs of opposite polarities have similar durations in the guinea pig LSO (average half-width of dPSP in guinea pig LSO = 2.71 ± 0.2 ms, n= 3 Vs. average half-width of hPSP in guinea pig LSO = 3.6 ± 1.15 ms, n=6).

The two similarities mentioned above also highlight how dPSPs from the LSO contrast in both the gerbil and guinea pig. It is useful to make this comparison as many studies have concentrated on understanding how the temporal profile of a dPSP is controlled biophysically in the gerbil MSO.

4.2.3 Temporal properties of dPSPs in guinea pig LSO and MSO

Coincidence detection in the MSO requires narrow time windows of synaptic integration for ITDs differing by tens of microseconds to be distinguished (Wu and Kelly, 1991; Chirila et al, 2007; Mathews et al, 2010). Comparing the temporal properties of dPSPs from the guinea pig MSO and LSO can therefore be a useful measure of how effective dPSPs are at producing ITD sensitivity in the guinea pig LSO. Fortunately such a comparison between SOC principal neurons is possible thanks to the data collected by Roberta Donato in the guinea pig MSO.

In order to make a fair comparison, dPSPs were selected in pMSO neurons using the same criteria applied to pLSO neurons in section 3.2.1 i.e. between 3 and 6 mV and occurring within the first five pulses in a train. The average half-width of these dPSPs was calculated as 0.8 ± 0.05 ms (n=3 guinea pig pLSO neuron pMSO neurons; Donato, personal communication), demonstrating how short duration dPSPs must be for coincidence detection. The average rise and decay times of dPSPs in the pMSO neurons were measured as 0.58 ± 0.06 ms and 0.64 ± 0.02 ms respectively (n =3 guinea pig pMSO neurons; Donato, personal communication).

Given the corresponding values in the three guinea pig pLSO neurons tested (average half-width = 2.71 ± 0.2 ms; the average rise time = 1.22 ± 0.15 ms; the average decay time = 3.08 ± 0.61 ms. $n= 3$ guinea pig pLSO neurons), it would appear that the dPSPs were at least 3 times as fast in the three pMSO neurons. As is evident in Figure 39 *b* where the time course of the average dPSP from one of the three pMSO neurons is compared with the time course of the average dPSP from one of the three guinea pig pLSO neurons, a combination of faster rise and decay phases meant that dPSPs in the sample guinea pig MSO were shorter than corresponding dPSPs in the guinea pig LSO. Since these pMSO neurons are large cells with extremely low input resistances, their membrane time constant is consistently in the sub-millisecond range (0.34 ± 0.04 ms in the 3 guinea pig pMSO neurons assessed in this study). It would therefore be expected that they will integrate synaptic inputs more rapidly than guinea pig pLSO neurons whose membrane time constants are, on average, much longer (1.0 ± 0.09 ms in the 3 guinea pig pLSO neurons assessed).

In addition to the effects of passive properties, some conductances can actively shape the time course of dPSPs and therefore further shorten their duration. Possibly the most important conductance in this regards is the low-threshold K^+ conductance, I_{KLT} . Its presence has been noted in both pMSO neurons from the gerbil and single-firing (type 1) pLSO neurons from the rat. However, only in the former have I_{KLT} 's effects on the time course of a dPSP been studied (Svirskis et al, 2003; Barnes-Davies et al, 2004; Scott et al, 2005; Mathews et al, 2010). Thanks to its fast kinetics and hyperpolarized voltage-activation range, I_{KLT} activates during the initial rising phase and helps to decrease dPSP rise times by dynamically reducing the membrane time constant as well as resisting the depolarization as an outward conductance (Mathews et al, 2010). It is difficult to state categorically, from the current findings, whether the impact of I_{KLT} on the rising phase of dPSPs was greater in the LSO or MSO since the slower average dPSP rise times in the LSO could easily have resulted from the longer membrane time constants of pLSO neurons at rest dominating the early dPSP time course.

I_{KLT} has also been previously implicated in the generation of dPSP after-hyperpolarizations in models of guinea pig pMSO neurons but not pLSO neurons (Rothman and Manis, 2003; Scott et al, 2005). By only reaching its maximum activity after the dPSP has peaked in pMSO neurons, the outward conductance of I_{KLT} rapidly repolarizes pMSO neurons during the decay phase, causing an after-hyperpolarizing potential (Mathews et al, 2010). This truncated decay further reduces the duration of dPSPs in pMSO neurons. The absence of a hyperpolarizing potential follows dPSPs in guinea-pig pLSO neurons therefore almost certainly reflects the reduced impact of I_{KLT} . It is not possible to say from this finding, however, whether this difference is generated by the reduced expression of I_{KLT} in pLSO neurons or whether the conductance's kinetic and voltage-sensitive properties differ.

However paramount I_{KLT} is in actively shaping the time course of dPSPs, it must not be forgotten that its constitutive activity also lowers considerably the membrane time constant at rest. I_{KLT} is not, however, the only conductance available to pMSO neurons affecting the passive properties, a fact best demonstrated by those studies which have employed the selective Kv1.1 blocker dendrotoxin (DTX-K) to block I_{KLT} in gerbil pMSO neurons. Input resistances increased between two- and three-fold on addition of the drug. Nevertheless, resulting values were still smaller than those calculated for pLSO neurons recorded under control conditions in the current study (Barnes-Davies, 2004; Scott et al, 2005, 2007; Mathews et al, 2010; Khurana et al, 2011). It therefore appears that other large conductances which are expressed in pMSO neurons are active at rest. They may not have similar kinetic or voltage-sensitive properties of I_{KLT} , but they do reduce the average input resistance (and therefore the membrane time constant) of pMSO neurons beyond that measured for control pLSO neurons. These should therefore also contribute to the faster time course of dPSPs in the MSO.

The relationship between peak amplitude and time course of dPSPs

The finding that the half-widths of dPSPs increased with peak amplitude in the guinea pig LSO (Figure 40) suggests that the electrotonic spread of dPSPs is passive in guinea-pig pLSO neurons. This contrasts with observations from both gerbil and guinea-pig pMSO neurons where half-widths of larger dPSPs are actually shorter than for smaller dPSPs (Mathews et al, 2010; Donato, personal communication). Since the phenomenon is reliant upon I_{KLT} being highly concentrated at the somata of pMSO neurons (Mathews et al, 2010), one can assume that this conductance is not found at such high densities in the somata of guinea-pig pLSO neurons. Since I_{KLT} may not only determine dPSP time course but also regulate pLSO neuronal excitability, it would be especially interesting to compare the half-widths of dPSPs from guinea pig pLSO neurons with different firing patterns. If I_{KLT} were indeed responsible for both phenomena, then it would be expected that dPSP time course should increase with the number of APs that could be maximally elicited by current injection. Alongside experiments using DTX-K to block Kv1.1 channels, results from such experiments could potentially describe the true impact of I_{KLT} 's active properties on the half-width and rise-time of dPSPs in guinea-pig pLSO neurons.

4.2.4 Temporal properties of hPSPs in the guinea pig LSO and MSO

The time course of inhibition has been considered an important parameter in explaining how ITD tuning curves are shifted in the gerbil MSO (Brand et al, 2002; Dodla et al, 2006). If the cycle-by-cycle interaction of hPSP and dPSP is vital to ITD processing then the hPSP time course should be as important as that of the dPSP. To perform a comparison between hPSPs in the guinea pig MSO and LSO, data was taken from two guinea pig pMSO neurons (Donato, personal communication). The average half-widths of hPSPs were 1.2 ms and 2.7 ms in the two guinea pig pMSO neurons, leading to an overall average across the sample of 2.2 ± 0.8 ms ($n=2$, Donato, personal communication). With such a high variability and

small sample size, it is impossible to say whether hPSPs were faster in the MSO than the LSO. It is noteworthy however that Magnusson and colleagues found hPSPs in the gerbil LSO possessed similar rise time and decay times to amplitude-matched hPSPs in the gerbil MSO (Magnusson et al, 2005).

If the time course of hPSPs is indeed constant across the guinea pig SOC nuclei, it is impossible to explain this finding by considering their principal neurons' passive properties alone: the average τ of the two guinea pig pMSO neurons was a factor of five faster than the average τ measured for the six guinea pig pLSO neurons (τ of pMSO neurons = 0.25 ± 0.0500 , n=2, Donato, personal communication; τ of pLSO neurons = 1.2 ± 0.25 ms, n= 6). This then suggests that a voltage-gated conductance was either prolonging the time courses of hPSPs in the MSO or shortening them in the LSO.

The observation that after-depolarizations followed hPSPs in the guinea-pig LSO, but not the MSO, supports the notion that a conductance actively accelerated hPSPs in the LSO. As an inward conductance activated by hyperpolarization, and being highly expressed in the LSO (Adam et al, 2001; Barnes-Davies et al, 2004; Leao et al, 2006), I_h is a very good candidate to perform this task. Although much slower than most voltage-gated channels, I_h can produce after-depolarizations 2-3mV large following hyperpolarizing current steps as short as 10ms duration in mouse pLSO neurons (Leao et al, 2006). It is therefore very feasible that it could underlie the smaller afterdepolarizations observed in the guinea pig and rat LSO after 7-8ms hPSPs. The absence of an after-depolarization following hPSPs in the MSO likely reflects another conductance masking the depolarizing overshoot caused by I_h . I_{KLT} could perform this role - its rapid activation time constant means that the conductance can recover quickly from the initial deactivation during the decay phase of the hPSP and prolong the course of the IPSC as the major outward current in pMSO neurons (Mathews et al, 2010). The increased expression of I_{KLT} in pMSO neurons, compared to pLSO neurons, would then explain why masking was more effective in the MSO and after-depolarizations were only observed following hPSPs in the LSO.

4.2.5 Comparing the temporal properties of hPSPs in the LSO of different species

Although Magnusson and colleagues did not directly measure the half-width of hPSPs in the gerbil LSO, they did demonstrate that the rise and decay times of hPSPs were similar in the gerbil MSO and LSO (Magnusson et al, 2005). Since the time course of hPSPs recorded in the gerbil MSO (average half-width= 3.1 ± 1.2 ms) proved analogous to the hPSP time course measured in the guinea pig LSO (average half-width= 3.6 ± 1.15 ms), it is likely that the same would be true for hPSPs from the gerbil and guinea pig LSOs. Neither were intrinsic differences in hPSP time course encountered when amplitude-matched hPSPs from rat and guinea pig pLSO neurons were compared (rat data was from pilot study performed by myself). The average half-width of the hPSPs in the rat pLSO neurons (3.5 ± 0.3 ms, n=3) closely matched the value observed in the six guinea pig neurons (3.6 ± 0.5 ms, n=6).

If hPSP time courses are invariant across the three species, these results suggest that the ability of pLSO neurons to process different binaural cues cannot be inferred from the time course of its hPSPs. Other factors such as the amount of input jitter as well as the sublocalization of the inhibitory inputs onto pLSO neurons could still modify inhibition's action allowing it to produce diverging binaural sensitivities in species with different hearing ranges.

4.2.6 Comparing the temporal properties of hPSPs and dPSPs in the guinea pig LSO

When compared to dPSPs, it has been shown previously that hPSPs have a slower time course in the gerbil and the guinea-pig MSO (Magnusson et al, 2005; Chirila et al, 2007; Couchman et al, 2010). Since the membrane time constant of these neurons at rest should remain the same for PSPs of different polarity, the differing time courses can be mainly attributed to the relative activation/deactivation of voltage-gated conductances in the

depolarizing and hyperpolarizing voltage direction. As mentioned previously, the major conductance in pMSO neurons is the low-threshold K^+ conductance, I_{KLT} , which is activated by depolarizing voltages and can therefore accelerate the time course of dPSPs. It is possible that I_{KLT} actually prolongs hyperpolarizing potentials by resisting the repolarization of the membrane voltage during the decay phase. Thus, in conjunction with a lack of hyperpolarization-activated conductances to shorten actively the time course of hPSPs, the relative activation/deactivation of I_{KLT} during depolarization and hyperpolarization can explain why hPSPs are slower than dPSPs in the gerbil and guinea pig MSO nuclei.

In the gerbil LSO, dPSPs were also found by Sanes (1990) to have shorter durations than amplitude-matched hPSPs. Even though the absence of hyperpolarizations following dPSPs in the gerbil LSO suggests that I_{KLT} is less prominent than in pMSO neurons (Sanes, 1990), the conductance must be sufficiently expressed in these neurons to help accelerate the time course of dPSPs, whilst simultaneously slowing down hPSPs. In the guinea-pig LSO, where hPSPs and dPSPs displayed similar half-widths, the aforementioned explanation cannot hold true. One simple explanation for this finding would be that the passive properties of guinea pig pLSO neurons influenced the time course of hPSPs and dPSPs more so than I_{KLT} .

4.2.7 Short term depression of dPSP amplitude

Short-term depression of dPSP amplitude was clearly evident over the course of 50Hz and 100Hz pulse trains in guinea pig pLSO neurons. Whilst previous studies have demonstrated that the probability of failure to generate APs increased towards the end of a train of pulses (Wu and Kelly, 1993), this is the first study to show conclusively that short-term depression affects excitatory transmission at the AVCN-LSO synapse. Importantly, the current study also shows no indication of long term plasticity across trials as peak amplitudes remained constant. This also indicates that the 10s interval between trials was sufficient for the recovery from STSD.

By altering the baseline membrane potentials of pLSO neurons whilst continuing to stimulate the trapezoid body fibres with current pulses (Figure 41), it was possible to exclude the influence of postsynaptic, voltage-gated channels on STSD of dPSP amplitude. Whilst the application of a pharmacological agent (such as CTZ or γ -D-glutamylglycine) would be necessary to prove that no postsynaptic component was involved at all, it is highly unlikely that the discreet bouton synapses between the AVCN and LSO are affected by the desensitization and saturation of glutamate receptors as much as the calyx of Held where large amounts of neurotransmitter are released into a small cleft volume, and yet studies still question the contribution of postsynaptic components to STSD at mature AVCN-MNTB synapses (Trussell, 1999; Ishikawa and Takahashi, 2001).

Several presynaptic mechanisms could underlie STSD at the AVCN-LSO synapse, including depletion of the vesicular pool as well as a decrease in the calcium influx over the course of the pulse train. The relative time courses in other auditory centres suggest that vesicular depletion may be the more prominent of the two mechanisms at 50Hz and 100Hz (Borst and Sakmann, 1996; Weis et al, 1999; Taschenburger and Von Gersdorff, 2000). This is further corroborated by the fact that single exponential decays which were used so effectively to fit STSD in this study can be reproduced by simple depletion models (Weis et al 1999).

The lack of STSD observed at 1kHz in Figure 42 *b1* is strange considering that STSD increases with frequency at the AVCN-MSO synapse until it reaches a plateau (Couchman et al, 2010). This is compounded by the fact that responses in the LSO were seen occurring regularly at an average frequency of ~60Hz; yet in the same neuron, STSD was very strong for a stimulus of 50Hz. One possible explanation for what was observed at 1kHz is that the failure to generate APs in multiple axonal inputs at such a high input rate led to several synaptic inputs contributing with only one or two regularly-timed dPSPs over the course of a single presentation of a train of pulses. As each input would be responding at a far lower input rate than 60Hz, the vesicular pool could then recover before the next AP arrived. This explanation perhaps requires an unrealistically high proportion of failures in stimulated

fibres given that AVCN bushy cell fibres can respond *in vivo* with instantaneous spike rates of up to 750 Hz (Rhode and Oertel, 1983). Another explanation for this phenomenon proposes that APs were indeed generated in the trapezoid body fibres at higher rates however the release mechanism at the presynaptic terminals adapted quickly. This could have been caused by the large influx of calcium, which has been shown to induce faster replenishment of vesicular pools in a calmodulin-dependent manner (Sahaba and Neher, 2001). In conjunction with this faster recovery from STSD, a decrease in the sensitivity of the calcium sensing mechanism for vesicular release (as has been observed at the squid giant synapse (Hsu et al, 1996)) might have supported more constant dPSP amplitudes as vesicles would have been sufficiently replenished when calcium concentration in the terminal reached this new higher threshold for release. Such a biophysical mechanism would not only provide a suitable manner to preserve the postsynaptic action of high frequency inputs but also ensure that dPSPs were still evoked with great temporal precision across trials as shown by Figures 42 *b1* and *b2*.

Summation of dPSPs

Although either presynaptic mechanism could also result in the lack of summation observed at 1kHz stimulation, neither is necessary to explain its absence at 50Hz and 100Hz stimuli. The somatic integration of dPSPs in guinea pig pLSO neurons was sufficiently fast that the longest dPSPs in trains of responses had durations between 5-8ms long; thus it would be expected that dPSPs would first start to summate at frequencies between ~125 and 200Hz. These values sit well within the range observed in mouse LSO neurons from the Wu and Kelly (1993) study.

Where summation was observed in pLSO neurons, it was never prolonged and did not appear sufficient to elicit an AP. It is difficult to state whether this is solely due to the depression in dPSP amplitude with increasing pulse number in a train or, if there are in fact,

some active mechanisms involved in dendritic/somatic processing of dPSPs. Interestingly Wu and Kelly (1993) observed that summation of dPSPs did not lead to linear summation and AP generation; a similar study of temporal summation by Leao and colleagues has shown that a 50Hz input can actually cause large summation when I_h is blocked using ZD7288 (Leao et al, 2011). Thus it would appear that active processing of dPSPs is also important in the pLSO neurons of many species. In fact, evidence from the study by Leao and colleagues points to the influence of dendritic processing: a phenomenon that has been demonstrated extensively in the gerbil MSO where the high dendritic expression of I_{KLT} actively controls the temporal integration and propagation of dPSPs (Chirila et al, 2007; Matthew et al, 2010; Leao et al, 2011)..

4.2.8 Short-term depression of hPSP amplitude.

STSD was prominent in all hPSP trains and appeared to be both largest and fastest in neurons of guinea-pig pLSO whose train of hPSPs had the largest initial amplitude (Figures 48 *b* and *c*). If differing number of excitatory synaptic inputs contacted each pLSO neuron, this could potentially explain the range of initial dPSP peak amplitudes observed in these neurons; but is unlikely to explain why the initial peak amplitude of dPSPs was correlated with the subsequent strength and speed of STSD, given this factor's dependence on slicing technique and not biological plausibility. Instead it is more likely that a post- or pre-synaptic mechanism associated with neurotransmission mediated this relationship.

If it is assumed that the desensitization of postsynaptic glycine receptors is too slow to be considered as a potential depressing mechanism here (Harty and Manis, 1997), then presynaptic components can be considered as prime candidates to explain the relationship between the peak amplitude of the initial dPSP and the size of the following STSD. Since a larger initial hPSP entails changes in several presynaptic parameters that could each lead to an increased STSD, it is difficult to identify which mechanism in particular is involved.

Chief amongst the candidate mechanisms however is the depletion of vesicular pool; increased neurotransmission after the first stimulus would lead to a faster decline in the number of readily available vesicles in the pool. If subsequent stimuli produced equally effective synaptic release then the eventual balance between the replenishment and release of vesicles would favour increased depression too. The apparent ease with which results were fit by single exponential decays suggests that simple vesicular depletion model would explain the phenomenon well (Weis et al 1999).

Frequency dependence of STSD in hPSP amplitude

When different rates of pulse presentation were used to stimulate the trapezoid body fibres, two different consequences on the strength of inhibition's STSD were observed in guinea pig pLSO neurons: in the first group, STSD increased with stimulus frequency (Figures 49 *a* and *d*) whilst in the second group, very little change was observed in the STSD strength with stimulus frequency (Figure 49 *b* and *c*).

The first class of effect reflects how STSD strength increases with stimulus frequency at the mammalian AVCN-MSO synapse as well as the chick NM-NL and ANF-NA synapses (Kuba et al, 2002; Cook et al, 2003; Couchman et al, 2010). Although the synaptic mechanism has not been studied thoroughly, it has been modelled empirically using a simple vesicular model of depletion: an increased input rate producing a dynamic balance which favours vesicular release over its recovery and therefore promotes an increased STSD (Cook et al, 2003).

Since STSD cannot increase with stimulus frequency until transmission is completely exhausted it instead reaches a plateau at a limiting stimulus frequency (Cook et al, 2003). This phenomenon might explain why STSD remained unchanged with increasing stimulus frequency in the second group of pLSO neurons. In the neuron in Figure 49 *c*, the STSD

had reached a maximum at 10Hz, which is surprisingly low. This would suggest that the probability of release is very high at this particular MNTB-LSO synapse causing large vesicular depletion after each stimulus pulse.

The variety of STSD frequency dependence in pLSO neurons does not extend as far as unmasking STSF at lower frequencies as has been noted in the chick NA however it does suggest that the guinea pig MNTB-LSO synapse may possess heterogeneous properties across the population of pLSO neurons. .

dPSPs undergo greater STSD than hPSPs in the guinea pig LSO

Using analysed data from 50Hz stimuli, dPSPs appear to experience a stronger STSD than hPSPs (STSD of dPSPs= 0.35 ± 0.02 , n=3 Vs. STSD of hPSPs 0.41 ± 0.02 . n = 3). Although this difference was not significant (independent two-tailed t-test), it is supported by the evidence from the 1kHz where trains of dPSPs did not display STSD whereas hPSPs did (Figures 42 *b1* and 51). This finding is in agreement with a very recent study in the gerbil LSO which showed that STSD at 50, 100 and 200Hz was greater for excitatory PSCs than inhibitory PSCs (Walcher et al, 2011). This could have potential functional effects on interaural processing for the ongoing component of auditory stimuli as the balance of contralateral excitation and inhibition would dynamically change over the course of prolonged stimulation.

4.2.9 Suprathreshold dPSPs and graded APs

In two of the three guinea pig pLSO neurons in which dPSPs were evoked, APs of graded amplitude were recorded somatically as a result of suprathreshold responses. This, therefore, represents the first study in which graded APs have been observed in pLSO

neurons as well as pMSO neurons from the same species. Importantly these graded APs were of much smaller amplitude when evoked by synaptic potentials rather than somatic current injections.

Several studies have described a similar phenomenon in gerbil pMSO neurons and chick NL (Scott et al, 2005; Kuba et al, 2006; Scott et al, 2007). They have suggested that attenuation is caused by APs backpropagating from a distal site of initiation towards the soma (Scott et al, 2005; Kuba et al, 2006; Scott et al, 2007). The capacitive load of pMSO neurons' large somata and broad proximal dendrites reduces the impact of depolarizing currents for signals returning from the AP initiation site whilst an unfavourable ratio of active conductances (i.e. greatly in favour of K^+ over Na^+ conductances) further helps to accentuate the region's low-pass filtering properties (Svirskis et al, 2002; Svirskis et al, 2004; Scott et al, 2007). These factors do not explain however why the somatic and synaptic stimulation have dissimilar effects on the attenuation of backpropagating AP in the guinea pig MSO and LSO.

Two possible solutions to this problem exist: firstly the difference in attenuation may be caused by properties varying during backpropagation in the two instances. When synaptic stimulation is utilised, evoked dPSPs propagating towards the soma will activate dendritic I_{KLT} before eliciting an AP (Mathews et al, 2010). This dendritic compartment becomes very leaky and therefore acts as a large current sink for backpropagating APs (Agmon-Snir et al, 1998). Injecting stepped current somatically, on the other hand, is conducive to a very different set of backpropagating properties. The relative timing of the AP initiation with respect to the poor spread of current into the dendrites (on account of poor space clamp associated with patching neurons of such low input resistance) means that very little dendritic I_{KLT} is active during AP backpropagation. As a result, the somatic AP amplitude will not be attenuated greatly by the backpropagation and will better represent the profile as might be measured at the AP initiation site.

An alternative explanation for somatic current injection and synaptic stimulation evoking APs of different amplitude is that the original amplitudes of the APs at the initiation site itself might differ for the two stimulation protocols. This could arise if one of the stimuli was recruited more voltage-gated Na⁺ channels at the initiation zone than the other. The somatic current step protocol represents the stimulus with the more rapid rise time and hence will likely activate more of the voltage-gated Na⁺ channels necessary for larger initial AP amplitudes (Colbert and Johnston, 1996). It is important to note that this latter solution would not affect the forward propagating AP as mechanisms of regenerative excitation would help to normalize their amplitude (Scott et al, 2007).

Given the prominent expression levels of I_{KLT} in the both SOC nuclei (Svirskis et al, 2002; Barnes-Davies et al, 2004; Mathews et al, 2010), the former scenario most likely determines AP attenuation in both guinea pig pLSO and pMSO neurons. Unfortunately it is difficult to confirm this from the few cells in Figure 44. This is especially true as there is greater temporal overlap between the backpropagating AP and the underlying, slower dPSP (Fig 41 *b*) thus other conductances may also act to shunt the backpropagating AP and help attenuate its amplitude in the LSO. Indeed it is most likely that both the varying recruitment of voltage-gated Na⁺ channels and the current sink created by active I_{KLT} combine as factors determining the different backpropagating conditions associated with somatically and synaptically evoked APs in the MSO and LSO.

Whatever the mechanism underlying the attenuation of back-propagating APs in the guinea pig MSO and LSO, the phenomenon bestows principal neurons in the guinea pig SOC with the ability to isolate the site of AP initiation from the somatic site of integration and hence improve sensitivity to temporal disparities in stimuli (Kuba et al, 2006).

Threshold for generating APs

Figure 44 *c* suggests that generation of APs in the pLSO neuron relies less on the rising slope of dPSPs and more on the absolute value of a neuron's membrane voltage. Figure 44 *d* also supports the premise that values of the absolute membrane voltage may determine when APs are initiated as the dPSP rise slope and its peak amplitude were shown to be interchangeable. This shift from dV/dT to absolute voltage as a determinant of AP generation may arise from I_{KLT} not being as predominant in pLSO as it is in pMSO neurons (Day et al, 2008). It is supported by evidence from the current step injections that even the most phasically firing guinea pig pLSO neurons fired at least two APs at current steps $>850\text{pA}$ (Fig 16 *a*). This shift could place fewer limitations on how quickly a dPSP must rise to recruit sufficient amount of excitatory conductance to initiate an AP in pLSO neurons. A functional consequence of this altered sensitivity may be that pLSO neurons maintain a tonic firing profile and respond better to synaptic inputs that have integrated over time (Gai et al, 2010). This may be especially important for the neurons if they wish to retain their sensitivity to the rate of input and hence code for interaural intensity differences.

4.3 Immunohistochemistry

Four main findings emerge from this part of the study. First, sub-localization of inhibitory synapses in cells of the guinea pig SOC (as judged by immunohistochemical staining for gephyrin - the scaffolding protein associated with GlyR in the auditory brainstem) indicates a highly peri-somatic pattern, suggesting inhibitory synapses are confined to the cell soma.. This includes the discovery of a potential postsynaptic specialization for glycinergic transmission in the guinea pig MSO. Second, specific cell types are identifiable for the first time in the guinea pig LSO, by virtue of their staining for MAP2. Third, when guinea pig LSO cells were assessed according to sub-localization of their gephyrin staining, a group of relatively smaller cells was apparent, likely representing neurons of the LOC, the efferent feedback pathway to the type 1 fibres synapsing at the base of the inner hair cells of the cochlea. Fourth, those cells not classified as LOC neurons formed a group of putative pLSO neurons that appear to be of heterogenous somatic size.

4.3.1 Quality of gephyrin staining in the SOC of guinea pig

When at its clearest, the gephyrin staining in this study is well defined and very punctate (Figures 53 *b*, 54 *b* and 55 *c*), appearing more defined than patterns of staining observed in gerbil MSO studies when GlyR alpha 1 subunit or gephyrin have been targeted previously (Friauf et al, 1997; Kapfer et al, 2002). This is likely associated with the preparation technique better preserving gephyrin's antigenicity (Schneider Gasser et al, 2006). Interestingly when the same preparation was used to probe gephyrin sub-localization in the rat LSO, absent punctate staining and high levels of background fluorescence made identification of pLSO neurons very difficult (Figure 65 *a*). This cannot be attributed to a reduced antigenicity in the rat as the very same antibody has been shown to function well in the rat by the group which originally introduced the technique (Schneider Gasser et al, 2006).

Instead this background staining like arose from suboptimal frozen slices. Since this technique requires instant freezing in liquid nitrogen in order to preserve morphology and antigenicity, any issue at this critical stage (e.g. excess ACSF on the harvested tissue during the freezing process) could compromise the slice preparation and lead to non-specific association of primary antibodies and epitopes, producing background staining. Other potential issues such as the duration of fixation; the time frozen tissue spent in freezer and whether tissue dried during the processing were all closely controlled, but little improvement in the contrast of staining was observed.

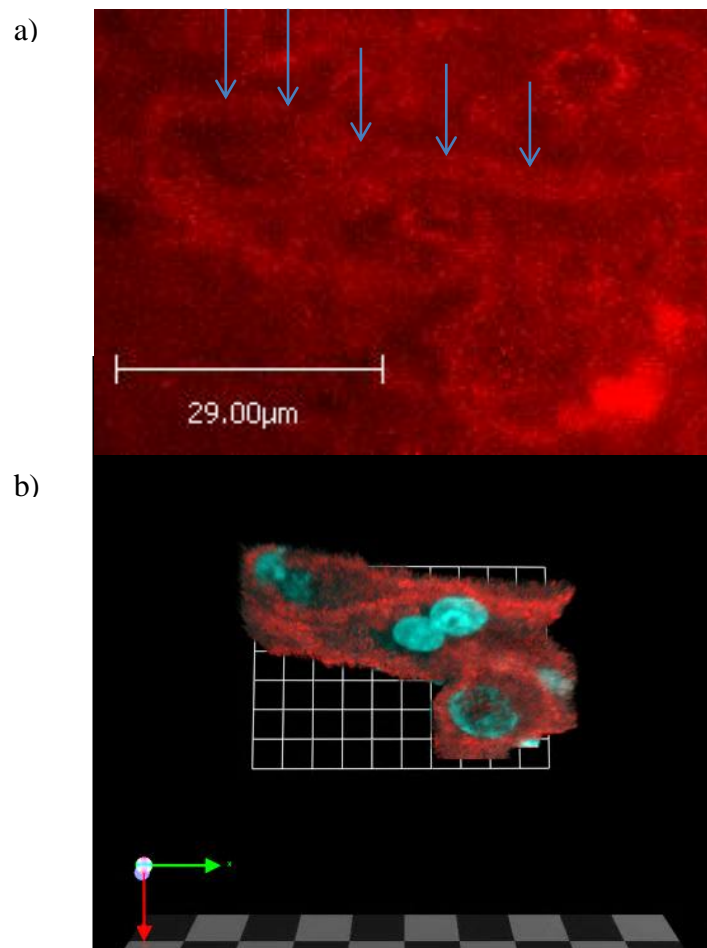


Figure 65. Gephyrin staining in rat pLSO neurons. Two unipolar cells can be seen as either a two-dimensional projection in *a* and a 3-D reconstruction in *b*. Gephyrin staining is in red and DAPI staining in blue. To improve visualization of the cells' outlines in *a*, all only gephyrin staining is shown. The average length of dendrite stained for gephyrin was $24.25 \pm 3.7\mu\text{m}$ ($n=4$). The scale grid in *b* = $5.4\mu\text{m} \times 5.4\mu\text{m}$.

4.3.2 The sublocalization of gephyrin staining in the guinea pig LSO.

One of the main consequences of the improved gephyrin antigenicity offered by rapid freezing may be the finding of ring-shaped structures gephyrin staining forms on the surface of pMSO neurons (Figure 58). The most obvious explanation for the rings would be that the empty space at the centre of these rings represents the outgrowth of a dendrite, although this is not consistent with the pattern of MAP2 staining (Figure 58 *a inset*). Instead, they may represent specializations to improve glycinergic transmission's efficiency by concentrating GlyRs around the bouton-like end-segments of MNTB fibres that contact pMSO cells (Werthat et al, 2008; Couchman et al, 2010). Such ring patterns were not as clear or frequent on pLSO neurons and thus may represent specializations of somatic inhibition in the MSO. Determining whether presynaptic terminals do indeed terminate in close proximity to the rings would require the use of an antibody for the glycine transporter, GlyT2 as presynaptic marker. This was not within the scope of this study.

That gephyrin staining is perisomatic in both the guinea pig MSO and LSO nuclei suggests that the sub-localization of glycinergic inhibitory input is homogeneous across the guinea pig's SOC. Studies of the adult gerbil MSO also demonstrate perisomatic localization (Kapfer et al, 2002; Couchman et al, 2010), and therefore the present study appears to corroborate the view that inhibition in the MSO of low-frequency hearing animals is largely peri-somatic (Kapfer et al, 2002). As the distribution of gephyrin only becomes somatic in the adult gerbil (Kapfer et al, 2002), data from this study advocates the precocious nature of the guinea pig as it already appears to possess an adult-like configuration at birth.

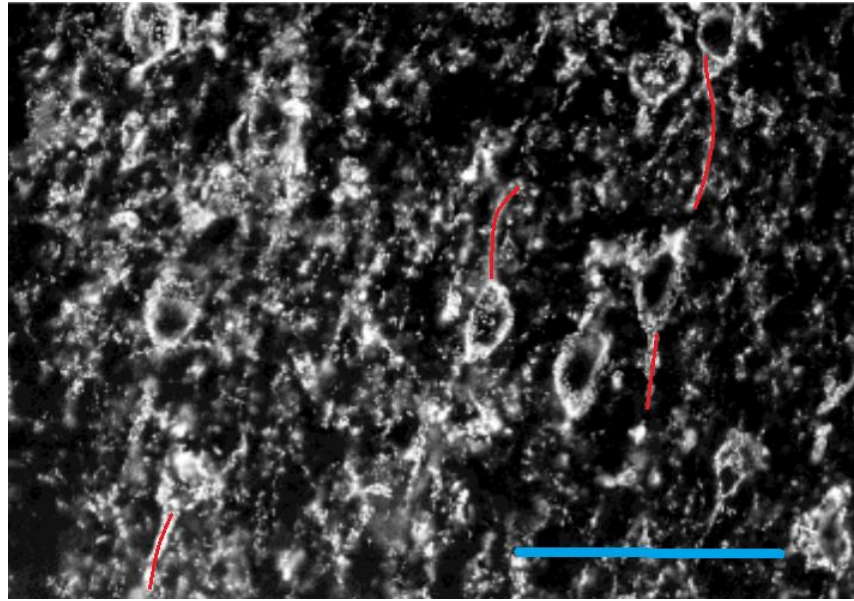


Figure 66. Medial region of rat LSO stained for GlyR alpha 1 subunit. Red lines trace individual dendrites whilst blue bar represents a scale of 100µm (Figure 2 b, taken from Friauf et al, 1997.)

In the LSO, the extent to which glycinergic inhibitory input impinged upon the dendritic length has not yet been quantified in any study. Thus, for the purposes of comparison with the current data set, data from a previous study of GlyR development in the rat (Figure 66, from Figure 2b in Friauf et al, 1997) was used to measure the extent of immunoreactivity for the GlyR alpha-1 subunit along the dendrites of cells in the medial limb of the LSO. An average value of $37.9 \pm 6.8\mu\text{m}$ (n=4) was calculated which is very similar to the $30.26 \pm 2.8\mu\text{m}$ (n=27) average in the guinea pig and the $24.25 \pm 3.77\mu\text{m}$ (n=4) average measured preliminarily in the rat. In spite of this similarity (no statistical test were performed due to small sample size), the average dendritic lengths stained of both studies appear unexpectedly low in light of the demonstrable contact between a MNTB fibre along the dendritic spread of a pLSO neuron (Kim and Kandler, 2003).

The most likely explanation for this disparity is that the length of immunoreactivity along dendrites was underestimated in the current study and that of Friauf et al (1997) by virtue of the severance of dendrites during slicing. This likely imposes an artificial limit on observed

length of gephyrin staining, and results in MAP2 and gephyrin staining to end concomitantly on the dendrites of all cells reported for the guinea pig LSO. In addition to the cutting of dendrites, tracking dendrites in slices was complicated by both high levels of background fluorescence (most prominently observed in the figure 65 for the rat and figure 55c for the guinea pig) and the densely complex network of dendrites in the brainstem (figure 55 *d* and 56 *a*). Both contribute to the underestimations of dendritic length stained for gephyrin by making judgment of where one dendrite's gephyrin staining started and another's terminated very difficult. As a result there will be many instances where staining was falsely identified to have abruptly stopped.

Evidence, obtained here for the guinea pig, of isolated dendrites being immunoreactive along their length for gephyrin also suggests that the dendritic length displaying gephyrin immunoreactivity was underestimated. Gephyrin staining extended as far as 82µm in some truncated dendrites (Figures 57 *b* and *c*) and had these dendrites remained attached to the soma it is very likely that the average dendritic length would have proven to be much larger.

To explore in greater detail dendritic staining of gephyrin would potentially require thicker slices than were employed in the current study, however these can notoriously lead to poorer penetration of the antibodies (Melvin and Sutherland, 2009). Serial reconstruction of slices would also achieve a similar aim although the more orthodox technique perfusion fixation might help to improve the efficiency of slicing given the difficulty in collecting sequential slices in this study.

4.3.3 Cell types encountered in guinea pig LSO

The observation of “banana-like” cells in all regions of the guinea pig LSO (Figures 56 *a* and 57 *a*) contrasts with data from the rat where they are restricted to the lateral limb and do not overlap with the dominant bipolar cells in the medial limb, suspected to be pLSO

neurons (Rietzel and Friauf, 1998). That both bipolar and “banana-like” cell types can be seen independently in the same regions of the guinea pig LSO would appear to agree with speculation, from the study of rate LSO, (Rietzel and Friauf, 1998) that they have different functional correlates.

A perspective for future investigation might be to determine the origins and the possible physiological implication of such variability within the population of LSO cells, by performing a systematic morphological analysis and correlating it with electrophysiological response properties. To do this, neurons might possibly be ‘patched’ and injected with neurobiotin. It would then be possible to reconstruct a more complete morphology and correlate this morphology with electrophysiological responses.

Evidence from a previous anatomical study in the guinea pig (Schofield and Cant, 1991) suggests that all cells in the LSO are either bipolar or multipolar, and it is interesting to note here that neurons with single dendrites were visible in both the rat and the guinea pig. It remains possible that these cells have had one or more dendrites severed due to the orientation of slicing. To definitively answer whether some pLSO neurons in the guinea pig are in fact unipolar, it would be necessary to fill neurons identified as principal neurons by their electrophysiological properties with a fluorescent dye. The absence of bipolar cells in the rat LSO, on the other hand, is most likely related to the restricted sampling from the medial limb of the rat LSO as their existence has been shown before in other regions of rat LSO (Rietzel and Friauf, 1998; Barnes-Davies et al, 2004).

4.3.4. Alternative cell types in the SOC of rats and guinea pigs

Non-principal neurons have been described in the SOC of many species (Smith, 1995; Adam et al, 1999; Sterenborg et al, 2010). Their shared topology and similar morphological

properties mean that at first viewing they can easily be mistaken for pSOC neurons (Smith; 1995; Adam et al, 1999).

In the guinea pig MSO, marginal non-principal cells are somatically very similar in size to pMSO cells; however they can be easily distinguished on account of their haphazard orientation and highly-arborized dendritic processes, which taper quickly as they extend from the soma (Smith, 1995). As the somata of MSO cells in the current study appeared to be arranged in parallel and their dendrites remained broad as far as 30 μ m from the somata (Figure 58 *a*), it is highly likely that all MSO cells imaged in this study were in fact pMSO neurons.

“Intrinsic” lateral olivocochlear neurons (LOC neurons) on the other hand are located within the LSO nucleus and provide efferent fibres to the inner hair cells of the cochlea as well as the cochlea nucleus (Warr and Guinan, 1979; Ryan et al, 1982; Vetter and Mugnaini, 1992). It has recently been confirmed in mice that LOC neurons receive glycinergic and GABAergic inhibition from the MNTB hence it is likely that they have been visualised in this study (Stereborg et al, 2010): especially as they are particularly prevalent in the guinea pig LSO (Robertson, 1985; Aschoff and Ostwald, 1987).

LOC and pLSO neurons have very similar somatic morphologies (Strutz and Bielenburg, 1984; Aschoff and Ostwald, 1987; Adam et al, 1999; Sanchez-Gonzalez et al, 2003); however, LOC neurons appear to have a significantly smaller somatic size (Aschoff and Ostwald, 1987; Adam et al, 1999). In the present study, when classifying the LSO cells by sub-localization of their gephyrin staining, it appears that LSO cells with somato-dendritic gephyrin staining possess a significantly smaller somata than those cells with purely somatic staining (Figures 61 *a* and *b*): this suggest that within the LSO, cells with purely somatic gephyrin staining represent an entirely different population of cells of smaller somata size. According to a previous study (Aschoff and Ostwald, 1987), these can be identified as LOC

neurons. A consequence of this, therefore, would be that all the neurons in the LSO with somato-dendritic gephyrin staining in the current study would represent pLSO cells.

It is interesting to note that the neurons identified in this study as candidate LOC neurons do not display dendritic staining (either MAP2 or gephyrin). This could be due to the fact that secondary cell types tend to project more extensively in the rostro-caudal plane i.e. perpendicular to the coronal slices which were cut (Schofield and Cant, 1991; Vetter and Mugnani, 1992; Adam et al, 1999) than the principal neurons, making it more likely that their dendrites were severed in the slicing procedure.

That the slicing protocol selectively preserved one cell type over another further supports the idea of the existence of two cell populations, which differ both in somatic size but also dendritic morphology. However an independent marker, such as the injection of a fluorescent retrograde tracer into the cochlea (Robertson et al, 1987), would be required to verify irrefutably this identification of LOC neurons in the guinea pig LSO.

4.3.5 pLSO neurons in the guinea pig LSO

In this study, LSO cells that show somatodendritic gephyrin staining in the guinea pig appear to be pLSO neurons. This observation is accompanied by a potential heterogeneity in the somatic areas across the axis of the guinea pig LSO: the average somatic size of putative pLSO neurons in the medial limb is larger than that of neurons in the mediolateral limb, which in turn is larger than that of neurons in the lateral limb. Whilst this trend may not be significant (Figure 61 *d*), the observation that only medial putative pLSO neurons are actually of a similar somatic size to pMSO cells would appear to affirm that tonotopic differences in somatic size do indeed exist across the guinea pig's pLSO population.

There is very little evidence in the literature with which to verify independently this observation. ³H-strychnine binding of GlyRs in adult guinea pig has shown that there is a

relative lower density of receptors in lateral limb as in the medial limb of the LSO (Suneja et al, 1998), and it is possible that putative pLSO neurons with smaller somatic areas would also possess less GlyRs if the receptor was expressed at the same density as larger pLSO neurons. A similar observation have been noted in the rat and gerbil LSO (Sanes et al, 1987; Friauf et al, 1997): in the rat it is also accompanied by evidence that the low-frequency lateral limb receives a much less-densely arborized MNTB input (Sanes and Siverls, 1991; Friauf et al, 1997). A lower density of pLSO neurons in the lateral limb than the medial limb would equally explain the findings from ^3H -strychnine binding as labelling in that study was quantified en masse in the LSO regions; nevertheless it has been contended that no such gradient exists in the rat and guinea pig LSOs (Schofield and Cant, 1991; Barnes-Davies et al, 2004).

Smaller cells are typically associated with higher input resistances and longer membrane time constants, prevent fast integration of temporal information. Were the membrane time constant too slow, this could potentially be debilitating for pLSO neurons of the lateral limb if they are indeed specialised to perform envelope ITD processing (Joris and Yin, 1995; Batra et al, 1997; Tollin and Yin, 2005). A possible means by which lateral limb pLSO neurons could avoid this fate would be to express a large conductance, active at rest, such as low-threshold potassium conductance, K_{LT} . It has been shown in the adult rat LSO that Kv1.1, the channel that mediates K_{LT} , is expressed prevalently in pLSO neurons of the lateral limb (Barnes-Davies et al, 2004). The use of an anti-Kv1.1 antibody to find out whether the putative pLSO neurons of the lateral limb stain positively for Kv1.1 would be useful in a future study.

General Conclusions

Functional implications of guinea pig pLSO neurons' intrinsic properties

Although the identity of bilateral synaptic inputs to a pSOC neuron ultimately determines the neuron's characteristic phase, its intrinsic properties actively regulate the time window for synaptic integration and then control the dynamic range of the resulting response (Chirila et al, 2007; Scott et al, 2007; Jercog et al, 2010). It is therefore likely that processing for different binaural cues actually requires a neuron with differing optimal parameters. These parameters have been explored most carefully in the MSO where phasic firing is associated with single-figure input resistances and extreme membrane time constants ($<0.4\text{ms}$, Scott et al, 2005; Mathews et al, 2010; Khurana et al, 2011). These active and passive properties not only institute the narrow window of integration that is considered so important for ITD processing but ensure that narrowband stimuli are encoded efficiently and accurately (Svirskis, et al, 2002; Day et al, 2008). Similar studies parameterizing the optimal neuronal properties for ILD processing have not been performed however it is presumed that the integration of intensity must be slower so that the power at either ear can be compared. By reducing the importance of temporal acuity to ILD processing, phasic encoding of this subthreshold signal is also redundant; thus tonic firing is perhaps expected to be predominant amongst ILD-sensitive neurons. Since the rat's hearing lies predominantly in the high frequency range (Fay, 1988), the LSO likely assumes the role of chief binaural nucleus processing ILDs and envelope ITDs in this species [as well as ITDs at lower frequencies potentially if rats display similar sensitivity to the cat (Tollin and Yin, 2005)] (Inbody and Feng, 1986; Yin, 2002). It is therefore quite understandable that the divide between more phasic (type 1) and tonic firing (type 2) in the rat LSO might be associated functionally with very different binaural cue processing: the fast membrane time constants of type 1 neurons permitting phase sensitivity in low frequency regions of the LSO and type 2 neurons

integrating amplitude signals over a longer time course as part of ILD processing in the high frequency.

If the above scenario is indeed true, then data collected from the guinea pig LSO offers a challenge to interpret its functional implications. The continuity of firing patterns as well as the homogeneously low input resistances and fast membrane time constants suggest that even the tonic firing neurons could represent rapidly changing ILDs of which envelope modulations are comprised and therefore these neurons too could contribute to envelope ITD processing. It would therefore appear likely that the “strategy” for encoding binaural cues may differ across the guinea pig and rat LSOs. This is not to say that certain similarities are present between species such as the tonotopic variations in passive properties: pLSO neurons in the high-frequency, medial limbs of the two species’ LSOs possessing larger input resistances and slower membrane time constants that might make them more suitable for ILD processing. Instead it is possible that any continuum of passive and active properties across the LSO may be biased towards processing different binaural cues in the two species: more emphasis being placed on envelope ITDs in the guinea pig and pure ILDs in the rat. This would be surprising given the relative ethological pressures their respective hearing ranges imply (Fay, 1988). The rat is mostly reliant on envelope ITDs for its binaural localization given its high frequency hearing range so where might envelope ITDs be processed in the rat?? One potential solution is the rat MSO. Although relatively small in the rat (likely as a result of its services not being required for ITD processing), its high frequency pMSO neurons in the rat could imaginably perform envelope ITD coding. A recent study has shown that whilst gerbil pMSO neurons will typically only respond with an AP to fast rising slopes, stochastic resonance helps elicit neural activity when slow sinusoidal signals are presented with white noise (Gai et al, 2010). This artificial stimulus could potentially be analogous to the subthreshold synaptic voltages produced by slow amplitude modulations in high frequency carriers (>3.5kHz): the poorly phasic encoding of the fine structure by the bushy cells taking the role of the white noise and the slow amplitude-modulated envelope potentially causing a sinusoidal voltage profile. Evidence for such envelope sensitivity in the MSO does exist in the literature from the cat (Joris and Yin, 1998) but is also potentially suggested in the current study

within the data from the subthreshold resonance assay. Impedance profiles from the high-frequency, ventral pole of the MSO demonstrated similar resonant peak frequencies to the highest values encountered in the low-frequency lateral limb of the LSO. If the rat relied even more on the MSO for envelope ITD coding then we might expect the average peak resonant frequency to be lower in its MSO.

Whilst this study suggests that resonance may be correlated with phase sensitivity in the guinea pig MSO and LSO, its actual biophysical role is far less clear. Since band-pass filters have been previously associated with reducing redundancy when coding signals in noise (van Hateren, 1992), a preliminary, theoretical study was performed in conjunction with the Rinzel group (NYU) to determine whether band-pass model pSOC neurons could display an improved ability to extract a natural signal in ambient noise. Using the same linear model that predicted the impedance profiles so well in Section 4.1.6; guinea pig vocalizations and white noise were passed through a cochlear model (Zilany et al, 2009) before the output was converted into synaptic conductances. These were then presented to the model cell “bilaterally” with different time delays between the two to simulate vocalizations originating in different locations. Although naturalistic sounds are amplitude modulated in nature, the model band-pass neurons could still extract the low frequency signal (<1.5kHz) well on a cycle-by-cycle basis. In fact, they differentiated between the various “ITDs” better than model low-pass neurons, displaying a larger dynamic range of spike rates. It would therefore appear that band-pass properties may especially be important to fine structure ITD processing in noisy environments.

Functional implications of guinea pig pLSO neurons’ synaptic properties.

Although it must typically be cautioned that using the passive properties of a pSOC neuron to speculate about ITD/ILD sensitivity only offers a very static perspective, it would appear that the synaptic integration was predominantly regulated by the pLSO neurons’ passive properties. The increasing dPSP half-width with amplitude was indicative of this and suggests that any resulting ITD in the guinea pig LSO would be highly level-dependent and might even support the temporal

summation of monoaural inputs. Such integration could in fact benefit envelope ITD processing as the energy in the envelope would be better encoded. If integration were too slow however, an upper frequency limit would be placed on the encoding of fast envelopes. One mechanism to prevent this would be the short-term synaptic depression of dPSP amplitude, which appeared frequency dependent in the guinea pig LSO. Aside from its importance in implementing ITD processing in the avian NL (Kuba et al, 2006), it has been speculated that short-term synaptic depression in the chick NM may in fact help to encode the onset intensity of an auditory stimulus (Macleod, 2011). Although information about the ongoing component of an auditory stimulus with static intensity would be lost as a result of STSD, this would not be problematic for amplitude-modulated stimuli, which incorporate fast envelopes and thus are constantly changing. Another factor which may have also prevented the summation of temporally asynchronous dPSPs in the guinea pig LSO is the activity of dendritic I_h . Its ability to promote detection of synchronous dPSPs in the mouse LSO has been proposed as a means of strengthening phase-locked responses to amplitude-modulated envelopes (Marsalek and Kofranek, 2005; Leao et al, 2011). It could therefore be very important to the dendritic processes that support envelope ITD encoding.

Much discussion has also been generated over the topic of hPSP kinetics in the pMSO neurons, with many groups believing that they must be unrealistically fast to implement shifts in the peaks of pMSO neurons' ITD tuning functions as proposed by Brand and colleagues (2002) (Zhou et al, 2005; Joris and Yin, 2007). It is therefore slightly surprising that hPSPs appear to possess similar average durations in the MSO and LSO considering the limits on fine structure/ envelope ITD processing that have been associated with the latter nucleus. Nevertheless, a recent model of MSO has suggested that hPSP kinetics observed in the gerbil (which are in line with data collected here for the guinea pig) are sufficient to reproduce the phase-frequency curves describing the relationship between fine structure ITD tuning function and stimulus frequency *in vivo*. Inhibition in the LSO should therefore be sufficiently fast to allow bilateral comparisons over short time windows. This could explain how narrow "troughs" in firing rates around 0 ITD as well as the encoding of amplitude-modulated

envelopes' ongoing portions are achieved biophysically in pLSO neurons (Joris and Yin, 1995; Tollin and Yin, 2005).

The current study presents evidence that contralateral excitation is more prevalent in the lateral limb of the rat and guinea pig LSO than has been previously thought. Data collected from the guinea pig IC has shown that only ~10% of 532 low frequency neurons appeared to be driven by “trougher” pLSO neurons. One possible explanation for the paucity of IC neurons with troughs in their noise-delay functions might be the convergence of inputs from multiple pSOC neurons possessing different binaural interactions (Tollin and Yin, 2005). Another possible explanation in light of results from this study is that many low-CF guinea pig pLSO neurons were in fact bilaterally excited. A similar observation was encountered in the rabbit LSO where bilateral excitation was universal in low CF neurons, contributing to the theory that a continuum of synaptic properties may also accompany a continuum in intrinsic properties and underlie the observed range of binaural tuning functions in the IC (Batra et al, 1997).

Summary of conclusions.

Although bilateral excitation may be prominent in the guinea pig LSO, it is very unlikely that it is conducive to a similar form of coincidence detection encountered in the MSO. In spite of this, both their intrinsic and synaptic properties put forward a clear case for guinea pig pLSO neurons possessing the necessary components to perform phase sensitive processing whether it be associated with the amplitude-modulated envelope in a high-frequency carrier or the low-frequency carrier itself. Several clues as to the existence of a continuum in pLSO neurons' intrinsic and synaptic properties were also found in the current study. It may in fact be the species differences between such continua that prove most insightful to understanding what strategies these animals employ to localize binaurally in light of differing head size and frequency hearing ranges.

List of guinea pig pLSO neurons and their properties

	Animal age (postnatal days)	LSO region	RMP (mV)	Rin (MOhm)	Tau (ms)	Max number of APs evoked	Resonance (Hz)	Synaptic activity
Cell 1	p1	Medial	-52	70	2.3	3	Low pass	N/A
Cell 2	p1	Lateral	-41	56	1.5	2	N/A	Excit
Cell 3	p2	Lateral	-45	30	0.73	11	N/A	N/A
Cell 4	p2	Lateral	-47	50	1	16	N/A	N/A
Cell 5	p3	Lateral	-51	38	1	2	N/A	Inhib
Cell 6	p3	Lateral	-57	60	2.02	2	Res (75Hz)	Excit
Cell 7	p3	Lateral	-41	50	0.84	16	Low pass	N/A
Cell 8	p4	Lateral	-46	36	1.09	2	N/A	Inhib
Cell 9	p4	Medial	-50	68	2.69	2	Low pass	Excit
Cell 10	p5	Medial	-54	88	3.6	15	Low pass	Excit
Cell 11	p8	Medial	-54	87	2	5	Low pass	Inhib
Cell 12	p9	Lateral	-50	38	1.74	2	Res (97Hz)	Inhib
Cell 13	p11	Medial	-45	55	2.4	5	Low pass	Inhib
Cell 14	p11	Lateral	-41	38	0.79	2	N/A	Inhib
Cell 15	p11	Lateral	-65	50	1.31	15	N/A	N/A
Cell 16	p13	Medial	-51	33	1.1	2	N/A	Mixed
Cell 17	p14	Medial	-50	60	1	2	N/A	N/A
Cell 18	p15	Lateral	-50	44	1.5	2	N/A	Excit
Cell 19	p19	Lateral	-52	50	0.84	21	N/A	N/A

References

Adam TJ, Schwarz DW and Finlayson PG (1999). Firing properties of chopper and delay neurons in the lateral superior olive of the rat. *Exp Brain Res* 124, 489-502.

Adam TJ, Finlayson PG and Schwarz DW (2001). Membrane properties of principal neurons of the lateral superior olive. *J Neurophysiol* 86, 922-934.

Adams JC and Warr WB (1976). Origins of axons in the cat's acoustic striae determined by injection of horseradish peroxidase into severed tracts. *J Comp Neurol.* 170, 107-121.

Agmon-Snir H, Carr CE and Rinzel J (1998). The role of dendrites in auditory coincidence detection. *Nature* 393, 268–272.

Art JJ, Crawford AC and Fettiplace R (1986). Electrical resonance and membrane currents in turtle cochlear hair cells. *Hearing Research* 22, 31-36.

Aschoff A and Ostwald J (1987). Different origins of cochlear efferents in some bat species, rats and guinea pigs. *J Comp. Neurol.* 264, 56-72.

Aschoff A and Ostwald J (1988). Distribution of cochlear efferents and olivo-collicular neurons in the brainstem of rat and guinea pig. *Exp Brain Res* 71, 241–251.

Attias H and Schreiner CE (1997). "Temporal low-order statistics of natural sounds". In: *Advances in Neural Information Processing Systems*, MIT Press.

Attneave F (1954). Some informational aspects of visual perception. *Psychological Review* 61, 183–193.

Bal R and Oertel D (2000). Hyperpolarization-activated, mixed-cation current ($I_{(H)}$) in octopus cells of the mammalian cochlear nucleus. *J Neurophysiol* 84 (2), 806-817.

Barlow H (1961). "Possible principles underlying the transformation of sensory messages". In: *Sensory Communication*, MIT Press.

Barnes-Davies M and Forsythe ID (1996). AMPA receptor mediated synaptic currents rectify with internal spermine in rat MNTB neurones. *J Physiol* 495:44.

Barnes-Davies M, Barker MC, Osmani F and Forsythe ID (2004). Kv1 currents mediate a gradient of principal neuron excitability across the tonotopic axis in the rat lateral superior olive. *Eur J Neurosci* 19, 325–333.

Batra R, Kuwada S and Fitzpatrick DC (1997). Sensitivity to interaural temporal disparities of low- and high-frequency neurons in the superior olivary complex. I. Heterogeneity of responses, *J Neurophysiol* 78 (3), 1222-1236.

- Beato M (2008). The time course of transmitter at glycinergic synapses onto motoneurons. *J Neurosci* 28 (29), 7412-7425.
- Beckius GE, Batra R and Oliver DL (1999). Axons from anteroventral cochlear nucleus that terminate in medial superior olive of cat: observations related to delay lines. *J Neurosci* 19, 3146–3161.
- Bernstein LR and Trahiotis C (1985). Lateralization of low-frequency, complex waveforms: The use of envelope-based temporal disparities. *JASA* 77 (5), 1868-1880.
- Bernstein LR and Trahiotis C (1994). Detection of interaural delay in high-frequency sinusoidally amplitude-modulated tones, two-tone complexes, and bands of noise. *JASA* 95 (6), 3561-3567.
- Bernstein LR and Trahiotis C (2002). Enhancing sensitivity to interaural delays at high frequencies by using "transposed stimuli", *JASA* 112(3 Pt 1), 1026-1036.
- Bernstein LR and Trahiotis C (2004). The apparent immunity of high-frequency "transposed" stimuli to low-frequency binaural interference. *JASA* 116 (5), 3062-3069.
- Blauert J (1982). Binaural localization. *Scand Audiol Suppl* 15, 7-26.
- Blauert J (1997). Spatial hearing: the psychophysics of human sound localization, *MIT Press*
- Boehlen A, Heinemann U and Henneberger C (2011). Heterogeneous voltage dependence of interneuron resonance in the hippocampal stratum radiatum of adult rats. *Synapse* 65 (12), 1378-1381.
- Borg E (1982). Auditory thresholds in rats of different age and strain. A behavioral and electrophysiological study. *Hear Res* 8, 101-111.
- Borst JG and Sakmann B (1996). Calcium influx and transmitter release in a fast CNS synapse. *Nature* 383 (6599), 431-434.
- Boudreau JC and Tsuchitani C (1968). Binaural interaction in the cat superior olive S-segment. *J Neurophysiol* 31, 442– 454.
- Bradaia A, Schlichter R and Trouslard J (2004). Role of glial and neuronal glycine transporters in the control of glycinergic and glutamatergic synaptic transmission in lamina X of the rat spinal cord. *J Physiol* 559, 169–186.
- Brand A, Behrend O, Marquardt T, McAlpine D and Grothe B (2002). Precise inhibition is essential for microsecond interaural time difference coding. *Nature* 417, 543–547.
- Brenowitz S and Trussell LO (2001). Maturation of synaptic transmission at end-bulb synapses of the cochlear nucleus. *J Neurosci* 21, 9487–9498.

Brown MC, Liberman MC, Benson TE and Ryugo DK (1988). Brainstem branches from olivocochlear axons in cats and rodents. *J Comp Neurol* 278, 591-603.

Brudzynski SM (2008). Communication of adult rats by ultrasonic vocalization: Biological, sociobiological, and neuroscience approaches. *ILARJ* 50, 43-50.

Caicedo A and Eybalin M (1999). Glutamate receptor phenotypes in the auditory brainstem and mid-brain of the developing rat. *Eur J Neurosci* 11, 51-74.

Caird D and Klinke R (1983). Processing of binaural stimuli by cat superior olivary complex neurons. *Exp Brain Res* 52, 385-399.

Cant NB (1984). The fine structure of the lateral superior olivary nucleus of the cat. *J Comp Neurol* 227 (1), 63-77.

Cant NB and Benson CG (2003). Parallel auditory pathways: projection patterns of the different neuronal populations in the dorsal and ventral cochlear nucleus. *Brain Res Bull* 60, 457- 474.

Cant NB and Casseday JH (1986). Projections from the anteroventral cochlear nucleus to the lateral and medial superior olivary nuclei. *J Comp Neurol* 247, 457- 476.

Cant NB and Hyson RL (1992). Projections from the lateral nucleus of the trapezoid body to the medial superior olivary nucleus in the gerbil. *Hear Res* 58, 26 -34.

Cao X and Oertel D (2010). Auditory nerve fibers excite targets through synapses that vary in convergence, strength and short-term plasticity. *J Neurophysiol* 104, 2308-2320.

Case DT and Gillespie DC (2011). Pre- and post-synaptic properties of glutamatergic transmission in the immature inhibitory MNTB-LSO pathway. *J Neurophysiol* 106 (5), 2570-2579.

Caspary DM and Faingold CL (1989). Non-N-methyl-D-aspartate receptors may mediate ipsilateral excitation at lateral superior olivary synapses. *Brain Res* 503, 83-90.

Chang EH, Kotak VC and Sanes DH. Long-term depression of synaptic inhibition is expressed postsynaptically in the developing auditory system. *J Neurophysiol* 90, 1479 - 1488.

Chirila FV, Rowland KC, Thompson JM and Spirou GA (2007). Development of gerbil medial superior olive: integration of temporally delayed excitation and inhibition at physiological temperature. *J Physiol* 584, 167-190.

Cody AR and Russell IJ (1987). The response of hair cells in the basal turn of the guinea-pig cochlea to tones. *J Physiol* 383, 551-569.

Colbert CM and Johnston D (1996). Axonal action-potential initiation and Na⁺ channel densities in the soma and axon initial segment of subicular pyramidal neurons. *J Neurosci* 16, 6676-6686.

Colburn HS and Esquissaud P (1976). An auditory-nerve model for interaural time discrimination of high-frequency complex stimuli. *JASA* 59 (S1), S23-S23.

Conlee JW and Kane ES (1982). Descending projections from the inferior colliculus to the dorsal cochlear nucleus in the cat: An autoradiographic study. *Neuroscience*. 7 (1), 161-178.

Cook DL, Schwandt PC, Grande LA and Spain WJ (2003). Synaptic depression in the localization of sound. *Nature* 421, 66–70.

Couchman K, Grothe B and Felmy F (2010). Medial superior olivary neurons receive surprisingly few excitatory and inhibitory inputs with balanced strength and short-term dynamics. *J Neurosci* 30, 17111–17121.

Crawford AC and Fetplace R (1980). The frequency selectivity of auditory nerve fibres and hair cells in the cochlea of the turtle. *J Physiol* 306, 79-125.

Day ML, Dorion B and Rinzel J (2008). Subthreshold K⁺ channel dynamics interact with stimulus spectrum to influence temporal coding in an auditory brain stem model. *J Neurophysiol* 99, 534-544.

Dodla R, Svirskis G and Rinzel J (2006). Well-timed, brief inhibition can promote spiking: postinhibitory facilitation. *J Neurophysiol* 95, 2664–2677.

Drewes G, Ebner A and Mandelkow EM (1998). MAPs, MARKs and microtubule dynamics. *Trends Biochem Sci* 23 (8), 307–311.

Dreyer A and Delgutte B (2006). Phase locking of auditory-nerve fibers to the envelopes of high-frequency sounds: implications for sound localization. *J Physiol* 96 (5), 2327-2341.

Ehrlich I, Lohrke S and Friauf E (1999). Shift from depolarizing to hyperpolarizing glycine action in rat auditory neurons is due to age dependent Cl⁻ regulation. *J Physiol (Lond)* 520, 121–137.

Escabi MA, Miller LM, Read HL and Schreiner CE (2003). Naturalistic auditory contrast improves spectrotemporal coding in the cat inferior colliculus. *J Neurosci* 23, 11489–11504.

Fatima-Shad K and Barry PH (1993). Anion permeation in GABA and glycine-gated channels of mammalian cultured hippocampal neurons. *Proc R Soc Lond B Biol Sci* 253, 69–75.

Fay RR (1988). *Hearing in Vertebrates: a Psychophysics Databook*. Hill-Fay Associates, Winnetka IL.

- Fettiplace R and Fuchs PA (1999). Mechanisms of hair cell tuning. *Annu Rev Physiol* 61, 809–834.
- Finlayson PG and Caspary DM (1991). Low-frequency neurons in the lateral superior olive exhibit phase-sensitive binaural inhibition. *J Neurophysiol* 65, 598 – 605.
- Friauf E, Hammerschmidt B and Kirsch J (1997). Development of adult-type inhibitory glycine receptors in the central auditory system of rats. *J Comp Neurol* 385, 117–134.
- Fitzpatrick DC, Kuwada S and Batra R (2002). Transformations in processing interaural time differences between the superior olivary complex and inferior colliculus: beyond the Jeffress model. *Hear Res* 168, 79 – 89.
- Frisina RD (2001). Subcortical neural coding mechanisms for auditory temporal processing. *Hear Res* 158, 1–27.
- Fuchs PA and Mann AC (1986). Voltage oscillations and ionic currents in hair cells isolated from the apex of the chick's cochlea. *J Physiol (Lond)* 371, 31P.
- Fujino K, Koyano K and Ohmori H (1997). Lateral and medial olivocochlear neurons have distinct electrophysiological properties in the rat brain slice. *J Neurophysiol* 77, 2788 –2804.
- Futai K, Okada M, Matsuyama K and Takahashi T (2001). High-fidelity transmission acquired via a developmental decrease in NMDA expression at an auditory synapse. *J Neurosci* 21, 3342–3349.
- Gai Y, Doiron B and Rinzel J (2010). Slope-based stochastic resonance: How noise enables phasic neurons to encode slow signals. *PLoS Comput Biol* 6 (6), e1000825.
- Galambos R, Schwartzkopf J and Rupert A. (1959). Micro-electrode study of superior olivary nuclei. *Am J Physiol* 197, 527-536.
- Garcia-Lazaro JA, Ahmed B and Schnupp JW (2006). Tuning to natural stimulus dynamics in primary auditory cortex. *Curr Biol* 16, 264–271.
- Glendenning KK, Hutson KA, Nudo RJ and Masterton RB (1985). Acoustic chiasm II: Anatomical basis of binaurality in lateral superior olive of cat. *J Comp Neurol* 232, 261-285.
- Goldberg JM and Brown PB (1968). Response of binaural neurons of dog superior olivary complex to dichotic tonal stimuli: some physiological mechanisms of sound localization. *J Neurophysiol* 69 (4), 1192.
- Grande LA and Spain WJ (2005). Synaptic depression as a timing device. *Physiology* 20, 201-210.

- Griffin SJ, Bernstein LR, Ingham NJ and McAlpine D (2005). Neural sensitivity to interaural envelope delays in the inferior colliculus of the guinea pig. *J Neurophysiol* 93, 3463–3478.
- Grothe B (2000). The evolution of temporal processing in the medial superior olive, an auditory brainstem structure. *Prog Neurobiol* 61, 581–610.
- Grothe B (1994). Interaction of excitation and inhibition in processing of pure tone and amplitude-modulated stimuli in the medial superior olive of the mustached bat. *J Neurophysiol* 71, 706–721.
- Grothe B and Sanes DH (1993). Bilateral inhibition by glycinergic afferents in the medial superior olive. *J Neurophysiol* 69, 1192–1196.
- Grothe B and Park TJ (1998). Sensitivity to interaural time differences in the medial superior olive of a small mammal, the Mexican free-tailed bat. *J Neurosci* 18, 6608 – 6622.
- Guinan JJ, Norris BE and Guinan SS (1972). Single units in the superior olivary complex. II. Location of unit categories and tonotopic organization. *Int J Neurosci* 4, 147–166.
- Gutfreund Y, Yarom Y and Segev I (1995). Subthreshold oscillations and resonant frequency in guinea pig cortical neurons: physiology and modelling. *J Physiol* 483, 621–640.
- Hancock KE and Delgutte B (2004). A physiologically based model of interaural time difference discrimination. *J Neurosci* 24, 7110–7117.
- Hardman RM and Forsythe ID (2009). Ether-à-go-go-related gene K⁺ channels contribute to threshold excitability of mouse auditory brainstem neurons. *J Physiol* 587, 2487–2497.
- Harper NS and McAlpine D (2004). Optimal neural population coding of an auditory spatial cue. *Nature* 430, 682–686.
- Harty TP and Manis PB (1998). Kinetic analysis of glycine receptor currents in ventral cochlear nucleus. *J Neurophysiol* 79, 1891–1901.
- Hassfurth B, Magnusson AK, Grothe B and Koch U (2009). Sensory deprivation regulates the development of the hyperpolarization-activated current in auditory brainstem neurons. *Eur J Neurosci* 30, 1227–1238.
- Held H (1893). Die centrale Gehörleitung. *Archiv für Anatomie und Physiologie. Anat Abt* 201–248.
- Helfert RH and Schwartz IR (1986). Morphological evidence for the existence of multiple neuronal classes in the cat lateral superior olivary nucleus. *J Comp Neurol* 244, 533–549.

- Henkel CK and Brunso-Bechtold JK (1991). Dendritic morphology and development in the ferret lateral superior olivary nucleus. *J Comp Neurol* 313, 259–272.
- Holmes G (1918). Disturbances of visual orientation. *Br J Ophthalmol* 2 (9), 449-468.
- Hsu SF and Augustine GJ and Jackson MB (1996). Adaptation of Ca²⁺-triggered exocytosis in presynaptic terminals. *Neuron*. 17, 501-512.
- Hu H, Vervaeke K and Storm JF (2002). Two forms of electrical resonance at theta frequencies, generated by M-current, h-current and persistent Na⁺ current in rat hippocampal pyramidal cells. *J Physiol (Lond)* 545, 783-805.
- Hudspeth AJ and Lewis RS (1988). A model for electrical resonance and frequency tuning in saccular hair cells of the bull-frog, *Rana catesbeiana*. *J Physiol* 400, 275–97.
- Hutcheon B, Miura RM and Pail E (1996). Subthreshold membrane resonance in neocortical neurons. *J Neurophysiol* 76, 683–697.
- Hutcheon B and Yarom Y (2000). Resonance, oscillation and the intrinsic frequency preferences of neurons. *TINS* 23(5), 216-22.
- Inbody SB and Feng AS (1986). Binaural response characteristics of single neurons in the medial superior olivary nucleus of the albino rat. *Brain Res* 210 (1-2), 361-6.
- Ingham NJ, Thornton SK, Comis SP and Withington DJ (1998). The auditory brainstem response of aged guinea pigs. *Acta Otolaryngol* 118, 673– 680.
- Inouye T (1909). Die Sehstörungen bei Schussverletzungen der kortikalen Sehsphäre nach Beobachtungen an Versundeten der letzten Japanische Kriege. *W. Engelmann Verlag*.
- Irvine DR, Park VN and McCormick L (2001). Mechanisms underlying the sensitivity of neurons in the lateral superior olive to interaural intensity differences. *J Neurophysiol* 86, 2647–2666.
- Ishikawa T and Takahashi T (2001). Mechanisms underlying presynaptic facilitatory effect of cyclothiazide at the calyx of Held of juvenile rats. *J Physiol (Lond)* 533, 423– 43.
- Izhikevich EM (2001). Resonate-and-fire neurons. *Neural Networks* 14, 883–894.
- Jeffress LA (1948). A place theory of sound localization. *J Comp Physiol Psychol* 41, 35–39.
- Jercog PE, Svirskis G, Kotak VC, Sanes DH and Rinzel J (2010). Asymmetric excitatory synaptic dynamics underlie interaural time difference processing in the auditory system. *PLoS Biol* 8, e1000406.
- Joris PX, Schreiner CE and Rees A (2004). Neural processing of amplitude-modulated sounds. *Physiol Rev* 84, 541–577.

Joris, PX and Yin, TC (1992). Responses to amplitude-modulated tones in the auditory nerve of the cat. *JASA* 91(1), 215-232.

Joris PX and Yin TC (1995). Envelope coding in the lateral superior olive. I. Sensitivity to interaural time differences. *J Neurophysiol* 73(3), 1043-1062.

Joris PX and Yin TC (1996). Envelope coding in the lateral superior olive. II. Characteristic delays and comparison with responses in the medial superior olive. *J Neurophysiol* 76(4), 2137-2156.

Joris PX and Yin TC (1998). Envelope coding in the lateral superior olive. III. Comparison with afferent pathways. *J Neurophysiol* 79, 253–269.

Joris PX, Smith PH and Yin TCT (1998). Coincidence detection minireview in the auditory system: 50 years after Jeffress. *Neuron* 21 (6), 1235-1238.

Joris PX, Schreiner CE and Rees A (2004). Neural processing of amplitude-modulated sounds. *Physiol Rev* 84, 541-577.

Joris PX and Yin TCT (2007) A matter of time: internal delays in binaural processing. *TINS* 30, 70-78.

Kaczmarek LK, Bhattacharjee A, Desai R, Gan L, Song P, von Hehn CA, Whim MD and Yang B (2005). Regulation of the timing of MNTB neurons by short-term and long-term modulation of potassium channels. *Hear Res* 206, 133–145.

Kandler K and Friauf E (1995). Development of electrical membrane properties and discharge characteristics of superior olivary complex neurons in fetal and postnatal rats. *Eur J Neurosci* 7(8), 1773-1790.

Kandler K, Clause A and Noh J (2009). Tonotopic reorganization of developing auditory brainstem circuits. *Nat Neurosci* 12, 711-717.

Kapfer C, Seidl AH, Schweizer H and Grothe B (2002). Experience-dependent refinement of inhibitory inputs to auditory coincidence-detector neurons. *Nat Neurosci* 5, 247–253.

Kern A, Heid C, Stebb WH, Stoop N and Stoop R (2008). Biophysical parameters modification could overcome essential hearing gaps. *PloS Comp Biol* 4(8), e1000161.

Khurana S, Remme MWH, Rinzel J and Golding NL (2011). Dynamic interaction of I_h and I_{K-LVA} during trains of synaptic potentials in principal neurons of the medial superior olive. *J Neurosci* 31(24), 8936-8947.

Kil J, Kageyama GH, Semple MN and Kitzes LM (1995). Development of ventral cochlear nucleus projections to the superior olivary complex in gerbil *J Comp Neurol* 353, 317–340.

Kim G and Kandler K (2003). Elimination and strengthening of glycinergic/GABAergic connections during tonotopic map formation. *Nat Neurosci* 6, 282-290.

Klumpp RG and Eady HR (1956). Some Measurements of Interaural Time Difference Thresholds. *JASA* 28(5), 859-860.

Koch U and Grothe B (2003). Hyperpolarization-activated current (I_h) in the inferior colliculus: distribution and contribution to temporal processing. *J Neurophysiol* 90, 3679 – 3687.

Kopp-Scheinflug C, Fuchs K, Lippe WR, Tempel BL and Rübsamen R (2003). Decreased temporal precision of auditory signalling in Kcna1-null mice: an electrophysiological study in vivo. *J Neuroscience* 23, 9199–9207.

Kotak VC and Sanes DH (1995). Synaptically evoked prolonged depolarizations in the developing auditory system. *J Neurophysiol* 74, 1611–1620.

Kotak VC, Korada S, Schwartz IR and Sanes DH (1998). A developmental shift from GABAergic to glycinergic transmission in the central auditory system. *J Neurosci* 18, 4646 – 4655.

Kretzmer ER (1954). Redundancy in Television. *Bell Lab Record*, 401

Kuba H, Ishii TM and Ohmori H (2006). Axonal site of spike initiation enhances auditory coincidence detection. *Nature* 444, 1069–1072.

Kuenzel T, Borst JG and van der Heijden M (2011). Factors controlling the input-output relationship of spherical bushy cells in the gerbil cochlear nucleus. *J Neurosci* 31: 4260–4273.

Leakey DM, Sayers BM and Cherry C (1958). Binaural fusion of low- and high-frequency sounds, *JASA* 30(3), 222-222.

Leão RN, Svahn K, Berntson A and Walmsley B (2005). Hyperpolarization-activated (I) currents in auditory brain stem neurons of normal and congenitally deaf mice. *Eur J Neurosci* 22 (1), 147–157.

Leão KE, Leão RN, Sun H, Fyffe RE and Walmsley B (2006). Hyperpolarization-activated currents are differentially expressed in mice brainstem auditory nuclei. *J Physiol* 576, 849 – 864.

Leão KE, Leão RN and Walmsley B (2011). Modulation of dendritic synaptic processing in the lateral superior olive by hyperpolarization-activated currents. *Eur J Neurosci* 33 (8), 1462-1470.

Leibold C (2010). Influence of inhibitory synaptic kinetics on the interaural time difference sensitivity in a linear model of binaural coincidence detection. *JASA* 127, 931–942.

Lesica NA and Grothe B (2008). Efficient temporal processing of naturalistic sounds. *PLoS One* 3:e1655.

Leung LS and Yu HW (1998). Theta-frequency resonance in hippocampal CA1 neurons in vitro demonstrated by sinusoidal current injection. *J. Neurophysiol* 79, 1592–1596.

Li WC, Soffe SR and Roberts A (2004). A direct comparison of whole-cell patch and sharp electrodes by simultaneous recording from single spinal neurons in frog tadpoles. *J Physiol.* 92, 380-386

Litvin Y, Blanchard DC and Blanchard RJ (2007). Rat 22-kHz ultrasonic vocalizations as alarm cries, *Behav Brain Res* 182, 166–172.

MacFadden D and Pasanen EG (1976). Lateralization at high frequencies based on interaural time differences. *JASA* 59 (3), 634-639.

MacLeod KM, Horiuchi TK and Carr CE (2007). A role for short-term synaptic facilitation and depression in the processing of intensity information in the auditory brain stem. *J Neurophysiol* 97, 2863-2874.

MacLeod KM and Horiuchi TM (2011). A rapid form of activity-dependent recovery from short-term synaptic depression in the intensity pathway of the auditory brainstem. *Biol Cybern* 104 (3), 209-223.

Macpherson EA and Middlebrooks JC (2002). Listener weighting of cues for lateral angle: The duplex theory of sound localization revisited. *JASA* 111 (5) 2219-2236.

MacKeith NW and Coles RRA (1971). Binaural advantages in hearing of speech. *J Laryngol Otol*, 85 (3), 213-232.

Macpherson EA and Middlebrooks JC (2002). Listener weighting of cues for lateral angle: The duplex theory of sound localization revisited. *J Acoust Soc Am* 111 (5), 2219-2236.

Madison brain collection, University of Wisconsin, <http://www.brainmuseum.org/Specimens/rodentia/guineapig/sections/thumbnail.html>

Magnusson AK, Kapfer C, Grothe B and Koch U (2005). Maturation of glycinergic inhibition in the gerbil medial superior olive after hearing onset. *J Physiol* 568, 497–51.

Margrie TW and Schaefer AT (2003). Theta oscillation coupled spike latencies yield computational vigour in a mammalian sensory system. *J Physiol (Lond)* 546, 363-374.

Marsalek P and Kofranek J (2005). Spike encoding mechanisms in the sound localization pathway. *Biosystems* 79, 191-198.

Martin P and Hudspeth AJ (2001). Compressive nonlinearity in the hair bundle's active response to mechanical stimulation. *Proc Acad Natl Sci USA* 98, 14386-14391.

Mast TE (1970). Binaural interaction and contralateral inhibition in dorsal cochlear nucleus of the chinchilla. *J Neurophys.* 33, 108-115.

Mathews PJ, Jercog PE, Rinzel J, Scott LL and Golding NL (2010). Control of submillisecond synaptic timing in binaural coincidence detectors by Kv1 channels. *Nat Neurosci* 13, 601– 609.

McAlpine D, Jiang D and Palmer AR (2001). A neural code for low-frequency sound localization in mammals. *Nat Neurosci* 4, 396 – 401.

McFadden D and Pasanen EG (1976). Lateralization at high frequencies based on interaural time differences, *JASA* 59 (3), 634-639.

Melvin NR and Sutherland RJ (2009). Quantitative caveats of standard immunohistochemical procedures: implications for optical dissector-based designs. *J Histochem Cytochem* 10, 1-28.

Mikiel-Hunter JAD, Donato R and McAlpine D (2010). Reassessing the intrinsic and synaptic properties of MSO and LSO Principal neurons in light of their interaural time difference sensitivity. *Poster at ARO 2009 conference.*

Morest DK (1968). The collateral system of the medial nucleus of the trapezoid body of the cat, its neuronal architecture and relation to the olivo-cochlear bundle. *Brain Res* 9, 288 – 311.

Nabekura J, Katsurabayashi S, Kakazu Y, Shibata S, Matsubara A, Jinno S, Mizoguchi Y, Sasaki A and Ishibashi H (2004). Developmental switch from GABA to glycine release in single centralsynaptic terminals. *Nat Neurosci* 7, 17-23.

Nagel KI and Doupe AJ (2006). Temporal processing and adaptation in the songbird auditory forebrain. *Neuron* 51, 845– 859.

Nelken I, Rotman Y and Bar Yosef O (1999). Responses of auditory-cortex neurons to structural features of natural sounds. *Nature* 397, 154 –15.

Nitschke W (1982). "Acoustic behaviour in the rat". New York: Praeger.

Nomoto M, Suga N and Katsuki Y (1964). Discharge pattern and inhibition of primary auditory nerve fibers in the monkey. *J Neurophysiol.* 27, 768-78.

Nuetzel JM and Hafter ER (1976). Lateralization of complex waveforms: Effects of fine structure, amplitude and duration. *JASA* 60 (6), 1339-1346.

Nyby J (2001). "Auditory communication in adults". In: *Handbook of Mouse Auditory Research: From Behavior to Molecular Biology*. James F Willott (Ed.) Boca Raton: CRC Press, 3-18.

- Palmer AR and Russell IJ (1986). Phase-locking in the cochlear nerve of the guinea-pig and its relation to the receptor potential of inner hair-cells, *Hear Res* 24 (1), 1-15.
- Palmer AR, Rees A and Caird D (1990). Interaural delay sensitivity to tones and broad band signals in the guinea-pig inferior colliculus. *Hear Res* 50, 71– 78.
- Paolini AG, FitzGerald JV, Burkitt AN and Clark GM (2001). Temporal processing from the auditory nerve to the medial nucleus of the trapezoid body in the rat, *Hear Res* 159 (1-2), 101-116.
- Park TJ, Monsivais P and Pollak GD (1997). Processing of interaural intensity differences in the LSO: role of interaural threshold differences. *J Neurophysiol* 77, 2863-2878.
- Paxinos G (2004). "The rat nervous system". *Gulf Professional Publishing*, p1013-1014.
- Pecka M, Brand A, Behrend O and Grothe B (2008). Interaural time difference processing in the mammalian medial superior olive: the role of glycinergic inhibition. *J Neurosci* 28, 6914-6925.
- Piechotta K, Weth F, Harvey RJ and Friauf E (2001). Localization of rat glycine receptor alpha1 and alpha2 subunit transcripts in the developing auditory brainstem. *J Comp Neurol* 438, 336-352.
- Puil E, Gimbarzevsky B and Miura RM (1986). Quantification of membrane properties of trigeminal root ganglion neurons in guinea pigs. *J Neurophysiol* 55, 995- 1016.
- Puil E, Gimbarzevsky BK and Spigelman I (1988). K⁺ conductances in membrane resonance of trigeminal root ganglion neurons. *J Neurophysiol* 59, 77-89.
- Rall W (1977). Core conductor theory and cable properties of neurons. *Handb Physiol* 1, 39-97.
- Rall W and Agmon-Snir H (1998). "Cable theory for dendritic neurons". In: *Methods in Neuronal Modelling: From Ions to Networks*. Koch C and Segev I (Eds.). MIT Press, Cambridge, Massachusetts. 2nd edition.
- Rayleigh, Lord (1907), On the dynamical theory of gratings, *Proc. Roy. Soc.*, 79, 399-416.
- Remme WH, Mikiel-Hunter JAD, Donato R, McAlpine D Rinzel J (2011) ITD sensitivity to naturalistic sounds in the superior olivary complex. *BMC Neuroscience*. 12, 1.
- Rhode WS, Oertel D and Smith PH (1983). Physiological response properties of cells labelled intracellularly with horseradish peroxidase in cat ventral cochlear nucleus. *J Comp Neurol* 213(4), 448-463.

Rhode WS and Smith PH (1986). Encoding timing and intensity in the ventral cochlear nucleus of the cat. *J Neurophysiol* 56, 261–286.

Rieke F, Bodnar DA and Bialek W (1995). Naturalistic stimuli increase the rate and efficiency of information transmission by primary auditory afferents. *Proc R Soc Lond B* 262, 259–265.

Rietzel H-J and Friauf E (1998). Neuron types in the rat lateral superior olive and developmental changes in the complexity of their dendritic arbors. *J Comp Neurol* 390, 20–40.

Rinzel J and Ermentrout GB (1989). “Analysis of neural excitability and oscillations”. In: *Methods in Neuronal Modeling*. Koch C and Segev I (Eds.). Cambridge, MA: MIT Press.

Robertson D, Anderson C-J and Cole K (1986). Segregation of efferent projections to different turns of the guinea pig cochlea. *Hearing Research* 25, 69-75.

Rodriguez FA, Chen C, Read HL and Escabi MA (2010). Neural modulation tuning characteristics scale to efficiently encode natural sound statistics. *J Neurosci* 30, 15969-15980.

Rosen R (1992). Temporal information in speech: acoustic, auditory and linguistic aspects philosophical transactions. *Royal Society, Biological Sciences* p367.

Rothman JS, Young ED and Manis PB (1993). Convergence of auditory nerve fibers onto bushy cells in the ventral cochlear nucleus: Implications of a computational model. *J Neurophysiol* 70, 2562–2583.

Rothman JS and Manis PB (2003). Kinetic analyses of three distinct potassium conductances in ventral cochlear nucleus neurons. *J Neurophysiol* 89, 3083–3096.

Rozov A and Burnashev N (1999). Polyamine-dependent facilitation of postsynaptic AMPA receptors counteracts paired-pulse depression. *Nature* 401, 594–598.

Ruggero MA, Rich NC, Recio A, Narayan SS and Robles L (1997). Basilar-membrane responses to tones at the base of the chinchilla cochlea, *JASA* 101, 2151–2163.

Ryan AF, Woolf NK and Sharp FR (1982). Tonotopic organization in the central auditory pathway of the mongolian gerbil: a 2-deoxyglucose study. *J Comp Neurol* 207, 369-380.

Sachs MB and Abbas PJ (1974). Rate versus level functions for auditory nerve fibres in cats: tone-burst stimuli. *JASA* 56, 1835-1847.

Sakaba T and Neher E (2001). Quantitative relationship between transmitter release and calcium current at the calyx of Held synapse. *J Neurosci* 21, 462-476.

Sanchez-Gonzalez MA, Warr WB and Lopez DE (2003). Anatomy of olivocochlear neurons in the hamster studied with FluoroGold. *Hear Res* 185, 65–76.

- Sanders I, Weisz DJ, Yang BY, Fung K and Amirali A (2001). The mechanism of ultrasonic vocalization in the rat. *Soc Neurosci Abstr* 27:88.19.
- Sanes DH and Rubel EW (1988). The ontogeny of inhibition and excitation in the gerbil lateral superior olive. *J Neurosci* 8, 682–700.
- Sanes DH (1990). An in vitro analysis of sound localization mechanisms in the gerbil lateral superior olive. *J Neurosci* 10, 3494–3506.
- Sanes DH and Siverls V (1991). The development and specificity of inhibitory axonal arborizations in the lateral superior olive. *J Neurobiol* 22, 837–854.
- Sanes DH (1993). The development of synaptic function and integration in the central auditory system. *J Neurosci* 13, 2627-2637.
- Sätzler K, Söhl LF, Bollman JH, Borst JG, Frotscher M, Sakmann B and Lübke JH (2002). Three-dimensional reconstruction of a calyx of Held and its postsynaptic principal neuron in the medial nucleus of the trapezoid body. *J Neurosci* 22 (24), 10567-10579.
- Sayers BM and Cherry EC (1957). Mechanism of binaural fusion in the hearing of speech, *JASA* 29 (9), 973-987.
- Schneider Gasser EM, Straub CJ, Panzanelli P, Weinmann O, Sassoè-Pognetto M and Fritschy JM (2006). Immunofluorescence in brain sections: simultaneous detection of presynaptic and postsynaptic proteins in identified neurons. *Nat Protocols* 1, 1887–1897.
- Schreiber S, Erchova I, Heinemann U, Herz AVM (2004). Subthreshold resonance explains the frequency-dependent integration of periodic as well as random stimuli in the entorhinal cortex. *J Neurophysiol* 92, 408 – 415.
- Schofield BR and Cant NB (1991). Organization of the superior Olivary complex in the guinea pig. I. Cytoarchitecture, cytochrome oxidase histochemistry, and dendritic morphology. *J Comp Neurol* 314, 645-670.
- Scott LL, Mathews PJ and Golding NL (2005). Posthearing developmental refinement of temporal processing in principal neurons of the medial superior olive. *J Neurosci* 25, 7887–7895.
- Scott LL, Hage TA and Golding NL (2007). Weak action potential backpropagation is associated with high-frequency axonal firing capability in principal neurons of the gerbil medial superior olive. *J Physiol* 583, 647– 666.
- Scott LL, Mathews PJ and Golding NL (2010). Perisomatic voltage-gated sodium channels actively maintain linear synaptic integration in principal neurons of the medial superior olive. *J Neurosci* 30, 2039 –2050.

Seidl AH and Grothe B (2005). Development of sound localization mechanisms in the Mongolian gerbil is shaped by early acoustic experience. *J Neurophysiol* 94, 1028-1036.

Shackleton T, Skottun B, Arnott R and Palmer A (2003). Interaural time difference discrimination thresholds for single neurons in the inferior colliculus of Guinea pigs. *J Neurosci* 23, 716–724.

Simon HJ, Collins CC, Jampolsky A, Morledge DE and Yu J (1994). The measurement of the lateralization of narrow bands of noise using an acoustic pointing paradigm: the effect of sound-pressure level. *JASA* 95 (3), 1534-1547.

Simpson GV, Knight RT, Brailowsky S, Prospero-Garcia O and Scabini D (1985). Altered peripheral and brainstem auditory function in aged rats. *Brain Res* 348, 28–35.

Singh NC and Theunissen FE (2003). Modulation spectra of natural sounds and ethological theories of auditory processing. *JASA* 114, 3394–3411.

Skaggs WE, McNaughton BL, Wilson MA and Barnes C (1996). Theta phase precession in hippocampal neuronal populations and the compression of temporal sequences. *Hippocampus* 6, 149–172.

Smith PH, Joris PX and Yin TCT (1993). Projections of physiologically characterized spherical bushy cell axons from the cochlear nucleus of the cat: evidence for delay lines to the medial superior olive. *J Comp Neurol* 331, 245–260.

Smith PH (1995). Structural and functional differences distinguish principal from nonprincipal cells in the guinea pig MSO slice. *J Neurophysiol* 73 (4), 1653-1667.

Smith AJ, Owens S and Forsythe ID (2000). Characterisation of inhibitory and excitatory postsynaptic currents of the rat medial superior olive. *J Physiol* 529, 681–698.

Song P, Yang Y, Barnes-Davies M, Bhattacharjee A, Hamann M, Forsythe ID, Oliver DL and Kaczmarek LK (2005). Acoustic environment determines phosphorylation state of the Kv3.1 potassium channel in auditory neurons. *Nat Neurosci* 8(10), 1335-1342.

Spitzer MW and Semple MN (1995) Neurons sensitive to interaural phase disparity in gerbil superior olive: diverse monaural and temporal response properties. *J Neurophysiol* 73 (4), 1668-1690.

Srinivasan G (2004). Characterization of neuronal activity in the auditory brainstem of rats: An optical imaging approach, *Dissertation zur Erlangung des Doktorgrades der Naturwissenschaften. Fachbereich Biologie Technische Universität Kaiserslautern.*

Staley KJ, Otis TS and Mody I (1992). Membrane properties of dentate gyrus granule cells: comparison of sharp microelectrode and whole-cell recordings. *J Physiol* 67, 1346-1358.

- Sterbing SJ, D'Angelo WR, Ostapoff E-M and Kuwada S (2003). Effects of amplitude modulation on the coding of interaural time differences of low-frequency sounds in the inferior colliculus. I. Response properties. *J Neurophysiol* 90, 2818–2826.
- Sterrenborg JC, Pilati N, Sheridan CJ, Uchitel OD, Forsythe ID and Barnes-Davies M (2010). Lateral olivocochlear (LOC) neurons of the mouse LSO receive excitatory and inhibitory synaptic inputs with slower kinetics than LSO principal neurons. *Hear Res* 270, 119-126.
- Stevens SS and Newman EB (1936). The localization of actual sources of sound, *Am J Psychol*, 297.
- Stotler WA (1953). An experimental study of the cells and connections of the superior olivary complex of the cat. *J Comp Neurol* 98, 401-431.
- Strohmann B, Schwartz DW and Puil E (1994). Subthreshold frequency selectivity in avian auditory thalamus. *J Neurophysiol.* 71, 1361- 1372.\
- Structure of organ of Corti (1997) *Encyclopedia Britannica, Inc.*
- Strutt JW (1907). On our perception of sound direction. *Philosophical Magazine A, Physics of condensed matter, defects and mechanical properties* 13, 214.
- Strutz J and Bielenberg K (1984). Efferent acoustic neurons within the lateral superior olivary nucleus of the guinea pig. *Brain Res* 299, 174-177.
- Suneja SK, Benson CG and Potashner SJ (1998). Glycine receptors in adult guinea pig brain stem auditory nuclei: regulation after unilateral cochlear ablation. *Exp Neurol* 154, 473–488.
- Svirskis G, Kotak V, Sanes DH and Rinzel J (2002). Enhancement of signal-to-noise ratio and phase locking for small inputs by a low-threshold outward current in auditory neurons. *J Neurosci* 22 (24), 11019-11025.
- Svirskis G, Kotak VC, Sanes DH and Rinzel J (2004). Sodium along with low threshold potassium currents enhance coincidence detection of subthreshold noisy signals in MSO neurons. *J Neurophysiol* 91, 2465–2473.
- Szalisznyó K (2006). Role of hyperpolarization activated conductances in the lateral superior olive: a modeling study. *J Comput Neurosci* 20 (2), 137-152.
- Taschenburger H and von Gersdorff H (2000). Fine-tuning an auditory synapse for speed and fidelity: developmental changes in presynaptic waveform, EPSC kinetics, and synaptic plasticity. *J Neurosci* 20 (24): 9162-9172.
- Tennigkeit F, Puil E and Schwarz DW (1997). Firing modes and membrane properties in lemniscal auditory thalamus. *Acta Otolaryngol* 117, 254–257.

Tollin DJ (2003). The Lateral Superior Olive: A Functional Role in Sound Source Localization, *Neuroscientist* 9 (2), 127–143.

Tollin DJ and Yin TCT (2002). The coding of spatial location by single units in the lateral superior olive of the cat. I. Spatial receptive fields in azimuth. *J Neurosci* 22, 1454-1467.

Tollin DJ and Yin TCT (2002). The coding of spatial location by single units in the lateral superior olive of the cat. II. The determinants of spatial receptive fields in azimuth. *J Neurosci* 22, 1468-1479.

Tollin DJ and Yin TC (2005). Interaural phase and level difference sensitivity in low-frequency neurons in the lateral superior olive. *J Neurosci* 25 (46), 10648-10657.

Trussell LO, Zhang S and Raman IM (1993). Desensitization of AMPA receptors upon multiquantal neurotransmitter release. *Neuron* 10, 1185–1196.

Trussell LO (1999). Synaptic mechanisms for coding timing in auditory neurons. *Annu Rev Physiol* 61, 477–496.

Tsuchitani C (1982). Discharge patterns of cat lateral superior olivary units to ipsilateral tone-burst stimuli. *J Neurophysiol* 47, 479 –500.

Tsuchitani C and Johnson DH (1985). The effects of ipsilateral tone burst stimulus level on the discharge patterns of cat lateral superior olivary units. *JASA* 77, 1484 –1496.

Tsuchitani C and Johnson DH (1991). "Binaural cues and signal processing in the superior olivary complex". In: *Neurobiology of Hearing: The Central Auditory System*, Raven Press Ltd, New York. Altschuler RA, Bobbin RP, Clopton BM and Hoffman DW (Eds), pp163–194.

van Hateren J.H. (1993), A theory of maximizing sensory information, *Biol Cybern* 68 (1), 23-29.

Vetter DE and Mugnaini E (1992). Distribution and dendritic features of three groups of rat olivocochlear neurons. *Anal Embryol* 185, 1-16.

von Gersdorff H and Borst JG (2002). Short-term plasticity at the calyx of held. *Nat Rev Neurosci* 3, 53–64.

Voss RF and Clarke J (1975). 1/f noise in music and speech. *Nature* 258, 317-318.

Walcher J, Hassfurth B, Grothe B and Koch U (2011). Comparative post hearing development of inhibitory inputs to the lateral superior olive in gerbils and mice. *J Neurophysiol* 106 (3), 1443-1453.

Wallace MN, Shackleton TM, Anderson LA and Palmer AR (2005). Representation of the purr call in the guinea pig primary auditory cortex. *Hear Res* 204, 115-126

- Warfield D (1973). The study of hearing in animals. In: *W Gay, ed., Methods of Animal Experimentation, IV. Academic Press, London*, pp 43-143.
- Warr WB and Guinan JJ (1979). Efferent innervation of the organ of Corti: Two separate systems. *Brain Res* 173, 152-155.
- Weedman DL and Ryugo DK (1996). Pyramidal cells in primary auditory cortex project to cochlear nucleus in rat. *J Comp Neurol* 706, 97-102.
- Weis S, Schneggenburger R and Neher E (1999). Properties of a model of Ca²⁺-dependent vesicle pool dynamics and short term depression. *Biophysical Journal*. 77, 2418-2429.
- Werthat F, Alexandrova O, Grothe B and Koch U (2008). Experience-dependent refinement of the inhibitory axons projecting to the medial superior olive. *Dev Neurobiol* 68, 1454–1462.
- Winter IM and Palmer AR (1990). Level dependence of cochlear nucleus onset unit responses and facilitation by second tones or broadband noise. *J Neurophys.* 73, 141-159
- Winter IM and Palmer AR (1991). Intensity coding in low-frequency auditory-nerve fibers of the guinea pig, *JASA* 90 (4), 1958-1967.
- Wu SH and Kelly JB (1991). Physiological properties of neurons in the mouse superior olive: membrane characteristics and postsynaptic responses studied in vitro. *J Neurophysiol* 65, 230-246.
- Wu SH and Kelly JB (1992). Synaptic pharmacology of the superior olivary complex studied in mouse brain slice. *J Neurosci* 12, 3084-3097.
- Wu SH and Kelly JB (1993). Response of neurons in the lateral superior olive and medial nucleus of the trapezoid body to repetitive stimulation: intracellular and extracellular recordings from mouse brain slice. *Hear Res* 68, 189-201.
- Wu SH and Kelly JB (1994). Physiological evidence from ipsilateral inhibition in the lateral superior olive: synaptic responses in mouse brain slice. *Hear Res* 73, 57-64.
- Wu YC, Art JJ, Goodman MB and Fettiplace R (1995). A kinetic description of the calcium-activated potassium channel and its application to electrical tuning of hair cells. *Prog Biophys Mol Biol* 63, 131-158.
- Yager DD and Hoy RR (1986). The cyclopean ear: a new sense for the praying mantis, *Science* 231 (4739), 727-729.
- Yin TCT (2002). "Neural mechanisms of encoding binaural localization cues in the auditory brainstem". In: *Integrative Functions in the Mammalian Auditory Pathway*. Oertel D *et al.* (Eds.), Springer pp. 99 – 159.

Yin TCT and Kuwada S (1983). Binaural interaction in low-frequency neurons in inferior colliculus of the cat. II. Effects of changing rate and direction of interaural phase. *J Neurophysiol* 50, 1000–1019.

Yin TC and Chan JC (1990). Interaural time sensitivity in medial superior olive of cat. *J Neurophysiol* 64, 465–48.

Zacksenhouse M, Johnson DH and Tsuchitani C (1995). Transient effects during the chopping response of LSO neurons. *JASA* 98, 1410–1422.

Zacksenhouse M, Johnson DH, Williams J and Tsuchitani C (1998). Single-neuron modeling of LSO unit responses. *J Neurophysiol* 79, 3098–3110.

Zar JH (1984). "Biostatistical analysis". 2nd Edition. Englewood Cliffs, NJ: Prentice-Hall. p130.

Zhou Y, Carney LH and Colburn HS (2005). A model for interaural time difference sensitivity in the medial superior olive: interaction of excitatory and inhibitory synaptic inputs, channel dynamics and cellular morphology. *J Neurosci* 25, 3046–3058.

Zhou N and Parks TN (1993). Divalent cation accumulation in chick brainstem auditory neurons induced by synaptic stimulation or by application of excitatory amino acids. *Soc Neurosci Abstr* 19, 534.

Zilany MSA, Bruce IC, Nelson PC and Carney LH (2009). A phenomenological model of the synapse between the inner hair cell and auditory nerve: Long-term adaptation with power-law dynamics. *JASA* 126, 2390-2412.

List of abbreviations and standard units of measurement

Abbreviations

4-AP	4-Aminopyridine
AC	Alternating Current
ACSF	Artificial cerebro-spinal fluid
AM	Amplitude-modulated
AMPA	2-amino-3-(5-methyl-3-oxo-1,2-oxazol-4-yl) propanoic acid
AMPARs	2-amino-3-(5-methyl-3-oxo-1,2-oxazol-4-yl) propanoic acid receptors
ANF	Auditory nerve fibre
AP	Auditory nerve
ASC	Ascorbic Acid
ATP	Adenosine triphosphate
AVCN	Anterior ventral cochlear nucleus
BAPTA	1,2-bis(o-aminophenoxy)ethane-N,N,N',N'-tetraacetic acid
BM	Basilar membrane
C	Capacitor
CCD	Charge-coupled device
CF	Characteristic frequency
CN	Cochlear nucleus
CNS	Central nervous system
CTZ	Cyclothiazide
DAPI	4',6-diamidino-2-phenylindole
DC	Direct current

DCN	Dorsal cochlear nucleus
dPSP	Depolarizing postsynaptic potential
DTX-K	Dendrotoxin-K
E_K	Reversal potential for potassium ions
EI	Neurons which receive excitatory inputs from one ear and inhibition from the other.
EPSC	Excitatory postsynaptic current
EPSP	Excitatory postsynaptic potential
FITC	Fluorescein isothiocyanate
FFT	Fast Fourier transform
GABA	Gamma-aminobutyric acid
GABAR	Gamma-aminobutyric acid receptor
GBC	Globular bushy cell
GluR	Glutamatergic receptor
GlyR	Glycinergic receptor
GlyT	Glycinergic transporter
hPSP	Hyperpolarizing postsynaptic potential
HEPES	4-(2-hydroxyethyl)-1-piperazineethanesulfonic acid
IC	Inferior colliculus
IHC	Inner hair cell
I_H	Hyperpolarization-activated mixed cationic current
I_{KIR}	Inward rectifying potassium current
I_{KLT}	Low threshold potassium current
I_{Na}	Sodium current
ILD	Interaural level difference
IPD	Interaural phase difference
IPSC	Inhibitory postsynaptic current

ISI	Inter-stimulus interval
ITD	Interaural time difference
L	Inductor
LNTB	Lateral nucleus trapezoid body
LOC	Lateral olivocochlear
LSO	Lateral superior olive
MAP2	Microtubule associated protein 2
MNTB	Medial nucleus trapezoid body
MSO	Medial superior olive
NA	<i>Nucleus angularis</i>
NL	<i>Nucleus Laminaris</i>
NM	<i>Nucleus Magnocellularis</i>
NMDA	N-Methyl-D-aspartic acid
NMDAR	N -methyl-D-Aspartate glutamate receptor
O.C.T	Optimum cutting temperature
OHC	Outer hair cell
pLSO	principal neurons of the lateral superior olive
pMNTB	principal neuron of the medial nucleus of the trapezoid body
pMSO	principal neuron of the medial superior olive
pSOC	principal neuron of the superior olive complex
PCr	Phosphocraatine
PFA	Paraformaldehyde
PBS	Phosphate buffer solution
PSC	Postsynaptic current
PSP	Postsynaptic potential
PVCN	Posterior ventral cochlear nucleus

Q factor	Quality factor
R	Resistor
R_{in}	Input resistance
SAM	Sinusoidally amplitude modulated
SBC	Spherical bushy cell
SD	Standard Deviation
SEM	Standard error of the mean
SOC	Superior Olivary complex
STSD	Short-term synaptic depression
STSF	Short-term synaptic facilitation
T	Time
TEA	Tetraethylammonium
V	Voltage
$V_{1/2}$ activations	Half-activation voltage
$Z(f)$	Impedance at frequency f.

Standard units of measurement

dB	Decibel
°C	Celsius
F	Capacitance
F_c	Peak resonant frequency
Hz	Hertz
ms	Milliseconds
mV	Millivolts

MOhm

MegaOhm

pA

Picoamps

pF

Picofarads